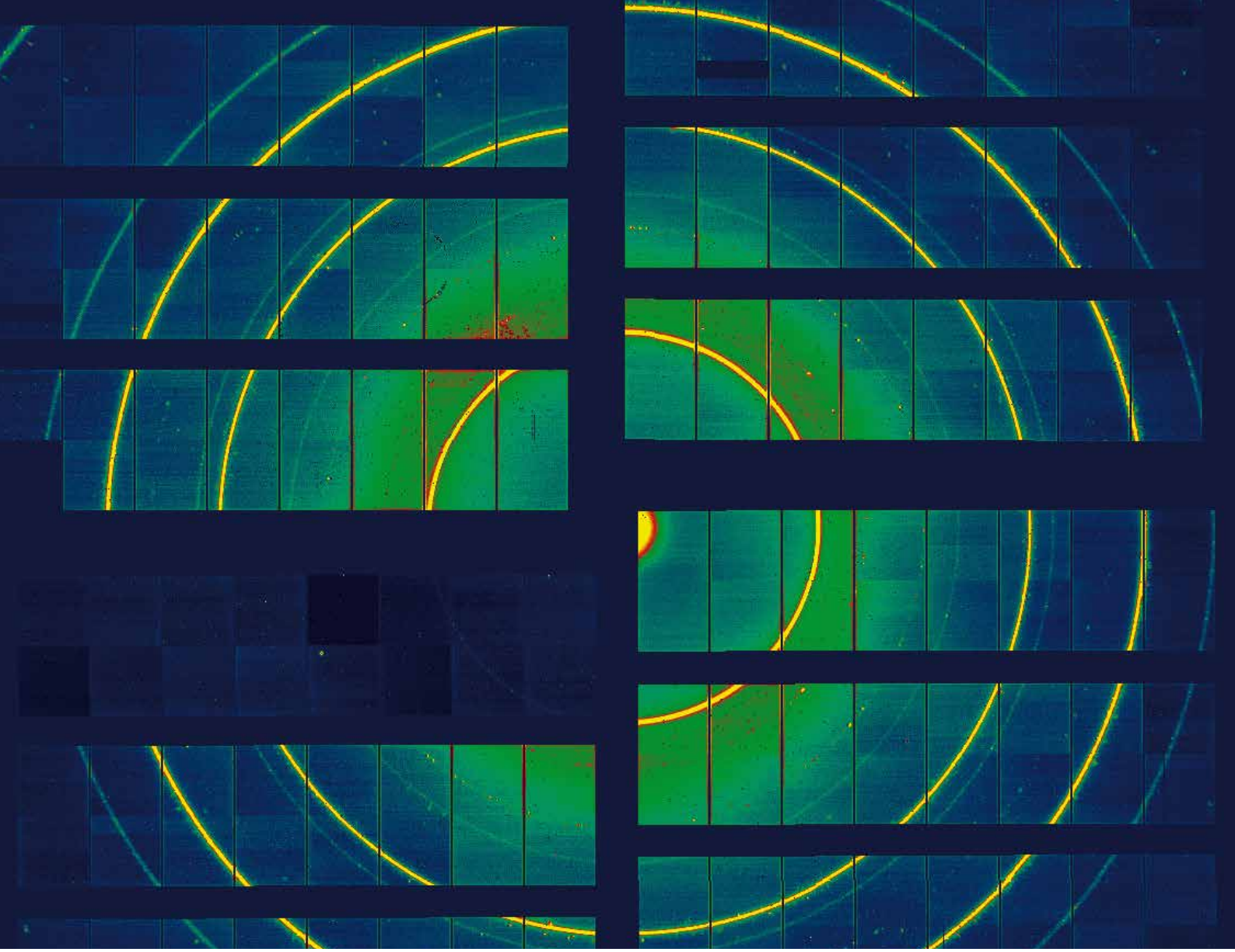

PHOTON SCIENCE 2017.

Highlights and Annual Report

Accelerators | Photon Science | Particle Physics

Deutsches Elektronen-Synchrotron
A Research Centre of the Helmholtz Association

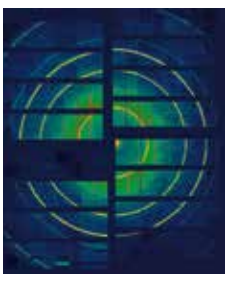

Cover

Diffraction data measured during the very first user experiment at the European XFEL.
The image shows measured test data ($Li_4Ti_5O_{12}$ powder) obtained at the SPB/SFX instrument using the AGIPD detector, which was made possible by the instrument team along with many supporting groups at the European XFEL. The AGIPD detector was specifically developed for the very high repetition rate (MHz) of the X-ray laser by the DESY detector group, headed by Heinz Graafsma. The first user experiment at the European XFEL during which this data was collected was led by Anton Barty and Henry Chapman from DESY (details on pages 98-100).

PHOTON SCIENCE 2017.

Highlights and Annual Report

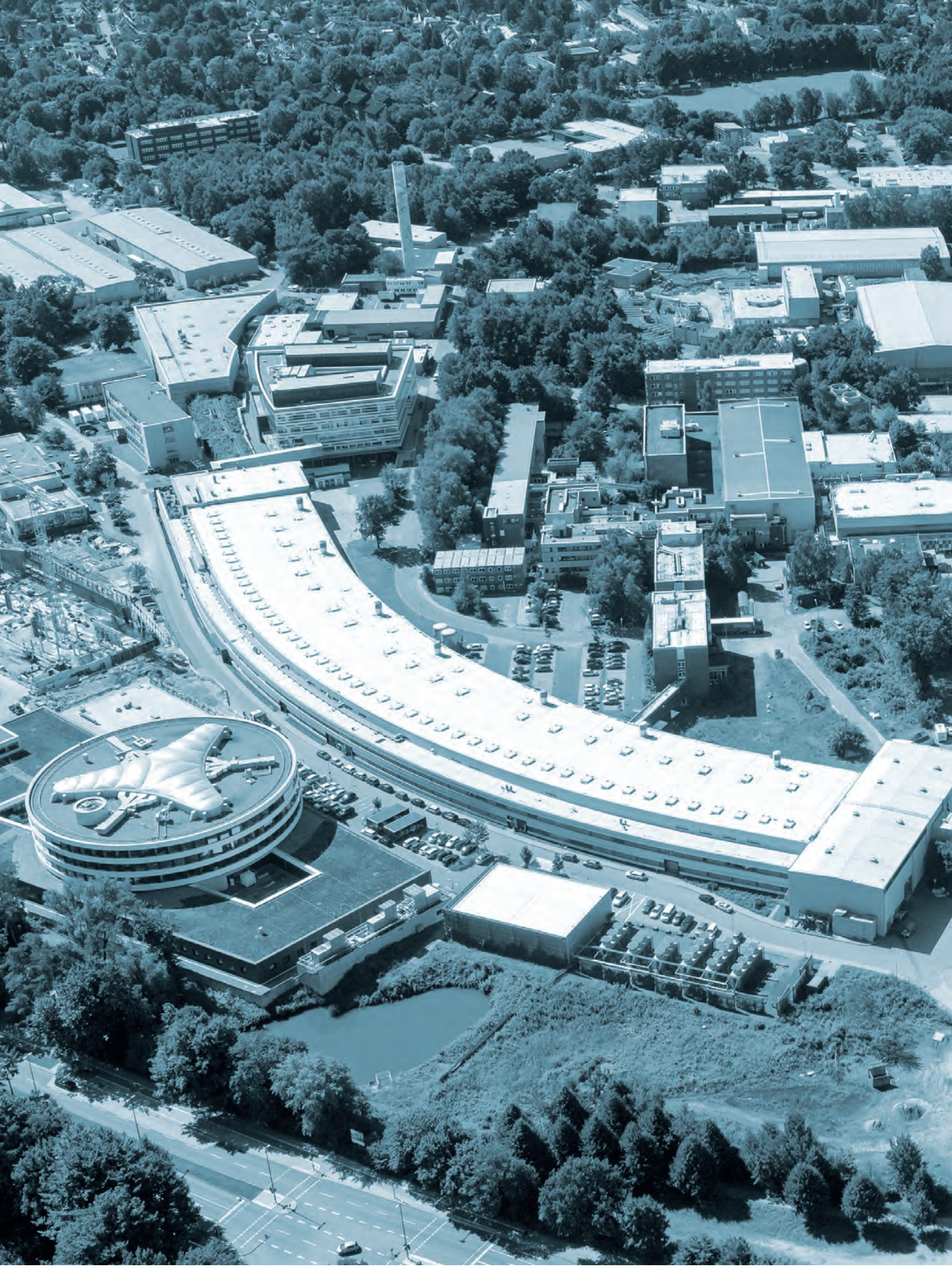

Contents.

Publications.

The list of publications based on work done at DESY Photon Science is accessible online:
http://photon-science.desy.de/research/publications/list_of_publications/index_eng.html

DESY tries to keep this list as complete and as updated as possible, and relies on the support by all users, who are kindly requested to register their publications via DOOR (door.desy.de).

The year 2017 at DESY.

Chairman's foreword

Dear Colleagues and Friends of DESY,

2017 will become known as a historical year for Photon Science in Hamburg. The European XFEL, the world´s most modern and most powerful X-ray laser facility has started user operation in September. The official inauguration of this international facility on 1 September created a worldwide echo in the scientific communities and in the media. DESY devised this facility, developed the superconducting accelerator technology and constructed the 2 km long linear accelerator beyond the original specification and has underlined with this great success its leading position as a top accelerator laboratory. It is now upon our accelerator crew to assure stable operation of the superconducting linear accelerator and upon our X-ray experts to exploit the unique potential of the facility for basic research. I am most curious to see the first breakthrough results emerging from the experiments in the coming years.

A further highlight of the year has been the official inauguration of the Centre for Structural Systems Biology (CSSB) on 29 June in the presence of Ministers, State Secretaries and the First and Second Mayor of Hamburg. It has become a wonderful science building offering a perfect interdisciplinary environment for our researchers. It has been most gratifying to see that the DFG proposal for the Cryo-EM laboratory has been fully approved, allowing now the implementation of a state-of-the-art Cryo-EM technology within CSSB. Most sadly, the excitement of the successful start of CSSB operations has been embittered by the tragic death of a worker. Our thoughts are with his family and friends.

Also our FLASH and PETRA III extension halls are now almost fully operational, offering additional and novel experimental capabilities to our users. We are currently analysing options of enhancing our bilateral co-operations with our Swedish, Indian and Russian partners.

The comprehensive DESY strategy process is in its final stage. Many brilliant ideas have been developed by our internal

Ribbon cutting in the experimental hall of the European XFEL: Prof. Dr. Johanna Wanka, German Minister for Education and Research (in the middle) and guests from across Europe.

CSSB official inauguration - ceremonial hand-over of the key: Schleswig-Holstein´s Scientific Senator Oliver Grundei, Helmut Dosch, Bärbel Brumme-Bothe from the Federal Ministry for Education and Research, CSSB´s Scientific Director Matthias Wilmanns, Lower Saxony´s Minister for Science Gabriele Heinen-Kljajić and Hamburg´s First Mayor Olaf Scholz (from left, photo: CSSB, T. Mavric).

competence teams which will enter into the DESY Strategy 2020-2035. It is most important that we have been able to identify not only future priorities but as well posteriorities. This will render the laboratory very robust to cope with the future challenges. Moreover the strategy process clearly positioned the PETRA III upgrade project ('PETRA IV') as the next large research infrastructure project and devised an ambitious future FEL plan.

PETRA IV has to be integrated in the national roadmap during the next update which will tentatively happen in 2019. This process will become embedded into the European initiative called LEAPS (League of European Accelerator-based Photon Sources) which has been initiated by DESY in 2015. LEAPS is aiming for a coordinated upgrade of the European X-ray/laser facilities and for a better integration of neighbouring communities. The launch event took place in Brussels on 13 November.

I am very pleased that the construction of the new Center for X-ray and Nano Science (CXNS) will start in 2018. It will focus our photon science research activities and also become the home of our Schleswig-Holstein partner institutes, the Helmholtz Centre Geesthacht and the Christian Albrechts University Kiel.

The DESY campus is developing very dynamically. DESY is making a strategic handshake with the University of Hamburg which is planning to allocate the physics and chemistry departments on the Bahrenfeld campus, in a later stage possibly also parts of the biology department. This will foster novel co-operations and new opportunities for the training of students and young scientists. DESY is preparing inter alia a new interdisciplinary Center for Water Science (CWS) together with the university and further partners. Thanks to a special financial support by the German Parliament, we are able to provide a substantial face lift to the laboratory including an upgrade of our guiding system ('Wegeleitsystem'), the construction of a visitor centre and the modernisation of our buildings.

Representatives of 16 light source organisations from across Europe met with Robert-Jan Smits, Director General for Research and Innovation of the European Commission at the European Union, at Brussels on 13 November to launch the new LEAPS initiative.

DESY's photon science infrastructure offers a unique inter-disciplinary research opportunity for scientists all over the world, but has also a great potential for industrial applications. This needs to be explored in all aspects in the coming years. The development of an 'Industrial Case' for PETRA IV is thus an important element of this strategy as well as the construction of the new Innovation Centre starting end of this year. We are currently investigating the options to launch a new Helmholtz Institute at the Otto-von-Guericke University in Magdeburg in collaboration with DESY, which will a have a focus on novel medical imaging tools for future applications.

I want to thank all members of the Photon Science division for their excellent work in the last years and look forward to the coming years which will be more brilliant than ever.

Helmut Dosch
Chairman of the DESY Board of Directors

Photon Science at DESY.

Introduction

The DESY site (Hamburg) with the European XFEL site in the far background (left upper corner) and the new CHyN building of the University of Hamburg (in the foreground), the new CSSB building and the construction site for the Max Planck Institute for the Structure and Dynamics of Matter (MPSD) (both close to the PETRA III hall 'Max von Laue') in August 2017.

The European XFEL site (Schenefeld) with the DESY site in the far background. The 3.4-kilometre-long European XFEL runs from DESY to the underground experimental hall in the main building (foreground).

Dear Colleagues and Friends,

The year 2017 has been a most exciting one for Photon Science in Hamburg and at DESY in particular. After many years of preparation, design and construction, and after successfully cooling down the superconducting linear accelerator (linac) over the season holidays 2016/2017, the European XFEL showed first time SASE lasing at the beginning of May. Already by the end of May the agreed commissioning goals of a wavelength of 0.2 nm and 1 mJ photon pulse energy were achieved. Meanwhile, a photon energy of about 0.13 nm is being delivered at a beam energy of roughly 14 GeV and at a repetition rate of 3000 pulses per second. My sincere congratulation goes to the entire team that made this happen not only at DESY and European XFEL but also to all collaboration partners around the world. After its official inauguration European XFEL started with first user experiments from September on in so called user assisted commissioning and later on with regular user proposals. DESY colleagues from CFEL were among the first experimentalists at European XFEL and they were very pleased with the outcome of their first experiments considering the complexity of the entire setup. Just to give you an idea: Some of us may still remember the time when we had NaI(Tl)-based point detectors as main counters on the diffractometers capable of a maximum count rate of roughly 10^5 counts per second. In comparison to these count rates the novel AGIPD detector, successfully used for some of the first experiments and developed by a consortium under the leadership of the DESY photon science detector group, can take 2D data of one mega pixel size at a frame rate of about 5 MHz. This example shows the significant progress made during the last years and needless to say that such a device is slightly more complicated and expensive than the 'good old' NaI-counters. Already now some exciting experiments were carried out at European XFEL and we are looking forward to all the ground-breaking results to come in the next years. We certainly will keep you updated.

Let's stay with free-electron lasers. Also at FLASH significant progress has been made to establish protocols for the parallel use of FLASH1 and FLASH2 in regular user operation. It is still not optimum due to the fact that we only have a fixed gap undulator at FLASH1, which needs an energy change of the linac for changing the photon energy and thus also affecting the operation of FLASH2. Therefore, a tuneable gap undulator for FLASH1 is of high priority for the next larger investments at FLASH. At present the installation of a high repetition rate pump-probe laser of the newest generation is ongoing at FLASH2. This will allow state of the art pump-probe experiments also at FLASH2 starting spring next year. At FLASH exciting scientific results have been obtained during this year, some of them are presented in this brochure.

Major progress has been made at our synchrotron source PETRA III as well. Some of the experiments in the experimental hall 'Max-von-Laue' already received a first upgrade like P01, the 'High resolution dynamics beamline', where now a crystal based in-vacuum RIXS spectrometer for photon energies as low as 2.5 keV is installed. This is a worldwide unique setup with two five metre undulators as a radiation source. In the PETRA III experimental hall 'Paul P. Ewald' the two EXAFS beamlines P65 and P64 started full user operation during the year 2016 and 2017, respectively, and three other beamlines P22 'Hard X-ray photoelectron spectroscopy', P23 'Russian-German *in situ* and nano-diffraction beamline' and P24 'Chemical crystallography' received first beam or are in commissioning and will start user operation in 2018. The P21 'Swedish materials science beamline' will see first beam from a 4 m in-vacuum undulator in mid 2018. This means, by the end of the year 2018 we should have 22 parallel operating beamlines at PETRA III, significantly increasing the portfolio of experimental techniques as compared to now. For three further beamlines P61 'High energy wiggler beamline', P62 'Small angle X-ray scattering' and P66 'Superlumi' design and tendering procedures are under way and first construction will start in January 2018. At present various discussions are ongoing for defining the science case and obtaining funding for the remaining two free undulator slots P25 and P63 in the PETRA III extension halls. Meanwhile more than 2400 scientists are performing experiments at PETRA III producing fantastic results of which only a few can be covered in this brochure.

Entrance of the new CSSB building.

In the past year DESY has carried out a thorough strategy process for defining its future beyond 2030. The ongoing PETRA IV project targeting for a hard X-ray source close to the diffraction limit received high priority in this process. The aim is to provide a first Conceptual Design Report by mid of 2018 and a more detailed Technical Design Report earliest by end of 2019. As mentioned already above, gap tunable undulators for FLASH and a number of further enhancements are also of high priority within the frame of a future FEL strategy.

Progress has also been made with all the construction projects on our campus. After some design changes, official ground breaking for the Center for X-ray and Nano Science (CXNS) took place on 27 March. This new photon science building will include the DESY NanoLab with complementary analysis techniques to prepare experiments at PETRA III and FLASH.

DESY is in close discussion with a number of national and international partners to explore the possibility of establishing a new Center for Water Science (CWS) on campus for the investigation of the peculiar properties of water that are accessible with our unique portfolio of photon based analytical techniques. On 9 June the laying of the foundation stone of the new building for the Max Planck Institute for Structure and Dynamics (MPSD) was celebrated. The new CSSB building has officially been inaugurated on 29 June and first groups are moving in. By the end of 2017 all five electron microscopes for CSSB have been delivered and installed adding this very advanced technique for single particle imaging and electron tomography to the analytical portfolio already available on the campus. The Center for Hybrid Nanostructures (CHyN) of the Universität Hamburg (UHH) was inaugurated on 19 July. Shortly before Christmas, on 21 December, the official ground breaking ceremony for the Hamburg Advanved Research Centre for Bioorganic Chemistry (HARBOR) of the UHH was celebrated. It does not need a prophet to predict that civil construction will continue for several years on our campus.

I am very thankful to all DESY staff as well as to our users and collaboration partners for the continued effort and support without that all these activities would not be possible.

Edgar Weckert
Director Photon Science

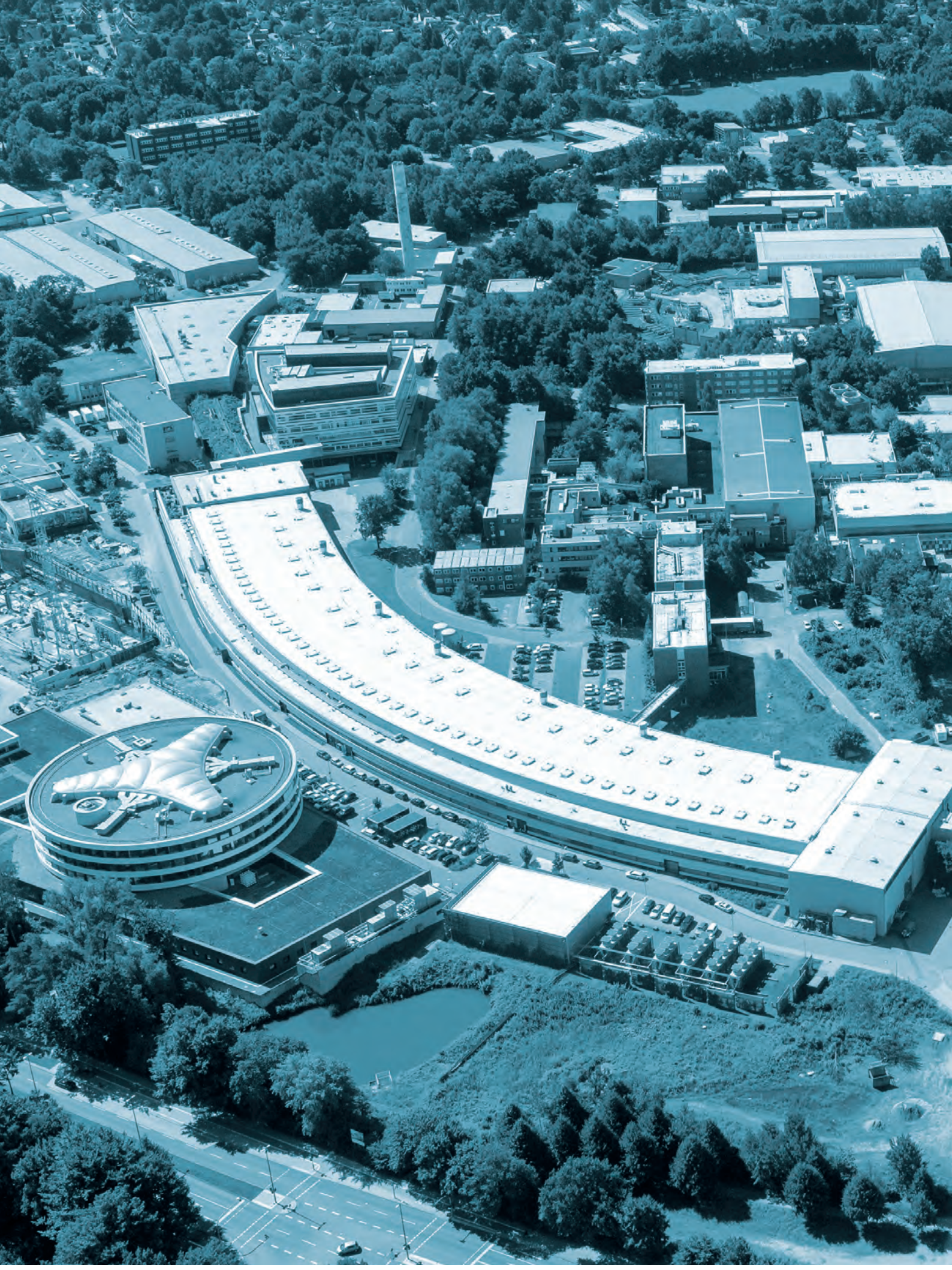

News and Events.

News and Events.

A busy year 2017

January

25 – 27 January:
New record participation in the joint users' meeting of DESY Photon Science and European XFEL

The joint users' meeting of the DESY light sources PETRA III and FLASH and of European XFEL attracted more participants than ever before. Around 1100 scientists from 30 countries and from more than 70 institutions had registered for this year's meeting to discuss research possibilities at these brilliant X-ray light sources, covering a broad range of applications from physics, chemistry, biology, and medicine to energy, materials and geoscience.

One of the highlights of the 2017 meeting was the outlook on the forthcoming start of European XFEL. Researchers from all over the world had been called to submit first proposals for experiments just before the users' meeting, and the new facility was looking forward to starting commissioning and welcoming first users for experiments. Additionally, DESY had just significantly expanded the research opportunities at its X-ray light sources PETRA III and FLASH with three new experimental halls. This not only offers additional capacities to meet the high demand for user beamtime at the facilities, but also provides new, previously unavailable experimentation techniques. In the last years DESY's light sources used to be heavily overbooked. Another focus of the users' meeting was on the scientific achievements at the facilities. Researchers presented the results of their recent work in 25 plenary talks, in a poster session with 338 posters and also in the frame of 15 satellite meetings on specific topics. In an accompanying exhibition about 50 companies showed their latest developments and products related to photon science.

Fully occupied DESY auditorium at the joint users' meeting.

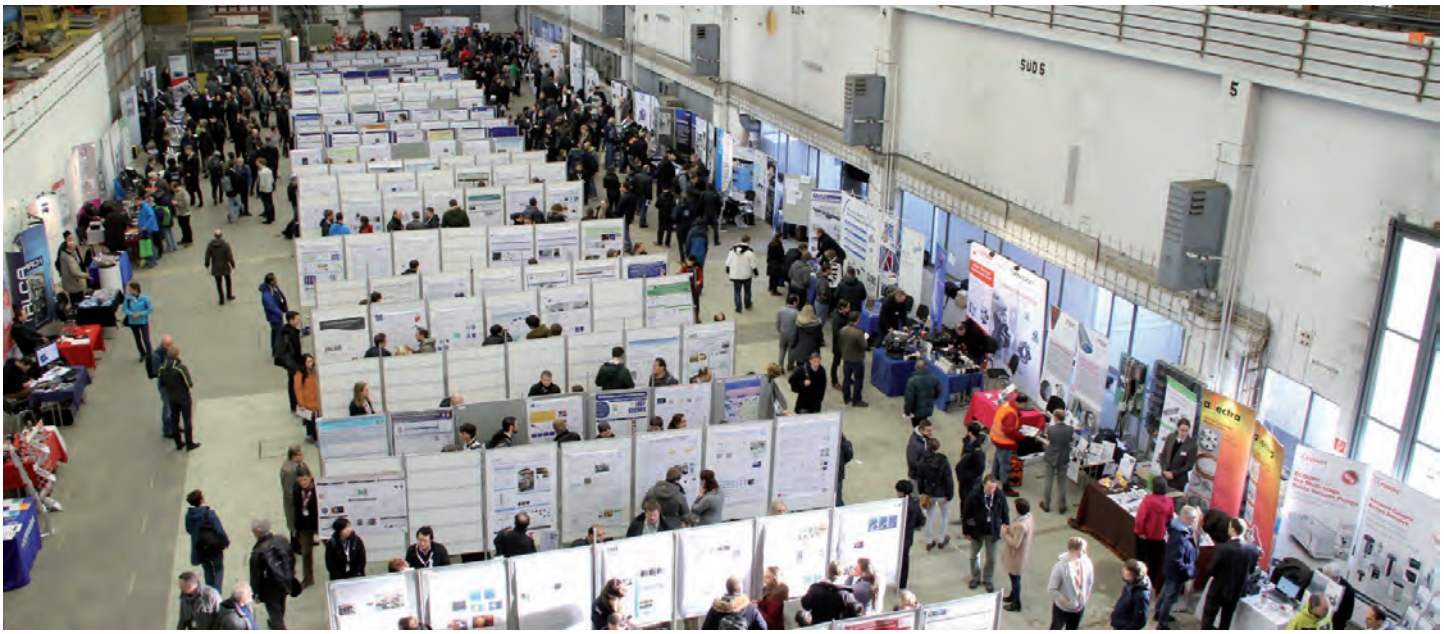

Poster session and vendor exhibition at the joint users' meeting.

March

1 – 3 March:
16th DESY Research Course

The series of DESY Research Courses addresses master and PhD students, young postdoctoral researchers, and interested scientists in general and offers the opportunity to learn about recent developments in a specific scientific field with special attention being paid to modern experimental techniques using X-ray scattering and spectroscopy.

The 16th DESY Research Course was entitled ‘Nanoscience at modern X-ray Sources’ and included topics like nanomembranes and nanodots, surfaces and interfaces, nanoelectronics, ptychography, approaches combining theory and experiment, and modern X-ray sources for nanoscience studies. The course comprised ten lectures, facility visits, and a poster session, and with 142 participants it was very well attended.

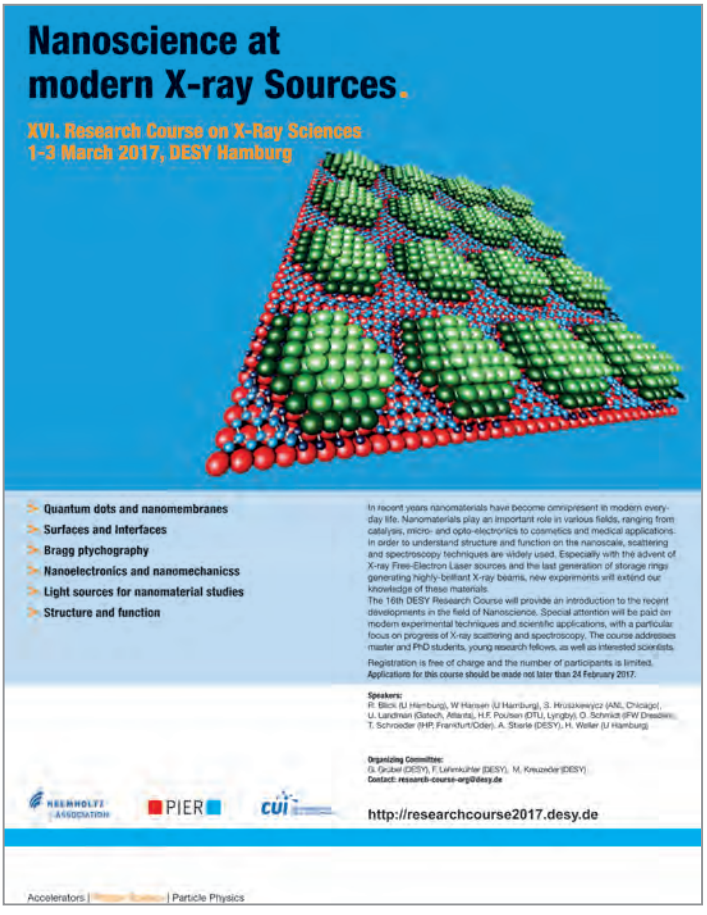

Announcement poster of the 16th DESY Research Course.

27 March:
Ground-breaking ceremony for a new Photon Science building

Joint ground-breaking. From the left: DESY director Helmut Dosch, HZG director Wolfgang Kaysser, Hamburg state secretary Eva Gümbel, Schleswig-Holstein research minister Kristin Alheit, CAU president Lutz Kipp, DESY´s director of administration Christian Harringa, and Andreas Stierle, head of the DESY NanoLab.

With a ground-breaking ceremony politicians and scientists celebrated the first step towards the construction of a new laboratory and office building at the DESY campus. It will host the Center for X-ray and Nano Science (CXNS) including the DESY NanoLab and is intended to become a focal point for nanoresearch and to complement the existing office buildings etc. for scientists from Helmholtz-Zentrum Geesthacht (HZG), Christian-Albrechts-Universität zu Kiel (CAU), and DESY. It will provide ideal conditions for preparing samples for experiments at PETRA III as well as complementary investigation techniques to make best possible use of the research potential offered by DESY’s light sources. With an envisaged close connection to research groups on campus it will provide ideal conditions for photon research and nanoscience. HZG’s activities at DESY are manifested by the German Engineering Materials Science Centre (GEMS), which acts as a user platform and operates various experimental equipment at DESY. The building will also provide a home on the DESY campus to the Ruprecht Haensel Laboratory, which is a successful cooperative venture between CAU and DESY for many years already. The building is scheduled to be finished in spring 2019.

April

28 March:
Thomas White receives Max von Laue Prize

Thomas A. White.

Thomas A. White, scientist at CFEL, was awarded the Max von Laue Prize of the German Crystallographic Society (DGK). Since 1996 the Max von Laue Prize is awarded each year to promising young scientists for outstanding scientific achievements in the field of crystallography. The prize committee recognises White's work which is basis for the unique software suite 'CrystFEL' without which the analysis of many of the ground-breaking experiments at X-ray free-electron lasers would have not been possible. Complex biomolecules like proteins often only crystallise in tiny crystals of micrometre size. Analysis of such extremely small crystals became possible by using the bright X-ray light produced in high energy free-electron lasers. With a technique called 'Serial Femtosecond X-ray crystallography' (SFX) thousands of these micro crystals are subsequently exposed to the pulses of the X-ray laser beam. 'CrystFEL' provides the tools to process the resulting huge amount of diffraction image data. Today the software package developed by White is used by scientists all over the world. By 2017 about 100 publications in peer reviewed journals report on results obtained with substantial use of the 'CrystFEL' suite.

7 April:
Röntgen Medal awarded to Henry Chapman

Henry Chapman, lead scientist at DESY and professor at Hamburg University, has received the Röntgen Medal 2017 from the City of Remscheid. Since 1951 the native town of Wilhelm Conrad Röntgen presents this award every year to individuals who made outstanding contributions towards improving and advancing the use of the X-ray radiation which was discovered by Röntgen. Henry Chapman who is head of the department for Coherent X-ray Imaging at the Center for Free-Electron Laser Science CFEL at DESY has been awarded the medal in recognition of his pioneering work on the application of X-ray lasers for determining the structure of biological macromolecules. His research team develops sophisticated new experimental techniques for making use of the excellent new opportunities offered by X-ray free-electron lasers like European XFEL which started operation this year. The aim is to use the laser-like beams to reveal structure and dynamics of proteins and their complexes—the molecular machinery of life. Chapman carried out ground-breaking experiments at DESY's free-electron laser FLASH and SLAC's Linac Coherent Light Source LCLS in California. He showed that the short FEL pulses can provide atomic scale information of the structure of nanocrystals before the crystals are destroyed by the radiation from the laser. This method of 'diffraction before destruction' forms the basis for exploiting the full potential of the new generation of X-ray lasers. Chapman has already used the method, for example, to establish the structure of a parasitic protein, the enzyme cathepsin B, in the pathogen that causes tropical sleeping sickness.

Burkhard Mast-Weisz (left), mayor of the City of Remscheid presents Henry Chapman with the Röntgen Medal. (credit: Deutsches Röntgen-Museum, Remscheid)

May

4 May:
European XFEL generates first X-ray laser light

The year 2017 saw European XFEL, the 3.4 km long largest X-ray free-electron laser in the world, coming into operation. The year started with cooling down the superconducting linear accelerator in the 2.1 km long accelerator tunnel. On the 4th of May the machine reached the next milestone when it produced first light in its 210 metres long magnetic structures called undulators. The generated X-rays had a wavelength of 0.8 nanometres. First lasing was reached at a repetition rate of one light pulse per second, the first step to the envisaged rate of 27000 pulses per second.

In the DESY accelerator control room: DESY scientist Winfried Decking (left) explains how to operate the accelerator of European XFEL.

Accelerator modules of European XFEL.

9 – 11 May:
Second workshop on science at PETRA IV

The participants of the 'Second Workshop on Science at PETRA IV'.

PETRA III is currently the world's most brilliant storage ring-based hard X-ray synchrotron radiation source. This opens up many unique scientific applications in the field of photon science. In order to keep the leading position in the future, a major strategic DESY project on a long-term scale will be the transformation of PETRA III into an ultimate storage ring named PETRA IV. This reconstruction will push the beam properties in terms of brilliance to the physical limits imposed by basic optics laws. In combination with the large circumference of the storage ring this will result in a light source with outstanding properties, significantly surpassing the existing ones. In order to collect scientists' views on the conceptual and technical design of such a new machine including the possible experimental techniques

13 February 2017: Workshop on research with high energy X-rays at PETRA IV.

15 March 2017: A PETRA IV workshop entitled 'Tribology and Interfaces in Functional Materials'.

27 March 2017: A workshop on time resolved studies at PETRA IV.

the ‘Second Workshop on Science at PETRA IV’ was organised at DESY in May 2017. It brought together experts from all the scientific fields which are currently served by PETRA III to discuss the impact of the upgrade for the various fields. The goal of the workshop was to find and exploit possible synergies and to inspire scientists to think about how to make use of new experimental opportunities that today may not be available yet. This workshop was accomplished by eight additional meetings which were spread over the entire year and addressed specific topics of future research at the envisaged storage ring PETRA IV like use of coherence, research with high energy X-rays, nanostructures at surfaces and interfaces, tribology and interfaces in functional materials, research on matter under extreme conditions, timing experiments, and experiments with soft X-rays.

26 June 2017: A PETRA IV workshop addressing coherent radiation, one of the most essential topics of a diffraction limited light source.

27 September 2017: PETRA IV workshop on research with soft X-rays.

9 October 2017: Participants of the workshop ‘Nanostructures at Surfaces and Interfaces’.

16 October 2017: Workshop on research on sample systems under extreme conditions.

June

12 – 15 June:
Ultrafast X-ray Summer School

The Center for Free-Electron Laser Science CFEL hosted the Ultrafast X-ray Summer School UXSS 2017 which was jointly organised by CFEL and the PULSE institute at SLAC National Accelerator Laboratory (United States). It was the 11th UXSS summer school since 2007.

Attendees of the Ultrafast X-ray Summer School at CFEL.

The school offered about 70 doctoral students and post-doctoral researchers the opportunity to get familiarised with the latest developments and opportunities in ultrafast X-ray science. The program was highly interdisciplinary, with nine lectures covering topics from accelerator physics to molecular biology and matter in extreme conditions. The school also included visits of instruments at DESY and European XFEL, as well as project work which concluded with a project presentation and prize ceremony honouring the best contributions.

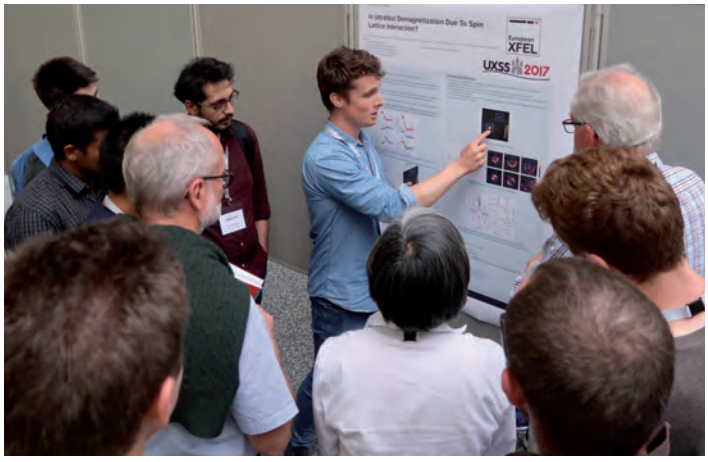

Students participating in the UXSS 2017 explain their project work.

July

29 June:
Opening ceremony for the new Centre for Structural Systems Biology

The Centre for Structural Systems Biology (CSSB) celebrated its grand opening. In this new interdisciplinary research centre, scientists from ten different research institutions will work together on some of the most challenging projects in structural biology: the functioning of viruses and bacteria. Research of CSSB will focus on the elucidation of mechanisms, structures, and dynamics of infection processes related to these pathogens. With these achievements, CSSB scientists in the end aim for contributing to the development of novel treatments and therapies. The involved partners are various Northern German institutions active in the field of infection related medical research. This outstanding cooperation of infection biologists, physicists, chemists and physicians is embedded in a unique research infrastructure.

Schleswig-Holstein´s scientific senator O. Grundei, H. Dosch, B. Brumme-Bothe from the federal ministry for education and research, M. Wilmanns, Lower Saxony´s minister for science G. Heinen-Kljajić, Hamburg´s first mayor O. Scholz, and CSSB partner institution representatives (credit: CSSB/T. Mavric).

The new CSSB building, specifically designed to foster collaboration, innovation and mentoring opportunities for young researchers, will provide scientists with state-of-the-art in-house techniques as well as with direct access to DESY's PETRA III and FLASH. The four-storey building with its combination of laboratory and office space will be home to approximately 180 scientists and staff members.

The building's basement was especially designed for the installation of five cryo-electron microscopes, which will enable CSSB scientists to visualise pathogens at various scales of resolution and complexity. Combining this in-house technology with DESY's X-ray light sources and the European XFEL will enable CSSB to apply different structural methods in an integrated manner thus advancing what scientists refer to as the 'resolution revolution'.

19 July:
DESY Summer Student Programme 2017

The DESY summer students of 2017 working in Photon Science.

The DESY summer student programme again offered the opportunity to international undergraduate students of natural sciences to join for about eight weeks the work of research groups at DESY and European XFEL. For the 2017 programme a total number of 575 students from more than 70 countries applied for attendance, more than 200 explicitly for the field of Photon Science. In the end 86 students were selected for the programme in Hamburg, 33 of them were going to work in research groups related to Photon Science. The combination of working in the groups with lectures, tours, and social events in an international, stimulating, lively and open-minded atmosphere was again highly appreciated by the participants and again made this stay in Hamburg an unforgettable experience for the students.

All students attending the 2017 summer students programme at the DESY site and at European XFEL.

August

28 August – 1 September:
10th International Conference on Inelastic X-ray Scattering

Inelastic X-ray scattering (IXS) is a powerful tool to study elementary excitations in matter. Since 1992 the International Conference on IXS had been organised nine times at different venues around the world. The 10th conference of this series, IXS2017, was now hosted by DESY and could welcome 150 attendees. It covered experimental techniques and technical development related to IXS, its applications in various scientific fields, and theory related to IXS and its applications. It comprised plenary and invited talks in twelve topical sessions with more than 70 contributions and various poster sessions, all with ample time for discussion.

The participants of the IXS2017 at DESY.

September

1 September:
Inauguration of European XFEL

European XFEL, the largest and most powerful X-ray free-electron laser in the world was inaugurated with an event attended by 800 international guests. This ceremony marked the official start of user operation.

Schleswig Holstein's minister of education, science, and cultural affairs, Karin Prien with DESY scientists Henry Chapman (left) and Anton Barty who received a symbolic access card for one of the very first user experiments at European XFEL.

Construction of the 3.4 km long facility started in January 2009, with construction costs of 1.2 billion Euro, funded by 11 countries, with Germany and Russia being the largest contributors. As many as 17 European institutes contributed in-kind to the accelerator complex. European XFEL GmbH is responsible for the construction and operation of the facility, especially of the X-ray photon transport and experimental stations, while its largest shareholder DESY is leading the construction and operation of the electron linear accelerator.

The audience of the European XFEL inauguration.

The City of Hamburg welcomed the new research facility with a special light installation: from 28 August to 3 September every evening green laser beams could be seen which originated from the Elbphilharmonie, Hamburg University and University of Applied Sciences, the Science Ministry, and the planetarium. All beams were directed to the Schenefeld site of European XFEL.

14 September:
Helmholtz Doctoral Prize for Johann Haber

In the course of the Helmholtz Association's Annual General Assembly DESY scientist Johann Haber received the Helmholtz Doctoral Prize 2017 for his PhD thesis in the research field Matter. Haber was born in Bonn and studied physics in Berlin and Göttingen and came to University of Hamburg and DESY to do his PhD work at the PETRA III storage ring. He worked in the research group of Ralf Röhlsberger on the topic 'Hard X-Ray Quantum Optics in thin-film nano structures' and discovered a new way to strongly amplify the interaction of X-rays with matter. He achieved this by embedding Mössbauer nuclei ^{57}Fe into coupled cavities and by resonantly exciting them with highly brilliant synchrotron radiation. In future applications his approach may be used to enhance nonlinear optical effects in the X-ray regime and eventually even to generate non-classical states of X-rays.

The Helmholtz Association aims to support talented young scientists at an early stage of their career. Awardees receive a prize money of 5,000 Euro and additionally 2,000 Euro per month for a research stay of up to six months at an international research institution of their choice.

20 September:
First experiment carried out at European XFEL

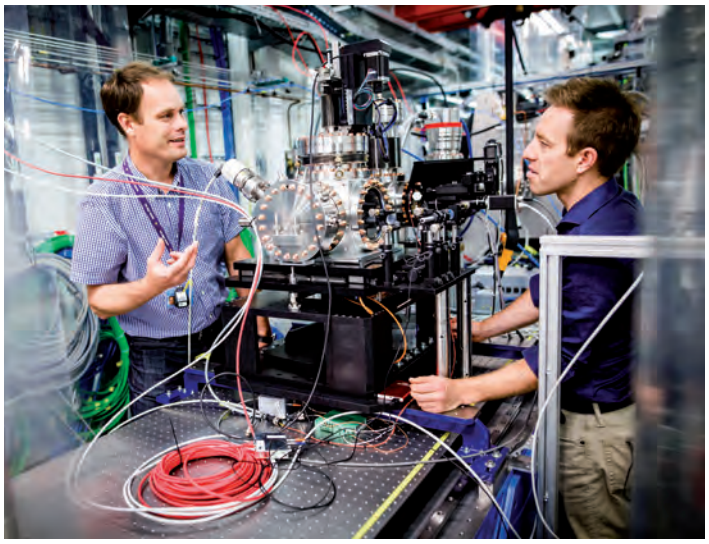

Anton Barty (DESY, left) and Richard Bean (European XFEL) at the SPB/SFX instrument.

A team of researchers from DESY has successfully started the first scientific experiments at European XFEL, the brand new X-ray free-electron laser. The aim of the team led by Anton Barty and Henry Chapman from the Center for Free-Electron Laser Science CFEL is to decode the atomic structure of complex biomolecules at the 'Single Particles, Clusters, and Biomolecules/Serial Femtosecond Crystallography' (SPB/SFX) instrument at European XFEL. The SPB/SFX instrument is headed by European XFEL scientist Adrian Mancuso and will be used to gain a better understanding of the shape and function of biomolecules, such as proteins, that are otherwise difficult or even impossible to study. During the first phase of their experiment, the scientists had to carefully calibrate and tune their instrumentation in order to learn how to use this new machine. This involves delivering the samples to the X-ray beam. The samples consist of tiny protein crystals that reveal information about their three-dimensional structure when exposed to X-rays. However, for each crystal, this is a one-shot-only experiment, as the intense flashes vaporise the crystals almost immediately. Thus, a new crystal has to be delivered into the X-ray beam every 220 nanoseconds – the temporal distance between subsequent light pulses of the X-ray laser.

Parallel to the SPB/SFX station, the 'Femtosecond X-Ray Experiments' (FXE) station headed by Christian Bressler also started scientific operation. FXE is designed to create 'molecular movies' showing the progression of chemical reactions.

25 September:
Uppsala University awards honorary doctorate to Henry Chapman

Henry Chapman, lead scientist at DESY, has been made honorary doctor at the Faculty of Science and Technology at Uppsala University in Sweden. The title will be conferred on him at the University in January 2018.

Chapman, who is also professor of physics at University of Hamburg, Germany, leads the coherent X-ray imaging division at the Center for Free-Electron Laser Science CFEL at DESY, where algorithms, instruments and methods for X-ray imaging are developed in co-operation with leading materials researchers and structural biologists. Together with researchers from Uppsala University, Chapman has conducted innovative experiments in which complex biological molecules were depicted by means of the ultrashort and extremely intensive X-ray pulses from a free-electron laser. This collaboration created a new interdisciplinary research domain which gathers researchers from various disciplines, ranging from biology to chemistry and physics, to develop new methods for atomic imaging. The collaborative work resulted in a large number of joint publications.

November

4 November:
Number of visitors at the DESY Day again marks a new record

For the seventh time DESY's open day took place as part of the Hamburg 'Night of Knowledge'. At DESY the doors were opened to the public already at 12 a.m., and at 5 p.m. when the Night of Knowledge started officially DESY had already welcomed more than 13000 curious visitors. And when the DESY Day ended at midnight, more than 20000 people had visited the site. This was a new record attendance with around 5000 more visitors than welcomed during the previous open days. DESY and the partner institutes again had prepared an attractive programme for visitors from different backgrounds and for all ages starting from young children at the age of six. About 1000 colleagues volunteered to present the experimental halls, laboratories, accelerator tunnels, workshops, and other facilities to the public. They explained their work and the research activities at DESY, organised a series of guided tours and brief talks on various topics and more than 150 demonstration and hands-on experiments. For the helpers the DESY Day again was a nice experience and the guests highly appreciated the effort and the friendly atmosphere in which they were welcomed.

During the Night of Knowledge many DESY buildings were colourfully illuminated.

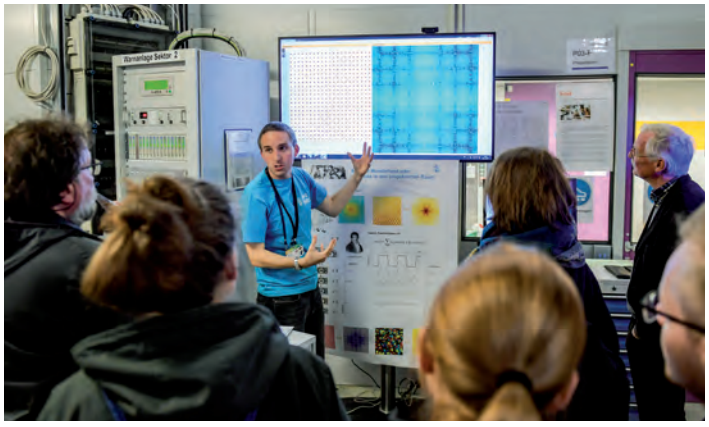

One of the numerous demonstration and hands-on experiments at the DESY Day: How to experience reciprocal space.

9-10 November:
Swedish Materials Science Beamline workshop

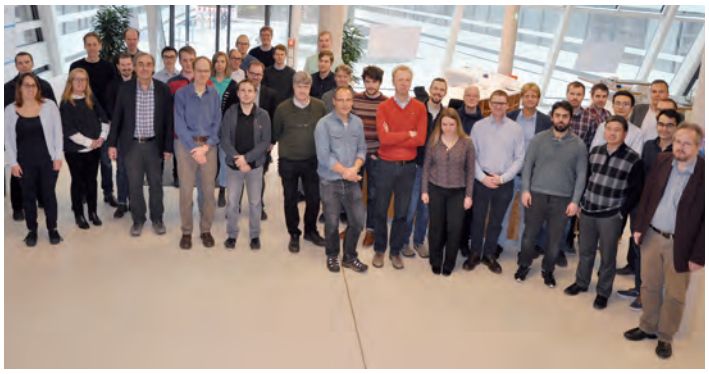

The participants of the workshop on the Swedish beamline for Materials Science.

The construction of the Swedish Materials Science (SMS) beamline P21 at PETRA III is approaching completion and first beam is anticipated in spring 2018. Therefore a workshop was organized at DESY for the Swedish user community and beyond to communicate the technical status and discuss user requirements, beamtime allocation and administrative measures to assure best use by the Swedish materials science community. The workshop was attended by about 40 participants who were interested to learn about the construction status of the in-line and side branches of the SMS beamline. The scope of scientific applications was highlighted in three sessions on catalysis and corrosion/electrochemistry, functional materials, and structural materials. Detailed beamline parameters and specific scientific applications were presented in a poster session.

13 November:
Launching a European consortium of accelerator-based photon sources

A new strategic alliance between European accelerator-based photon sources was launched in Brussels. The League of European Accelerator-based Photon Sources (LEAPS) is aiming for a big change in European cooperation through a common vision of enabling scientific excellence solving global challenges, and boosting European competitiveness and integration. Representatives of sixteen organisations from across Europe approved the consortium declaration in the presence of Robert-Jan Smits, Director General for Research and Innovation (RTD) at the European Commission. Helmut Dosch, the chairman of DESY's board of directors was a major driving force supporting the idea of LEAPS and is the first chairman of the consortium. The new form of collaboration between the participating institutions is supposed to ensure that the large European research infrastructures in the future can be used even more efficiently than already today and that major scientific and technological challenges will be

tackled with joint effort. This will not only be of benefit for fundamental and applied research, but also for industrial research carried out at accelerator-based photon sources.

DESY director Helmut Dosch with logos of the sixteen organisations who approved the LEAPS consortium declaration.

The institutions serve a community of more than 24000 researchers from a wide range of scientific fields. The new consortium shall encourage the exchange of ideas between its member institutions and their users.

15 November:
PhD thesis prize for Johann Haber

The 2017 PhD thesis prize of the Association of the Friends and Sponsors of DESY was awarded in a prize ceremony as part of this year's DESY Science Day. The prize was shared between Volodymyr Myronenko (DESY and University of Hamburg) for his combined analysis of data from HERA detectors H1 and ZEUS, and Johann Haber (DESY and University of Hamburg), who worked on quantum optics in the X-ray regime using synchrotron radiation at PETRA III.

The winners of the PhD thesis award, Johann Haber (right) and Volodomyr Myronenko (second from the left), with Helmut Dosch (left) and Friedrich-Wilhelm Büßer, chairman of the 'Association of the Friends and Sponsors of DESY'.

23-24 November:
Hard X-Ray Photoelectron Spectroscopy at PETRA III: new possibilities at the dedicated P22 beamline

The P22 beamline in the PETRA III experimental hall 'Ada Yonath' is one of three new beamlines that saw first light in 2017. The beamline is dedicated to hard X-ray Photoelectron Spectroscopy (HAXPES) techniques and comprises a number of specialised instruments built and operated in collaboration with external user groups. These include a HAXPES spectroscopy setup with optional multi-channel spin detection using a 2D spin filter, an energy filtered hard X-ray excited PEEM (HAXPEEM) for spatially resolved spectroscopy, k-space microscopy using a time-of-flight spectrometer and a high-pressure HAXPES instrument designed to reach pressures up to 10 bar.

Attendees of the workshop on Photoelectron Spectroscopy at PETRA III beamline P22.

In view of the upcoming first proposal call for this beamline, the workshop aimed at bringing together the groups contributing to the P22 project as well as presenting the unique capabilities to a wider user community. The strong interest and diversity of the field was illustrated in 13 scientific talks and 53 participants from ten countries.

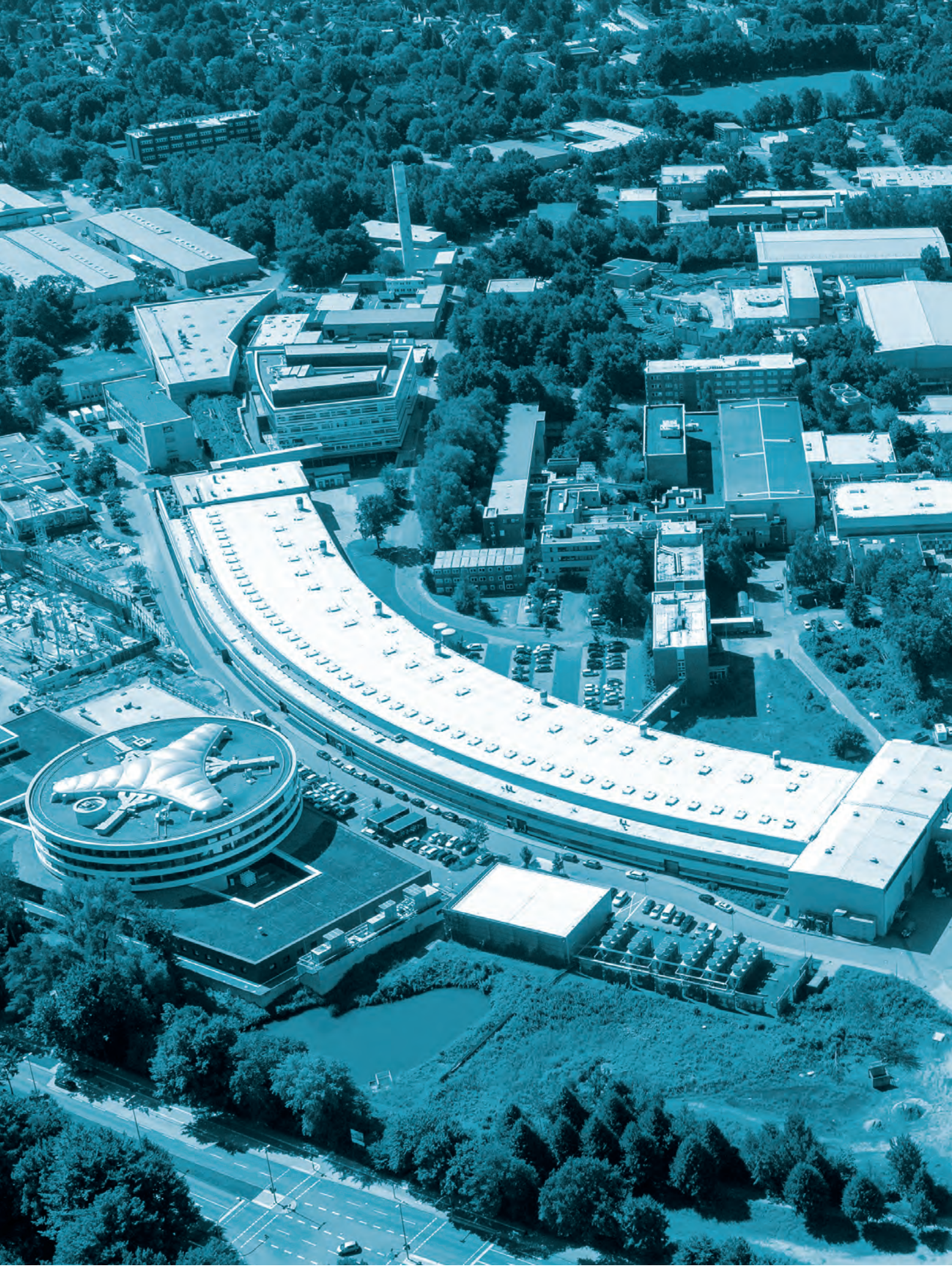

Science Highlights.

Squeezing electrons out: formation of helium compounds.

New high-pressure induced stable compound of helium and sodium, Na_2He

Helium is the most chemically inert element in the periodic table and is not known to form thermodynamically stable compounds except a few inclusion compounds. Recently, using the *ab initio* evolutionary algorithm USPEX and subsequent high-pressure synthesis experiments in a diamond anvil cell, a thermodynamically stable compound, Na_2He, has been discovered. It is stable at pressures above 113 GPa. This phase is an electride with electron pairs localised in interstices, forming eight-centre two-electron bonds within empty Na_8 cubes. The presence of He atoms causes strong electron localization and makes this material insulating.

Helium is the most inert element in the periodic table. It is the second most abundant element in the universe and is present in large quantities in normal stars and gas giant planets [1]. In the last decades, many scientists tried to find stable compounds involving helium. The most successful example is the HeH^+ radical [2] (and, in general, He_nH^+ radicals, n = 1-6), which is stable only in the charged form, extremely aggressive and protonating any base. All neutral molecules involving He known from theory or experiment are metastable and have very high energies. Stable solid compounds involving helium are exclusively van der Waals compounds, such as $NeHe_2$ [3] and $He@H_2O$ [4]. For inclusion compounds, the enthalpy of formation is close to zero and removal of He atoms has little effect on host's electronic structure.

Pressure greatly affects chemistry of elements. Using the variable-composition evolutionary structure prediction algorithm as implemented in the USPEX code [5] we identified Na_2He as new compound predicted to be stable at pressures above 160 GPa to at least 1000 GPa. In chemistry textbooks, the structure of ionic crystals is associated with the electrostatic attraction among cations and anions. However, some compounds have bare electrons instead of anions, these are called 'electride'.

According to the Pauli exclusion theory two or more identical fermions (such as electrons) cannot occupy the same quantum state. This results in a strong repulsion between valence electrons and inner-layer electrons. When external pressure forces the overlap between valence electrons and inner-layer closed-shell electrons, this repulsion will push the valence electrons out to interstitials. Usually the localized electrons in these high pressure electrides are paired which is quite different from zero-pressure electrides, which rely on the spin polarisation.

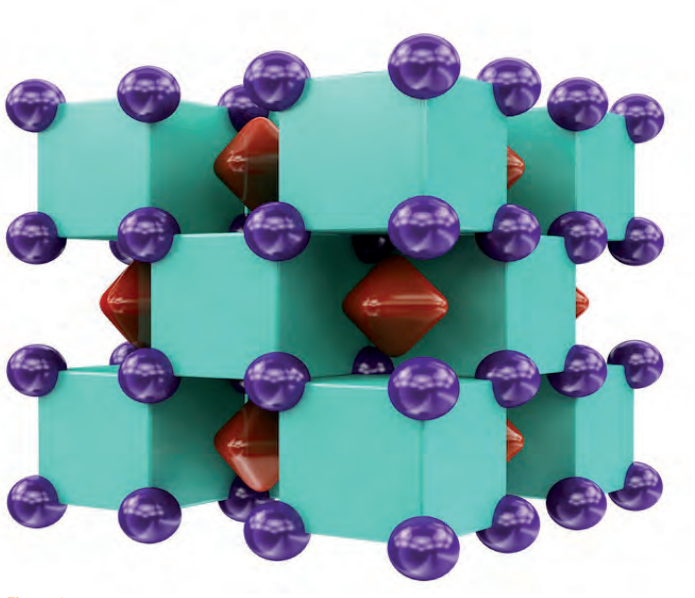

Figure 1

Sodium and helium react at high pressure to form the fluorite-type structure Na_2He (violet: Na, turquoise: Na_8 cube, red: localised electron pair).

A representative example of a high-pressure electride is hP4-Na [6]. The formation of semi-conductive Na_2He is similar to hP4-Na that converts into an insulator at high pressure with the formation of an electride state.

In the Na sublattice, on average there is only one electron in every Na_8 cube. The insertion of He atoms pushes away the electron gas out of the Na_8He cube into the neighbouring empty Na_8 cubes, leading to localisation of valence electrons and the formation of eight-centre two-electron bonds, resulting also in the opening of a wide band gap. The eight-centre two-electron bonds are essential for the stability of Na_2He.

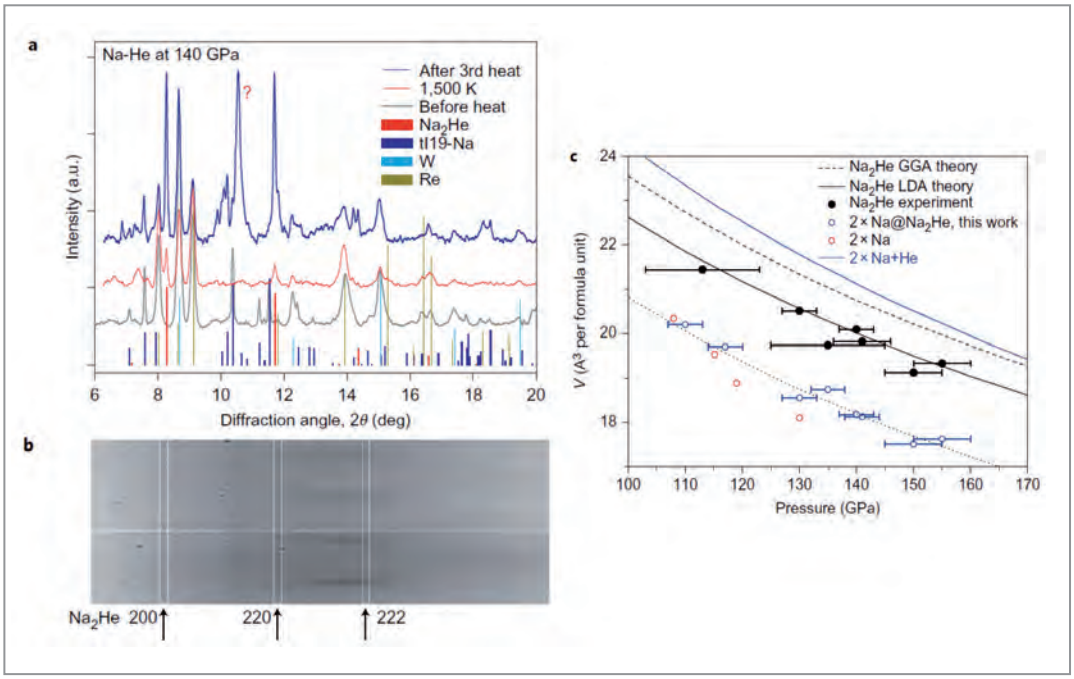

Figure 2

Experimental data on Na_2He: (a) Integrated XRD patterns before heating and after the second and third heating to ~1200 and >1500 K, respectively. (b) Two-dimensional image after the third heating, in radial coordinates, showing single-crystal reflections of tI19-Na and Na_2He, marked by light blue circles and white rectangles, respectively. (c) Equation of state (EOS) of Na_2He synthesised in a DAC at 113–155 GPa in comparison with the EOS of Na. Filled circles: experimental unit cell volumes of Na_2He. Open blue circles: volumes per two Na atoms in this work. Open red circles: volumes of Na phases reported in [7].

The analysis of Bader charges proves that He contributes its Pauli repulsion to the localised electrons and accordingly is accepting a small number of electrons of 0.15 e. This means when the electrons are pushed out to interstitials under high pressure, an electronic redistribution takes place indicating the weak electronic affinity of He.

To synthesise Na_2He, Na was loaded into a He medium in a diamond anvil cell (DAC) and compressed up to 155 GPa. The sample was monitored using synchrotron X-ray diffraction (XRD), Raman spectroscopy, and visual observation at PETRA III beamline P02.2. The latter verified that there was He in the DAC high-pressure cavity, as there were transparent areas around the Na sample, which remained to the highest pressure reached. Below ~110 GPa, only single crystal reflections of elemental Na were observed in XRD, above 113 GPa, we detected the appearance of new single-crystal reflections, which became stronger after laser heating to T >1500 K. A prolonged heating at 140 GPa (Fig. 2a and b) yielded quasi-continuous diffraction lines, which revealed a substantial production of a new phase.

We hypothesised that Na_2He with a bare interstitial electron pair might be stabilised by a strong acceptor of an electron pair – for example, oxygen. Our extensive variable-composition searches showed that indeed Na_2HeO has the same Heusler-type structure as Na_2He where O^{2-} (i.e. oxygen with the absorbed electron pair) occupies the position of the localised electron pair, and can be considered as salt. However, because of the anti-bonding between O^{2-} and He, Na_2HeO only exist as a thermodynamically stable phase in the pressure range from 15 to 106 GPa.

Our prediction of both compounds Na_2He and Na_2HeO change the hitherto bare field of helium chemistry and will have an impact on the understanding of chemical bonding and processes inside giant gas planets.

Contact: Artem R. Oganov, a.oganov@skoltech.ru
Hui-Tian Wang, htwang@nankai.edu.cn

Authors

Xiao Dong, Artem R. Oganov, Alexander F. Goncharov, Elissaios Stavrou, Sergey Lobanov, Gabriele Saleh, Guang-Rui Qian, Qiang Zhu, Carlo Gatti, Volker L. Deringer, Richard Dronskowski, Xiang-Feng Zhou, Vitali Prakapenka, Zuzana Konôpková, Ivan Popov, Alexander I. Boldyrev and Hui-Tian Wang

See original publication for affiliation details.

Original publication

'Stable Compound of Helium and Sodium at High Pressure', Nat. Chem. 9, 440–445 (2017), DOI: 10.1038/nchem.2716

References

1. D. J. Stevenson, 'Metallic helium in massive planets', Proc. Natl. Acad. Sci. 105, 11035–11036 (2008).
2. J. W. Hiby, 'Massenspektrographische Untersuchungen an Wasserstoff- und Heliumkanalstrahlen (H^{3+}, H^{2-}, HeH^+, HeD^+, He^-)'. Annalen der Physik 426, 473–487 (1939).
3. P. Loubeyre, M. Jean-Louis, R. LeToullec and L. Charon-Gerard, 'High pressure measurements of the He-Ne binary phase diagram at 296 K: Evidence for the stability of a stoichiometric $Ne(He)_2$ solid', Phys. Rev. Lett. 70, 178–181 (1993).
4. H. Liu, Y. Yao and D. D. Klug, 'Stable structures of He and H_2O at high pressure', Phys. Rev. B 91, 014102 (2015).
5. A. R. Oganov and C. W. Glass, 'Crystal structure prediction using ab initio evolutionary techniques: Principles and applications', J. Chem. Phys. 124, 244704–244704 (2006).
6. Y. Ma et al., 'Transparent dense sodium', Nature 458, 182–185 (2009).
7. E. Gregoryanz et al., 'Structural diversity of sodium', Science 320, 1054–1057 (2008).

Silk from milk.

Spinning of all-protein fibres from aligned protein nanofibrils

Many of nature's high-performance materials are built from proteins, e.g. silks and muscle fibres. The properties of these materials are closely associated with their hierarchical architecture. Protein nanofibrils offer a promising route to mimic such assemblies, as they are formed by self-assembly and have mechanical properties comparable to silk. For the first time, we could demonstrate that micrometer sized fibres can be assembled from protein nanofibrils using a microfluidics setup without any plasticizers or crosslinkers. Microfocus small-angle X-ray scattering (SAXS) measurements allowed us to monitor the alignment of the fibrils in the microfluidic channel and to compare the assembly processes of nanofibrils of distinct morphologies. We found that the mechanical properties of the fibre are related to the nanostructure of the fibrils.

Protein-based materials from nature have served as inspiration for man-made structures for a long time, however it remains a challenge to produce synthetic materials with comparable properties from bio-based resources. Increased knowledge about the assembly of hierarchical structures from bio-molecules opens the possibility to create novel materials for a variety of applications. In this perspective, the ability of protein molecules to self-assemble into highly ordered nanofibrils, also known as amyloid fibrils, is of significant interest [1]. Proteins from e.g. milk, egg, and soybean form such fibrils when heated in acidic solutions (low pH). The structure of protein nanofibrils has similarities with the ordered domains of natural silk fibres, including the arrangement of the protein chains into strongly hydrogen-bonded sheet-like structures, so-called β-sheets, and the mechanical properties, like strength and elastic modulus, of isolated nanofibrils appear to be in the same range as for silk. However, the knowledge about how to control the microscale structure of materials built from protein nanofibrils is limited so far.

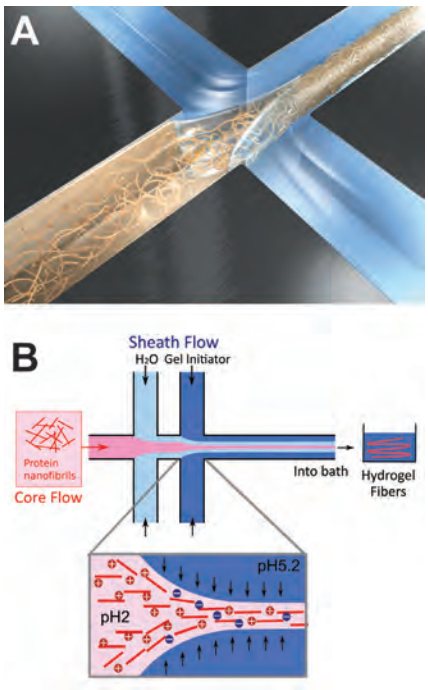

Figure 1
A) Graphical illustration of the assembly process of nanostructured protein fibres. B) Schematic of the double flow-focusing device used for fibre assembly. The core flow, containing the protein nanofibril dispersion, encounters two sheath flows that align the fibrils and then lock the structure into a hydrogel by changing the pH. Fig. 1B taken from original publication, reprinted with permission from PNAS.

Our recent studies showed that the alignment of the *cellulose* nanofibrils under elongational flow significantly improves the mechanical properties of the resulting fibres [2]. Here, we use the same double flow-focusing device (Fig. 1) with a core flow of *protein* nanofibril dispersion and two focusing steps of sheath flows [3]. The first focusing step aligns the fibrils in the presence of an elongational flow field, whereas the second step locks the structure by a change of the pH value.

Protein nanofibrils were prepared from whey protein isolate from milk by incubation at pH 2 and 90 °C. We found that the morphology of the nanofibrils could be altered simply by changing the initial protein concentration. At protein concentrations below 4 % we obtained straight and up to several micrometres long fibrils while at higher concentrations, the fibrils were short and curved (Fig. 2A). Atomic force microscopy and image analysis were used to estimate the mechanical properties of the fibrils. The persistence length of the straight fibrils was found to be almost 50 times higher than for the curved fibrils. The straight fibrils are also thicker (4.1 ± 1.1 nm) than the curved fibrils (2.5 ± 0.5 nm). These estimates indicate that the two types of nanofibrils have distinct mechanical properties: The elastic modulus of the curved fibrils is 15 – 25 times higher compared to the straight fibrils.

The behaviour of protein nanofibrils under elongational flow was explored using the small-angle X-ray scattering (SAXS) method at the PETRA III beamline P03 with a microfocus

beam of 20 × 10 μm² [4]. The flow focusing setup used in this experiment had the second focusing step replaced by a contraction step, which creates an elongational flow-field that is similar to the second focusing step (Fig. 2B). The alignment of the fibrils was quantified in terms of an order parameter calculated from μSAXS images [2], with the values of 0 and 1 corresponding to an isotropic distribution and fully aligned fibrils, respectively. Obvious differences were observed for the straight and curved fibrils with the order parameter for the curved fibrils only reaching approximately half of that for the straight fibrils (Fig. 2D).

The double flow-focusing channel with the pH-induced gel transition in the second step was used to assemble the protein nanofibrils into microfibers. Both types of fibrils were examined and found to produce hydrogel fibres. However, to our surprise we found that only the fibres from the curved nanofibrils were strong enough to overcome the surface tension and could be picked out from the bath solution of the spinning setup. Moreover, non-fibrillar protein solutions did not produce hydrogel fibres at all, further highlighting the importance of the nanostructure.

The microfibers obtained from the curved nanofibrils were dried and characterized. The nanofibrils stay intact in the fibre and the elastic modulus is of the same order of magnitude as in the individual nanofibrils. Further investigations of the fibrils in the bulk gel state revealed substantial differences for the two types of nanofibrils. We concluded that the higher ability of entanglement of the curved nanofibrils provide improved possibilities of fibril crosslinking in bulk gel as well as under flow alignment compared to the straight fibrils.

Our findings stand in contrast to the behaviour of many other systems, including our previous study of cellulose nanofibrils [2], where the alignment of nanofibrils leads to improved mechanical properties. Although protein- and cellulose nanofibrils might appear similar they represent distinct classes of nanomaterials and behave differently when assembled into macroscopic materials.

We also note some similarities between the formation of nanostructured protein fibres and the assembly mechanism of spider silk. Both materials are built from proteins with a high degree of β-sheet secondary structure and the fibres are formed in a spinning process with elongational flow and pH changes. However, unlike our approach, the molecular- and supramolecular structures of spider silk are formed simultaneously, resulting in entangled structures with optimized intermolecular contacts at the same time as ordered β-sheet regions are created. Our results show that the balance between ordered regions and inter-chain entanglements is critical also for the assembly of fibres from protein nanofibrils.

Contact: Christofer Lendel, lendel@kth.se,
Fredrik Lundell, fredrik@mech.kth.se,
Stephan V. Roth, stephan.roth@desy.de

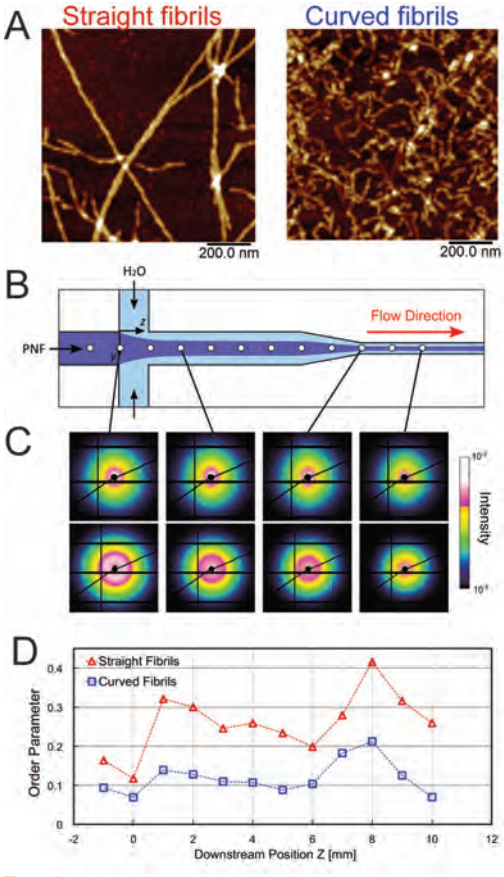

Figure 2

A) Whey protein can form fibrils with distinct morphologies; either long and straight or short and curved. Here illustrated by AFM images. B) Schematic of the flow-focusing setup used for the μSAXS studies. Measurements were carried out at the positions indicated with white spots. C) μSAXS patterns at selected locations in the channel for straight (upper row) and curved (lower row) fibrils. C) Order parameters for straight and curved fibrils at different positions along the channel. Fig. 2B-D is taken from the original publication.

Authors

Ayaka Kamada[1], Nitesh Mittal[1,2], L. Daniel Söderberg[1,2], Tobias Ingverud[2,3], Wiebke Ohm[4], Stephan V. Roth[3,4], Fredrik Lundell[1,2] and Christofer Lendel[5]

1. Linne FLOW Centre, Department of Mechanics, KTH Royal Institute of Technology, Stockholm, Sweden
2. Wallenberg Wood Science Center, KTH Royal Institute of Technology, Stockholm, Sweden
3. Department of Fiber and Polymer Technology, KTH Royal Institute of Technology, Stockholm, Sweden
4. Deutsches Elektronen-Synchroton DESY, Hamburg, Germany
5. Department of Chemistry, KTH Royal Institute of Technology, Stockholm, Sweden

Original publication

'Flow-assisted assembly of nanostructured protein microfibers', Proc Natl Acad Sci 114, 1232-1237 (2017). DOI: 10.1073/pnas.1617260114

References

1. T. P. Knowles and R. Mezzenga, 'Amyloid fibrils as building blocks for natural and artificial functional materials', Adv Mater 28, 6546-6561 (2016).
2. K. M. O. Håkansson, A. B. Fall, F. Lundell, S. Yu, C. Krywka, S. V. Roth, G. Santoro, M. Kvick, L. Prahl Wittberg, L. Wågberg and L. D. Söderberg, 'Hydrodynamic alignment and assembly of nanofibrils resulting in strong cellulose filaments', Nat. Commun. 5, 4018 (2014).
3. K. M. O. Håkansson, 'Online determination of anisotropy during cellulose nanofibril assembly in a flow focusing device', RSC Adv. 5, 18601-18608 (2015).
4. A. Buffet, A. Rothkirch, R. Dohrmann, V. Korstgens, M. M. Abul Kashem, J. Perlich, G. Herzog, M. Schwartzkopf, R. Gehrke, P. Müller-Buschbaum and S. V. Roth, 'P03, the microfocus and nanofocus X-ray scattering (MiNaXS) beamline of the PETRA III storage ring: the microfocus endstation', J Synchrotron Radiat 19, 647-653 (2012).

Long-range correlations in a tiny focus.

Unravelling the structural details of mesocrystals by angular X-ray cross-correlation analysis

Ordered arrays of oriented nanocrystals are obtained by directional linking of nanocrystals with organic semiconductor molecules. Detailed knowledge about the structure of the superlattice and its angular correlations with the atomic lattice of the constituting nanocrystals is pivotal in elucidating the relationship between structure and charge transport in these materials. We show how X-ray cross-correlation analysis in combination with a nanofocused X-ray beam rewards such information. This allows for future *in situ* studies of exploiting direction-dependent transport properties in nanocrystal superlattices for optoelectronic applications.

Advances in the synthesis, device fabrication and structural analysis of nanoscale materials have enabled the design and application of "mesocrystals", which are three-dimensional, macroscopic arrays of iso-oriented nanocrystals. In many ways, these nanomaterials mimic classical crystals in which atoms have been replaced by nanocrystals. Mesocrystals play an important role in biology, where their extraordinary structure determines the properties of bones, teeth and sea urchin spines to name only a few examples. Synthetic mesocrystals are already applied and/or currently studied as materials for lighting applications (lasing by photonic crystals) or cloaking devices [1].

The physical properties of mesocrystals are largely determined by their structural coherence, for which the angular correlation between their individual atomic lattice and the underlying superlattice of nanocrystals is a key ingredient. Colloidal nanocrystals stabilized by organic surfactants have been shown to pose excellent building blocks for the design of synthetic mesocrystals with tailored structural properties [2]. Of particular relevance for optoelectronic applications are synthetic mesocrystals with sufficient electronic coupling and charge carrier mobilities. To this end, ligand exchange procedures have been developed to increase the carrier mobilities within the mesocrystal [3]. However, a persisting problem of these protocols is that they are prone to introduce defects in the superlattice structure with some degree of granularity and significantly smaller grain sizes. This poses difficulties in determining the angular correlation between the superlattice and the atomic lattice with a meaningful statistical distribution. Here, we show how angular X-ray cross correlation analysis (XCCA) [4], (for a review, see [5]) in conjunction with a nanofocused X-ray beam can address this problem. Such a method should facilitate the application of synthetic conductive mesocrystals with strong angular correlation for thermoelectrics, spintronics, (magneto-) electronics and optics.

We investigated a conductive mesocrystal on the basis of PbS nanocrystals cross-linked with the organic semiconduc-

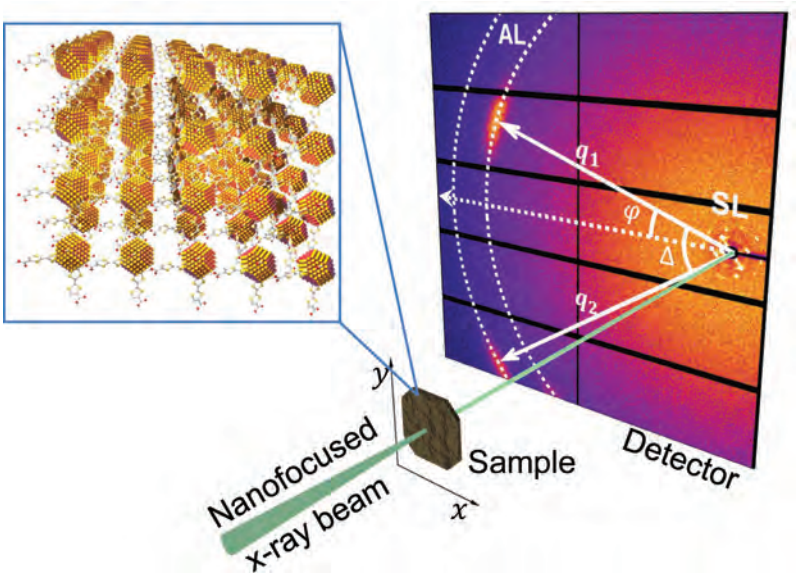

Figure 1

Scheme of the X-ray scattering experiment performed at beamline P10 of PETRA III. Using the large PILATUS 1M detector it was possible to record the scattering signal from both the superlattice (SL) and the atomic lattices (AL) of individual nanocrystals. The inset schematically shows the structure of the mesocrystal consisting of PbS NCs connected by organic ligands.

tor tetrathiafulvalenedicarboxylate (TTFDA). The X-ray scattering experiment was performed at beamline P10 of PETRA III, where the X-ray beam was focused down to about 400 nm. Small-angle X-ray scattering (SAXS) from the nanocrystal superlattice and wide-angle X-ray scattering (WAXS) from the PbS atomic lattice of individual nanocrystals were recorded simultaneously by a large detector positioned behind the sample (Fig. 1). We performed spatially resolved studies of the mesocrystal structure by scanning the sample in the plane perpendicular to the beam, see Fig. 2 (a,b). One can clearly see the granular structure of the sample with typical domain size of about 6-8 μm^2. Interestingly, the same domain structure can be observed in both SAXS and WAXS regions, which indicates that the orientation of the individual nanocrystals is correlated with the orientation of the superlattice.

To analyse this finding in more detail, angular XCCA was applied. This technique is based on the analysis of a two-point angular cross-correlation function between the scattered intensity at two different values of momentum transfer corresponding to scattering from the superlattice and the atomic lattice (Fig. 2c). XCCA revealed that the angular positions of the SAXS diffraction peaks imply a tetragonal distortion along the [001] direction of the superlattice. Therefore, some crystallographic directions are collinear in the atomic lattice of the nanocrystal and the superlattice of the mesocrystal (all three ⟨100⟩ axes as well as the family of ⟨110⟩ directions), while the ⟨111⟩ directions are not (Fig. 2d). Another finding of XCCA is the robust angular correlation between the orientation of the mesocrystal superlattice and individual nanocrystals. The angular disorder between individual nanocrystals was determined to be about 10°, while the average orientation of the nanocrystals coincides with the orientation of the superlattice within the accuracy of few degrees. Such a strong angular correlation preserved over entire domains highlights the mesocrystalline nature of the material.

We anticipate that the future exploration of synthetic mesocrystals with increasing complexity, e.g., binary nanocrystal superlattices, nanorod assemblies, honeycomb lattices, will strongly benefit from the present study. The experiment allows quantifying the structure of the superlattice, its angular correlation with the atomic lattices and the average orientational disorder between atomic lattices simultaneously. In addition, a meaningful statistical distribution of these parameters as well as the length scale of the domains and their boundaries are obtained. This should greatly facilitate the understanding of structure–property relationships in mesocrystals.

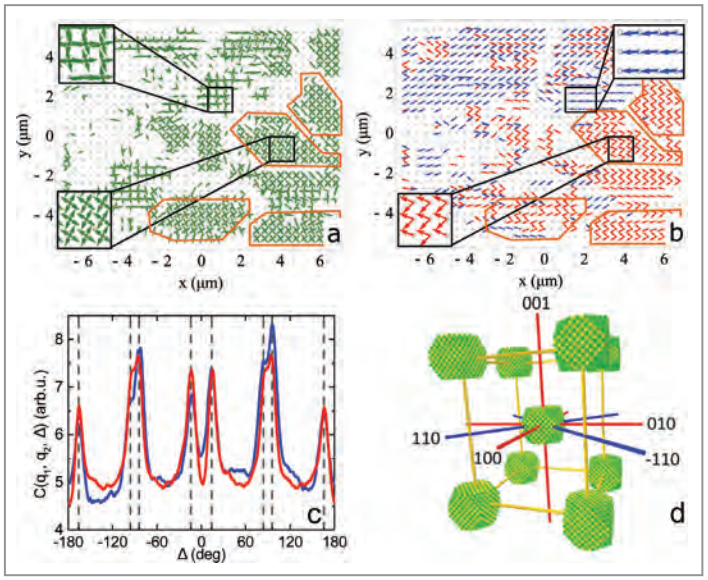

Figure 2

(a) Spatially resolved maps of angular orientation of diffraction peaks of the superlattice (green arrows). (b) Angular orientation of ⟨111⟩ (red arrows) and of ⟨200⟩ (blue arrows) Bragg reflections. Domains are indicated by orange lines. (c) Comparison between the experimentally obtained angular cross-correlation function (blue line) and the model (red line) based on a tetragonal distortion of the mesocrystal superlattice. (d) Schematic of the mesocrystalline unit cell displaying the angular correlation between atomic lattices and the superlattice; collinear axes are indicated in red (⟨100⟩ directions) or blue (⟨110⟩ directions).

Contact: Ivan Vartaniants, ivan.vartaniants@desy.de; Frank Schreiber, frank.schreiber@uni-tuebingen.de; Marcus Scheele, marcus.scheele@uni-tuebingen.de

Authors

Ivan. A. Zaluzhnyy[1,2], Ruslan P. Kurta[3], Alexander André[4], Oleg Y. Gorobtsov[1], Max Rose[1], Petr Skopintsev[1,5], Ilya Besedin[1,2,6], Alexey V. Zozulya[1,3], Michael Sprung[1], Frank Schreiber[4], Ivan A. Vartanyants[1,2] and Marcus Scheele[4]

1. Deutsches Elektronen-Synchrotron DESY, Hamburg, Germany
2. National Research Nuclear University MEPhI, Moscow, Russia
3. European XFEL GmbH, Schenefeld, Germany
4. Eberhard Karls Universität Tübingen, Tübingen, Germany
5. Paul Scherrer Institute, Villigen, Switzerland
6. National University of Science and Technology MISIS, Moscow, Russia

Original publication

'Quantifying Angular Correlations between the Atomic Lattice and the Superlattice of Nanocrystals Assembled with Directional Linking', Nano Lett. 17, 3511–3517 (2017). DOI: 10.1021/acs.nanolett.7b00584

References

1. H. Cölfen and M. Antonietti, 'Mesocrystals: Inorganic Superstructures Made by Highly Parallel Crystallization and Controlled Alignment', Angew. Chem. Int. Ed. 44, 5576–5591 (2005).
2. M. C. Weidman, D.-M. Smilgies and W. A. Tisdale, 'Kinetics of the self-assembly of nanocrystal superlattices measured by real-time in situ X-ray scattering', Nat. Mater. 15, 775–781 (2016).
3. M. Scheele, W. Bruetting and F. Schreiber, 'Coupled Organic-Inorganic Nanostructures', Phys. Chem. Chem. Phys. 17, 97–111 (2015).
4. P. Wochner, C. Gutt, T. Autenrieth, T. Demmer, V. Bugaev, A. D. Ortiz, A. Duri, F. Zontone, G. Grübel and H. Dosch, 'X-ray cross correlation analysis uncovers hidden local symmetries in disordered matter', Proc. Natl. Acad. Sci. 106, 11511–11514 (2009).
5. R. P. Kurta, M. Altarelli and I. A. Vartanyants, 'Structural analysis by X-ray intensity angular cross correlation analysis', in Adv. Chem. Phys., John Wiley & Sons, Inc., 1–39 (2016).

Two liquid states in deeply supercooled water.

Coherent X-rays probe diffusion in the ultraviscous regime

The importance of liquid water is greatly recognized over many fields, even though a fundamental molecular level understanding of its structure and dynamics is still lacking. That is due to the ability of water molecules to form a complex hydrogen-bonding network, which is hypothesized to form high- and low-density structural components. It has been postulated that the observed high- and low-density amorphous ice forms of water, HDA and LDA, can be related to the two hypothesized liquid forms, HDL and LDL, through two distinct glass transitions. Here, we provide evidence of a liquid-liquid transition in the ultraviscous regime, as the high-density state transforms into the low-density liquid.

The proposed glass-to-liquid transition in amorphous ice and a hypothesized liquid-liquid transition between HDL and LDL is controversially discussed over decades [1]. Theoretical investigations predict a liquid-liquid transition terminating in a second-critical point, i.e. a point on a phase diagram at which both liquids would coexist, deeply in the supercooled region [2]. Supercooling is the process of lowering the temperature of a liquid below its freezing point without it becoming freezing, which can be very challenging experimentally because liquid water tends to crystalize in this regime on a very fast timescale.

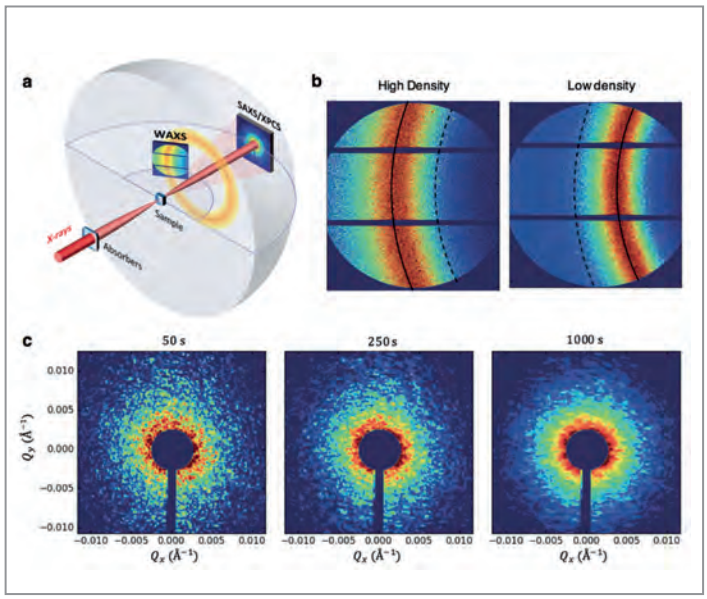

Figure 1

The experimental setup combining WAXS with XPCS in SAXS. (a) The geometry used employs two detectors for WAXS and SAXS. (b) From the WAXS scattering pattern we distinguish high- and low-density forms. (c) Using XPCS we extract the dynamics by looking at the changes of the speckle patterns as a function of time. Here the actual data obtained at beamline P10 of PETRA III are shown.

Studying LDA and HDA amorphous ice is an alternative approach since the dynamics are much slower in the ultra-viscous range, where the viscosity is very high. At ambient pressure HDA expands by almost 20 % and transforms to the low-density state. Previous experiments gave evidence for a glass transition in HDA prior to the structural transformation [3], so the question at hand is: Does a comparable transition occur between two liquid states in the ultraviscous regime [4]? To investigate this question, we combine wide-angle X-ray scattering (WAXS) with X-ray photon-correlation spectroscopy (XPCS) in the small-angle X-ray scattering (SAXS) geometry to probe both the structural and dynamical properties during the high-to-low-density transition in amorphous ice.

In Fig. 1a the experimental setup is shown that was used at beamline P10 at PETRA III (DESY). Using X-ray diffraction in WAXS geometry, one can distinguish between the high- and low-density forms (Fig. 1b) due to changes in the static structure factor S(Q), with Q being the momentum transfer in the scattering process. In the SAXS geometry, we use XPCS to access dynamics at the nanometre length scale. A speckle contrast arises due to the illumination with the coherent X-ray beam. For longer exposure time the speckle contrast is gradually lost because of dynamics in the sample, giving rise to a more uniform scattering pattern (Fig. 1c).

Figure 2a shows the structure factor S(Q) for HDA at low temperatures and the transition to LDA upon warming. At intermediate temperatures, the two structures coexist. However, based purely on the S(Q), one cannot distinguish a transition between two amorphous forms or between two liq-uids. Therefore, dynamical information accessible by XPCS is needed (Fig. 2b). The intermediate scattering function is fitted with a double-exponential function. At 90 K a single time constant is obtained, whereas at temperatures above 110 K

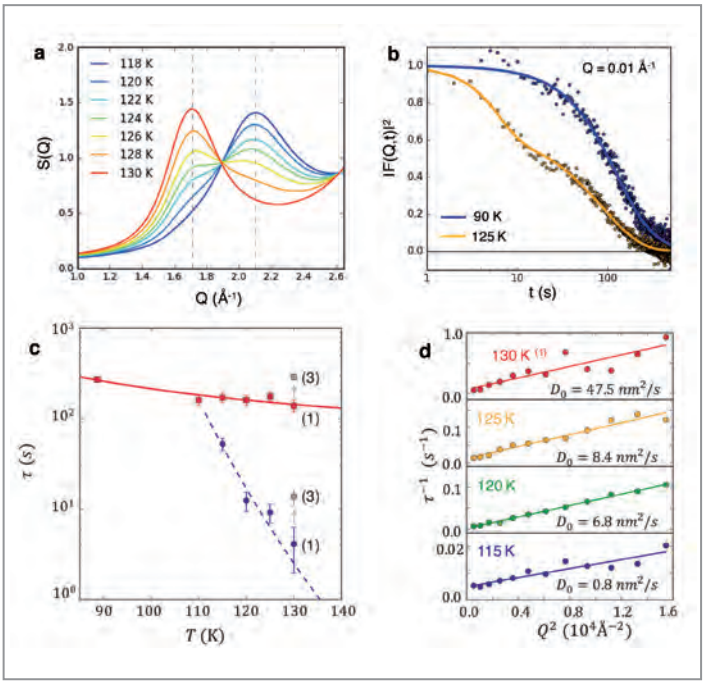

Figure 2

Structural and dynamical information during the high-to-low transition. (a) The structure factor S(Q), obtained from wide-angle x-ray diffraction. (b) The intermediate scattering function F(Q,t) reflects structural relaxation on the nanometre length scale. (c) Time constants obtained from the intermediate scattering function F(Q,t) at different temperatures at Q = 0.01 Å^{-1}. The labels (1) and (3) indicate the data points obtained during the first and last 300 seconds of the total 1000 seconds. For the lower temperatures (T = 89 and 110 K) only a single, slow component is obtained (red squares), whereas at higher temperatures a second, faster component appears (blue circles). (d) The fast time constant obtained from the double exponential fit plotted as $1/\tau$ over Q^2. The solid lines depict the result of a fit of the diffusion constant D_0.

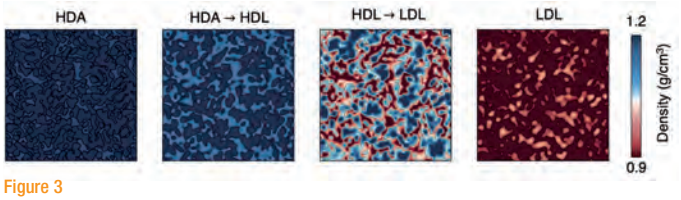

Figure 3

Schematic depiction of the dynamical and structural heterogeneities during the gradual transition from HDA ice (blue) to ultraviscous HDL (light blue) and finally to LDL (red).

we find an additional faster component. The two time constants are shown in Fig. 2c, the solid and dashed lines depict results of two Arrhenius fits. The slower component appears nearly temperature-independent, whereas the faster component, manifested at 115 K, accelerates ~100-fold upon heating to 130 K. One can derive the diffusion constant D_0 on nanometre length scales by the Q dependence of the characteristic time constant by the relation $1/\tau = D_0Q^2$ [5]. Figure 2d shows $1/\tau$ versus Q^2 for temperatures of 115 K and above. D_0 is determined for the fast component to vary from 0.8 to 47.5 nm^2/s in the range of 115 – 130 K. The diffusion involves translational motion at the nanometre length scale and is the strongest indication of liquid-like motion between 115 and 130 K and evidence for HDL and LDL.

The interpretation is schematically summarized in Fig. 3. Initially, HDA exhibits nanoscale structural heterogeneities and slow heterogeneous dynamics due to viscoelastic relaxation. In the temperature range of 110 K to 120 K, the appearance of a faster component indicates translational diffusion on a 100 nm length scale due to rearrangement of the heterogeneity boundaries. This dynamical transition occurs while still in the high-density form which, together with a previously proposed glass transition [3], points to an ultraviscous HDL state. Upon further heating to 130 K, the structure changes locally to the low-density form and the corresponding diffusive dynamics suggest that the transition occurs while in the liquid state. Therefore, the observed liquid-liquid transition occurs as HDA transitions to HDL and then to LDL at ambient pressure conditions.

Contact: Fivos Perakis, f.perakis@fysik.su.se
Katrin Amann-Winkel, katrin.amannwinkel@fysik.su.se
Anders Nilsson, andersn@fysik.su.se

Authors

Fivos Perakis[1,2,*], Katrin Amann-Winkel[1,*], Felix Lehmkühler[3,4], Michael Sprung[3], Daniel Pettersson[1], Jonas A. Sellberg[5], Harshad Pathak[1], Alexander Späh[1], Filippo Cavalca[1,2], Daniel Schlesinger[1,†], Alessandro Ricci[3], Avni Jain[3], Bernhard Massani[6], Flora Aubree[6], Chris J. Benmore[7], Thomas Loerting[6], Gerhard Grübel[3,4], Lars G. M. Pettersson[1] and Anders Nilsson[1]

1. Department of Physics, AlbaNova University Center, Stockholm University, Sweden
2. SLAC National Accelerator Laboratory, Menlo Park, USA
3. Deutsches Elektronen-Synchrotron DESY, Hamburg, Germany
4. Hamburg Centre for Ultrafast Imaging, Hamburg, Germany
5. Biomedical and X-ray Physics, Department of Applied Physics, AlbaNova University Center, KTH Royal Institute of Technology, Stockholm, Sweden
6. Institute of Physical Chemistry, University of Innsbruck, Austria
7. X-ray Science Division, Advanced Photon Source Argonne National Laboratory, Argonne, USA

* These authors contributed equally to this work

† Present address: Department of Environmental Science and Analytical Chemistry & Bolin Centre for Climate Research, Stockholm University, Stockholm, Sweden

Original publication

'Diffusive dynamics during the high-to-low density transition in amorphous ice', Proc. Natl. Acad. Sci. 114, 8193–8198 (2017); DOI: 10.1073/pnas.1705303114

References

1. K. Amann-Winkel, R. Böhmer, F. Fujara, C. Gainaru, B. Geil and T. Loerting, 'Colloquium: Water's controversial glass transitions', Rev. Mod. Phys. 88, 011002 (2016).
2. O. Mishima and H. E. Stanley, 'The relationship between liquid, supercooled and glassy water', Nature 396, 329 (1998).
3. K. Amann-Winkel et al., 'Water's second glass transition', Proc. Natl. Acad. Sci. 110, 17720 (2013).
4. F. Sciortino, 'Which way to low-density liquid water?', Proc. Natl. Acad. Sci. 114, 8141 (2017).
5. H. Conrad et al., 'Correlated heterogeneous dynamics in glass-forming polymers', Phys. Rev. E 91, 042309 (2015).

Architecture of a type VII secretion complex from Mycobacterium tuberculosis.

First insight by an integrative structural biology approach

The infectious disease tuberculosis kills millions of people every year worldwide. The pathogen responsible for the disease is the Gram-positive bacterium *Mycobacterium tuberculosis*. Specialised molecular machines known as type VII secretion systems located in the mycobacterial cell membrane are crucial for the pathogen's virulence and survival in the host. As such, they are critical targets for urgently needed novel anti-tuberculosis drugs. We used electron microscopy and small angle X-ray scattering techniques, as well as associated biophysical analyses to reconstruct the overall architecture of one of these secretions systems in mycobacteria and help further our understanding of the biology of these and related pathogens.

In 2016, tuberculosis resulted in over 1.7 million deaths and around 10 million new infections, making it one of the top ten causes of death worldwide. Among HIV/AIDS patients, it is the number one cause of death [1]. Treatment involves extensive courses of multiple antibiotics, however, the increase in the number of cases of drug-resistant tuberculosis makes the need of novel treatment avenues ever more urgent. Tuberculosis is caused by the bacterium *Mycobacterium tuberculosis (Mtb)*, which is transmitted through the air and generally infects the host lung. *Mtb* has a complex life cycle and can remain dormant and undetected for decades in the host, before becoming active when the conditions are more favourable, such as when the host's immune defences become depleted as in HIV/AIDS patients.

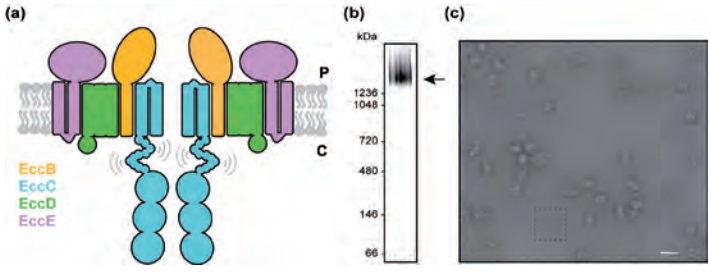

Figure 1

(a) Model of the ESX-5 membrane complex of *Mycobacterium xenopi* composed of $EccB_5$, $EccC_5$, $EccD_5$ and $EccE_5$; $EccD_5$ is an integral membrane protein, while the major part of $EccB_5$ and $EccE_5$ is localised in the periplasm (P) as determined by gold labelling and molecular docking approaches combined with segmentation analysis of the electron microscopy density map. The flexible tail-like extensions of $EccC_5$, each containing three ATPase domains, are found in the cytoplasm (C) where they can bind secretion effectors. (b) Blue native-polyacrylamide gel electrophoresis of purified ESX-5 complex solubilised in amphipol A8-35. The size of the intact complex is approximately 1.8 MDa as indicated by a black arrow. (c) Representative electron micrograph showing ESX-5 particles in several orientations. A top view of the hexameric complex is boxed with a dotted line. Scale bar, 50 nm.

Mycobacteria are atypical Gram-positive bacteria, characterised by an unusual double cell membrane structure including a chemically distinct outer layer known as the mycomembrane and an inner plasma membrane, separated by the periplasm. The outer membrane is highly impermeable due to the presence of long chain fatty acids, known as mycolic acids. To translocate substances, including molecules known to be vital for the pathogen's virulence and survival in the host across the cell envelope, mycobacteria use five related and highly specialised secretion machineries, known as ESX type VII secretion systems [2,3]. To date, there is no structural information on any of the type VII secretion systems. The ESX-5 system is only found in the slow-growing pathogenic species of mycobacteria, including *Mtb*. Due to its evidently important role for transporting key proteins across the cell membrane and hence its central role in the progress of the disease in the host, it is an important target for future drug development [4].

To unravel the mechanism of ESX-5 secretion, we set up a collaboration between three research groups. Based on the ground-breaking work for the biochemical isolation of the secretion system by the group of Wilbert Bitter and Edith Houben, the group of Annabel Parret and Matthias Wilmanns developed novel protocols to purify the active macromolecular secretion complex from the mildly pathogenic, slow-growing mycobacterial species *Mycobacterium xenopi* to a level suitable for subsequent structural analysis. The system comprises four core proteins – $EccB_5$, $EccC_5$, $EccD_5$, $EccE_5$ – and has an estimated size of 1.8 MDa [5]. Biophysical analyses showed that the complex is able to assemble

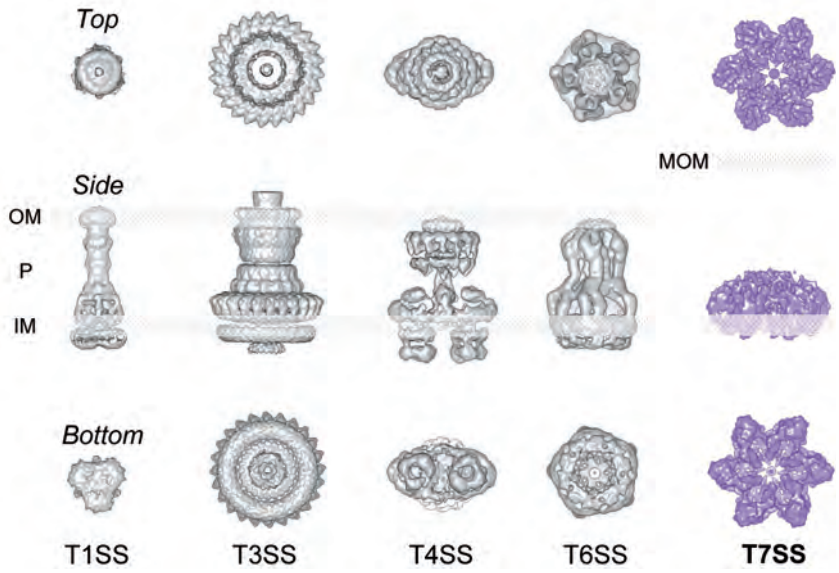

Figure 2

Unique features of the mycobacterial ESX-5 type VII secretion system in comparison to other bacterial secretion systems. Electron microscopy density maps were retrieved from the Electron Microscopy Data Bank (EMDB; https://www.ebi.ac.uk/pdbe/emdb/). From left to right: type I secretion system from *E. coli*, AcrAB-TolC multi-drug efflux pump (T1SS; EMD-5915); type III secretion system from *Salmonella thyphimurium* (T3SS; EMD-1875); type IV secretion system from *E. coli* (T4SS; EMD-2567); type VI secretion system from *E. coli* (T6SS; EMD-2927); and type VII secretion system from *M. xenopi* (this study, T7SS; EMD-3596). Top, side and bottom views are shown for comparison, demonstrating the overall symmetry of each secretion system. The positions on the inner membrane (IM), outer membrane (OM), mycobacterial outer membrane (MOM) and periplasm (P) are indicated.

independently of its secreted substrates. The group of Thomas Marlovits used electron microscopy (EM) to reconstruct the overall architecture of the ESX-5 type VII secretion system at 13 Å resolution. While the data were collected in Vienna, the data were processed using the DESY IT infrastructure in Hamburg. By the additional use of mass spectrometry at the EMBL facilities we determined the ESX-5 complex to consist of 24 subunits: six copies of each of the four proteins. The overall dimensions of the complex are 28 × 16 nm with a central channel of approximately 5 nm suggesting that the complex is embedded only within the inner membrane of the cell rather than extending across both membranes. The central pore observed in the system is large enough to accommodate folded protein substrates.

In addition, we identified the tail-like protein extensions protruding from the complex as the cytosolic domains of $EccC_5$, a core component of the type VII secretion system. These tail-like extensions are highly flexible as determined by Small Angle X-ray Scattering (SAXS) experiments performed at the EMBL beamline P12 at the PETRA III storage ring. The flexible nature of the $EccC_5$ protein which contains recognition sites for substrates may be crucial for substrate transfer across membranes. As the complex only spans the inner membrane, additional components are required to complete the transport of substrates across the mycomembrane. The identification of these components, however, requires future investigation.

Our findings are an important step forward in our understanding of the structure and function of type VII secretion systems. Since these structures are similar across all mycobacterial species, this adds to our knowledge of the biology of not only tuberculosis but also other pathogenic mycobacterial diseases, such as leprosy. The results also serve as a blueprint for other type VII secretion systems in related bacterial species. A key goal for the near future is to achieve at least residue-resolution to allow probing the function of type VII secretion systems and related secretion complexes further by targeted mutagenesis.

Contact: Thomas Marlovits, marlovits@marlovitslab.org
Annabel H. A. Parret, parret@embl-hamburg.de
Edith N. G. Houben, e.n.g.houben@vu.nl

Authors

Katherine S.H. Beckham[1], Luciano Ciccarelli[2,3,4], Catalin M. Bunduc[5], Haydyn D.T. Mertens[1], Roy Ummels[6], Wolfgang Lugmayr[2,3,4], Julia Mayr[2,3,4], Mandy Rettel[7], Mikhail M. Savitski[7], Dmitri I. Svergun[1], Wilbert Bitter[5,6], Matthias Wilmanns[1,4,8], Thomas C. Marlovits[2,3,4,8,9], Annabel H.A. Parret[1] and Edith N.G. Houben[5]

1. European Molecular Biology Laboratory, Hamburg Unit, Hamburg, Germany
2. Research Institute of Molecular Pathology, Vienna, Austria
3. Institute of Molecular Biotechnology, Austrian Academy of Sciences, Vienna, Austria
4. University Medical Centre Hamburg-Eppendorf, Hamburg, Germany
5. Vrije Universiteit Amsterdam, Amsterdam, The Netherlands
6. VU University Medical Center, Amsterdam, The Netherlands
7. European Molecular Biology Laboratory, Heidelberg, Germany
8. Centre for Structural Systems Biology, Hamburg, Germany
9. Deutsches Elektronen-Synchrotron DESY, Hamburg, Germany

Original publication

'Structure of the mycobacterial ESX-5 type VII secretion system membrane complex by single particle analysis', Nature Microbiology 2, 17047 (2017) DOI: 10.1038/nmicrobiol.2017.47

References

1. **Global tuberculosis report 2017, World Health Organization (http://www.who.int/tb/publications/global_report/en/).**
2. **M.I. Gröschel, F. Sayes, R. Simeone, L. Majlessi and R. Brosch, 'ESX secretion systems: mycobacterial evolution to counter host immunity', Nature Reviews Microbiology 14, 677-691 (2016).**
3. **L.S. Ates, E.N.G. Houben and W. Bitter, 'Type VII Secretion: A Highly Versatile Secretion System', Microbiology Spectrum 4, 1-21 (2016).**
4. **M.E. Feltcher, J.T. Sullivan and M. Braunstein, 'Protein export systems of *Mycobacterium tuberculosis*: novel targets for drug development?', Future Microbiol. 5, 1581–1597 (2010).**
5. **E.N.G. Houben, J. Bestebroer, R. Ummels, L. Wilson, S.R. Piersma, C.R. Jiménez, T.H.M. Ottenhoff, J. Luirink and W. Bitter, 'Composition of the type VII secretion system membrane complex', Mol. Microbiol. 86, 472–484 (2012).**

Crystal structure of the 15-subunit core Mediator at 3.4 Å extends the structural understanding of transcription.

Accurate structural models by homogeneous X-ray illumination of crystals

In the process of transcription of DNA into messenger RNA, Mediator is the central multi-subunit complex directing RNA polymerase II (Pol II) to transcription start sites. We solved the crystal structure of the 15-subunit core Mediator (~400 kDa). After improving the diffraction limit of Mediator crystals from ~8 Å to better than 4 Å resolution by controlled crystal dehydration, complete diffraction data to 3.4 Å resolution were collected with a collimated synchrotron beam on EMBL P14 beamline at PETRA III. The accurate interpretation of electron densities was facilitated by locating sulphur and selenium atoms based on their anomalous signals as optimized by tuning the X-ray energy. The refined model revealed important structural details of the core Mediator and suggested revisions for significant portions of a previous single particle electron microscopy reconstruction at lower resolution.

High-resolution structural information of biological macromolecules allows to understand the biochemical mechanisms underlying life. For large complex structures, during recent years, cryo-electron microscopy (Cryo-EM) has become a standard tool especially for those complexes that are difficult to crystallize. For the Mediator complex, comprising 25 subunits with a total mass of 1.4 MDa, Cryo-EM reconstructions have revealed the subunit organization and delivered important information about how Mediator acts as a platform for the transcription initiation by Pol II. However, atomic details of a large portion of the complex remained invisible and the mechanism of how Mediator enables regulation of transcription was still poorly understood. In an effort to understand the Mediator mechanism, we solved the crystal structure of the essential core Mediator (cMed) consisting of 15 subunits by combining several crystallographic methods and techniques.

Post-crystallization methods, in particular those reducing the solvent content of macromolecular crystals and thus resulting in a tighter packing and improved crystalline order can often convert poorly diffracting crystals into crystals delivering high-quality diffraction data [1]. Indeed, after reviewing different dehydration methods, the typical diffraction limit of cMed crystals were dramatically improved from ~8 to ~4 Å resolution. The most suitable method for the dehydration of cMed crystals was to harvest crystals into a 12-well depression plate containing 50 µl mother liquor followed by incremental increases in the concentration of a strongly hydrophilic polyethylene glycol (PEG400). This was accomplished by removing 25% of the mother liquor and replacing it with the dehydration solution [mother liquor + 30 (w/v) PEG 400]. Crystals were allowed to equilibrate for 15 min. before repeating the partial buffer exchange. These incremental steps were repeated until 90–95% of the well was composed of the dehydration solution, with a final step in which the crystal was transferred into 100% dehydration solution with a nylon loop.

Initial crystallographic phases were determined through the method of molecular replacement combined with single anomalous dispersion (MR-SAD, [2]) using the previously determined crystal structure of the Mediator head module in combination with anomalous diffraction data collected from a crystal soaked with tantalum bromide clusters ($Ta_6Br_{12}^{2+}$). Improved phases were obtained through MR-SAD exploiting optimized anomalous signals from selenium (Se) and sulphur (S) -atoms. While S atoms are naturally present in the Mediator complex, Se atoms were introduced artificially by replacing the natural amino-acid Methionine with its Se analogue. For obtaining high-resolution datasets beyond 4 Å resolution with accurate anomalous signals for Se and S atoms, the use of

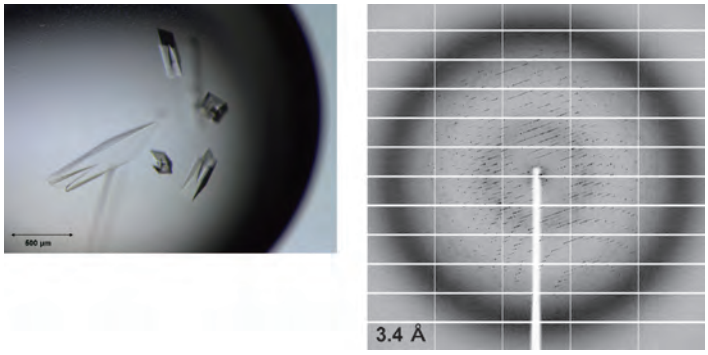

Figure 1

Native crystals of the core Mediator (cMed) protein (left side) and best diffraction pattern after the collimated beam was applied (right side).

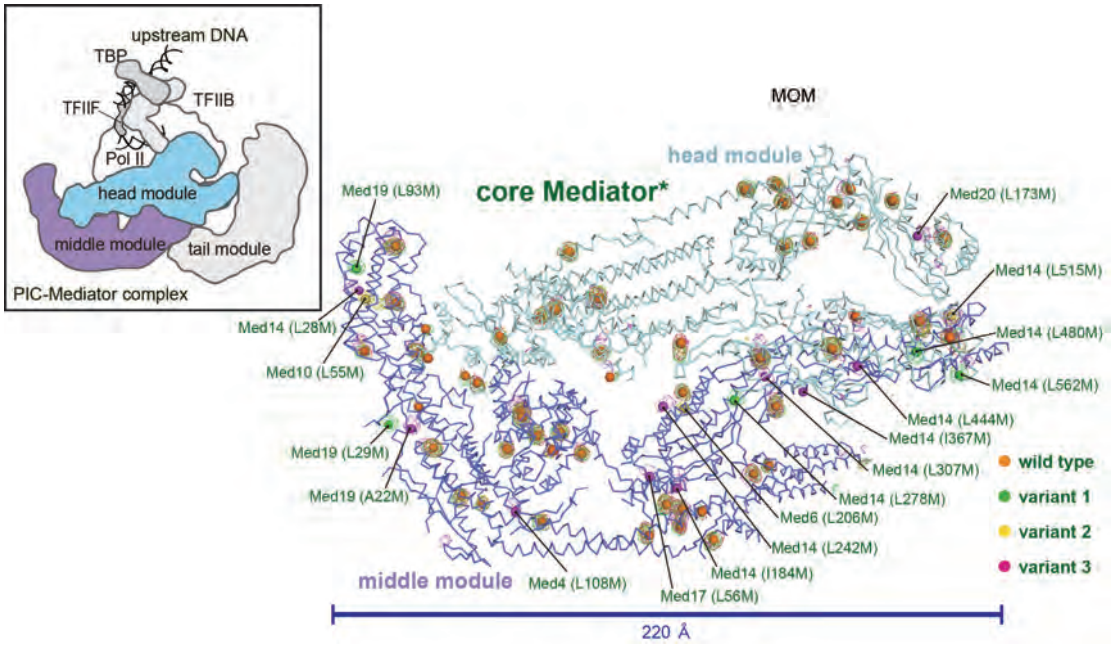

Figure 2

Schematic view of the architecture of the transcription pre-initiation complex (PIC)–Mediator complex (left) and superposition of four anomalous difference electron density maps, contoured at 3σ revealing peaks for anomalously scattering Se-atoms that indicate the position of methionine residues (right). A total of 29 additional methionine residues were introduced in three mutant variants of cMed. The large number and wide distribution of sequence markers facilitated modelling and led to a refined atomic model of very high confidence. (Figure adapted from original publication).

the EMBL P14 beamline on PETRA III at DESY was essential. Using a 200 µm × 200 µm collimated X-ray beam in combination with a kappa-goniostat and the helical-scan data collection strategy, 180 degrees of diffraction data could be collected from single crystals at this beamline, compared to typically < 20 degrees under different experimental conditions. Out of a total of ~200 crystals tested, the very best crystal yielded a complete diffraction data set to 3.4 Å resolution (Fig. 1).

The 'collimated' quasi-parallel X-ray beam on beamline P14 is generated via compound refractive lenses (CRLs). With this beam, large (> 50 µm in linear dimensions) crystals can be illuminated homogeneously allowing for extraction of highly accurate data under low-dose - but still high-flux - conditions. Furthermore, the P14 MXCuBE user interface allows to easily match the beam-shape precisely to the shape of the crystal thus reducing background scatter from non-crystalline material to the minimum.

In addition to enabling crystallographic phase determination, Se and S atoms can also serve as reliable sequence marker providing important information not available in the cryo-EM method. During the construction of the atomic model for the cMed, the locations of 53 out of 78 naturally present methionine residues and of 35 out of 40 cysteine residues where identified from anomalous difference data collected at optimized X-ray energies of 12.7 and 6.5 keV, respectively. We also prepared three Mediator variants with 29 additional methionine residues for the use as sequence markers (Fig. 2). The large number and wide spatial distribution of sequence markers facilitated accurate modelling and led to a refined atomic model with a confidently assigned sequence register. In fact, when compared to the crystal structure, the EM-derived model for cMed [3] contained regions where subunits or parts of subunits were differently assigned, regions where the amino acid sequence remained unassigned, and regions where the register of the amino acid sequence was shifted.

Macromolecular crystallography using the collimated and tunable beam of P14 allowed the accurate structural analysis of a large protein complex, the core Mediator. While EM analyses prior to our study had revealed the subunit organization, our crystallographic analysis unveiled the detailed structure and lead to a revision of significant portions of previously available EM-based models at lower resolution.

Contact: Patrick Cramer, patrick.cramer@mpibpc.mpg.de

Authors

Kayo Nozawa[1], Thomas R. Schneider[2] and Patrick Cramer[1]

1. Max Planck Institute for Biophysical Chemistry, Department of Molecular Biology, Göttingen, Germany.
2. European Molecular Biology Laboratory (EMBL), Hamburg Outstation c/o Deutsches Elektronen-Synchrotron (DESY), Hamburg, Germany.

Original publication

'Core Mediator structure at 3.4 Å extends model of transcription initiation complex.', Nature 545, 248-251 (2017). DOI: 10.1038/nature22328

References

1. M. Frey, 'Water structure associated with proteins and its role in crystallization', Acta Crystallogr. D: Biol. Crystallogr. 50, 663-666 (1994).
2. J.P. Schuermann, and J.J. Tanner, 'MRSAD: using anomalous dispersion from S atoms collected at Cu Kα wavelength in molecular-replacement structure determination', Acta Crystallogr. D: Biol. Crystallogr. 59, 1731-1736 (2003).
3. K-L.Tsai, et al, 'Mediator structure and rearrangements required for holoenzyme formation', Nature 544, 196-201 (2017).

Capturing biochemistry in action.

Novel mix-and-inject technology allows imaging of intermediate states in biochemistry

Technologies to determine static structures of biomacromolecules have been around for more than sixty years. But biomolecular structures are not static – they are dynamic and often transient (short lived). They change shape upon interactions with other molecules to convey biological signals, which control many biological functions and processes relevant to life. We have now demonstrated the capability to capture the three-dimensional structures of short-lived intermediates in real time. We use a novel mix-and-inject technology, coupled to serial femtosecond crystallography at an X-ray free-electron laser (XFEL), to study the adenine riboswitch, an RNA molecule that switches on/off the production of proteins or other biomolecules upon a direct interaction with a small triggering molecule.

Found in all organisms, riboswitches are structural elements in certain messenger RNAs (mRNAs) that act as regulators of gene expression, controlling the production of proteins. They consist of two parts: aptamer and expression platform domains. When the term 'riboswitch' first appeared about 15 years ago, it referred literally to the distinct conformational switching upon ligand binding, resulting in an altered pattern of gene expression [1,2]. For most riboswitches, the key to the mechanism is a 'switching sequence', which is part of either the first helix (P1) of the aptamer domain, or the expression platform, depending on the ligand-triggered conformational changes [3]. How such structural changes are 'transmitted' from the binding pocket, where a specific small molecule (ligand) interacts and stays, to the 'switching sequence', and subsequently the expression platform, has been under extensive investigations [3].

A number of studies have suggested the presence of multiple conformational states of riboswitches, both in the presence and absence of ligand. However, such a hypothesis lacks direct structural evidence to support it. Before our work, very little experimental structural information was available about the existence of a distinct conformation of ligand-free riboswitches. Thus, in reality, any differences between the structure of a riboswitch aptamer domain in its unbound state to that of its bound state are not known. That is, conformational changes induced by the absence or presence of a ligand had not been directly visualised at the atomic level. A clear understanding of the nature of binding and 'switching' requires detailed structural information on unbound aptamers [3] as well as any short-lived intermediate structures that are formed after binding.

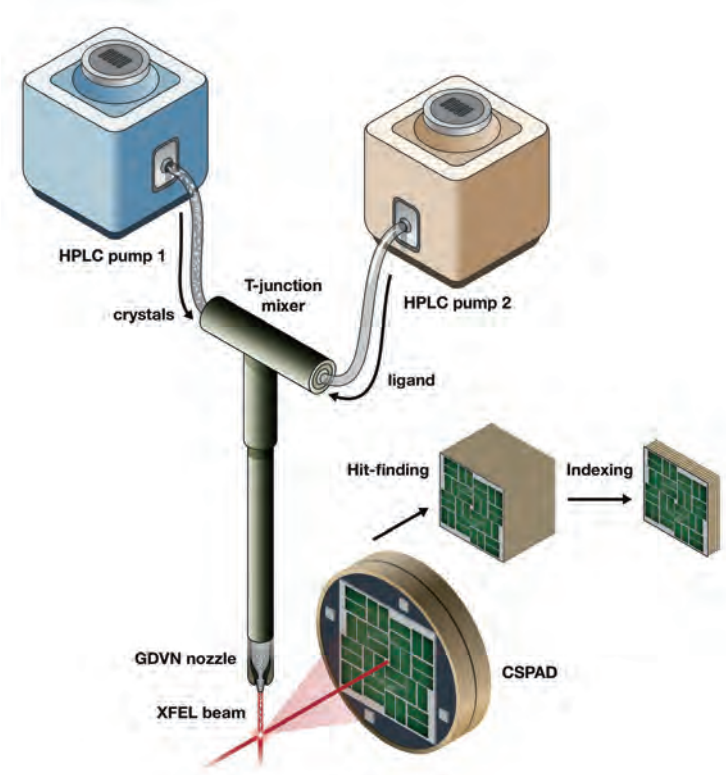

Figure 1

A schematic illustration of the mix-and-inject technology. Nanocrystals were pumped into a narrow chamber ('T-junction'), where they mixed with a stream of a fluid containing the ligand. Mixing results in rapid diffusion of ligand molecules into crystals within hundreds of microseconds. The mixture then continued to travel for a given time before being intercepted by an XFEL pulse and the diffraction pattern recorded. Image: Joseph Meyer

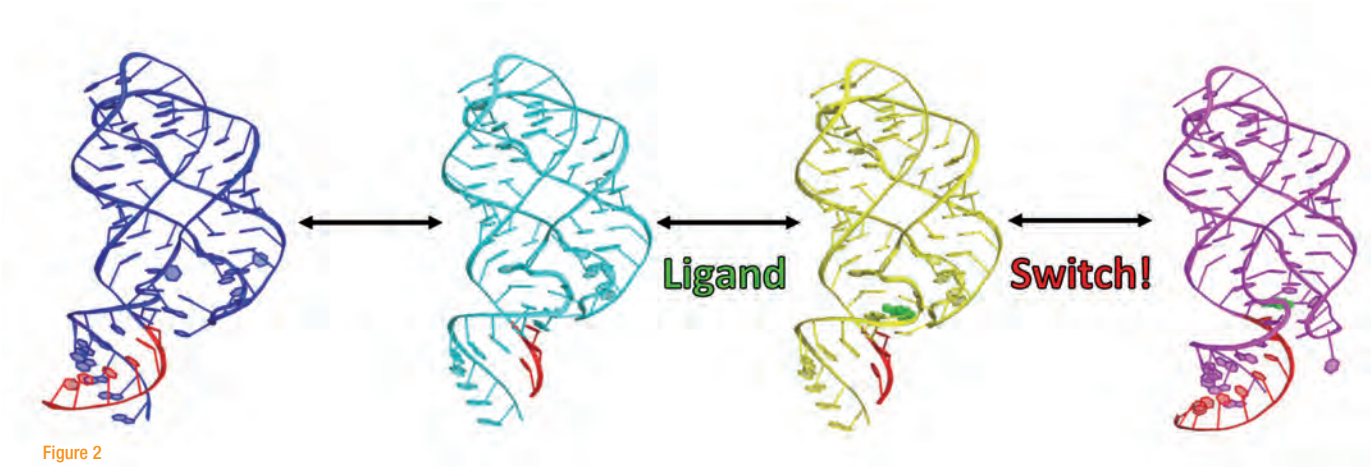

Figure 2

A ribbon diagram showing the three dimensional structure of the adenine riboswitch in four conformational states: blue (unbound), cyan (alternate unbound), yellow (transient intermediate) and magenta (bound). The ligand is drawn as a green ball-and-stick model. The active switching sequence is highlighted in red. In solution, conformational change occurs on the millisecond to microsecond timescale, but in the crystalline state takes place within seconds.

Determining structures of RNA is significantly more difficult than for proteins. Less than 3 % of the entries in the protein data bank are for RNA and RNA-containing complexes, of which fewer than 100 entries are unique and larger than 70 nucleotides. Limited RNA structural information is due in part to the intrinsic dynamics and conformational flexibility of RNA, as well as methodological limitations. New approaches and tools are therefore acutely needed to study RNA structure.

By combining a novel mix-and-inject approach with serial femtosecond crystallography at an XFEL, we have now been able to determine the structures of intermediate states of the adenine riboswitch. The mix-and-inject technology allows streams of tiny crystal slurry and the buffer containing ligand to rapidly mix in a mixing device for a well-determined time before their exposure to an XFEL pulse for a snapshot diffraction measurement, as shown in Fig. 1. This mix-and-inject technique requires the use of serial femtosecond crystallography [4] at an XFEL because, in order to observe diffraction from a crystal that has ligand diffused into it, the time for the diffusion must be negligible compared to the time it takes for the conformation change to occur. As such, the crystal has to be sufficiently small to ensure a rapid uniform spread of ligand within the crystal, so that all molecules in the crystals undergo cooperative conformation changes without cracking the crystals. In the meantime, the XFEL pulse used to take snapshots of the system has to be so short and bright that it can catch actions in tiny crystals via diffraction measurements on the scale of microseconds and milliseconds. The short XFEL pulses hence not only ensure accurate timing, but also allow the necessary high-dose exposures for diffractive imaging of tiny crystals by outrunning radiation damage.

Our experiments, carried out at the CXI beamline of the Linac Coherent Light Source, showed that structural changes to the adenine riboswitch aptamer domain occurred just seconds after mixing with the ligand adenine (Fig. 2). The measurements showed that the changes in the binding pocket of the aptamer occurred after a 10-second delay and 10 minutes later the RNA molecules were fully converted to the ligand-bound state. Surprisingly, the RNA crystals changed space group in this process, but the crystals were small enough to sustain such drastic changes without ill effect.

Using our novel approach, a large number of biochemical systems, such as enzymatic, transport, drug-binding, and other ligand-triggered reactions, can be studied at the structural level and in real time. This will potentially allow us to observe the full course of reaction states – from initiation to activation, to transitional intermediates, to termination.

Contact: Yun-Xing Wang, wangyunx@mail.nih.gov
Henry Chapman, henry.chapman@desy.de

Authors

Jason R. Stagno, Yu Liu, Yuba R. Bhandari, Chelsie E. Conrad, Sujay Panja, M. Swain, Lin Fan, Garrett Nelson, Chufen Li, Derrick R. Wendel, Thomas A. White, Jesse D. Coe, Max O. Wiedorn, Juraj Knoska, Dominik Oberthuer, Ryan A. Tuckey, Ping Yu, Marzena Dyba, Sergey G. Tarasov, Uwe Weierstall, Thomas D. Grant, Charles D. Schwieters, Jinwei Zhang, Adrian R. Ferré-D'Amaré, Petra Fromme, David E. Draper, Meng Liang, Mark S. Hunter, Sebastien Boutet, Kemin Tan, Xiaobing Zuo, Xinhua Ji, Anton Barty, Nadia A. Zatsepin, Henry N. Chapman, John C.H. Spence, Sarah A. Woodson and Yun-Xing Wang

Affiliation details at: https://www.nature.com/articles/nature20599

Original publication

'Structures of riboswitch RNA reaction states by mix-and-inject XFEL serial crystallography', Nature 541, 242–246 (2017). DOI: 10.1038/nature20599

References

1. A. Nahvi et al., 'Genetic control by a metabolite binding mRNA', Chem Biol 9, 1043 (2002).
2. W.C. Winkler and R.R. Breaker, 'Genetic control by metabolite-binding riboswitches', Chembiochem : a European journal of chemical biology 4, 1024–1032 (2003).
3. R.T. Batey, 'Structure and mechanism of purine-binding riboswitches' Q. Rev. Biophys. 45, 345–381 (2012).
4. S. Boutet et al., 'High-resolution protein structure determination by serial femtosecond crystallography', Science 337, 362 (2012).

Pumping spins.

Ultrafast spin currents by magnetization dynamics

The generation of spin currents sets the basis for spin-based electronics. One mechanism to generate spin current is called spin pumping. It is present in nanometre thin bilayer systems consisting of a ferromagnetic material and a non-magnetic layer. When the magnetization precesses, spins are pumped across the interface. This process relies on spin angular momentum transfer. So far, experiments detecting this spin current operate at the ferromagnetic resonance at GHz frequencies because the magnetization response is large for these frequencies. In our work, spin pumping is calculated for much higher frequencies. It turns out that spin currents can be efficiently generated up to THz frequencies and coherently controlled by the external magnetic driving field.

The manipulation of the electron spin in condensed matter systems reaches for new applications in information technology. This field of research is known as spintronics, in analogy to electronics. Spintronic devices are already used for read heads of magnetic hard disks and for magneto-resistive field sensors. But the full potential of spintronics is by far not exploited today. Spintronics applications are expected to have lower power consumption and faster processing times than electronics nowadays.

In electronics the electrons move in an electrical field and their spins are randomly distributed. The average spin direction is zero and thus the spin cannot be used to process any information. However in ferromagnetic materials the electrons are spin-polarized, which means that the randomness is lifted by the magnetic interactions in the ferromagnet. The spins are thus aligned to the magnetization direction of the magnet and additionally they have an excess of spins being parallel to the magnetization. The difference between a normal current and such a spin-polarized current is depicted in Figs. 1a and b. Ferromagnets can be used as a source and a detector, or can even be switched by spin-polarized currents if the current is large enough. Modern spintronic devices rely on this principle.

The generation of spin currents used in this work relies on another mechanism. At the interface between a ferromagnet and a non-magnetic material, electrons in the non-magnetic layer get spin-polarized. If the magnetization direction is changed there is a mismatch between this spin direction and the magnetization that has to equilibrate via a pure spin current. In this way the spin excess that builds up will be compensated. This spin current can be illustrated by spin-up and spin-down electrons flowing in opposite directions.

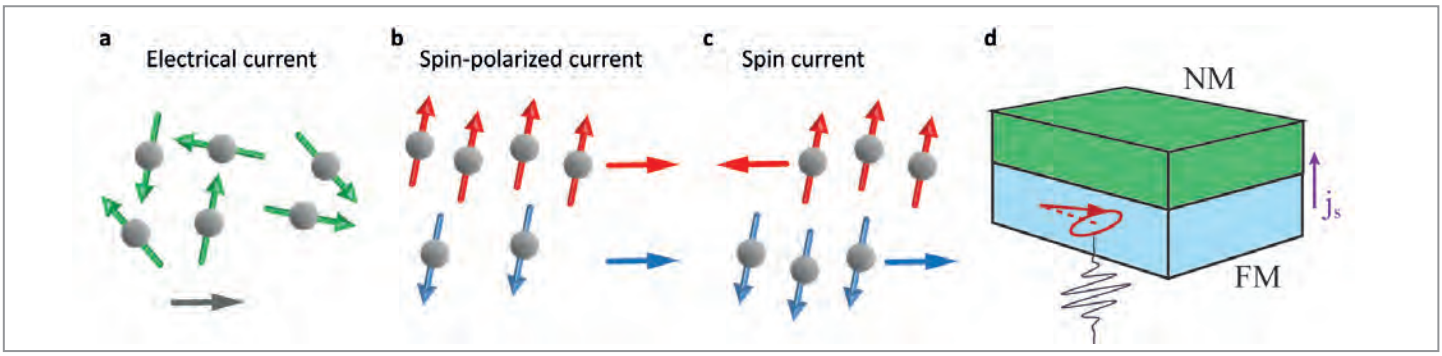

Figure 1

(a) An electrical current, indicated by the grey arrow, carries electrons that have a charge (sphere) and a spin (arrow). In an electrical current the spins are randomly distributed.

(b) In magnetic materials the spins are aligned with the magnetization, either parallel (red) or antiparallel (blue). The electrical current is spin-polarized due to an excess of parallel spins.

(c) In a pure spin current as discussed here, spin-up and spin-down electrons flow in opposite directions. No net charges are transported.

(d) Bilayer of a ferromagnetic (FM) and a non-magnetic material (NM) used for spin pumping. The magnetization (red) is excited to precess by a THz field pulse (black), which generates a spin current j_s flowing at the interface. The spin current oscillates at the same frequency as the magnetization.

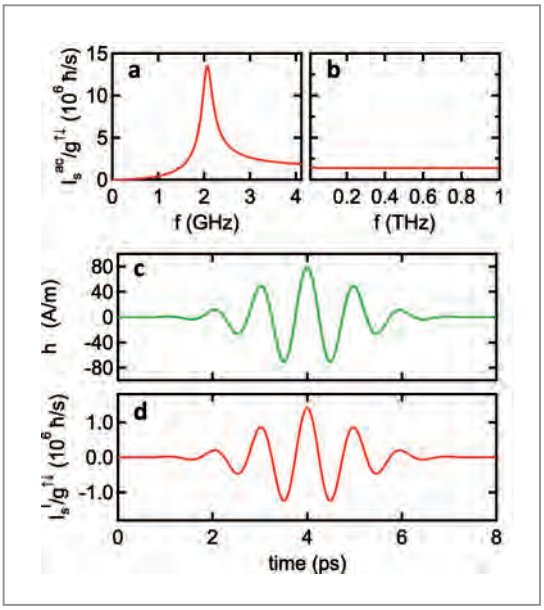

Figure 2

Magnitude of the generated spin current I_s^{ac} for a magnetization precessing at frequency f around the ferromagnetic resonance at GHz frequencies (a) and at much higher frequencies in the THz range (b).
(c) Evolution of a THz magnetic field pulse exciting the magnetization in the ferromagnetic layer.
(d) The resulting THz spin current in the non-magnetic layer is coherent to the excitation field pulse shown in (c).

Effectively no charge is flowing but spins are transported (see Fig. 1c). By changing the magnetization continuously one can keep up such a spin current that flows from the ferromagnet to the non-magnetic layer as depicted in Fig. 1d. This process is called spin pumping [1].

The effect is particularly pronounced when the changes of the magnetization are large. The spin current depends on the cross product of the magnetization and its time derivative. It is maximized when the ferromagnet is excited by an external magnetic field to precess at its ferromagnetic resonance because then the precession angle and the associated changes in the magnetization direction are large. This frequency typically lies around a few GHz as shown in Fig. 2a for a ferromagnetic thin film.

In the present work the spin current generated by spin pumping is calculated for frequencies far above the resonance frequency. Magnetization dynamics up to the THz range have been in focus recently [2] due to possible ultrafast magnetic switching applications. By modelling the THz dynamics of the magnetization [3,4] one can also calculate the THz spin current that is generated by spin pumping. One of the main findings for the THz range is the small precession angle of the magnetization, so it seems unlikely that a large spin current is generated. However, the loss of precession amplitude is exactly compensated by the very fast changes of the magnetization far above resonance. A spin current generated by spin pumping will persist up to the THz range. It will not depend on the excitation frequency and its amplitude is about one tenth of the current generated at the resonance (see Fig. 2b). The calculations show that ultrafast spin currents can be generated efficiently by spin pumping although the ferromagnetic materials do not possess any resonances at these high frequencies. This is important because for antiferromagnetic materials, which exhibit resonances in this frequency range, there are still many unanswered questions like how to efficiently detect spin currents or how to incorporate these systems into current technologies.

Spin pumping at THz frequencies will have some advantages compared to another recently discovered method to generate THz spin currents by laser heating [5]. This method relies on the excitation of electrons with eV energies and their transport in magnetic mulitlayers. Thus, it is restricted to conducting materials and the spin current cannot be controlled coherently by the laser pulse. Spin pumping is based on spin diffusion and is present in different materials as found in magnetic or topological insulators for example. Furthermore, the spin current oscillates in unison with the magnetic field that stimulates the magnetization (see Figs. 2c and d). Therefore, it can be coherently controlled externally via the driving THz magnetic field, in other words, additional control power over the spins.

The calculations show an interesting way to bring spintronics to much higher frequencies than used today. With THz sources that are present at table-top laser systems or at FLASH, experiments that inject and detect such ultrafast spin currents can be performed in the future.

Contact: Lars Bocklage, lars.bocklage@desy.de

Author

Lars Bocklage[1,2]

1. Deutsches Elektronen-Synchrotron DESY, Hamburg, Germany
2. The Hamburg Centre for Ultrafast Imaging, Hamburg, Germany

Original publication

'Coherent THz Transient Spin Currents by Spin Pumping', Physical Review Letters 118, 257202 (2017). DOI: 10.1103/PhysRevLett.118.257202

References

1. Y. Tserkovnyak, A. Brataas and G. E. W. Bauer, 'Enhanced Gilbert Damping in Thin Ferromagnetic Films', Phys. Rev. Lett. 88, 117601 (2002).
2. C. Vicario, C. Ruchert, F. Ardana-Lamas, P. M. Derlet, B. Tudu, J. Luning and C. P. Hauri, 'Off-resonant magnetization dynamics phase-locked to an intense phase-stable terahertz transient', Nat. Photonics 7, 720–723 (2013).
3. L. Bocklage, 'Model of THz Magnetization Dynamics', Sci. Rep. 6, 22767 (2016).
4. L. Bocklage, 'Transient magnetization dynamics in the free energy formulation of the Landau-Lifshitz equation', J. Magn. Magn. Mater. 429, 324–329 (2017).
5. T. Kampfrath, M. Battiato, P. Maldonado, G. Eilers, J. Nötzold, S. Mährlein, V. Zbarsky, F. Freimuth, Y. Mokrousov, S. Blügel, M. Wolf, I. Radu, P. M. Oppeneer and M. Münzenberg, 'Terahertz spin current pulses controlled by magnetic heterostructures', Nat. Nanotechnol. 8, 256–260 (2013).

Foundation for new type of solar cell.

Using hot polarons to harvest sunlight

In conventional solar cells, the interaction between the electrons and the lattice vibrations can lead to unwanted losses, causing substantial problems like reduction of efficiency and lowering of the long-term stability of the cells. This study reveals the foundation for an entirely new type of photovoltaic cell based on hot polaron excitation. Here, polaronic distortions, due to non-linear electronic excitations, and the inherent properties of the manganite perovskite material prevent an ultra-fast electron hole recombination. Accordingly, this leads to increased life-times of the excited state, which is beneficial for harvesting the converted energy of the sunlight.

In order to satisfy the growing energy demand of human mankind, scientific advances are necessary as the traditional energy sources will be either running short in the next decades or comprise an indefensible danger. The ideal energy source has to be based on renewable energy, safe to use, rather cheap and highly efficient. Harvesting solar energy thereby plays a major and growing role. But nowadays existing solar cell devices involve mainly toxic materials, have low efficiencies or costs that exceed the budget of the average consumer.

Recently developed ultra-fast methods based on optical lasers and highly brilliant X-ray sources like synchrotrons and free-electron lasers are thereby a key step towards the optimization of photovoltaic devices [1]. Only these ultra-fast methods enable unravelling the atomistic mechanisms and understanding the underlying charge transfer processes. This understanding might lead to the control of the occurring relaxations of optically excited charge carriers and optimization of the photon-induced structural dynamics.

In our study we present the application of such an ultrafast method in combination with detailed theoretical studies and photovoltaic measurements (Fig. 1a). The occurring processes are investigated after photoexcitation of a 100 nm thick film of the manganite $Pr_{0.65}Ca_{0.35}MnO_3$ (PCMO) as a representative for the broad variety of ABX_3 perovskite type materials. These types of materials are characterized by their crystal structure, were each B-type atom (here Mn) is centred in an octahedron built of six X-type atoms (here O), whereas every X-type atom is shared with the neighbouring octahedra, as indicated in Fig. 1b. These octahedra are deformed due to the Jahn-Teller (JT) effect, which energetically splits the usually degenerated d-orbitals of the B-type atom metal as the Mn 3d orbitals are not completely occupied. Additionally, the octahedra are tilted against each other, which further lowers the total energy of the system (Fig. 1c) [2,3].

Although a direct transition between two d-orbitals on a single manganese site is unlikely to occur, the investigated

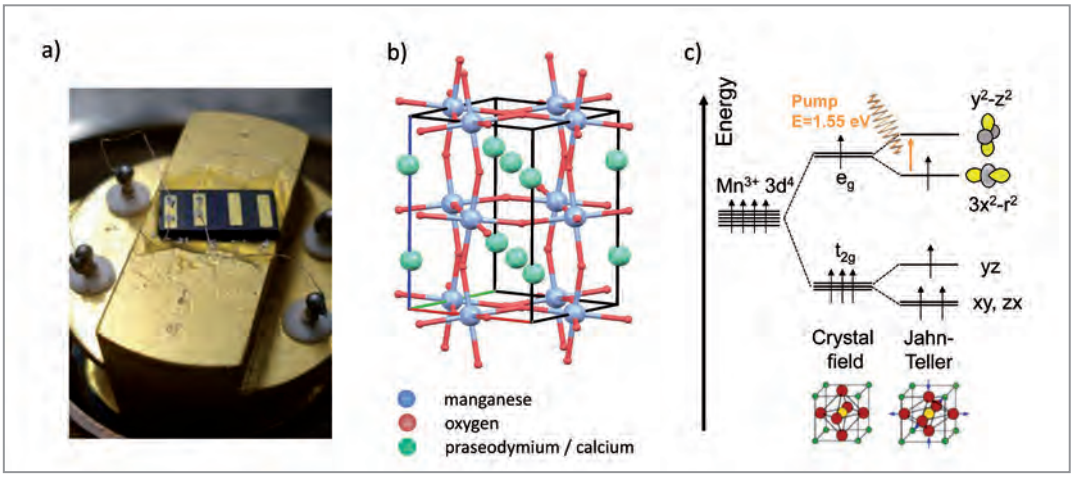

Figure 1

a) Solar cell device.

b) Crystal structure of the perovskite $Pr_{1-x}Ca_xMnO_3$.

c) Scheme of the crystal field and Jahn-Teller splitting of the degenerated Mn 3d levels in undoped $PrMnO_3$.

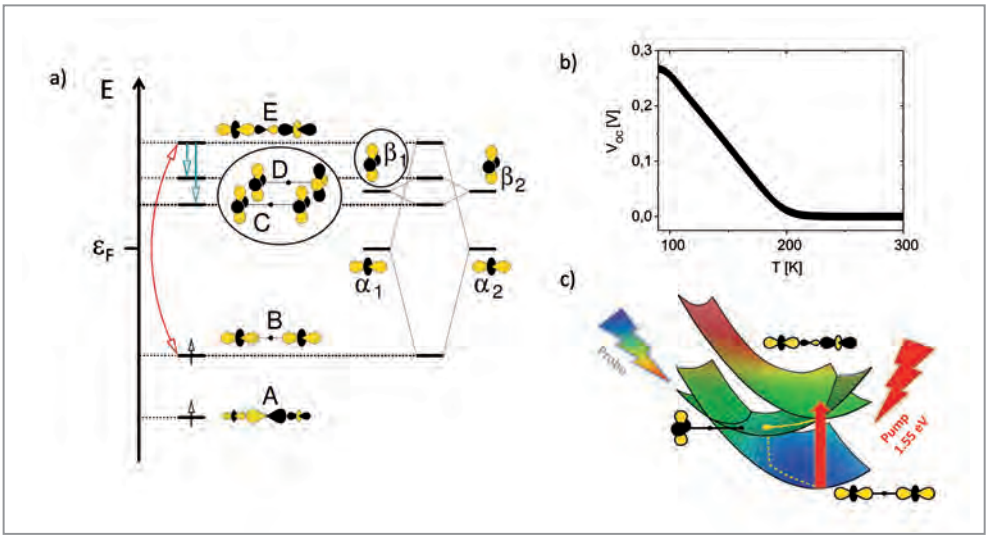

Figure 2

a) Schematic orbital diagram based on the model of a coupled Jahn-Teller dimer. The dipole-allowed polaron transition and subsequent temporal evolution of the hot polaron state are indicated by red and green arrows, respectively. The transitions are obtained by first-principles calculations.
b) Photovoltage under open-circuit conditions V_{OC} as a function of temperature showing the photovoltaic effect in a PCMO/Nb:STO heterojunction under monochromatic illumination at an energy of 1.55 eV.
c) Scheme of the Jahn-Teller dimer potential energy hypersurfaces which are involved in the photo-induced effect, including the respective relevant molecular orbitals of the dimer.

material shows a strong absorption in the visible to infrared range due to the formation of JT dimers according to the theoretical simulations (Fig. 2a). This makes PCMO an ideal material for light harvesting from the solar spectrum. At the given calcium doping level, the charge carriers of this manganite form an interacting dense system of small polarons, i.e. local polarizations of the crystal lattice due to charged particles.

At low temperatures below 200 K these polarons lose their random orientations and form a charge-ordered state. In our study we found that photo-excitation of the material in or into this charge-ordered state in a non-linear manner is responsible for the nanosecond long lasting life times at low temperatures and the resulting photovoltaic properties (Fig. 2b). The photovoltaic measurements were carried out on a heterojunction of PCMO and niobium doped strontium titanat (Nb:STO) under monochromatic illumination with an energy of 1.55 eV (λ = 800 nm). The excited electrons are thereby locked in an excited state, whose life-time is greatly increased due to the structural reconfiguration of the lattice caused by the photo-excitation and the resulting charge shifts (Fig. 2c). This locking, however, is only possible due to a given sufficiently strong cooperative coupling of the polarons in the electronical ground state. Unfortunately, the investigated material loses this property when thermal effects break up the crystallinity of the polarons above the critical charge ordering transition temperature of about 200 K.

Despite the revelation of a revolutionary new mechanism referred to as the hot polaron state, these findings do not immediately lead to a new jack of all trades device with practical application. But knowledge about the existence of this mechanism has now opened the way to expediently search for other materials that exhibit charge ordered polaron states at higher temperatures in order to exploit the newly revealed mechanism of hot polaron formation in perovskites in solar cells. With the current restriction to temperatures well below the temperatures that can be naturally encountered on earth, this new finding is momentarily rather attractive for space craft industries or other low-temperature applications.

Nevertheless, the search for further materials, that exhibit strong polaronic correlations at higher temperatures is already ongoing and will hopefully soon lead to new photovoltaic solar cell with a great common relevance.

Contact: Simone Techert, simone.techert@desy.de

Authors

Dirk Raiser[1,2], Stephanie Mildner[3], Benedikt Ifland[3], Mohsen Sotoudeh[4], Peter Blöchl[3,4], Simone Techert[1,2,5] and Christian Jooss[3]

1. Structural Dynamics of (Bio)chemical Systems, Max-Planck-Institute for Biophysical Chemistry, Göttingen, Germany
2. Deutsches Elektronen-Synchrotron DESY, Hamburg, Germany
3. Institute for Material Physics, University of Göttingen, Germany
4. Institute for Theoretical Physics, University of Clausthal, Clausthal-Zellerfeld, Germany
5. Institute for X-ray Physics, University of Göttingen, Germany

Original publication

'Evolution of Hot Polaron States with a Nanosecond Lifetime in a Manganite Perovskite', Adv. Energy Mater. 7, 1602174 (2017). DOI: 10.1002/aenm.201602174

References

1. S. Bari, R. Boll, K. Idzik, K. Kubicek, D. Raiser, S. Thekku Veedu, Z. Yin and S. Techert, 'Ultrafast Time Structure Imprints in Complex Chemical and Biochemical Reactions', Chapter 15 in 'X-Ray Free Electron Lasers: Applications in Materials, Chemistry and Biology', The Royal Society of Chemistry, 301 (2017).
2. H. A. Jahn and E. Teller, Proc. R. Soc. London, Ser. A 161, 220 (1937).
3. E. Dagotto, 'Nanoscale Phase Separation and Colossal Magneto-Resistance: The Physics of Manganites and Related Compounds', Springer Series in Solid-State Sciences, Vol. 136, Springer, Berlin, 2003.

Revealing complex magnetic order in nanostructure patterns.

GISAXS and surface diffraction go nuclear

Determining magnetic properties of nanostructured materials is a key issue for designing functional nanodevices for information storage, sensor technology, or medical diagnostics. Recent development of new magnetic nanopatterns raised the need for advanced tools to quantify lateral heterogeneous magnetisation states. Addressing this demand, we have introduced two new X-ray scattering approaches, namely nuclear grazing incidence small angle scattering and nuclear surface diffraction. Both techniques employ resonant off-specular scattering to allow for a unique insight into complex lateral magnetisation states of nanopatterned systems – especially under *in situ* conditions.

In the last decades, various synchrotron based X-ray scattering techniques have proven to be essential for nanoscopic magnetic characterisation of ultra-thin films and multilayers. Experiments benefitted from the high sensitivity of polarised X-rays to magnetic moment orientations and their relatively large penetration depth. Hence, the determination of *magnetisation depth profiles* even in relatively thick layered structures of a few tens of nanometres could be performed with sub-nanometre spatial resolution [1].

Recently, a new field of research has emerged, which focusses on the lateral *magnetisation state* of nanopatterns like spin ice and skyrmion lattices or magnetic nanostructure arrays with tilted or curved surface morphology. Their heterogeneous magnetisation state within the sample plane hinders a characterisation with X-rays via specular scattering. In such a reflectivity measurement only integral magnetic information can be extracted. We developed two new scattering approaches, which overcome this limitation and allow to disentangle magnetic contributions from selected parts of magnetic nanopatterns.

In the first experiment (PETRA III, P01 and ESRF, ID18) we demonstrated how the resonant analogue of the widely applied grazing incidence small angle X-ray scattering (GISAXS) can be used to disentangle nanomagnetic information from a sample with facetted surface morphology. For this purpose, we sputter-deposited iron onto a nanofacetted sapphire template to form a continuous magnetic film with periodically varying thickness (Fig. 1).

Performing non-resonant grazing incidence small angle X-ray scattering on this sample *in situ* allows to precisely follow the growth of the nanostructured film. Thickness oscillations with decreasing period become visible during deposition along the two scattering rods (Fig. 1a) oriented perpendicular to both facet nanosurfaces. Their evaluation reveals a thickness ratio of the stripe-shaped film regions of 4:3 during the entire deposition run.

To correlate this high-resolution structural information with the nanomagnetic state of the sample we additionally recorded the time dependent nuclear resonant scattering (NRS) signal [1] of iron in the same GISAXS configuration (Fig. 1b, top). To separately extract the magnetic signal from both types of

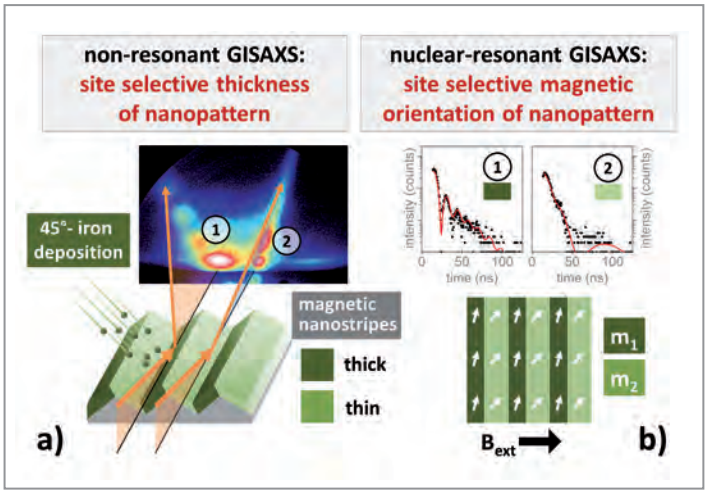

Figure 1

Illustration of the principle of nuclear resonant (magnetic) GISAXS. The technique is applied to monitor the formation of a magnetic nanopattern with periodically varying thickness via iron deposition at non-normal incidence onto a nanofacetted sapphire substrate. (a) Conventional, non-resonant GISAXS allows to precisely follow the growth of both types of nanostripes via detection of diffuse thickness oscillations along scattering rods normal to the nanofacets. (b) Nuclear resonant time spectra detected at both GISAXS scattering rods (position 1 and 2) allow to disentangle the magnetic moment orientation and strength in both types of nanostripes during growth and subsequent field dependent reversal. The study reveals an unexpectedly complex magnetic behaviour on the nanoscale in this simple sample system.

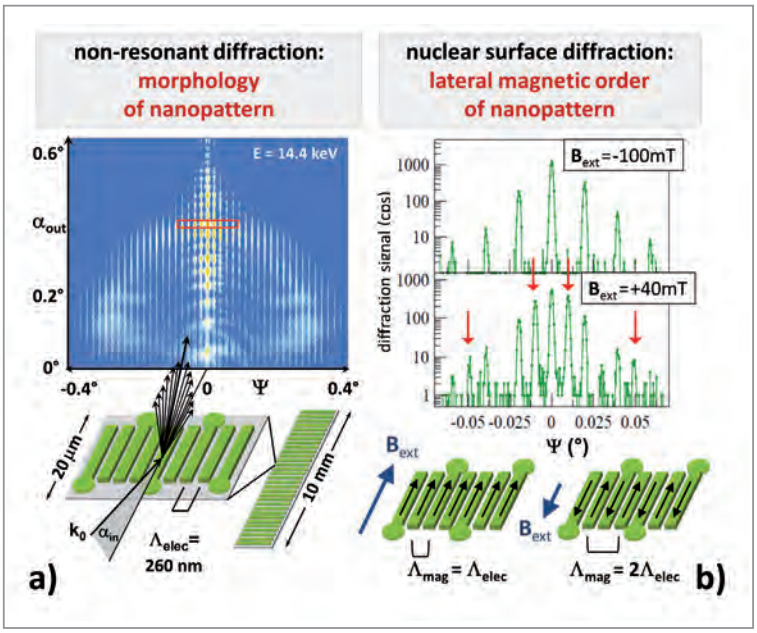

Figure 2

Illustration of nuclear resonant surface diffraction.
(a) Performing non-resonant surface diffraction on a grating of magnetic nanostripes results in formation of a scattering pattern from which the morphology of the nanostructure can be determined with sub-nanometre precision. The box marked in red shows the area analysed in experiment (b). (b) Performing nuclear resonant GISAXS in identical scattering geometry results in a diffraction pattern which is in addition sensitive to the lateral magnetic ordering in the grating. During field-dependent reversal of this nanograting [2], pure nuclear superstructure peaks (red arrows) appear, which identify a ferromagnetic-antiferromagnetic transition on the nanoscale. Tracking these resonant superstructure peaks in an external field thus constitutes an advanced technique to detect the appearance and strength of magnetic superstructures also in more complex nanopatterns.

nanostripes we did not collect the NRS signal along the specular scattering direction but on both scattering rods (Fig. 1a, marked as positions 1 and 2). This allowed us to follow the evolution of magnetic order in the nanostripes during the deposition run. During magnetic field cycles after the deposition we found an unexpected heterogeneous nanomagnetic behaviour: The magnetic moments in the thinner nanostripes tend to follow the external magnetic field much stronger than the thicker ones and show a different magnetic hysteretic behaviour in general (Fig. 1b, bottom). This observation on the nanoscale became only possible using this new resonant GISAXS approach which can be generally applied to magnetic nanopatterns with 3D morphology.

In the second experiment (PETRA III, P01) we applied nuclear resonant surface diffraction as a new technique for the characterisation of lateral magnetic order in magnetic nanopatterns. For this purpose, we fabricated a custom-made permalloy nanograting [2], which was intended to undergo a ferromagnetic-antiferromagnetic transition upon field cycling. The non-resonant scattering signal in the GISAXS configuration shows a diffraction pattern from which the morphology of the nanograting was determined with sub-nanometre precision. To be sensitive to the lateral magnetisation state we collected the nuclear resonant diffraction pattern via horizontal line scans (Fig. 2b). It turned out that during magnetic reversal strong pure magnetic superstructure peaks (red arrows) are formed, which are caused by an antiferromagnetic superstructure in the grating with a lateral correlation length of twice the structural one.

The angular position, relative strength and field-dependent intensity of these superstructure peaks enabled us to precisely study the nanoscale magnetic reversal. The experiment thus successfully demonstrated that nuclear surface diffraction is technically feasible and could offer a completely new insight into a wide range of nanomagnetic sample systems with its high sensitivity to spin dynamics [3].

Contact: Kai Schlage, kai.schlage@desy.de,
Denise Erb, d.erb@hzdr.de

Authors

Kai Schlage[1], Denise Erb[1,3], Lars Bocklage[1,2], Hans-Christian Wille[1], Liudmila Dzemiantsova[1,2], René Hübner[3], Guido Meier[2,4], Daniel Geza Merkel[5], Matthias Pues[6], Rudolf Rüffer[5] and Ralf Röhlsberger[1,2]

1. Deutsches Elektronen-Synchrotron DESY, Hamburg, Germany
2. The Hamburg Centre for Ultrafast Imaging, Hamburg, Germany
3. Institute of Ion Beam Physics and Materials Research, Helmholtz-Zentrum Dresden-Rossendorf, Dresden, Germany
4. Max Planck Institute for the Structure and Dynamics of Matter, Hamburg, Germany
5. European Synchrotron Radiation Facility, Grenoble, France

Original publications

'Disentangling magnetic order on nanostructured surfaces', Physical Review Materials 1, 023001(R) (2017). DOI: 10.1103/PhysRevMaterials.1.023001

'Nuclear Resonant Surface Diffraction of Synchrotron Radiation', Physical Review Letters 118, 237204 (2017). DOI: 10.1103/PhysRevLett.118.237204

References

1. K. Schlage and R. Röhlsberger, 'Nuclear resonant scattering of synchrotron radiation: Applications in magnetism of layered structures', J. Electron Spectrosc. Relat. Phenom 189, 187 (2013)
2. M.-Y. Im, L. Bocklage, P. Fischer and G. Meier, 'Direct Observation of Stochastic Domain-Wall Depinning in Magnetic Nanowires', Phys. Rev. Lett. 102, 147204 (2009)
3. L. Bocklage, C. Swoboda, K. Schlage, H.-C. Wille, L. Dzemiantsova, S. Bajt, G. Meier and R. Röhlsberger, 'Spin Precession Mapping at Ferromagnetic Resonance via Nuclear Resonant Scattering of Synchrotron Radiation', Phys. Rev. Lett. 114, 147601 (2015)

X-rays reveal weaving of golden coatings.

Tailoring ultra-thin metallic coatings on polymer surfaces

The tuning of size-dependent properties of ultra-thin metallic coatings is a desirable but challenging goal in applied nanotechnology. We present a comprehensive real-time investigation of the metal growth from small nuclei to a complete gold layer during sputter deposition on a polystyrene thin film at different deposition rates. Using time resolved surface-sensitive X-ray scattering, the impact of deposition rates on the growth regimes were identified: At higher rates an earlier onset of thin film percolation occurs and initial particle densities are higher due to an increase of the nucleation probability. This study provides a better understanding of the growth kinetics of ultra-thin gold cluster films on polymer substrates needed for an optimized fabrication of tailored polymer-metal interfaces.

Our modern society more and more relies on high speed exchange of information. Electronic devices based on polymer-metal-composites gained significant relevance due to their high performance, flexibility and low-cost production. These polymer-metal-nanocomposites are employed in a broad spectrum of attractive applications as inexpensive and flexible organic photovoltaic components, organic light emitting diodes, organic field effect transistors and sensors [1,2]. Depending on their application, an efficient tailoring of the structure on different length scales ranging from micrometre to nanometre and below is required to fully exploit their great potential. The properties of the metal coatings need to be precisely adjusted, depending on the application requested. Here, the utilization of sputter deposition stands out as a versatile routine method in industry and science.

During sputtering, a solid target is bombarded with ions leading to the release of individual atoms, which can then form an ultra-thin layer of nanoparticles on the substrate material. The advantage of this method is that the atoms self-organize on the surface into clusters and therefore adopt the most favourable configuration. In addition, one can adjust the average spacing and the size of the nanoparticles more or less at the push of a button [3]. In order to tune the morphology-dependent properties of such metal cluster layers, it is mandatory to monitor how the deposition rate affects the growth kinetics.

In this study, we deposited a nanolayer of gold atoms on a thin polymer film made of polystyrene, whereby the growth behaviour of the layers was studied as a function of the deposition rate. Particularly at high growth rates, like those used in industrial applications, advanced imaging equipment with sufficiently high temporal resolution in the milliseconds regime is required in order to observe the fast processes involved. High frame-rate two-dimensional X-ray detectors (PILATUS 300k, Dectris Ltd.) in combination with the high photon flux (≈ 10^{12} photons per second) in a micro beam with a spot size of 31 × 24 µm^2, available at the PETRA III beamline P03, enables a non-invasive *in situ* and real-time investigation of gold growth kinetics during sputter deposition on a thin polymer layer [4]. Using surface-sensitive X-ray scattering (GISAXS) [5], we were able to observe the way in which the radii of and the spacing between the tiny gold clusters varied in dependence on the effective deposition rates (Fig. 1).

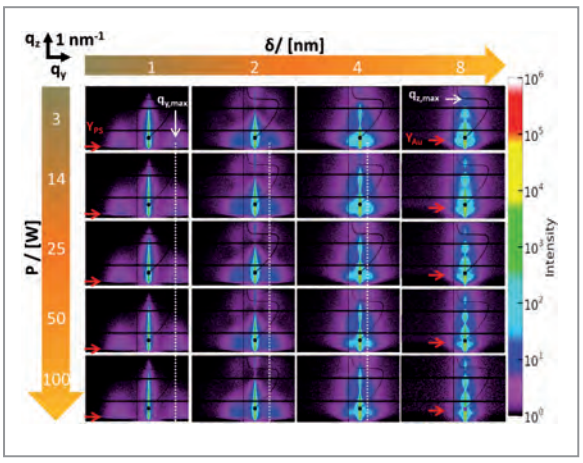

Figure 1

Selected GISAXS patterns illustrate the dependence of the evolution of key scattering features with increasing effective Au film thicknesses δ (from left to right: 1, 2, 4, 8 nm) on the sputter power (from top to bottom: 3, 14, 25, 50, 100 W). The coordinate system (q_y, q_z), corresponding key scattering features, Yoneda peak position of polystyrene (Y_{PS}) and gold (Y_{Au}) and scale bars are indicated. The vertical dashed white lines indicate the $q_{y,max}$ position at 3 W and are guides for the eye to visualize the shifts in peak positions at higher deposition rates. The dark circles correspond to the specular beam stop used to avoid detector saturation. The black horizontal stripes correspond to the detector intermodular gaps. Figure is reprinted with permission from ACS Appl. Mater. Interfaces 9, 5629–5637 (2017). Copyright 2017 American Chemical Society.

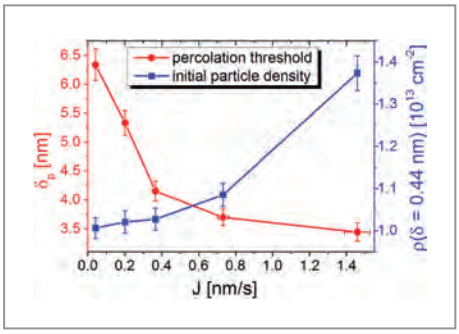

Figure 2

Shift of percolation threshold (red circle) and initial particle densities at effective thickness δ = 0.44 nm (blue rectangle) as a function of the effective deposition rate. Figure is reprinted with permission from ACS Appl. Mater. Interfaces 9, 5629–5637 (2017). Copyright 2017 American Chemical Society.

With an acquisition throughput of 20 frames per second, the fast surface processes of initial nucleation and subsequent cluster growth in dependence on the effective deposition rate could be followed on the nanoscale.

Sputtering gold onto a polymer is rather like a shower of gold atoms raining onto a sheet of plastic. Different structures form on the sheet, depending on whether it 'rains' harder or more gently, even when total amount of material deposited remains the same. We discovered two main differences between low and high sputter deposition rates (Fig. 2 and Fig. 3). Firstly, at the start of the deposition process, during nucleation, the density of particles is higher at higher rates, i.e. more clusters of gold atoms are formed, but the individual clusters are smaller. Secondly, at higher deposition rates the percolation threshold is reached earlier, i.e. with thinner layers. This threshold describes the point beyond which all gold clusters are assumed to touch each other, meaning there are hardly any gaps left in the layer. This is because at higher deposition rates, branching structures are formed, whereas at lower rates larger blobs are formed which only form interconnected networks at a later stage. This in turn means that metal coatings created at high deposition rates are smoother and more compact.

These observations now allow researchers to deduce what sputter deposition rates are best suited for specific applications. For example, if the material is to be used as a catalyst, its structure ought to consist of many small gold clusters showing a high surface/mass ratio. This can be achieved using a high sputter rate and an ultra-thin layer thickness. If the material is intended for sensors, on the other hand, a low sputter deposition rate with a comparatively high layer thickness is appropriate, as the latter results in a structure made up of larger, more separated metal clusters.

As the next step we intend to study how different properties of the layer change during sputter deposition. For example, we are using simultaneously spectroscopic methods to examine how the optical properties of the layer differ for the different morphologies [6]. This could provide a better understanding of how the use of sputter deposition can be optimised for industrial applications.

Contact: Matthias Schwartzkopf, matthias.schwartzkopf@desy.de

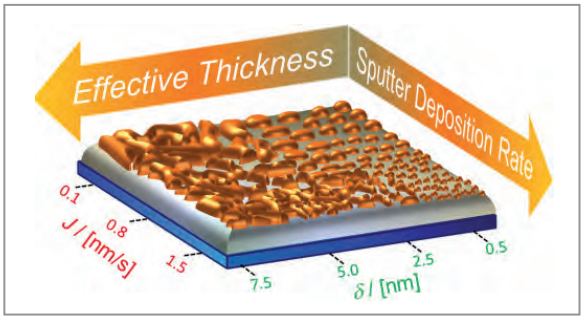

Figure 3

Schematic representation of the influence of sputter deposition rates on the morphology of nanogranular gold structures on polymer surfaces at different effective film thicknesses. Figure is reprinted with permission from ACS Appl. Mater. Interfaces 9, 5629–5637 (2017). Copyright 2017 American Chemical Society.

Authors

Matthias Schwartzkopf[1], Alexander Hinz[2], Oleksandr Polonskyi[2], Thomas Strunskus[2], Franziska C. Löhrer[3], Volker Körstgens[3], Peter Müller-Buschbaum[3], Franz Faupel[2] and Stephan V. Roth[1,4]

1. Deutsches Elektronen-Synchrotron DESY, Hamburg, Germany
2. Lehrstuhl für Materialverbunde, Institut für Materialwissenschaft, Christian Albrechts-Universität zu Kiel, Kiel, Germany
3. Lehrstuhl für Funktionelle Materialien, Physik-Department, Technische Universität München, Garching, Germany
4. KTH Royal Institute of Technology, Department of Fibre and Polymer Technology, Stockholm, Sweden

Original publication

'Role of sputter deposition rate in tailoring nanogranular gold structures on polymer surfaces', ACS Appl. Mater. Interfaces 9, 5629–5637 (2017). DOI: 10.1021/acsami.6b15172

References

1. F. Faupel, V. Zaporojtchenko, T. Strunskus and M. Elbahri, 'Metal-Polymer Nanocomposites for Functional Applications', Adv. Eng. Mater. 12, 1177–1190 (2010).
2. J.-L. Wu, F.-C. Chen, Y.-S. Hsiao, F.-C. Chien, P. Chen, C.-H. Kuo, M. H. Huang and C.-S. Hsu, 'Surface Plasmonic Effects of Metallic Nanoparticles on the Performance of Polymer Bulk Heterojunction Solar Cells', ACS Nano 5, 959–967 (2011).
3. M. Schwartzkopf, A. Buffet, V. Körstgens, E. Metwalli, K. Schlage, G. Benecke, J. Perlich, M. Rawolle, A. Rothkirch, B. Heidmann, G. Herzog, P. Müller-Buschbaum, R. Röhlsberger, R. Gehrke, N. Stribeck and S. V. Roth, 'From Atoms to Layers: *In Situ* Gold Cluster Growth Kinetics during Sputter Deposition', Nanoscale 5, 5053–5062 (2013).
4. A. Buffet, A. Rothkirch, R. Döhrmann, V. Körstgens, M. M. Abul Kashem, J. Perlich, G. Herzog, M. Schwartzkopf, R. Gehrke, P. Müller-Buschbaum, P. and S. V. Roth, 'P03, the Microfocus and Nanofocus X-Ray Scattering (MiNaXS) Beamline of the PETRA III Storage Ring: The Microfocus Endstation', J. Synchrotron Radiat. 19, 647–53 (2012).
5. M. Schwartzkopf and S.V. Roth, 'Investigating Polymer–Metal Interfaces by Grazing Incidence Small-Angle X-Ray Scattering from Gradients to Real-Time Studies', Nanomaterials 6, 239 (2016).
6. M. Schwartzkopf, G. Santoro, C. J. Brett, A. Rothkirch, O. Polonskyi, A. Hinz, E. Metwalli, Y. Yao, T. Strunskus, F. Faupel, P. Müller-Buschbaum and S. V. Roth, 'Real-Time Monitoring of Morphology and Optical Properties during Sputter Deposition for Tailoring Metal–Polymer Interfaces', ACS Appl. Mater. Interfaces 7, 13547–13556 (2015).

3D imaging of strain in a nanowire LED.

Bragg ptychography on a single nanowire

The future of solid state lighting can be potentially driven by utilizing InGaN/GaN core-shell nanowires. These radial heterostructures provide the possibility for fine tuning of functional properties by controlling a strain state between mismatched layers. We present a non-destructive study of a single 400 nm thick InGaN/GaN core-shell nanowire using two-dimensional (2D) X-ray Bragg ptychography with a nanofocused X-ray beam. The XBP reconstruction enabled the determination of a detailed three-dimensional (3D) distribution of the strain in the particular nanowire using a model based on a finite element method.

The field of solid-state lighting is one of the rapid growing directions in applications of III-V semiconductor materials and their compounds [1]. Nowadays, the best performance in terms of external quantum efficiency (EQE) in the blue range of the visible spectrum is achieved by III-nitride semiconductors [2]. A significant improvement in performance of LEDs across the whole visible range is expected with the use of III-nitride based nanowires (NWs). They possess outstanding mechanical and optoelectronic properties because of a high surface-to-volume aspect-ratio. One of the main advantages of NWs is their ability to relax mechanical strain without plastic deformations. While the mechanical properties are tightly connected with optoelectronic characteristics, there is high demand for tools providing information on the inner structure of NWs without destructive sample preparation.

X-ray Bragg ptychography (XBP) is a scanning version of the coherent X-ray diffractive imaging technique and is a field of active development during the last decade. It has a great potential to provide in a non-destructive way structural and strain information for extended samples. In this technique the sample is scanned by a localized illumination with overlapping adjacent positions and 2D diffraction patterns are recorded in the far-field. Employing iterative phase retrieval algorithms, the real space image of the sample is retrieved [3,4].

We investigated a wurtzite (WZ) core-shell InGaN/GaN nanowire grown in Lund University using selective area metal-organic chemical vapour deposition (MOCVD). GaN NWs were grown to be 340 nm thick and 2 µm long. The growth of the InGaN shell was performed at 30 % concentration of In. The total final diameter of the NW from facet to facet was 390 nm (see Fig. 1a, b). One can see that the surface of the InGaN shell is rough. This surface morphology can be explained by the uneven process of the radial growth of the shell. A misfit strain induced by lattice mismatch at the interface between the core and shell (see Fig. 1b) was expected to partially relax due to the formation of misfit dislocations.

The XBP experiment was performed at the nanoprobe end-station of the P06 beamline at PETRA III. The photon energy of the X-ray beam was 15.25 keV. An X-ray fluorescence detector was used for locating the sample. The diffraction patterns were recorded in the far-field by the 2D detector. The incident beam was focused using nano-focusing lenses down to 100 nm (see Fig. 1c for the experimental geometry). A series of 2D ptychographic scans were performed for a set of angular positions θ around the Bragg condition for the $10\bar{1}0$ reflection of GaN. The angular range of the measurement was ±0.3° with 0.1° increment. At each

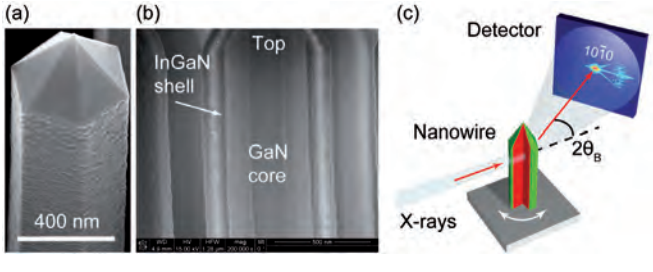

Figure 1

(a) SEM image showing the typical surface morphology of a nanowire under investigation in side view.

(b) Cross-sectional SEM image taken at the top of the NW similar to the studied one.

(c) Experimental setup of the XBP measurements. A single NW consisting of the GaN core (red) and the InGaN shell (green) was mounted in Bragg condition of the $10\bar{1}0$ GaN diffraction peak.

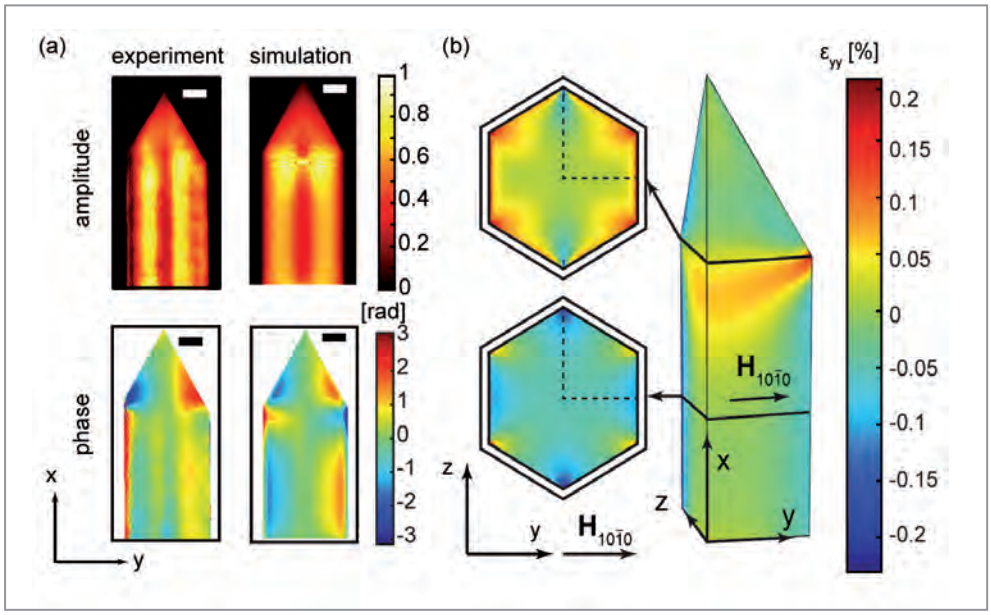

Figure 2

(a) Amplitude and phase of the ptychographic reconstruction at the central angular position of the NW as obtained from the experimental data (left) and from FEM based simulation (right).
(b) 3D render of the radial yy component of strain distribution in the NW core obtained from the FEM model after fitting to the experimental results.

rotational step, an area of 500 × 500 nm^2 in the upper part of the NW was scanned.

The reconstruction of the ptychographic datasets was performed using the ePIE algorithm [5] for every angular position. The amplitude and phase of the 2D XBP reconstruction corresponding to the central angular position near the Bragg angle of the sample is shown in Fig. 2a (left). As it can be seen from these results, both the amplitude and phase have a stripe-like structure. These features arise from the fact that the measurement was performed detuned by -0.03° from the exact Bragg condition.

In order to interpret the result of the 2D XBP reconstruction, a 3D model of a strained GaN NW was developed using the Finite Element Method (FEM). By simulating the 2D XBP reconstruction it was possible to fit the major parameters of the core-shell NW to the experimental results (see Fig. 2a right column). The 3D representation of the obtained model is shown in Fig. 2b. Radial strain values of about 0.2 % were observed in the region of the NW close to the tip. Below that region, the NW is more relaxed and strain values do not exceed ±0.05 %. The maximum value of the strain component normal to the facets was concentrated in the transition region between the central part of the NW and the GaN tip. In addition, a stronger plastic relaxation was found along the axial growth direction compared to the radial one.

Non-uniformity of strain distribution in NWs leads to a change of the band gap and, consequently, in charge carrier mobility that affects an overall performance of the devices. The results of our work provide important information for understanding the relation between the structural and optoelectronic properties of semiconductor core-shell NWs with high spatial resolution. Therefore, the technique of X-ray Bragg ptychography combined with simulation such as FEM is capable of providing a detailed information and feedback on how to improve the growth of the nanowires. We believe that the proposed approach will open possibilities for an improved performance of core-shell NW-based devices.

Contact: Dmitry Dzhigaev, dmitry.dzhigaev@desy.de, Ivan Vartaniants, Ivan.Vartaniants@desy.de

Authors

Dmitry Dzhigaev[1], Tomaš Stankevič[2], Zhaoxia Bi[3], Sergey Lazarev[1,4], Max Rose[1], Anatoly Shabalin[1], Juliane Reinhardt[1], Anders Mikkelsen[3], Lars Samuelson[3], Gerald Falkenberg[1], Robert Feidenhans'l[5] and Ivan A. Vartanyants[1,6]

1. Deutsches Elektronen-Synchrotron DESY, Hamburg, Germany
2. Niels Bohr Institute, University of Copenhagen, Copenhagen, Denmark
3. NanoLund, Department of Physics, Lund University, Lund, Sweden
4. National Research Tomsk Polytechnic University (TPU), Tomsk, Russia
5. European XFEL GmbH, Schenefeld, Germany
6. National Research Nuclear University MEPhI (Moscow Engineering Physics Institute), Moscow, Russia

Original publication

'X-ray Bragg Ptychography on a Single InGaN/GaN Core–Shell Nanowire', ACS Nano, 11, 6605–6611 (2017). DOI: 10.1021/acsnano.6b08122

References

1. M. H. Crawford, 'LEDs for Solid-State Lighting: Performance Challenges and Recent Advances', in IEEE Journal of Selected Topics in Quantum Electronics, 15, 4, 1028–1040 (2009).
2. H. X. Jiang and J. Y. Lin, 'Nitride micro-LEDs and beyond - a decade progress review', Opt. Express 21, A475–A484 (2013).
3. I. A. Vartanyants and O. M. Yefanov, 'X-ray Diffraction. Modern Experimental Techniques', O. H. Seeck and B. M. Murphy, Eds.; Pan Stanford Publishing: Singapore, Chapter 12, 341–384 (2015).
4. D. Dzhigaev et al., 'Theoretical analysis of the strain mapping in a single core-shell nanowire by x-ray Bragg ptychography', X-Ray Nanoimaging: Instruments and Methods II, edited by Barry Lai, Proc. of SPIE, 9592, 95920S (2015).
5. A. M. Maiden and J. M. Rodenburg, 'An improved ptychographical phase retrieval algorithm for diffractive imaging', Ultramicroscopy 109, 1256–1262 (2009).

Colour tuning in metal-halide perovskites through confinement in nanoporous thin films.

Microfocus high energy X-ray depth profiling of crystallite sizes

Metal-halide perovskites are inexpensive and easily processable next generation semiconductors. They show narrow band emission, at wavelengths that can be tuned by exploiting quantum size effects. In this work the perovskite solid-state confinement in nanoporous oxide matrices was demonstrated as a general strategy to control the size of the nanocrystallites (< 10 nm). Under these conditions strong quantum size effects are observed. Tuning of photoluminescence in the range between near infrared and ultraviolet was achieved by manipulating the size of perovskite crystals through confinement in nanoporous alumina or silicon scaffolds.

Tuning the band gap of semiconductors via quantum size effects fostered the development of optoelectronics [1] and photovoltaics [2]. For metal-halide perovskites colour tuning approaches vary between altering halide stoichiometry [3] and synthesis of colloidal particles [4]. The use of nanoporous alumina (npAAO) or silicon (npSi) scaffolds as templates for growth allows fine tuning of the photoluminescence (PL) across the visible spectrum and increased PL stability within device-relevant architecture without colloidal stabilization. The template-controlled size of the perovskite crystals was quantified in nanoporous silicon with microfocus high-energy X-ray depth profiling in transmission geometry, verifying the growth of perovskite nanocrystals throughout the entire thickness of the nanoporous films. Low-voltage light-emitting diodes (LEDs) with narrow, blue-shifted emission fabricated from nanocrystalline perovskites grown in embedded npAAO thin films support the general concept for next-generation photonic devices. Potential applications range from photon detectors and polarized or non-polarized electroluminescent devices to single-photon sources and metasurfaces.

The preparation of npSi is a galvanostatic electrochemical procedure which yields a spongy network of pores (Fig. 1a). The anodization current density during the procedure affects the pore diameter, therefore it is defining the upper size limit to perovskites nanocrystallites formed within. By reducing the current density and hence the pore size, normally infrared-emitting perovskites become visibly red, and green-emitting materials become cyan or blue (Fig. 1b). The potentiostatic electrochemical process is used to produce npAAO which results in an analogous matrix with pores at around 10 nm in diameter. This matrix was used for fabrication of perovskite LEDs with blue-shifted electroluminescence.

The wide angle X-ray scattering (WAXS) technique was used to investigate the size of the crystallites that form within the

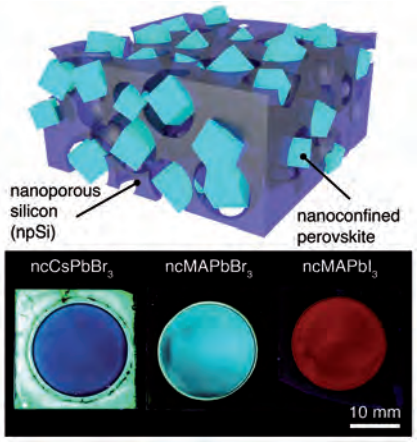

Figure 1
a) Schematic of npSi matrix with embedded perovskite nanocrystallites. b) Silicon samples with nanoporous area (circular) containing different confined perovskites under UV illumination. The difference between bulk (outside) and confined (inside) is especially pronounced in the $CsPbBr_3$ sample.

porous layers. The microfocused (vertical size 2-5 µm (FWHM)) and high energy (~100 keV) X-ray beam at the PETRA III beamline P07 allowed to probe the perovskite filled porous layers with the incident beam parallel to the sample surface. Due to this unusual geometry we were able to scan the few tens of µm thick layers in depth while reaching a good signal to noise ratio by letting the beam propagate for several millimetres through the sample. The measured diffraction patterns (Fig. 2a) show broadened Debye rings resulting from the perovskite crystallites. This signal is superimposed by a complex background, whose most prominent contribution are strongly broadened Si peaks due to the remaining single crystalline Si scaffold between the pores. In the background corrected and azimuthally averaged data, broadening of all perovskite peaks is clearly visible. Fig. 2b shows diffraction profiles for three methylammonium lead triiodide ($MAPbI_3$) filled porous layers which were etched at different current densities. Analogous diffraction profiles were acquired at different depths within the porous layers and the depth-dependent sizes of the $MAPbI_3$ crystallites were calculated for the three different samples using the Scherrer equation [5]. In Fig. 2c the results for $MAPbI_3$ in a porous Si layer that was etched at 15 mA cm^{-2} are

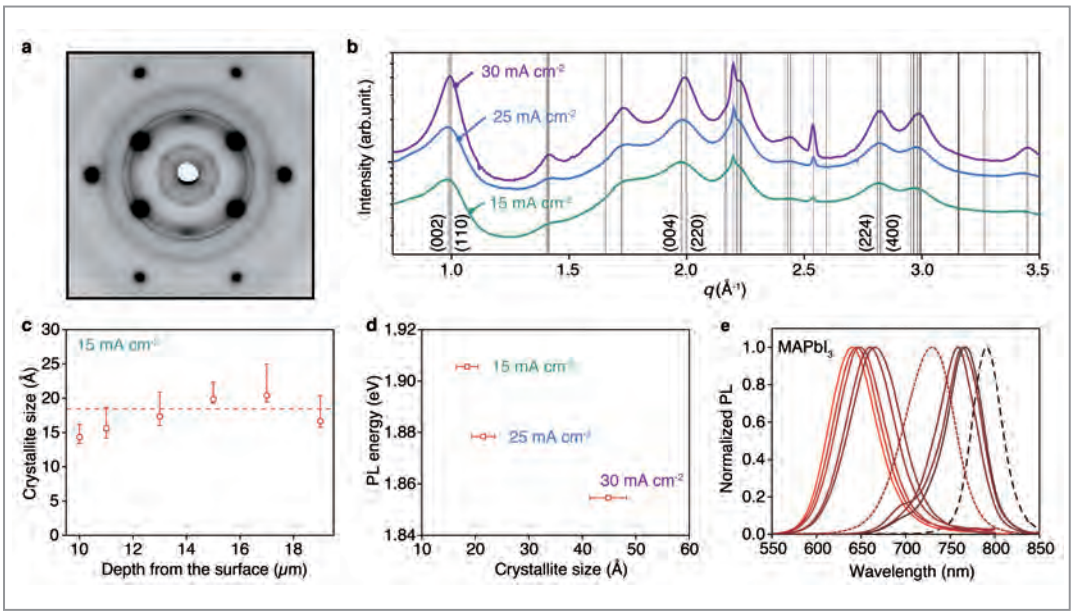

Figure 2

a) Diffraction pattern of $MAPbI_3$ nanocrystallites confined in npSi etched at 15 mA cm^{-2} probed 15 µm below the surface. b) Logarithmic plot of the background corrected azimuthally averaged intensity profiles of $MAPbI_3$ nanocrystals in npSi etched at different current densities as a function of the scattering vector q. The curves are normalized and vertically shifted for clarity. c) Crystallite size as function of depth (circles) and averaged over the entire layer (dashed line) for $MAPbI_3$ confined in npSi etched at 15 mA cm^{-2}. d) PL peak emission energy against the average size of crystallites formed in three npSi layers prepared with indicated anodization current density. e) PL spectra of $MAPbI_3$ confined in npSi etched at different current densities (lines) and npAAO (dots) compared to bulk $MAPbI_3$ (dash) emission.

presented as an example, showing a narrow distribution of crystallite sizes with the depth. We averaged the crystallite size over the whole layer thickness, yielding values of 1.8, 2.1 and 4.5 nm for $MAPbI_3$ crystallites in npSi etched at 15, 25 and 30 mA cm^{-2}, respectively. This decrease of the average crystallite size with decreasing current density directly causes an increase of the PL peak emission energy (Fig. 2d). Consequently, this is an strong indication that the observed blue shifts can be attributed to quantum size effects. The inference is in line with the fact that the calculated crystallite sizes are of the same order of magnitude compared to values reported for the Bohr radius of excitons in $MAPbI_3$ (2.2 and 2.8 nm) [6,7]. Other pore and crystallite sizes can be achieved by adjusting the current density, which is applied for the npSi preparation, allowing to control the peak PL wavelength (Fig. 2e).

From additional SAXS measurements performed at the PETRA III beamline P08 and analysed according to the Porod method [8] we estimated an average pore diameter of 4.0 nm in npSi etched at 15 mA cm^{-2}. This value is much bigger than the average crystallite size within these pores (4.0 nm vs. 1.8 nm). This result is an indication that the pore volume limits the amount of perovskite precursor solution accessible for the formation of each crystallite, which leads to an upper boundary of the crystal size.

We introduced a promising method to tune the optical properties of metal halide perovskites, by confining their growth in nanoporous thin films. Combining microfocus high energy WAXS experiments with SAXS measurements enables us to evaluate the sizes of the formed perovskite crystallites and the surrounding pores contributing to a better understanding of how the observed changes in the emission spectra arise.

Contact: Bert Nickel, nickel@lmu.de
Martin Kaltenbrunner, martin.kaltenbrunner@jku.at

Authors

Stepan Demchyshyn, Janina M. Roemer, Heiko Groiß, Herwig Heilbrunner, Christoph Ulbricht, Dogukan Apaydin, Anton Böhm, Uta Rütt, Florian Bertram, Günter Hesser, Markus Clark Scharber, Niyazi Serdar Sariciftci, Bert Nickel, Siegfried Bauer, Eric Daniel Głowacki and Martin Kaltenbrunner

Affiliation details at: http://advances.sciencemag.org/content/3/8/e1700738.full

Original publication

'Confining metal-halide perovskites in nanoporous thin films', Science Advances 3, e1700738 (2017). DOI: 10.1126/sciadv.1700738

References

1. P. O. Anikeeva, J. E. Halpert, M. G. Bawendi and V. Bulović, 'Quantum dot light-emitting devices with electroluminescence tunable over the entire visible spectrum', Nano Lett. 9, 2532–2536 (2009).
2. M. Yuan, M. Liu and E. H. Sargent, 'Colloidal quantum dot solids for solution-processed solar cells', Nat. Energy 1, 16016 (2016).
3. G. Nedelcu, L. Protesescu, S. Yakunin, M. I. Bodnarchuk, M. J. Grotevent and M. V. Kovalenko, 'Fast anion-exchange in highly luminescent nanocrystals of cesium lead halideperovskites ($CsPbX_3$, X = Cl, Br, I)', Nano Lett. 15, 5635–5640 (2015).
4. L. Protesescu, S. Yakunin, M. I. Bodnarchuk, F. Krieg, R. Caputo, C. H. Hendon, R. X. Yang, A. Walsh and M. V. Kovalenko, 'Nanocrystals of cesium lead halide perovskites ($CsPbX_3$, X = Cl, Br, and I): Novel optoelectronic materials showing bright emission with wide color gamut', Nano Lett. 15, 3692–3696 (2015).
5. P. Scherrer, 'Bestimmung der Größe und der inneren Struktur von Kolloidteilchen mittels Röntgenstrahlen', Göttinger Nachrichten Gesell. 2, 98–100 (1918).
6. K. Tanaka, T. Takahashi, T. Ban, T. Kondo, K. Uchida and N. Miura, 'Comparative study on the excitons in lead-halide-based perovskite-type crystals $CH_3NH_3PbBr_3$ $CH_3NH_3PbI_3$', Solid State Commun. 127, 619–623 (2003).
7. M. Hirasawa, T. Ishihara, T. Goto, K. Uchida and N. Miura, 'Magnetoabsorption of the lowest exciton in perovskite-type compound $(CH_3NH_3)PbI_3$', Phys. B Condens. Matter 201, 427–430 (1994).
8. G. Porod, 'Small Angle X-ray Scattering', Academic Press, (1982).

Vesicle origami.

Changing the shape of phospholipid vesicles

The route to a next generation of drug delivery vehicles leads through the advancement of basic physical properties of phospholipid liposomes. Here, the frontiers of phospholipid self-assembly have been expanded, and the first template-free self-assembled cuboid vesicles are presented. Experiments performed at DESY's PETRA III have been crucial in understanding phospholipids' biophysics. The phospholipids of interest build a hydrogen bonding network akin to the β-sheet of proteins and this is leading to very stiff membranes. Trapped into a 3D arrangement, the vesicles optimise the ratio of flat faces versus round edges so that a new, mechanoresponsive cuboid structure is formed.

Targeted drug delivery, the encapsulation and transport of a medication to a specific location in the human body, is still a formidable challenge for science. In order to achieve targeted delivery, a drug is typically enclosed in a nanosized carrier such as a phospholipid liposome to which a biological or chemical marker is attached acting as 'address tag'. Unfortunately, this concept only works well *in vitro* and the high hopes associated with this approach have not been confirmed for application in humans. As a new targeting strategy, we explore a trigger that is more fundamental than a biochemical or chemical marker: physics. A typical example for a physical (mechanoresponsive) trigger is the change of wall shear stress in healthy vs. narrowed or blocked human arteries. Using mechanoresponsive drug delivery devices, we and others are taking advantage of increased shear stress to release drugs locally [1]. In order to advance to the next generation of mechanoresponsive nanocontainers, a deeper understanding of the basic phospholipid vesicle biophysics is needed.

Mechanoresponsive nanocontainers can be self-assembled from phospholipids. However, phospholipids are designed by nature to form highly adaptable membranes that are not compromised by mechanical stress. To obtain a stiff membrane susceptible to mechanical stress the intermolecular attractive forces have to be made much stronger. Our group is specialised in the synthesis of artificial phospholipids and we exchanged the natural phospholipid fatty acyl esters (1) with amide moieties as depicted in Fig. 1. This led to strong intermolecular hydrogen bonding networks. Additional aspects under consideration were fatty acyl chain length and interleaflet interdigitation. This resulted in highly faceted phospholipid vesicles with membrane defects (Fig. 2) that are

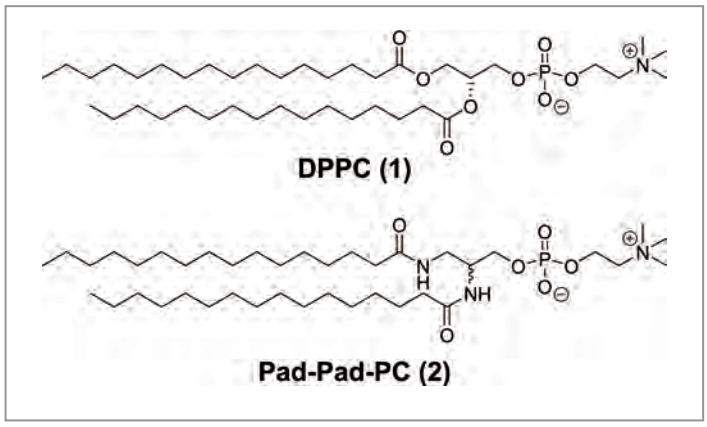

Figure 1

Chemical structure of the natural phospholipid DPPC (1) and the artificial diamidophospholipid Pad-Pad-PC (2). The fatty acyl ester functions have been exchanged by amide moieties.

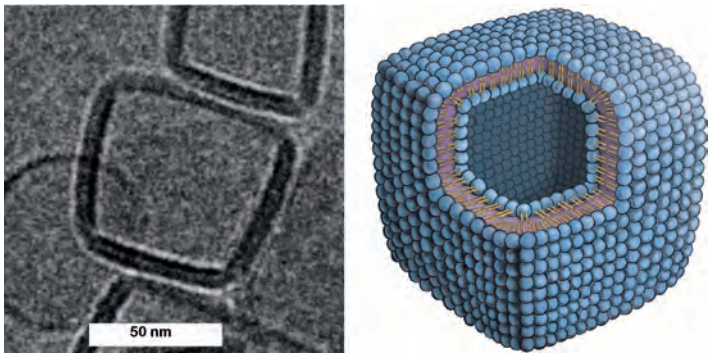

Figure 2

Cryo-transmission electron micrograph of a cuboid phospholipid vesicle. The figure has been adapted from the original publication. On the right an artist's rendering of the cube. The outer bilayer membrane leaflet is continuous, the inner leaflet is discontinuous. This results in membrane defects that are attenuated when the vesicle is exposed to shear stress and is the basis for mechanoresponsive drug delivery.

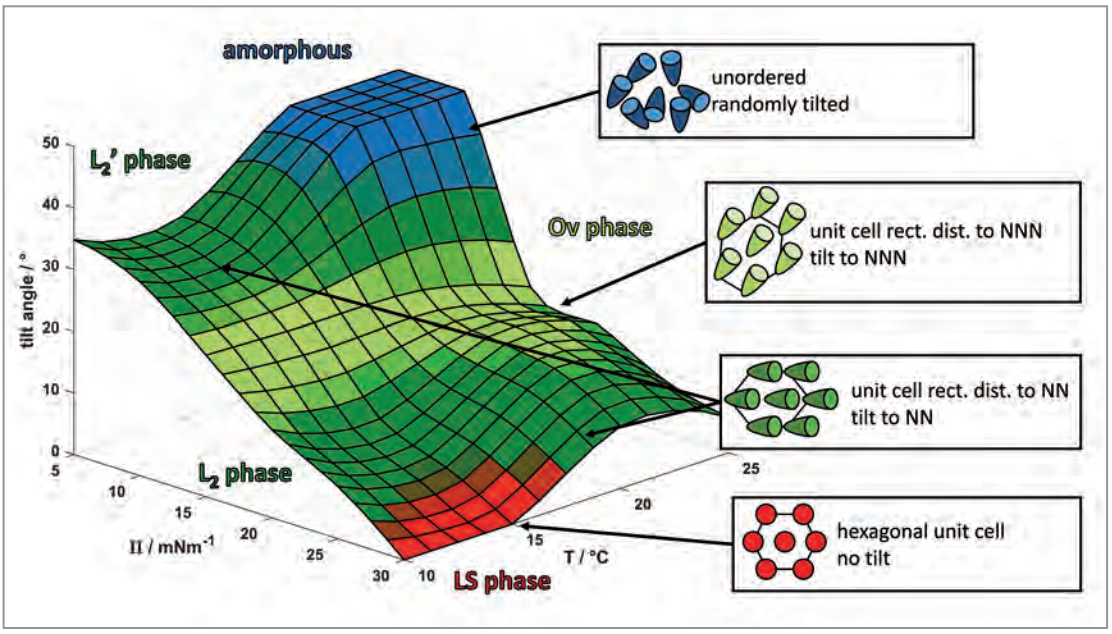

Figure 3

Phase diagram of the artificial phospholipid Pad-Pad-PC (2) measured under variable temperature T and surface pressure Π at the PETRA III beamline P08 taking the lipid tail tilt angle into account. The abbreviations describe the different monolayer phases (NN nearest neighbour, NNN next nearest neighbour). The cubes are formed when the phospholipids assemble in a subgel herringbone packing, which corresponds to the L_2' phase in the diagram.
The figure was adapted from the original publication.

attenuated under mechanical stress [2]. The membrane interdigitation and the hydrogen bonding interaction between phospholipid head groups are mutually exclusive forces, and we were interested in the effect of increased hydrogen bonding without interdigitation. Therefore, we have resynthesised a 1,2-diamidophospholipid that we termed Pad-Pad-PC (2). The molecule itself was already investigated in the 1990s when it was explored as an anti-HIV agent but was found to be of low activity [3]. At that time, however, the biophysics of the molecule was not studied so its surprising properties were left undiscovered.

Pad-Pad-PC (2) is the first phospholipid that self-assembles into cuboids (Fig. 2). Apparently, the hydrogen bonding network results in a tight lipid packing and very stiff layer inhibiting membrane curvature typically found in spherical vesicles. Energy minimisation of such a three-dimensional structure with flat stiff faces over edges is satisfied by the observed geometry of a cube. This should also be reflected in very tight phospholipid packing at the air/water interface during our monolayer experiments using a Langmuir-Pockels film balance. This long-established type of experimental setup allows studies of the phospholipid packing under defined lateral pressure and temperature, thus the film balance is still highly attractive and very versatile. At DESY's PETRA III beamline P08, a Langmuir-Pockels film balance is coupled with a synchrotron radiation source to enable grazing incidence-angle X-ray diffraction measurements.

Pad-Pad-PC (2) monolayers at low temperatures arrange into an extremely dense packing in a L_2' phase, with an area per fatty acyl chain of 19.2 Å^2 [4], as shown in Fig. 3. This is corroborated by bilayer small- and wide-angle X-ray scattering experiments and reflects a β-sheet packing found in natural proteins. The observed very dense packing of the fatty acyl chains is the main reason ultimately resulting in the cuboid vesicle geometry.

These results show that it is feasible to influence the shape of a soft matter object such as a vesicle by changing the physical forces at play such as hydrogen bonding and membrane interdigitation.

Contact: Andreas Zumbuehl, andreas.zumbuehl@unifr.ch

Authors

Frederik Neuhaus[1,2], Dennis Mueller[1], Radu Tanasescu[1], Sandor Balog[3], Takashi Ishikawa[4], Gerald Brezesinski[5] and Andreas Zumbuehl[1,2]

1. Department of Chemistry, University of Fribourg, Fribourg, Switzerland
2. National Centres of Competence in Research in Chemical Biology (Geneva) and Bio-inspired Materials (Fribourg), Switzerland
3. Adolphe Merkle Institute, University of Fribourg, Fribourg, Switzerland
4. Paul Scherrer Institute (PSI), Villigen PSI, Switzerland
5. Max Planck Institute of Colloids and Interfaces, Research Campus Potsdam-Golm, Potsdam, Germany

Original publication

'Vesicle Origami: Cuboid Phospholipid Vesicles Formed by Template-Free Self-Assembly', Angewandte Chemie, International Edition, 56, 6515–6518 (2017).
DOI: 10.1002/anie.201701634

References

1. **D. Mellal, A. Zumbuehl and 'Exit strategies – smart ways to release phospholipid vesicle cargo', J. Mater. Chem. B 2, 247–252 (2014).**
2. **M. N. Holme, I. A. Fedotenko, D. Abegg, J. Althaus, L. Babel, F. Favarger, R. Reiter, R. Tanasescu, P.-L. Zaffalon, A. Ziegler, B. Müller, T. Saxer and A. Zumbuehl, 'Shearstress sensitive lenticular vesicles for targeted drug delivery', Nat. Nanotechnol. 7, 536–543 (2012).**
3. **C. Jia and A. H. Haines, 'Diamide analogues of phosphatidyl choline as potential anti-AIDS agents', J. Chem. Soc. Perkin Trans 1, 2521–2523 (1993).**
4. **V. M. Kaganer, H. Möhwald and P. Dutta, 'Structure and phase transitions in Langmuir monolayers', Rev. Mod. Phys. 71, 779–819 (1999).**

Sudden shifts sharpen X-ray pulses.

Spectrally broad X-ray pulses can be sharpened by mechanical means

Nuclear resonance techniques use only a narrow fraction of the broad spectrum of pulses delivered by state-of-the-art X-ray sources. By squeezing off-resonant photons onto resonance via the precisely controlled motion of a resonant target, we have significantly increased the number of resonant photons in a given X-ray pulse. The enhanced intensity permits experiments that were previously unfeasible and further optimisation will open the door for new experimental possibilities with ultranarrow X-ray resonances.

Narrow X-ray resonances such as those of Mössbauer nuclei form the basis for a broad range of experiments based on high-precision spectroscopy and are a decisive component for novel applications in the realm of X-ray quantum optics [1-3]. However, the spectra of the short pulses delivered by modern X-ray sources are orders of magnitude broader in energy than the narrow resonances. Only a tiny fraction of the available photons interacts resonantly with the sample, while the vast majority of the photons produce an off-resonant background. This restricts the achievable spectral, spatial and temporal resolution for commonly-used narrow resonances, and has prevented experiments with the sharpest available resonances thus far.

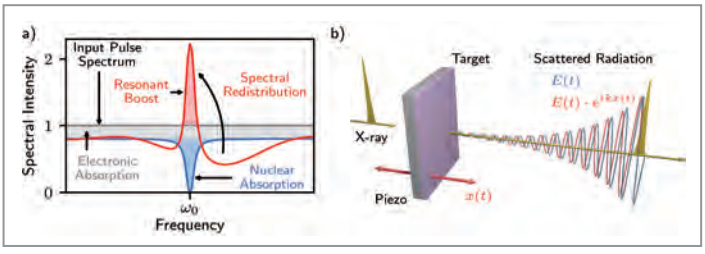

Figure 1

a) A target containing a narrow nuclear resonance usually imprints a resonant absorption dip onto the X-ray spectrum, accompanied by broadband electronic absorption (blue line, compared to the grey normalized input spectrum). Here, we manipulate this interaction and redistribute off-resonant photons of the X-ray pulse into resonance (red). Thus, the resonant intensity of the X-ray pulse increases rather than decreases, while the undesired off-resonant background is reduced.

b) The redistribution is achieved by applying fast mechanical displacements to the target, such that a time-dependent phase is imprinted onto the scattered light (red), compared to the case without motion (blue). Consequently, the interference with the unscattered light (yellow) is modified and enables one to tailor the spectrum of the resulting X-ray pulse.

To overcome this restriction, we developed and implemented a novel method to amplify spectrally-broad X-rays of pulsed X-ray sources in a narrow spectral region. Unlike monochromators, this method does not simply remove the undesired off-resonant background. Instead, off-resonant photons are converted into resonant ones, such that the number of resonant photons in the pulse is increased.

Pictorially, the method works like a mechanical digger that shapes a hill out of a flat landscape by removing earth at the sides and piling it up. Analogously, the new method removes photons in the off-resonant spectral region, and piles them up in a narrow resonant spectral region (Fig. 1a). In the actual experiments performed at the Dynamics Beamline P01 at PETRA III and the Nuclear Resonance Beamline ID18 at the ESRF, the role of the digger is taken by a piezoelectric material which performs specific motions upon precisely characterised and controlled electric signals. The ‘photon shovel’ is formed by a thin iron absorber foil on the piezo, which temporarily stores X-ray photons while it performs its motion (Fig. 1b). The operation of the piezoelectric photon shovel exploits the Mössbauer effect: Resonant nuclei, such as ^{57}Fe used in this experiment, can absorb and emit X-ray photons essentially without recoil, when embedded in a solid-state environment.

The working principle of the photon shovel is based on interference effects: Incoming resonant X-ray photons either pass through the sample without interaction or are temporarily absorbed by the ^{57}Fe foil. This absorption and re-emission of the light in the ^{57}Fe foil leads to a phase shift, such that the scattered photons destructively interfere with the non-interacting part. As a consequence, a dip due to absorption is observed in the spectrum. If instead the absorber foil is

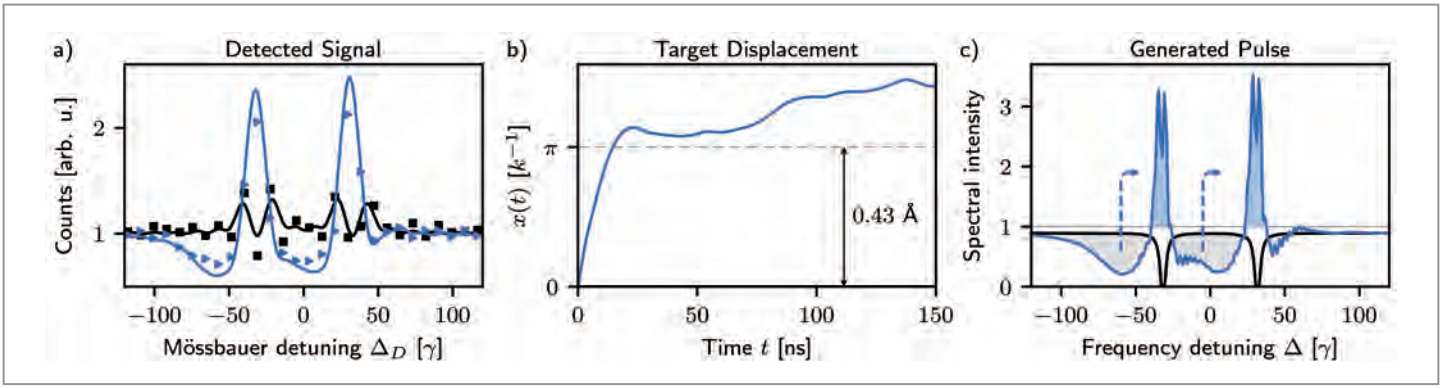

Figure 2

a) Experimental data together with fits. The Figure shows the number of photons in an integration window of 60 – 168 ns after the excitation as function of the Mössbauer detuning of the analyser foil. b) Actual piezo motion as a function of time, recovered from the experimental data. The indicated displacement of 0.43 Å is half the resonant X-ray wavelength. c) X-ray pulse spectra behind the piezo 'photon shovel' recovered from the experimental data and normalised to the input pulse spectrum. The black lines show the usual absorption dips of the magnetically-split nuclear resonance without motion. The blue curves show the spectrum for the motion in b), and clearly exhibit the conversion of absorption into enhancement on resonance. The dashed arrows indicate the spectral redistribution, which can be controlled via the piezo motion. Grey shaded areas indicate spectral regions from which photons were redistributed onto resonance.

displaced by half the resonant wavelength after the non-interacting part has passed the sample, but before most absorbed photons have been reemitted, the destructive interference can be converted into constructive interference. In this way, the number of resonant photons is increased. The motion not only affects the resonant photons, but conversely also attenuates the X-ray pulse in a spectral range around the narrow resonance. Overall, the enhancement of the resonant photon number is thus achieved by shovelling off-resonant photons onto the resonance.

Our experiments were performed with samples enriched in the isotope ^{57}Fe, which features a nuclear transition at 14.4 keV. Their displacements by half the resonant wavelength had to be controlled to less than a tenth of a nanometre, and took place within a few nanoseconds. The reconstruction of these motions from the measured spectra constituted a considerable part of the analysis. With the desired step-like displacements by half the resonant wavelength, an enhancement by a factor of up to four was observed for the number of photons on resonance as compared to the incoming photon number (Fig. 2). Theoretical calculations suggest that an enhancement by a factor of ten should be feasible with an optimised absorber foil and corresponding motion, limited only by the additional electronic attenuation due to the photon-shovel material. In a subsequent experiment, the possibility for further enhancements with multiple successive shovels was successfully demonstrated.

In the future, this new technique could be deployed in the routine operation of beamlines at synchrotrons and free-electron lasers. The increased intensity results in shorter measurement times and enables measurements with presently too low signal rates. Also, the higher signal rates translate into better energy and spatial resolution. Using different displacement patterns enables a more general manipulation of the X-ray spectra [4]. Furthermore, the mechanical control of X-ray-matter interactions could become a valuable tool in X-ray quantum optics, alleviating the need for additional X-ray control fields in certain settings. Finally, the technique also opens the possibility to track motions on atomic length scales in a wide range of scientific and technological applications.

Contact: Jörg Evers, joerg.evers@mpi-hd.mpg.de

Authors

Kilian P. Heeg[1], Andreas Kaldun[1], Cornelius Strohm[2], Patrick Reiser[1], Christian Ott[1], Rajagopalan Subramanian[1], Dominik Lentrodt[1], Johann Haber[2], Hans-Christian Wille[2], Stephan Goerttler[1], Rudolf Rüffer[3], Christoph H. Keitel[1], Ralf Röhlsberger[2], Thomas Pfeifer[1] and Jörg Evers[1]

1. Max-Planck-Institut für Kernphysik, Heidelberg, Germany
2. Deutsches Elektronen-Synchrotron DESY, Hamburg, Germany
3. ESRF – The European Synchrotron, Grenoble, France

Original publication

'Spectral narrowing of X-ray pulses for precision spectroscopy with nuclear resonances', Science 357, 375 (2017). DOI: 10.1126/science.aan3512

References

1. B. W. Adams, C. Buth, S. M. Cavaletto, J. Evers, Z. Harman, C. H. Keitel, A. Pálffy, A. Picón, R. Röhlsberger, Y. Rostovtsev and K. Tamasaku, 'X-ray quantum optics', Journal of Modern Optics 60, 2 (2013).
2. F. Vagizov, V. Antonov, Y. V. Radeonychev, R. N. Shakhmuratov and O. Kocharovskaya, 'Coherent control of the waveforms of recoilless γ-ray photons', Nature 508, 80 (2014).
3. J. Haber, K. S. Schulze, K. Schlage, R. Loetzsch, L. Bocklage, T. Gurieva, H. Bernhardt, H.-C. Wille, R. Rüffer, I. Uschmann, G. G. Paulus and R. Röhlsberger, 'Collective strong coupling of X-rays and nuclei in a nuclear optical lattice', Nat. Photonics 10, 445 (2016).
4. C. Ott, A. Kaldun, P. Raith, K. Meyer, M. Laux, J. Evers, C. H. Keitel, C. H. Greene and T. Pfeifer, 'Lorentz meets Fano in spectral line shapes: A universal phase and its laser control', Science 340, 716 (2013).

Incoherent diffractive imaging via intensity correlations.

A novel method allows for X-ray structure determination with atomic resolution using incoherently scattered light

Established X-ray diffraction methods like coherent diffraction imaging (CDI) rely on coherent scattering mechanisms for which incoherent processes like fluorescence emission or Compton scattering, often predominant, are usually considered detrimental. In a recent theoretical proposal and a first experimental verification at FLASH, we showed that also incoherently scattered X-ray radiation can be used for imaging. The novel method exploits intensity correlations rather than the intensity alone and offers a number of properties that are conceptually superior to coherent diffraction methods.

Since the discovery of X-ray diffraction from crystals over 100 years ago, X-ray crystallography has developed into a robust method for crystal structure determination with atomic resolution. However, many biologically relevant molecules cannot be crystallised, rendering them inaccessible for conventional crystallography methods. Here, modern accelerator-driven free-electron lasers (FELs) have opened new avenues that go far beyond conventional X-ray crystallography. The most prominent method in this field is coherent diffractive imaging (CDI) [1], the central goal of which is imaging of single nanoscopic objects, such as nanocrystals or even single molecules.

The above mentioned techniques rely on coherent scattering, i.e. scattering processes that maintain the first-order coherence of the radiation field throughout the imaging procedure. The fixed phase relation between incoming and scattered photons produces a stationary interference pattern upon measurement of a large number of photons, a central paradigm of the approach. However, the cross-sections of coherent scattering processes are often significantly lower than those of incoherent scattering, such as fluorescence emission or Compton scattering. This poses a strong challenge for CDI of single particles. In contrast, the new approach, termed incoherent diffractive imaging (IDI), relies on incoherently scattered or emitted X-ray radiation and as such benefits from considerably higher cross-sections.

IDI can be illustrated by Young's double slit experiment where we assume the fields at both slits possess randomly fluctuating phases, thus emulating the fluctuating phases of fluorescence emission by two atoms. On a short time scale, i.e. shorter than the coherence time of the fields, a detector in the far field will observe a stationary interference pattern. However, due to the randomly fluctuating phases, the pattern will shift in position on the detector if observed for times longer than the coherence time – even though the strength and period of the fringes remain constant as they depend only on the slit arrangement. Consequently, when averaging over times longer than the coherence time the intensity pattern vanishes, together with all structural information encoded in the pattern.

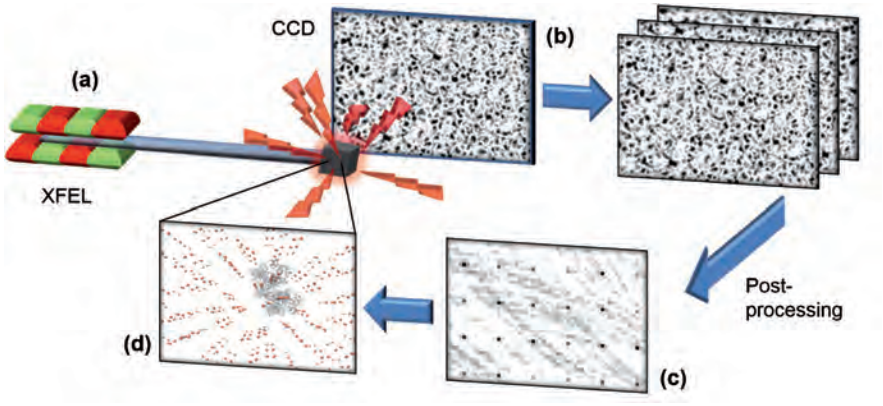

Figure 1

Schematic setup of IDI. Light from a XFEL (a) is incoherently scattered from the sample (red flashes). A CCD camera captures a snapshot (b) of the incoherently scattered light. Taking a series of snapshots and evaluating the intensity correlation function yields the Fourier transform (c) of the original sample, allowing reconstruction of the object (d).

The central idea of IDI is to capture snapshots of the diffraction pattern with exposure times shorter than the coherence time (Fig. 1b). Averaging the intensity patterns over many such snapshots would again wipe out the structural information. However, computing the autocorrelation of the intensity pattern for each snapshot and averaging the autocorrelations over many snapshots builds up a fringe pattern, as the autocorrelations are insensitive to the shift of the fringes (see Fig. 1c). As it turns out, the resulting fringe pattern is identical to the interference pattern of CDI, apart from a decrease in contrast.

For incoherent X-ray fluorescence, the coherence time is on the order of a few femtoseconds. Fortunately, the corresponding temporal resolution can be achieved with the ultrashort pulses from current FELs such as the Linac Coherent Light Source (USA) or the European XFEL (Germany).

In a first demonstration of IDI at FLASH, the coherent VUV radiation of the FEL beam was spatially and temporally randomised to produce incoherent light. The radiation was then sent to a hexagonal arrangement of six square-cut holes of micrometre size, etched into an opaque mask. This arrangement effectively mimics the fluorescence emission by the six carbon atoms of a benzene molecule. A CCD detector placed in the far field of the mask measured the shot-to-shot interference pattern, where each shot created a different pattern (Fig. 2a). For the reconstruction of the object, we did not rely only on the second-order intensity correlations, but evaluated correlations up to the fourth order (Fig. 2b). This allowed the isolation of different spatial frequencies of the object within different correlation orders, enabling a sequential determination of all spatial frequencies with higher precision and potentially sub-Abbe resolution (Fig. 3) [2].

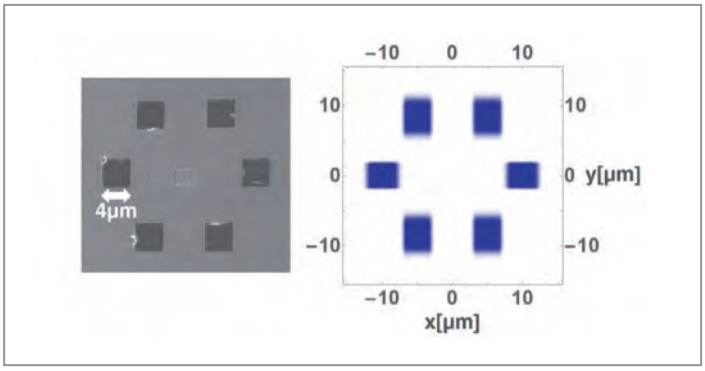

Figure 3

Left: Electron microscope image of the sample, mimicking a hexagonal benzene ring structure. Right: Reconstructed image of the benzene ring structure using the new method based on IDI. Image: Nature Physics

IDI bears a number of advantages with respect to coherent diffraction methods. Since the method uses fluorescence, typically a much stronger signal is obtained. Moreover, the signal is scattered to significantly larger angles, thereby increasing the spatial information and resolution. In addition, filters can be used to measure the light of specific atomic species only. This makes it possible to determine the position of individual atoms in molecules and proteins with significantly higher resolution compared to CDI. This method could give new impetus to structure determination of proteins in structural biology and medicine down to the level of single molecules.

Contact: Joachim von Zanthier, joachim.vonzanthier@fau.de

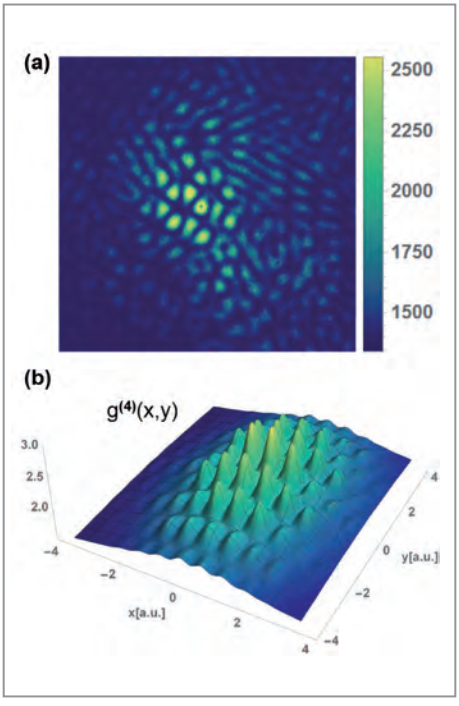

Figure 2

(a) Example of a single shot speckle pattern as measured by the CCD. (b) 10.800 single shot speckle pattern were processed to obtain the fourth order intensity correlation function $g^{(4)}(x,y)$, where three pixel detectors are fixed at specific locations and $g^{(4)}$ is plotted as function of the position (x,y) of the last detector.

Authors

A: Anton Classen, Kartik Ayyer, Henry N. Chapman, Ralf Röhlsberger and Joachim von Zanthier
Affiliation details at: https://journals.aps.org/prl/abstract/10.1103/PhysRevLett.119.053401

B: Raimund Schneider, Thomas Mehringer, Giuseppe Mercurio, Lukas Wenthaus, Anton Classen, Günter Brenner, Oleg Gorobtsov, Adrian Benz, Daniel Bhatti, Lars Bocklage, Birgit Fischer, Sergey Lazarev, Yuri Obukhov, Kai Schlage, Petr Skopintsv, Jochen Wagner, Felix Waldmann, Svenja Willing, Ivan Zaluzhnyy, Wilfried Wurth, Ivan A. Vartanyants, Ralf Röhlsberger and Joachim von Zanthier
Affiliation details at: https://www.nature.com/articles/nphys4301

Original publications

A: 'Incoherent Diffractive Imaging via Intensity Correlations of Hard X Rays', Phys. Rev. Lett. 119, 053401 (2017). DOI: 10.1103/PhysRevLett.119.053401
B: 'Quantum imaging with incoherently scattered light from a free-electron laser', Nature Physics, published online October 30, 2017; DOI: 10.1038/nphys4301

References

1. A. Barty, J. Küpper and H. N. Chapman, 'Molecular Imaging Using X-Ray Free-Electron Lasers', Annu. Rev. Phys. Chem. 64, 415 (2013).
2. A. Classen, F. Waldmann, S. Giebel, R. Schneider, D. Bhatti, T. Mehringer and J. von Zanthier, 'Superresolving Imaging of Arbitrary One-Dimensional Arrays of Thermal Light Sources Using Multiphoton Interference', Phys. Rev. Lett. 117, 253601 (2016).

Nuclei exchange photons.

Observation of strong coupling Rabi oscillations between nuclear ensembles in a multilayer cavity

Coherent control of light is at the heart of most modern applications of optics, for example for spectroscopy and technology. To achieve coherent control, it is crucial to reach the strong coupling regime between light and matter. In this regime, two degrees of freedom couple so strongly with each other that they exchange a photon several times before the combined system dissipates its energy. Usually, this takes place between a light field and an electromagnetic resonance of some material. Here, we observe the temporal signature of this phenomenon, the so-called Rabi oscillations in the X-ray regime between two ensembles of resonant nuclei.

Rabi oscillations are the repeated absorption and re-emission of a photon by a resonance of matter. Their observation permits a host of subtle and sophisticated experiments in quantum optics: for instance, the observation of photon entanglement and the control and manipulation of quantum states of matter [1]. The latter is needed for the implementation of quantum technologies and novel spectroscopic techniques. Particularly for this reason, the observation of Rabi oscillations in the X-ray range is a sought-after result [2]. Unfortunately, the observation of Rabi oscillations in the X-ray regime is hampered by the fact that strong coupling with Rabi oscillations requires that the decay constants of the participating degrees of freedom are much smaller than the interaction constant between the light field and the resonance. In other words, Rabi oscillations cannot be observed if an excitation's decay takes place on a timescale shorter than that of the Rabi oscillations. Commonly, Rabi oscillations are observed by coupling a light mode to a matter resonance in a high-quality cavity. In the X-ray range though, cavities of sufficient quality are not yet available.

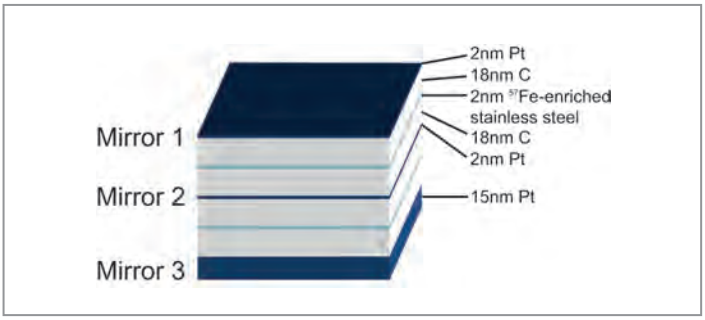

Figure 1

Sketch of the cavity. Sandwiched by Pt mirrors, two identical carbon cores contain ^{57}Fe-enriched stainless steel. Standing waves form inside the carbon cores. This compound has only weak magnetic hyperfine fields, and thus forms an almost perfect single-resonance line sample. A thin Pt layer between the cavities serves both as a mirror and a coupler.

We present here a different approach which has allowed us to observe Rabi oscillations and equivalently, the Rabi splitting in energy-space. We make use of the 14.4 keV nuclear resonance of ^{57}Fe – a workhorse resonance of quantum optics in the X-ray range [3,4]. The main advantage is a very long decay time of 144 ns, corresponding to a spectral width of only 5 neV. This decay can be monitored in the time domain with fairly standard detection electronics.

When a thin layer of ^{57}Fe is placed in a cavity, the latter will change the spectral properties of the nuclear resonance. As described before, strong coupling cannot directly be reached in that way. Two other effects stand out: (1) superradiance, i.e. a speed-up of the nuclear decay and (2) the collective Lamb shift, an energy shift resulting from mutual dipole-dipole interactions of the nuclei in the layer. The collective Lamb shift can be tuned in sign and magnitude by varying the detuning between the nuclear and cavity resonance. This also changes the superradiant decay time, albeit with the natural lifetime as a lower bound. In a sense, the complete cavity-nuclear layer-system may be regarded as an artificial atom with tunable spectroscopic properties.

The novel idea of our experiment is to place two nuclear ensembles in two cavities and couple these cavities with each other. This is done simply by sputter depositing identical copies of the same cavity on top of each other on a silicon substrate (Fig. 1), which is like coupling two artificial atoms

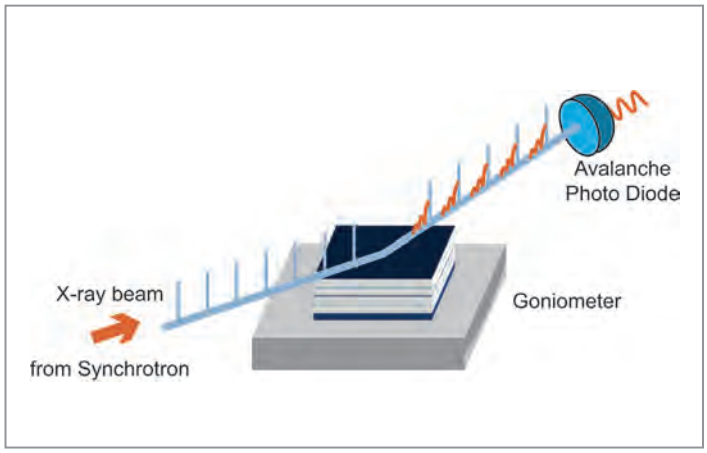

Figure 2

Setup of the experiment. A pulsed beam from the synchrotron illuminates the sample, which is placed on a goniometer. The latter is used to position the sample at an appropriate angle, detuned from the cavity modes. The pulses that get reflected from the sample carry a tail of delayed photons (orange) with them; this delayed part of the pulse has the temporal shape of Rabi oscillations.

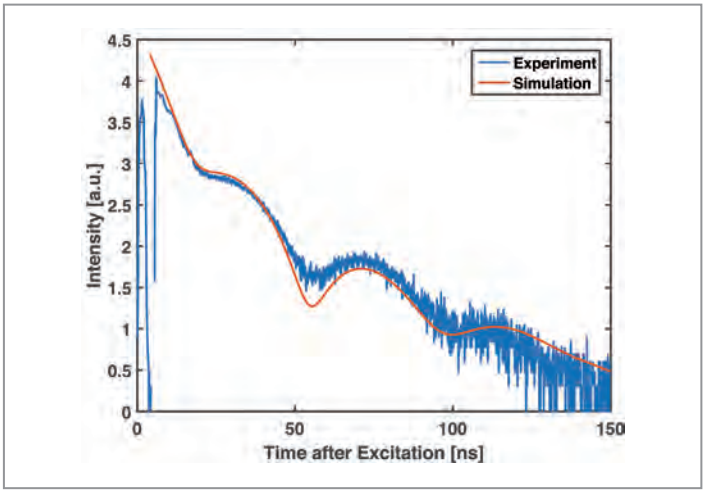

Figure 3

Observation of the temporal signature of Rabi oscillations. In the experimental data, the exponential decay (corresponding to the lifetime of ^{57}Fe) is superimposed with an oscillatory component, the signature of Rabi oscillations. The quantum optical model (orange) describes the experimental observation very well.

with each other. This provides now the degrees of freedom to achieve Rabi oscillations. The decay times are the superradiant decays of the individual ^{57}Fe layers; the interaction is between the layers and the coupling strength can be tuned by varying the thickness. It turns out that the magnitude of the coupling strength follows the same dispersion as the collective Lamb shifts. An examination of a theoretical model of the system reveals that when detuning the cavity modes from the ^{57}Fe-layers, this Lamb shift dispersion decays much slower than the superradiant decay strength. In other words, if the cavity modes are detuned far enough, the interaction between the two ^{57}Fe-layers will inevitably be stronger than their superradiant decay constants. Therefore, the precondition for strong coupling with Rabi oscillations is fulfilled: the decay constants of two degrees of freedom are smaller than their mutual interaction strength.

In order to actually observe the above phenomena, we performed an experiment at the ID18 beamline of the ESRF. A double cavity system was sputter-deposited on top of a silicon substrate. The resonant layers were made of stainless steel with an ^{57}Fe-content enriched to a purity of 95 %, yielding effective single-line resonances. The experiment was carried out in 16-bunch mode, leaving 170 ns between the pulses. The incoming beam illuminated the sample in grazing incidence, detuned far enough from the cavity modes. A high-resolution monochromator was used to narrow down the bandwidth of the incoming beam to 1 meV. A sketch of the setup is shown in Fig. 2.
In this configuration, non-resonant photons were reflected, while a resonant photon was absorbed by one of the two layers, starting the process of exchange between the layers. The temporal signal is shown in Fig. 3. When the photon was in the upper layer, it could be either emitted out of the system towards the detector, or to the other ensemble for absorption. This is the origin of the sinusoidal signal visible in the data, which corresponds to the probability of the photon being absorbed by the upper layer.

These results open up new avenues for quantum optical studies in the X-ray regime and are the first step to realise the entanglement of X-ray photons.

Contact: Ralf Röhlsberger, ralf.roehlsberger@desy.de

Authors

Johann Haber[1], Xianjing Kong[2], Cornelius Strohm[1], Svenja Willing[1], Jakob Gollwitzer[1], Lars Bocklage[1], Rudolf Rüffer[3], Adriana Palffy[2] and Ralf Röhlsberger[1]

1. Deutsches Elektronen-Synchrotron DESY, Hamburg, Germany
2. Max-Planck-Institut für Kernphysik, Heidelberg, Germany
3. European Synchrotron Radiation Facility, Grenoble, France

Original publication

'Rabi oscillations of X-ray radiation between two different nuclear ensembles', Nature Photonics 11, 720-725 (2017). DOI:10.1038/s41566-017-0013-3

References

1. J. M. Raimond, M. Brune and S. Haroche, 'Manipulating quantum entanglement with atoms and photons in a cavity', Rev. Mod. Phys.73, 565 (2001).
2. J. Haber, K. S. Schulze, K. Schlage, R. Loetzsch, L. Bocklage, T. Gurieva, H. Bernhardt, H.-C. Wille, R. Rüffer, I. Uschmann, G. G. Paulus and R. Röhlsberger, 'Collective strong coupling of x-rays and nuclei in a nuclear optical lattice', Nature Photonics 10, 445–449, (2016).
3. F. Vagizov, V. Antonov, Y. V. Radeonychev, R. N. Shakhmuratov and O. Kocharovskaya, 'Coherent control of the waveforms of recoilless gamma-ray photons', Nature 508, 80–83 (2014).
4. R. Röhlsberger, K. Schlage, B. Sahoo, S. Couet and R. Rüffer, 'Collective Lamb shift in Single-Photon Superradiance', Science 328, 1248–1251 (2010).

Four isomers hidden in ten millions of possibilities.

Revealing molecular structure of giant icosidodecahedral supramolecule

An unprecedented nanosized spherical supramolecule with a unique organometallic core beyond the fullerene topology was synthesised. According to the X-ray structure analysis, 20 copper atoms and 12 pentaphosphaferrocene units form a giant icosidodecahedron. The copper atoms are statistically distributed over 30 vertices of the polyhedral core. Therefore, the true molecular structure is hidden by this disorder. A synergy of chemical, structural and mathematical methods was required to reveal the structure of the individual molecule. It was shown that among millions of possible combinations, only two pairs of enantiomeric supramolecules are possible given the bidentate bridging coordination of the $(CF_3SO_3)^-$ ligands. DFT calculations for optimised geometries of each isomer proved that they are equally stable suggesting their co-crystallisation.

The world of hollow discrete spherical supramolecules based on the family of R-substituted pentaphosphaferrocenes $[Cp^RFe(\eta^5\text{-}P_5)]$ and copper(I) halides (X = Cl, Br) is a world of unceasing fascination due to the beauty and elegant complexity of supramolecular aggregation [1]. The diversity of polyhedral shapes and molecular topologies arises via the self-assembly of fivefold-symmetric building blocks provided by five phosphorus atoms of $[Cp^RFe(\eta^5\text{-}P_5)]$ according to [2-4]. Among them, the most symmetrical supramolecule to date consists of 12 $[Cp^{Bn}Fe(\eta^5\text{-}P_5)]$ units (1) and 20 Cu atoms ($Cp^{Bn} = \eta^5\text{-}C_5(CH_2Ph)_5$) (see Fig. 1). Its 80-vertex dodecahedral core contains only five- and six-membered rings and represents an inorganic analogue of C_{80} fullerene (Fig. 1c) [5]. To access supramolecules with an even larger core, the use of multifunctional anions is a logical step. In contrast to the terminal halides, they can be embedded in the molecular core between the units 1 and therefore expand it (Fig. 1a, c). We chose triflate (OTf = $CF_3SO_3^-$) as a convenient anion, which can be 3-coordinated towards copper. The desired scaffold-constructing role of the triflate would alter the common fullerene-topology opening a new chapter in supramolecular aggregation using a fivefold symmetric building block.

The self-assembly of the pentaphosphaferrocene 1 with Cu(OTf) leads to a spherical supramolecule $[\{1\}_{12}\{Cu(OTf)\}_{19.6}]$ (3) with a diameter of 3.3 nm (Fig. 1). The idealised inorganic scaffold of the supramolecule 3 is constructed by 12 units of 1 with the same dodecahedral arrangement as in the supramolecule $[(1)_{12}(CuX)_{20}]$ (2). However, the scaffold in 3 is expanded through the insertion of the bridging triflate ligands between the P_5 rings (Fig. 1a, b). Each of the twenty vertices of the parent dodecahedron is truncated by triangles of the triflate anions to give an icosidodecahedron consisting of 12 pentagonal and 20 triangular faces (Fig. 1c, d). The resulting icosidodecahedral supramolecule $[\{1\}_{12}Cu_{30}(OTf)_{20}]^{10+}$ would be tenfold positively charged. However, the supramolecule 3 is neutral and must have ten empty positions among 30 copper positions somehow distributed over the vertices of the icosidodecahedron. In other words, in the scaffold of 3 with the ideal composition $[\{1\}_{12}Cu_{20}(OTf)_{20}]$, intrinsically one third of copper positions are vacant. The X-ray structure analysis for 3, performed at the P11 beamline of PETRA III, reveals 30 unique Cu sites, which all have occupancy factors between 0.2 and 0.9. This means that, in the solid state, only the so-called average structure of 3 can be verified and, in contrast

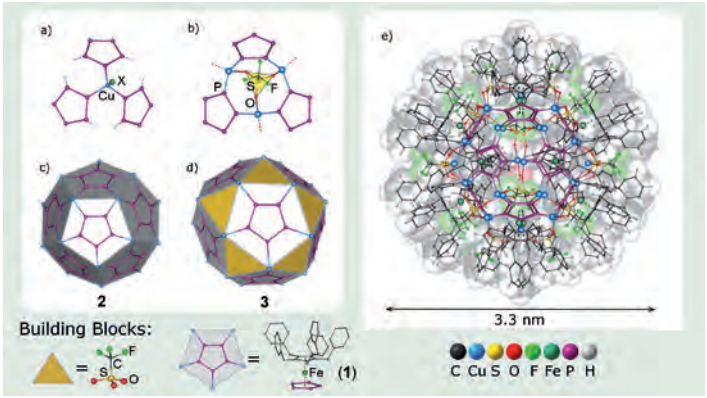

Figure 1

Rational design of the supramolecule 3. Modification of the (a) known dodecahedral inorganic core of 2 to the (b) novel core 3 by insertion of triangles of the triflate ligands between the P_5 rings of the core. Resulting transformation of the (c) 80-vertex dodecahedron 2 into the (d) 90-vertex icosidodecahedron 3. (e) The X-ray average structure of the icosidodecahedral supramolecule 3 (shown by van der Waals spheres), which is 0.2 nm larger than the 80-vertex fullerene-analogue 2.

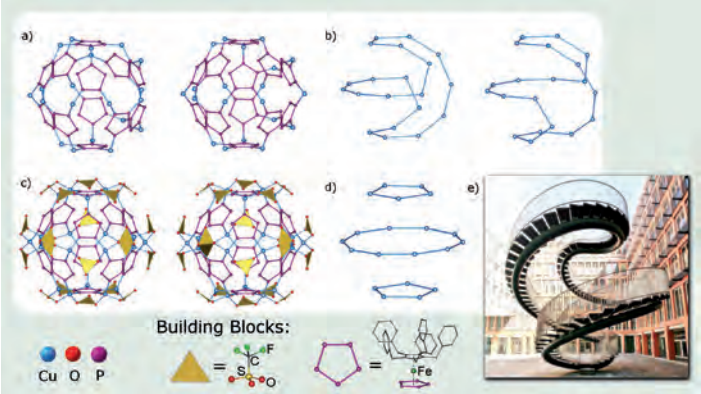

Figure 2

Isomerism of the supramolecule 3. (a) The chiral $Cu_{20}P_{60}$ cores and the (b) chiral arrangements of copper atoms in two enantiomers of D_2 isomer; (c) Two enantiomers of D_5 isomer with chiral arrangements of the triflate anions; (d) achiral arrangement of copper atoms in the core of both D_5 enantiomers; (e) the 'Endless staircase' sculpture by Olafur Eliasson (KPMG company office in München).

to small molecules, the structure of individual supramolecules cannot be determined explicitly by X-ray structural analysis.

There are different possibilities to occupy the two thirds of the copper sites in the icosidodecahedral scaffold. One would intuitively think that the number of these possibilities or, in other words, permutational isomers of the supramolecule must be huge. In fact, the upper estimate resulted in 10015005 possible isomers! With a computer program coded for this purpose, all of them were generated. The number of the resulting isomers was additionally restricted with justified structural requirements. First, any copper arrangement must not fragment the supramolecular core. This implies that each triflate must be at least bidentate towards copper atoms. After exclusion of all isomers with terminal triflates, only 12 arrangements were left. Then, the truly unique isomers were further distinguished regarding their rotations or reflections. Finally, only four individual isomers of the scaffold 3 were derived, namely two enantiomeric pairs with D_2 and D_5 point symmetries, respectively (Fig. 2).

In the D_5 isomer, the Cu atoms form three distinct rings around the fivefold axis, whereas two units of 1 show 1,2,3,4,5- and ten 1,2,4-coordination modes to copper, respectively (Fig. 2c). The $Cu_{20}P_{60}$ part of the scaffold itself is not chiral, and only the slight mutual rotation of the SO_3 groups of the coordinating triflate anions gives rise to enantiomers (Fig. 2d).

In the D_2 isomer, Cu atoms run over the surface of the icosidodecahedron in a loop (Fig. 2b). This arrangement is a more uniform one than in the D_5 configuration and resembles the 'Endless Staircase' sculpture by Olafur Eliasson (Fig. 2e). The four and eight units of 1 possess 1,2,3,4- and 1,2,4-coordination modes, respectively. This scaffold is truly chiral, since one D_2 enantiomer cannot be transformed into the other without breaking chemical bonds with the copper atoms (Fig. 2a,b).

Yet, which of these isomers is more stable, the more symmetrical D_5 isomer or the more uniform D_2 isomer? To answer this question, DFT geometry optimisations at the EDF1/SBKJC level were performed resulting in the difference in energy of only 2.5 kcal/mol. Therefore, both D_5 and D_2 isomers should be equally stable and able to co-exist in the solid state.

Isomerism manifested by crystallographic disorder in molecules and ions is an ordinary phenomenon. However, the disorder of the giant clusters has only formally been described in scientific literature as an average structure. The resulting chemically essential interpretation is a constant challenge in this area. To the best of our knowledge, the modelling of isomers has never been attempted for giant clusters so far. In this work, we used the synergy of different scientific methods to present a first mathematical reconstruction of individual isomers of the novel icosidodecahedral supramolecule based on X-ray diffraction data.

Contact: Manfred Scheer, Manfred.Scheer@ur.de
Eugenia Peresypkina, peresyp@niic.nsc.ru
Alexander V. Virovets, a_v_virovets@yahoo.com

Authors

Claudia Heindl[1], Eugenia Peresypkina[1,2], Alexander V. Virovets[1,2], Ivan S. Bushmarinov[3], Michael G. Medvedev[3,4], Barbara Krämer[1], Birger Dittrich[5] and Manfred Scheer[1]

1. Institute of Inorganic Chemistry, Universität Regensburg, Regensburg, Germany
2. Nikolaev Institute of Inorganic Chemistry, Siberian Division of Russian Academy of Science, Novosibirsk, Russia
3. A. N. Nesmeyanov Institute of Organoelement Compounds, Russian Academy of Science, Moscow, Russia
4. N. D. Zelinsky Institute of Organic Chemistry, Russian Academy of Science, Moscow, Russia
5. Institute of Inorganic Chemistry and Structural Chemistry, Heinrich-Heine-Universität Düsseldorf, Germany

Original publication

'An Icosidodecahedral Supramolecule Based on Pentaphosphaferrocene: From a Disordered Average Structure to Individual Isomers', Angew. Chem. Int. Ed. 56, 13237–13243 (2017). DOI: 10.1002/anie.201706756

References

1. E. Peresypkina, C. Heindl, A. Virovets and M. Scheer, 'Inorganic Superspheres', Structure and Bonding 174, 321–373 (2016).
2. A. Schindler, C. Heindl, G. Balázs, C. Gröger, A. Virovets, E.V. Peresypkina and M. Scheer, 'Size-determining dependencies in supramolecular organometallic host-guest chemistry', Chem. Eur. J. 18, 829–835 (2012).
3. C. Heindl, E.V. Peresypkina, A.V. Virovets, W. Kremer and M. Scheer, 'Giant Rugby Ball $[\{Cp^{Bn}Fe(\eta^5\text{-}P_5)\}_{24}Cu_{96}Br_{96}]$ Derived from Pentaphosphaferrocene and $CuBr_2$', J. Am. Chem. Soc. 137, 10938-10941 (2015).
4. F. Dielmann, C. Heindl, F. Hastreiter, E.V. Peresypkina, A.V. Virovets, R. Gschwind and M. Scheer, 'A nano-sized supramolecule beyond the fullerene topology', Angew. Chem. Int. Ed. 53, 13605-13608 (2014).
5. F. Dielmann, A. Schindler, S. Scheuermayer, J. Bai, R. Merkle, M. Zabel, A.V. Virovets, E.V. Peresypkina, G. Brunklaus, H. Eckert and M. Scheer, 'Coordination polymers based on $[Cp^*Fe(\eta^5\text{-}P_5)]$: Solid-state structure and MAS NMR studies', Chem. Eur. J. 18, 1168-1179 (2012).

The longest bond.

Imaging the He_2 quantum halo

Usually the bond length of two particles is within the range of their interaction potential. For quantum halos it is the opposite: their particle density is mainly outside the range of the interaction potential, leaking into the potential barrier. Examples of quantum halos are known from nuclear, atomic and molecular physics. Their extended wavefunction goes along with an almost vanishing binding energy between the constituents. The faint van der Waals bond between two helium atoms is a prime example, where the largest part of the wavefunction is outside the potential well. Using FLASH as a light source and a COLTRIMS reaction microscope as a camera, we experimentally imaged the spectacular exponential decay of the tunnelling He_2-wavefunction over a range of more than 500 times the radius of the individual atoms.

Attractive and repulsive forces form the potential landscape between two particles. If this landscape allows for minima, the particles can condense into bound matter. The distance between the bound particles is typically defined by the position of those minima, this is where normally the wavefunction has its maxima. But in contrast to classical particles in a potential well the wavefunction is allowed to tunnel into the barrier of the potential, showing an exponential decay in this classical forbidden region [1]. The exponent of this decay depends on the height of the potential barrier. In the limit of a vanishingly low barrier the exponent gets so small that the wavefunction spreads so far into the barrier that much more probability density is found at large distances than in the potential well. Such a super extended feeble system, delocalised by quantum tunnelling, is called a quantum halo.

The van der Waals system consisting of two helium atoms, the helium dimer, fulfils the requirements to show this peculiar behaviour. The He–He interaction potential has a minimum of about 1 meV [2]. It is so shallow that it was debated for a long time if the zero point energy is larger than its potential depths or not. The existence of He_2 was proven experimentally in 1993 and 1994 [3,4] and the mean bond length was estimated to be 52 Å in 2000 [5], confirming the halo character of the dimer. This set the stage for the current work. Having the unprecedented power of FLASH and the possibilities offered by modern COLTRIMS reaction microscopes [6] in our hands allowed us to shoot for a far reaching goal. We aimed to obtain the first ever image of the wavefunction of a quantum halo. If successful, this would then allow us to determine the mean value of the bond length and establish a new reference value for the binding energy of He_2.

The dimer was investigated by ionising both atoms and detecting the two generated ions. The kinetic energy the two fragments acquire during Coulomb repulsion is dependent on their distance at the instance of ionisation. Therefore the internuclear distance can be reconstructed by measuring the kinetic energy release. As the bond is very weak any perturbation of the system during the ionisation process would affect the measured distance. Furthermore the ionisation probability must be independent of the internuclear distance and the alignment of the molecular axis. The process of single photoionisation at each centre fulfilled those conditions. In addition an ionisation

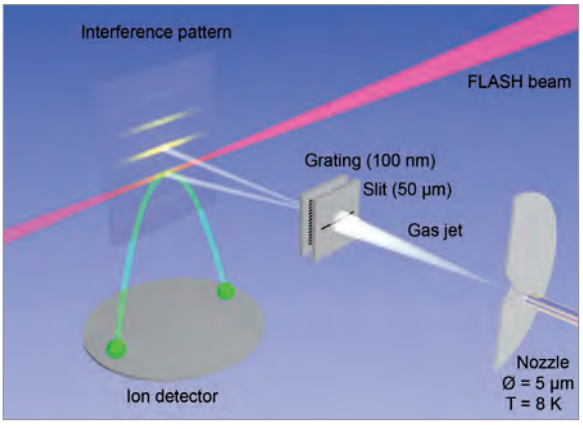

Figure 1
Experimental setup. Helium clusters are produced by expanding cooled gas through a 5 µm nozzle. A grating diffracts the different cluster sizes according to their mass. The FLASH beam ionises the first diffraction order of dimers while other cluster sizes do not reach the focus of the beam. An electric field deflects ionised particles onto a time and position sensitive detector.

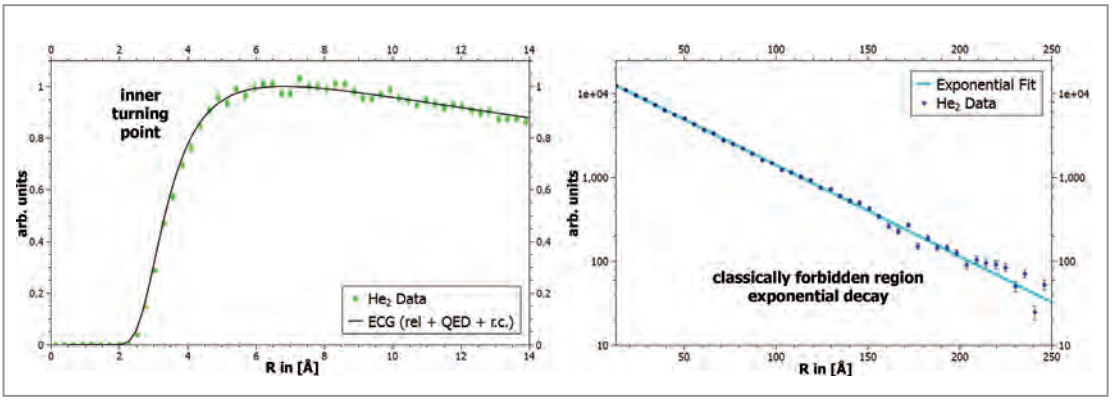

Figure 2

Measurement of the helium-dimer wavefunction. (left) Region of the inner turning point in agreement with theoretical calculations. (right) Classically forbidden tunnelling region on logarithmic scale. The binding energy of the system was obtained from the exponential slope. To conclude the exact value of 151.9 ± 13.3 neV the electron recoil has to be taken into account.

probability of unity was required for working with a very dilute target, given by the need to employ a pure helium dimer target.

The fragile helium dimers were generated by expanding cooled helium gas through a 5 µm nozzle (Fig. 1). This expansion, however, produces a mix of cluster sizes, which would render the results useless. To isolate the dimers the gas beam was split into mass selected sub beams using matter wave diffraction at a 100 nm transmission grating. The FLASH pulses (<100 fs, 18.5 nm) was then used to singly photoionise each of the atoms of the dimer inducing a Coulomb explosion, where from the measured energy of the fragments the internuclear distance can be inferred.

The probability distribution of the measured internuclear distances in the dimer is shown in Fig. 2. As there is only one bound state in the dimer (all excited rotational and vibrational states are unbound) this distribution represents a direct measurement of the square of the wavefunction of the helium dimer ground state $|\Psi|^2$. The distribution shows a wide range of distances, beginning at the inner turning point of the potential at around 2.5 Å and reaching several hundred Å into the classical forbidden tunnelling region. For internuclear distances larger than 30 Å the helium dimer potential is two orders of magnitude smaller than the predicted ground-state binding energy and therefore can safely be approximated to zero. So in this region the wavefunction is the solution of the Schrödinger equation below a step-like barrier which is given by a strict exponential decay. The slope of this decay is, besides the mass and Planck's constant ħ, only dependent on the height of the step-like barrier, which is the binding energy of the dimer. This enables to obtain the binding energy by an exponential fit to the measured distribution, resulting in a value of 151.9 ± 13.3 neV.

The theoretical value for the binding energy was disputed for many years. While early calculations predicted that the system might even be unbound, newer results give values between 44.8 and 161.7 neV. The most recent calculations include the quantum electrodynamical effect and relativistic effects in a full configuration interaction approach [2]. These supposedly most precise calculations predict a binding energy of 139.2 ± 2.9 neV, which is in good agreement with our measurement, while both, our measurement and this calculation, are in clear disagreement with several older predictions and the pioneering experimental results from Grisenti et al. [5], which were based on a much more indirect and error-prone technique.

Our study demonstrates the advantages of combining ultra-intense soft X-ray laser pulses with the spectroscopic possibilities of modern COLTRIMS reaction microscopes. Even so the high power light pulses of FLASH might seem like a hammer, in reality single photon ionisation is an extremely gentle and well controlled process which surprisingly makes FLASH the perfect tool to conduct measurements with neV (sub mK) precision.

Contact: Stefan Zeller, zeller@atom.uni-frankfurt.de
Reinhard Dörner, doerner@atom.uni-frankfurt.de

Authors

Stefan Zeller[1], Maksim Kunitski[1], Jörg Voigtsberger[1], Anton Kalinin[1], Alexander Schottelius[1], Carl Schober[1], Markus Waitz[1], Hendrik Sann[1], Alexander Hartung[1], Tobias Bauer[1], Martin Pitzer[1], Florian Trinter[1], Christoph Goihl[1], Christian Janke[1], Martin Richter[1], Gregor Kastirke[1], Miriam Weller[1], Achim Czasch[1], Markus Kitzler[2], Markus Braune[3], Robert E. Grisenti[1,4], Wieland Schöllkopf[5], Lothar Ph. H. Schmidt[1], Markus S. Schöffler[1], Joshua B. Williams[6], Till Jahnke[1] and Reinhard Dörner[1]

1. Institut für Kernphysik, Goethe-Universität Frankfurt, Frankfurt, Germany
2. Photonics Institute, Vienna University of Technology, Vienna, Austria
3. Deutsches Elektronen-Synchrotron DESY, Hamburg, Germany
4. GSI Helmholtz Centre for Heavy Ion Research, Darmstadt, Germany
5. Department of Molecular Physics, Fritz-Haber-Institut, Berlin, Germany
6. Department of Physics, University of Nevada, Reno, NV, US

Original publication

'Imaging the He_2 quantum halo state using a free electron laser', PNAS 113, 14651-14655 (2016). DOI: 10.1073/pnas.1610688113

References

1. A. S. Jensen, K. Riisager, D. V. Fedorov and E. Garrido, 'Structure and reaction of quantum halos', Rev. Mod. Phys. 76, 215–261 (2004).
2. M. Przybytek et al., 'Relativistic and quantum electrodynamics effects in the helium pair potential', Phys. Rev. Lett. 104, 183003 (2010).
3. W. Schöllkopf and J. P. Toennies, 'Nondestructive mass selection of small van der Waals cluster', Science 266, 1345–1348 (1994).
4. F. Luo, G. C. McBane, G. Kim, F. C. Giese and W. R. Gentry, 'The weakest bond: Experimental observation of helium dimer', J. Chem. Phys. 98, 3564–3567 (1993).
5. R. E. Grisenti et al., 'Determination of the bond length and binding energy of the helium dimer by diffraction from a transmission grating', Phys. Rev. Lett. 85, 2284–2287 (2000).
6. J. Ullrich et al., 'Recoil-ion and electron momentum spectroscopy: Reaction-microscopes', Rep. Prog. Phys. 1463–1545 (2003).

Attosecond metrology exposes dichotomy of electron motion.

Reversible and irreversible facets of strong light–matter interaction

Attosecond pump-probe spectroscopy has opened up the possibility to study light–matter interaction with unprecedented time resolution. Here, such spectroscopy is used to investigate the strong-field–driven electron dynamics of 'fuzzy' xenon atoms inside each laser cycle. We observe two opposite types of ultrafast electron motion induced by intense lasers: one corresponds to an irreversible, monotonic ion build-up process as predicted by a widely used model; another one is associated with a reversible, periodic electron displacement due to transient ground-state polarisation. Albeit well known in the weak-field regime, the role polarisation had so far been unnoticed, both experimentally and theoretically, in the strong-field regime.

Photoionisation is one of the most probable processes that can happen when light is coupled to matter's electronic degrees of freedom. More than fifty years ago, Keldysh introduced the tunnelling model of optical strong-field ionisation [1]. In his picture, the light field deforms the binding potential and creates a potential barrier that allows a bound electron to tunnel through and, thus, to become ionised. This mechanism marks the starting point for our understanding of various nonlinear phenomena caused by strong light–matter interaction. High-harmonic generation, for example, converts incident infrared radiation into a broad spectrum extending into the soft x-ray regime. Such a spectrum can then be used to synthesise attosecond bursts of light, making it possible to track and manipulate electron motion on its intrinsic time scale [2].

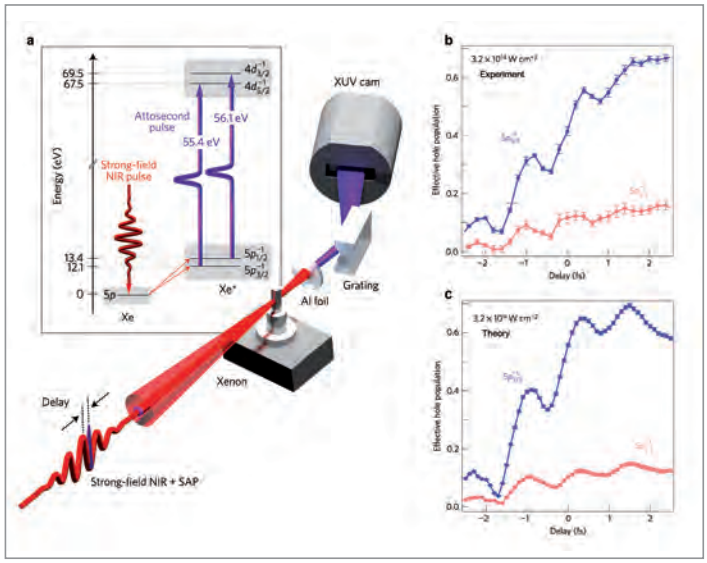

Figure 1

(a) Illustration of the ATAS experiment. An intense, few-cycle NIR laser (red) tunnel-ionises a 5p electron of xenon. A delayed single attosecond XUV pulse (violet, SAP) probes the valence hole by moving it to the 4d inner shell. Hole population dynamics, as a function of the delay, retrieved from the ATAS measurement (b) and predicted by quantum calculation (c).

Until recently, Keldysh's original idea and its extensions had been tested experimentally only in a time-integrated manner. The high-power laser fields that trigger tunnel ionisation typically oscillate with a period of a few femtoseconds. Thanks to the birth of attosecond spectroscopy [2], such tunnelling can now be examined in greater detail—by directly looking into each laser cycle. In this joint experiment-theory collaboration, we apply attosecond transient absorption spectroscopy (ATAS) to follow the strong-field electron dynamics of atomic xenon. We find that only part of the electron wave packet is actually ionised via the tunnel effect, while another part remains bound to the ion and undergoes strong periodic deformation. Although the latter aspect, polarisation, is well understood in weak-field scenarios, its significance had been overlooked in the strong-field context.

The concept of our ATAS experiment is shown in Fig. 1a. An intense, few-cycle near infrared (NIR) laser is used to ionise an electron out of the 5p valence shell of xenon. The system is subsequently probed by a weak, attosecond extreme-ultraviolet (XUV) pulse. If there is an electron vacancy, or a hole, in the 5p shell, an XUV photon can be absorbed, transferring the valence 5p hole down to an inner 4d hole. Intuitively, the strength of a characteristic XUV absorption line is proportional to the hole population in a specific valence orbital. By changing the delay between the NIR and XUV pulses, one can therefore map out the 5p hole population dynamics during strong-field ionisation.

The subcycle-resolved hole-creation processes in the two spin-orbit–split 5p levels of xenon are reconstructed from the ATAS spectrogram (Fig. 1b). At the given NIR intensity, tunnel ionisation is expected to govern the dynamics. This should

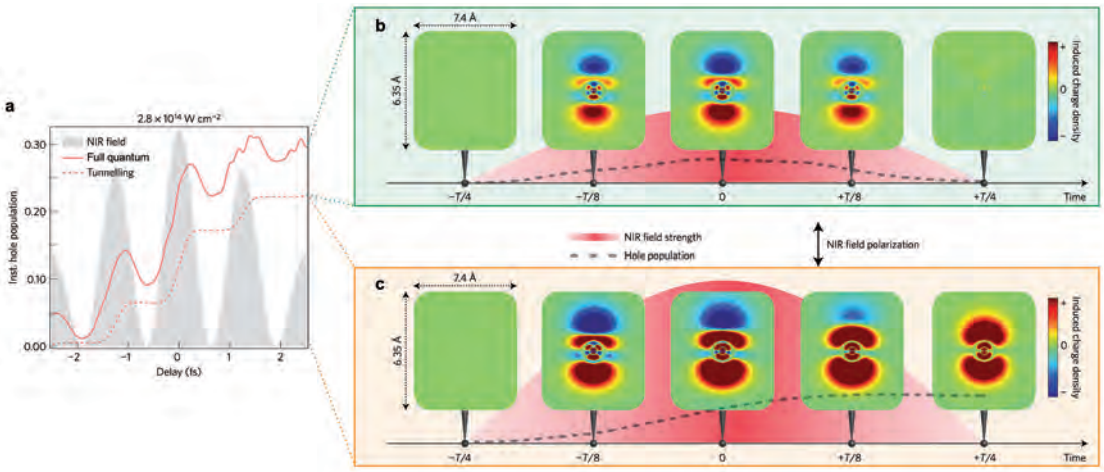

Figure 2

(a) Comparison between the full quantum dynamics (solid line) and the pure tunnel-ionisation dynamics (dashed line). (b) Evolution of the NIR-induced charge density of xenon within half of an NIR cycle. Polarisation leads to temporary separation of the positive and negative charges. After the half cycle, the electron cloud flows back and fills in the hole; i.e., this hole-creation pathway is reversible. (c) Tunnel ionisation results in irrecoverable loss of the negative charge. After the half cycle, part of the electron cloud disappears from the atom and permanently leaves a hole behind; i.e., this different hole-creation pathway is irreversible.

give rise to monotonically growing hole populations in sharp steps, separated by half of the NIR period. Particularly, around the nodes of the NIR field, the hole populations are supposed to form plateaus, since the instantaneous tunnel rates drop to zero. In our measurement, however, the hole dynamics exhibit a pronounced oscillatory feature superimposed on a rising background without any plateau structure. This departure from the anticipated tunnel behaviour is well captured by our first-principles quantum simulation under the experimental conditions (Fig. 1c).

Our theoretical tool may be utilised to reveal the mechanism behind the oscillatory character of the hole evolutions. To this end, the full quantum dynamics are compared with the pure tunnel-ionisation dynamics in Fig. 2a. As a first observation, the hole population in the full theory lies above the stepwise increasing tunnel background, so the oscillations represent overshoots, i.e., temporary enhancement of the hole population. Next, subtracting the tunnel reference from the full dynamics, we find that the overshoots are in synchrony with the NIR instantaneous intensity and scale linearly with the NIR peak intensity as it varies. This provides clear evidence that strong-field–induced polarisation of the atomic electron cloud is responsible for the recurring enhancement of the measured hole populations.

Polarisation periodically stretches the electron cloud back and forth from its field-free ground-state distribution, leading to an oscillatory component in the hole dynamics (Fig. 2b). On the other hand, tunnel ionisation permanently strips away an electron from its parent ion, resulting in a monotonic increment in the hole populations (Fig. 2c). Whereas the two mechanisms seem to dominate the electronic response of matter separately in the weak- and strong-field limits, our study shows the breakdown of such a clear-cut classification scheme: even deep in the strong-field regime, the two pathways, one reversible (polarisation) and one irreversible (tunnel ionisation), always coexist and both contribute to the electronic behaviour. This dichotomy of electron motion in intense laser fields, undetected in previous ultrafast experiments on lighter atoms [3,4], comes to light as a consequence of the high polarisability of xenon. Indeed, photoionisation is one, but not the only one, of the most probable processes in strong light–matter interaction.

Contact: Yi-Jen Chen, yi-jen.chen@cfel.de
Robin Santra, robin.santra@cfel.de

Authors

Mazyar Sabbar[1*], Henry Timmers[1*], Yi-Jen Chen[2*], Allison K. Pymer[3], Zhi-Heng Loh[4], Scott G. Sayres[5], Stefan Pabst[6], Robin Santra[2] and Stephen R. Leone[1,7]

1. Department of Chemistry, University of California, Berkeley, California, USA
2. Center for Free-Electron Laser Science, DESY and Department of Physics, University of Hamburg, Hamburg, Germany
3. Eastman Chemical Company, Kingsport, Tennessee, USA
4. Division of Chemistry and Biological Chemistry and Division of Physics and Applied Physics, School of Physical and Mathematical Sciences, and Centre for Optical Fibre Technology, The Photonics Institute, Nanyang Technological University, Singapore
5. School of Molecular Sciences and Biodesign Center for Applied Structural Discovery, Arizona State University, Tempe, Arizona, USA
6. ITAMP, Harvard-Smithsonian Center for Astrophysics and Physics Department, Harvard University, Cambridge, Massachusetts, USA
7. Chemical Sciences Division, Lawrence Berkeley National Laboratory and Department of Physics, University of California, Berkeley, California, USA

* These authors contributed equally to this work.

Original publication

'State-resolved attosecond reversible and irreversible dynamics in strong optical fields', Nature Physics 13, 472–478 (2017). DOI: 10.1038/nphys4027

References

1. L. V. Keldysh, 'Ionization in the field of a strong electromagnetic wave', Sov. Phys. JETP 20, 1307–1314 (1965).
2. F. Krausz and M. Ivanov, 'Attosecond physics', Rev. Mod. Phys. 81, 163–234 (2009).
3. M. Uiberacker et al., 'Attosecond real-time observation of electron tunnelling in atoms', Nature 446, 627–632 (2007).
4. A. Wirth et al., 'Synthesized light transients', Science 334, 195–200 (2011). laser field', Phys. Rev. A 62, 063204 (2000).

Cold, locked and rotating.

Tiny molecular motor caught on-the-fly by microwaves

Scientists often find inspiration in nature's fascinating designs, which drive, regulate, and boost the very fabric of life as we know it. The synthesis of artificial constructs with similar or even enhanced performances for tasks taking place at the molecular level are today's quests in modern synthetic chemistry. A recently introduced design of a molecular rotary motor is able to perform unidirectional motion triggered by light and heat. The functional performance of such a molecular machine emerges from its unique structural properties. We performed high-resolution microwave spectroscopy of an artificial molecular motor which allowed us to take a snapshot of the tiny molecule in the gas phase and determine its structure.

Molecular nanotechnology is strongly driven by our ability to observe, interpret and mimic the functionalities of naturally occurring molecular machinery. Inspired by nature's designs, synthetic chemists have engaged on a quest to synthesise artificial molecular machines that can perform similar functions at the molecular level, such as rotary [1-3] or translational [4] motion. These tasks can be today elegantly driven either chemically, with heat or simply by exposing the molecules to light. Light-driven molecular machines have the potential to trigger molecular responses giving a control-switch to a specific molecular action.

Much like its macroscopic counterpart, a molecular rotary motor has three components: a stator and a rotor, connected by an axle. The rotary motion occurs when the rotor rotates with respect to the stator via the axle. An artificial molecular motor with these structural properties has been designed by Chemistry Nobel laureate Ben L. Feringa at the University of Groningen in the Netherlands. The chemical structure of the motor and its components are shown in Fig. 1 and its operation mechanism can be shortly described in two key steps: first, an ultrafast light-driven process, followed by a thermally-driven helix inversion that brings the motor to a stop completing a half turn. Further photo-isomerisation and thermal steps return the motor to its initial configuration. This motion is unidirectional, i.e. the motor only works in one direction, which is a fairly useful functionality if one intends to incorporate it to perform tasks at the molecular level in a controlled manner.

In the study conducted at DESY, we used advanced high-resolution spectroscopy methods that combine microwave radiation with isolated molecules in a gas. A brief description of our experiment is given next, following the scheme given in Fig. 2. The motor molecules are heated to ca. 180° C and brought into the gas phase mixed with an inert carrier gas neon using a pulsed valve, generating a molecular beam via a so-called supersonic expansion. In this regime, the molecules in the molecular beam collide with the carrier gas and cool down to rotational temperatures close to 1 K. At this point the molecules are not interacting anymore with each other in the expansion and can be treated as being in isolation and internally cold.

The experiment continues as follows: a microwave chirp [5] (linear sweep covering 6 GHz of frequency bandwidth) is broadcast into the chamber containing the molecular beam thereby exciting the molecules in the beam and creating a macroscopic dipole moment arising from the generated polarisation of polar molecules in the expansion. Once the excitation stops, the molecules relax in a coherent manner in the form of a free induction decay (FID), similar to NMR spectroscopy. The FIDs are then detected, averaged and Fourier transformed to obtain the high-resolution rotational spectrum. At a repetition rate of 72 Hz, millions of acquisitions containing numerous rotational transitions can be averaged within a few hours. The duration of the detected FID defines the resolution obtained in the final spectrum. For this particular experiment, we detected the FIDs for 40 microseconds, which translates to a resolution of 25 kHz. 6 GHz of bandwidth at

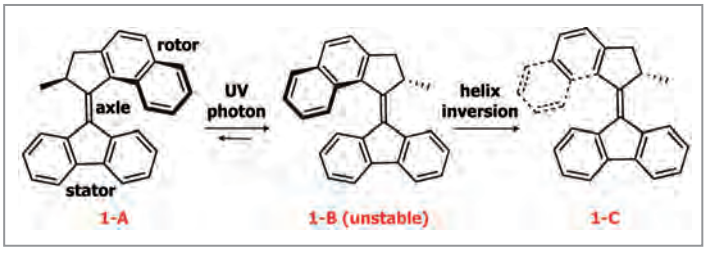

Figure 1

Structure of the molecular motor. The three components, namely rotor, axle and stator are indicated as well as the light-driven (power) and thermal strokes (helix inversion) required for operation. Further photon-driven and thermal isomerisation events return the motor to its original configuration 1-A.

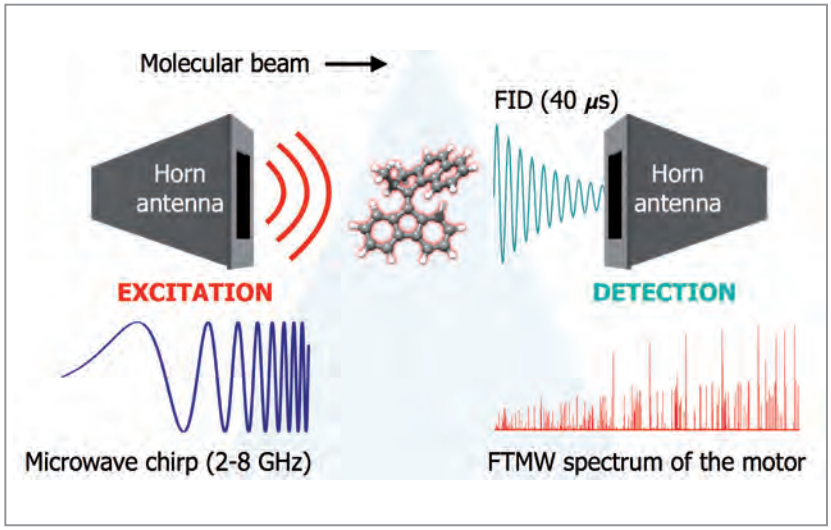

Figure 2

A microwave chirp (2-8 GHz) is broadcasted into the vacuum chamber via a horn antenna (excitation). The molecules interacting with the microwave field will generate a polarisation that is then recorded as a free induction decay (FID, detection) and Fourier transformed to obtain the final Fourier transform microwave (FTMW) spectrum of the molecular motor.

this resolution means that one can in principle resolve more than 300.000 transitions in our spectrum. These transitions form a fingerprint for each of the many molecular species that may be thermally populated in the molecular beam, and enable us to assign them to definite molecular structures. Owing to their unique moments of inertia, each conformation of a particular molecule can be differentiated by its rotational spectrum.

Using this experimental approach, more than 200 rotational transitions could be detected and assigned to the ground-state structure of the molecular motor. This study provided the first observation of a motor of this class in the gas phase. Its geometrical parameters could be compared with the ones obtained using other structure elucidation tools in the condensed phase [1-3]. In particular, comparing it with the crystal structure obtained with X-ray diffraction, structural changes are noted that, while not drastic, are noticeable and indicate that the motor is unmistakably affected by its environment. Moreover, due to the elevated heating necessary to generate vapour pressure to transport the motor into the gas phase, some of the motor molecules broke down at the axle. The not-so-unfortunate event allowed us to also detect transitions from the isolated motor components as dissociation products, namely the stator and the rotor.

While the observation of a molecular system of this size is certainly a milestone for the microwave spectroscopy community, molecular nanotechnology also gained a new, unexpected method to assist in the structure elucidation of functional molecular systems. Follow-up experiments include activation of the molecular motor on-the-fly using UV photons to drive the power stroke, initiating its unidirectional motion. Due to the long-lived intermediate conformations within the photo-cycle of this molecular machine, we aim to obtain the first direct observation of the actual structures of these key steps and further contribute to the understanding of the structure-function relations that emerge from these highly functional artificial molecular motors.

Contact: Melanie Schnell, melanie.schnell@desy.de
Sérgio Domingos, sergio.domingos@desy.de

Authors

Sérgio R. Domingos[1,2,3], Arjen Cnossen[4], Wybren J. Buma[5], Wesley R. Browne[4], Ben L. Feringa[4] and Melanie Schnell[1,2,3]

1. Deutsches Elektronen-Synchrotron DESY, Hamburg, Germany
2. Max Planck Institute for the Structure and Dynamics of Matter, Hamburg, Germany
3. Christian-Albrechts-Universität zu Kiel, Institute of Physical Chemistry, Kiel, Germany
4. Stratingh Institute for Chemistry and Zernicke Institute for Advanced Materials, University of Groningen, Groningen, The Netherlands
5. Van't Hoff Institute for Molecular Sciences, University of Amsterdam, Amsterdam, The Netherlands

Original publication

'Cold Snapshot of a Molecular Rotary Motor Captured by High-Resolution Rotational Spectroscopy', Angew. Chem. Int. Ed. 56, 11209–11212 (2017).
DOI: 10.1002/anie.201704221

References

1. J. Vicario, A. Meetsma, and B. L. Feringa, 'Controlling the speed of rotation in molecular motors. Dramatic acceleration of the rotary motion by structural modification', Chem. Commun. 5910–5912 (2005).
2. J. Conyard, A. Cnossen, W. R. Browne, B. L. Feringa, and S. R. Meech, 'Chemically optimizing operational efficiency of molecular rotary motors', J. Am. Chem. Soc. 136, 9692–9700 (2014).
3. J. Conyard, K. Addison, I.A. Heisler, A. Cnossen, W.R. Browne, B.L. Feringa, and S. R. Meech, 'Ultrafast dynamics in the power stroke of a molecular rotary motor', Nat. Chem. 4, 547–551 (2012).
4. M. R. Panman, P. Bodis, D. J. Shaw, B. H. Bakker, A. C. Newton, E. R. Kay, A. M. Brouwer, W. J. Buma, D. A. Leigh, and S. Woutersen, 'Operation mechanism of a molecular machine revealed using time-resolved vibrational spectroscopy', Science 328, 1255–1258 (2010).
5. G. G. Brown, B. C. Dian, K. O. Douglas, S. M. Geyer, S. T. Shipman, and B. H. Pate, 'A broadband Fourier transform microwave spectrometer based on chirped pulse excitation', Rev. Sci. Instrum. 79, 053103 (2008).

Molecules respond differently to high-intensity X-rays.

Discovery of new X-ray ionisation enhancement mechanism for molecules exposed to ultra-intense hard X-rays

Understanding how matter interacts with high-intensity X-ray fields is essential for most X-ray free-electron laser (XFEL) applications. The interaction of XFEL pulses with molecules, however, had never been quantified and its description had been relying on a simple atomic picture so far. Here we present a joint experimental and theoretical study of small polyatomic molecules irradiated by ultra-intense hard X-rays, capturing a detailed picture of ultrafast ionisation and fragmentation dynamics of molecules. Our results demonstrate that ionisation of molecules at high X-ray intensity is substantially enhanced and fundamentally different from that of isolated atoms, providing new insights for future XFEL applications.

XFELs have brought an impact on various scientific fields, including material science, molecular biology, and astrophysics. All XFEL applications, for example, diffractive imaging of biological or solid-state samples and the investigation of matter under extreme conditions relevant to astrophysics, require the knowledge of the fundamental interaction between matter and intense X-rays. There have been several groundbreaking studies on the XFEL–matter interaction, but most of them have focused on gas-phase atomic systems [1,2]. Exposed to extremely intense X-ray pulses, an atom absorbs many X-ray photons sequentially and ejects many electrons, turning into a highly charged ion within a femtosecond time scale. The interactions of XFEL pulses with molecules are more complicated; however, no quantitative study had been established yet. It was believed instead that the induced charge of a molecule can be inferred from the charge induced in an isolated atom with the same absorption cross section under comparable irradiation conditions. This is called the independent-atom model and was employed in several previous experiments with less-intense X-ray pulses [3,4].

One question arises: Is this independent-atom model still valid when the X-ray intensity becomes extremely high, especially when it reaches the regime required for molecular imaging or plasma formation experiments? A closely related question: Do we have the capability of predicting the behaviour of matter under such conditions? Our present study clearly answers both questions: No for the first and yes for the other.

In our experiment, we expose isolated xenon atoms and gas-phase molecules containing iodine, whose cross section is comparable to that of xenon, to ultra-intense X-ray pulses generated by LCLS. The photon energy is 8.3 keV, which selectively ionises the iodine atom within the molecule. The light atoms are transparent to hard X-rays owing to very small

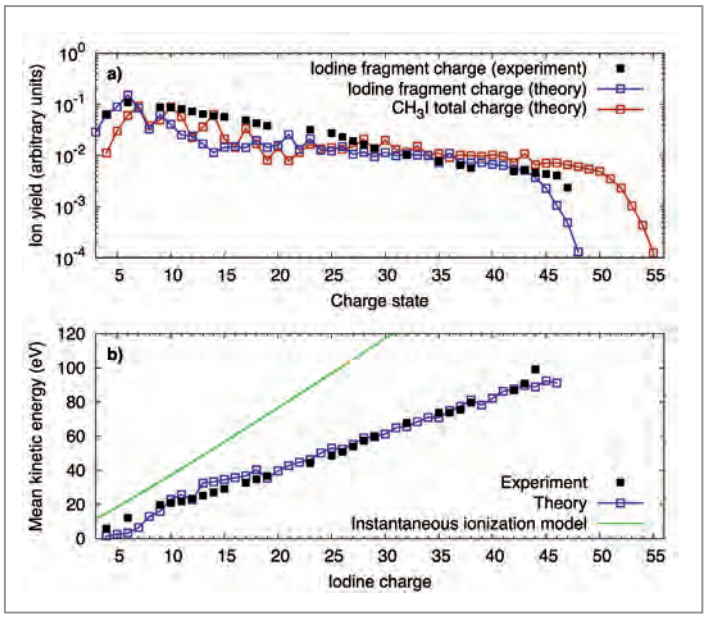

Figure 1

a) Calculated (blue) and measured (black) charge-state distribution of iodine ions from CH_3I molecules. The calculated total charge of the molecule is shown in red.
b) Calculated (blue) and measured (black) mean values of the kinetic-energy distribution of iodine ions from CH_3I molecules as a function of the iodine charge state. The green line indicates the energies that are expected for the instantaneous ionization model.

cross sections. The peak intensity approaches 2×10^{19} W/cm^2 using a nano-sized focused beam, which is orders of magnitude higher than in previous experiments. Then we measure the yields and kinetic energies of the ionic fragments. For iodomethane (CH_3I), we observe the iodine ion yields with a charge up to +47. Combined with C^{4+} and $3H^+$ fragments, the total molecular charge is +54. To the best of our knowledge, this is the highest charge state in matter ever produced using light. Analysing the measured ion yields (Fig. 1a) and their

kinetic energies (Fig. 1b), we capture detailed ionisation and nuclear dynamics during the ultrafast Coulomb explosion.

Interpreting these dynamics requires theory. To describe the ionisation dynamics, we employ a rate-equation model based on first-principles electronic structure calculations. In the course of multiphoton multiple ionisation of CH_3I under given XFEL beam parameters, we need to solve more than 200 trillion coupled rate equations. When nuclear motions are taken into consideration, the computational task becomes even more difficult. To overcome all these gigantic challenges, we have newly developed the XMOLECULE toolkit [5,6], dedicated to describe ionisation and fragmentation dynamics at high X-ray intensity. Our experimental and theoretical results are in good agreement for both ion yields and kinetic energies as shown in Figure 1. It indicates that our theoretical model adequately describes the essential mechanisms underlying explosion dynamics of molecules in ultra-intense hard X-ray pulses.

The most striking feature of our study is that the degree of ionisation in a molecule is significantly enhanced in comparison with the independent-atom model, as shown in Figure 2. The results show that for low fluences, at which earlier experiments were conducted [3,4], the total charge state is equivalent to the case of the independent-atom model, whereas molecular effects considerably enhance the level of ionisation at higher fluences. This new phenomenon, called charge-rearrangement-enhanced X-ray ionisation of molecules (CREXIM), can be understood by recurrent charge redistribution upon multiphoton X-ray absorption, as sketched in Figure 3. The created positive charge, initially localised at the iodine site, sucks electrons away from the methyl group. In the high-fluence regime, multiphoton X-ray absorption occurs on the iodine atom, so the transferred electrons are available for further ionisation there, which would not be available for direct ionisation if they stayed in the methyl group. We expect that the CREXIM effect will be more pronounced for larger systems because the heavy atom can suck in more electrons from more neighbours.

Our results establish that the interaction of ultra-intense hard X-rays with molecules is fundamentally different from that with isolated atoms. Our theoretical model captures the essence of the ionisation and fragmentation dynamics under these conditions. The CREXIM effect plays an important part in the quantitative understanding of XFEL–molecule interactions and will need to be taken into account for future XFEL applications.

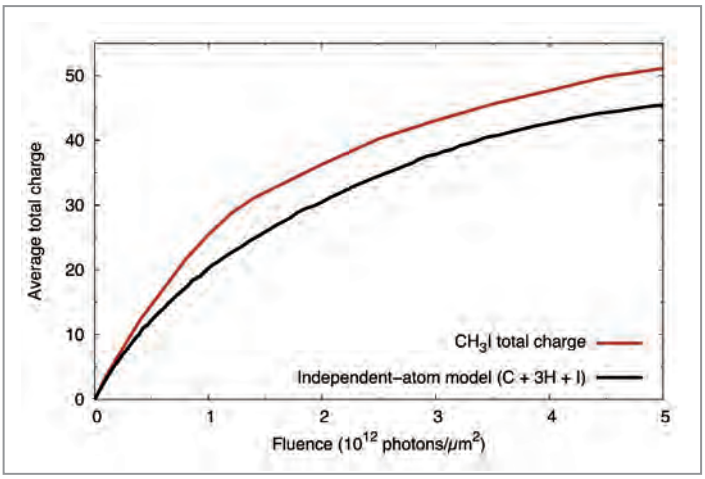

Figure 2

Average total molecular charge as a function of fluence calculated for CH_3I molecules (red) and within the independent-atom model (black).

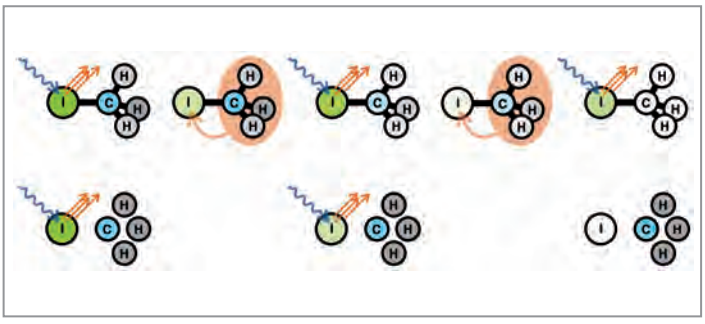

Figure 3

Illustration of the CREXIM mechanism. In the molecule (upper row), the repeated ionization (blue and orange arrows) of the iodine atom drives electrons from the methyl group to the iodine (orange shading), such that there are more electrons available for ionization compared to independent atoms (lower row). The darkness of the shading of the atoms indicates the number of electrons that remain in the atoms.

Contact: Sang-Kil Son, sangkil.son@cfel.de
Robin Santra, robin.santra@cfel.de

Authors

Artem Rudenko, Ludger Inhester, Kota Hanasaki, Xiang Li, Seyyed J. Robatjazi, Benjamin Erk, Rebecca Boll, Koudai Toyota, Yajiang Hao, Oriol Vendrell, Cedric Bomme, Evgeny Savelyev, Benedikt Rudek, Lutz Foucar, Stephen H. Southworth, Carl S. Lehmann, Bertold Krässig, Tatiana Marchenko, Marc Simon, Kiyoshi Ueda, Ken R. Ferguson, Maximilian Bucher, Tais Gorkhover, Sebastian Carron, Roberto Alonso-Mori, Jason E. Koglin, Jonathan Correa, Garth J. Williams, Sébastien Boutet, Linda Young, Christoph Bostedt, Sang-Kil Son, Robin Santra, and Daniel Rolles

Affiliation details at
http://www.nature.com/nature/journal/v546/n7656/full/nature22373.html

Original publication

'Femtosecond response of polyatomic molecules to ultra-intense hard X-rays', Nature 546, 129–132 (2017). DOI: 10.1038/nature22373

References

1. L. Young et al., 'Femtosecond electronic response of atoms to ultra-intense X-rays', Nature 466, 56–61 (2010).
2. B. Rudek et al., 'Ultra-efficient ionization of heavy atoms by intense X-ray free-electron laser pulses', Nat. Photonics 6, 858–865 (2012).
3. B. Erk et al., 'Ultrafast charge rearrangement and nuclear dynamics upon inner-shell multiple ionization of small polyatomic molecules', Phys. Rev. Lett. 110, 053003 (2013).
4. B. Erk et al., 'Imaging charge transfer in iodomenthane upon X-ray photoabsorption', Science 345, 288–291 (2014).
5. Y. Hao, L. Inhester, K. Hanasaki, S.-K. Son, and R. Santra, 'Efficient electronic structure calculation for molecular ionization dynamics at high X-ray intensity', Struct. Dyn. 2, 041707 (2015).
6. L. Inhester, K. Hanasaki, Y. Hao, S.-K. Son, and R. Santra, 'X-ray multiphoton ionization dynamics of a water molecule irradiated by an X-ray free-electron laser pulse', Phys. Rev. A 94, 023422 (2016).

Perfect X-ray focusing.

Glasses for X-ray optics enable diffraction-limited focusing at the nanoscale

Due to their short wavelength, X-rays can in principle be focused down to a few nanometres and below. At the same time, it is this short wavelength that puts stringent requirements on X-ray optics and their metrology. Both are limited by today's technology. Here, we show the accurate determination of residual aberrations of an X-ray lens using ptychography to create corrective glasses. Equipped with these glasses the optics achieve a diffraction-limited performance better than otherwise attainable. The scheme can be applied to any other focusing optics, thus solving the X-ray optical aberration problem generally for synchrotron radiation facilities and X-ray free-electron lasers (XFELs).

The ever-increasing brightness of modern storage ring sources and XFELs enables studying the structure and dynamics of matter with unprecedented spatial and temporal resolution. To fully benefit from the power of these sources, it is crucial to confine the X-ray beam and concentrate the radiation onto the sample. This is essential to improve not only the spatial resolution and sensitivity of X-ray analytical techniques, but also to generate highly intense X-rays that facilitate the generation of extreme states of matter and enable the study of non-linear X-ray phenomena. However, this requires X-ray optics with high numerical aperture (NA) that can withstand the extremely bright pulses of modern sources. Unfortunately, suitable X-ray optics are limited by fabrication technology, and trade-offs need to be made between aberration-free performance and highest possible NA.

Metrology to detect subtle optical imperfections and to characterise the tightly focused nanobeam has become very demanding. Over the past years, X-ray scanning coherent diffraction microscopy, also known as ptychography [1], has evolved to one of the most important methods for X-ray beam and optics characterization. In this method a nanostructured sample, positioned in the vicinity of the focal plane, is scanned through the beam and far-field diffraction patterns are recorded with appropriate spatial overlap between neighbouring scan points. Elaborate phase retrieval algorithms [2] can unambiguously retrieve the complex wavefield of the focused X-ray beam and, hence, reveal wavefront errors with unprecedented sensitivity and spatial resolution [3-5].

In this study, we present a general scheme to correct residual aberrations of X-ray optics by introducing corrective glasses into the optical path in order to achieve diffraction-limited focusing. We do so by assessing the quality of these optics under working conditions using ptychography. From the gathered information, suitable corrective elements were modelled – exactly like visiting an optician. As optics, we used a stack of 20 beryllium compound refractive lenses (Be CRLs) to focus the X-rays down to below 160 nm at the storage ring sources PETRA III at DESY (beamline P06) and Diamond Light Source (beamline I13-1), as well as at the XFEL source LCLS (MEC instrument). All measurements were performed with monochromatic X-rays at an energy of 8.2 keV. Similar spherical aberration was observed across all experiments, originating from tiny but repetitive shape errors of individual Be CRLs within the large lens stack. Numerical simulations revealed the deformation for an individual lens surface, shown in Fig. 1a. These lenses are fabricated via a coining process by pressing two parabolic stamps into a Be foil. To improve the already very small deformation error of 500 nm during production by over an order of magnitude is very challenging. Instead, we designed corrective glasses with the gathered data from

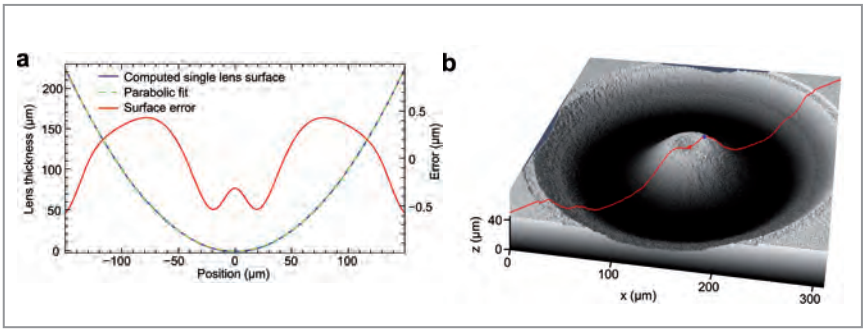

Figure 1

The error of the uncorrected optics was determined by retrieving the complex wave field via ptychography. With this information, the deformation of a single lens surface within a stack of 20 bi-concave Be CRLs was modelled (a). As these surface deformations are within current manufacturing limitations and are difficult to reduce any further, a tailor-made phase plate was manufactured by ultrashort-pulse laser ablation from fused silica in order to correct the whole lens stack at once for aberrations (b). The device operates like corrective glasses in the X-ray regime.

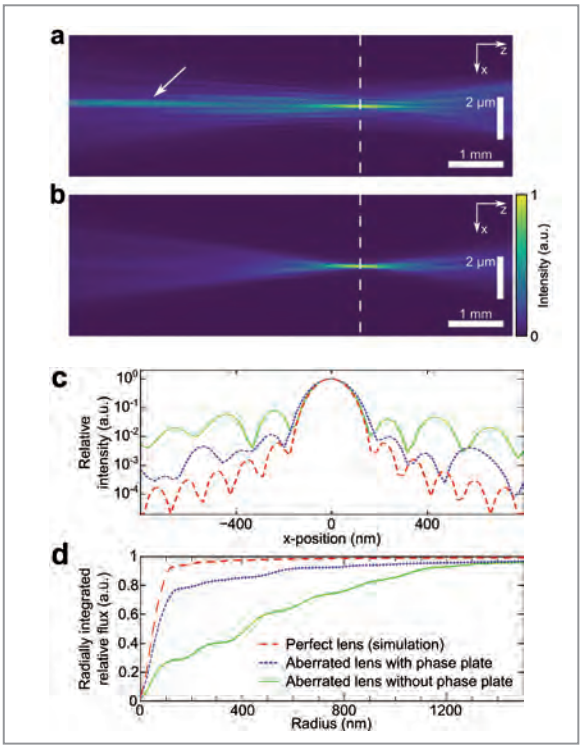

Figure 2

(a) Beam caustic in horizontal projection along the optical axis. For Be CRLs with spherical aberration the paraxial rays are focused further upstream (arrow), leading to pronounced side lobes in the main focal plane (dashed vertical line). (b) The Be CRLs equipped with the phase plate show almost no aberration. (c) While the central focal spot is unaffected in size, intensity in side lobes is reduced due to the phase plate. Colours as in panel (d). Red: simulated perfect lens, blue: measured corrected, green: measured uncorrected. (d) By concentrating most of the radiation in the central speckle, the effective focal spot radius is reduced from over 800 nm to 125 nm, close to the theoretical limit of about 80 nm.

With this novel scheme, many X-ray optics can be improved in performance beyond current manufacturing limitations. The principle is not only applicable to refractive optics as shown in this study, but can also be transferred to reflective and diffractive optics as well. As the glasses are very compact and easy to align, they can also be retrofitted to existing beamline optics. This benefits not only the resolution and sensitivity in classical X-ray microscopy schemes, but may also lead to new opportunities for isochoric X-ray heating and non-linear X-ray optics at XFEL sources.

Contact: Frank Seiboth, frank.seiboth@desy.de

ptychography in order to correct the whole lens stack at once. The tailor-made phase plate, manufactured by ultrashort-pulse laser ablation out of fused silica [6], is shown in Fig. 1b.

Due to spherical aberration, the nanofocus using the uncorrected optics was spoiled by X-rays being partly focused further upstream, highlighted by the arrow in Fig. 2a. This led to unwanted radiation around the focal spot, shown by the solid green line in the focal plane profile of Fig. 2c. Compared to a perfect lens (dashed red line in Fig. 2c), intensities in side lobes were increased by over an order of magnitude. In practice, these side lobes reduce the attainable resolution in X-ray microscopy applications due to an effective spot size broadening, illustrated by the radially integrated intensity profile in Fig. 2d. In addition, the peak intensity in the main focal spot is significantly reduced, as most of the radiation is distributed in the outer lobes.

By installing the manufactured phase plate, the corrective glasses, behind the lenses, the performance of the optics was strongly improved. With the suppression of spherical aberration, most X-rays were now focused within the same focal plane, illustrated by the clean beam caustic in Fig. 2b. This resulted in lowered intensities by an order of magnitude in lobes surrounding the focal spot, shown by the dotted blue line in Fig. 2c, and ultimately a reduced effective focal spot size as shown in Fig. 2d. The phase plate transformed the Be CRL optics from an aberrated system into a diffraction-limited hard X-ray optics. While the uncorrected optics could only focus less than 30 % of the radiation compared to the ideal optics (Strehl ratio below 0.3), the corrected focus gathered more than 85 % (Strehl ratio 0.85). At the same time the optical system stays radiation resistant and maintains its high NA of 0.5×10^{-3} in combination with a large aperture of 300 µm.

Authors

Frank Seiboth[1,2], Andreas Schropp[1], Maria Scholz[1], Felix Wittwer[1], Christian Rödel[2,3], Martin Wünsche[3], Tobias Ullsperger[4], Stefan Nolte[4], Jussi Rahomäki[5], Karolis Parfeniukas[5], Stylianos Giakoumidis[5], Ulrich Vogt[5], Ulrich Wagner[6], Christoph Rau[6], Ulrike Boesenberg[1], Jan Garrevoet[1], Gerald Falkenberg[1], Eric C. Galtier[2], Hae Ja Lee[2], Bob Nagler[2] and Christian G. Schroer[1,7]

1. Deutsches Elektronen-Synchrotron DESY, Hamburg, Germany
2. Linac Coherent Light Source, SLAC National Accelerator Laboratory, Menlo Park, California, USA
3. Institute of Optics and Quantum Electronics, Friedrich-Schiller-Universität Jena, Jena, Germany
4. Institute of Applied Physics, Friedrich-Schiller-Universität Jena, Jena, Germany
5. KTH Royal Institute of Technology, Biomedical and X-ray Physics, Albanova University Center, Stockholm, Sweden
6. Diamond Light Source Ltd, Diamond House, Harwell Science and Innovation Campus, Didcot, Oxfordshire, UK
7. Department Physik, Universität Hamburg, Hamburg, Germany

Original publication

'Perfect X-ray focusing via fitting corrective glasses to aberrated optics', Nature Communications 8, 14623 (2017). DOI: 10.1038/ncomms14623

References

1. P. Thibault, M. Dierolf, A. Menzel, O. Bunk, C. David and F. Pfeiffer, 'High-resolution scanning X-ray diffraction microscopy', Science 321, 379–382 (2008).
2. A.M. Maiden and J.M. Rodenburg, 'An improved ptychographical phase retrieval algorithm for diffractive imaging', Ultramicroscopy 109, 1256–1262 (2009).
3. C.M. Kewish, M. Guizar-Sicairos, C. Liu, J. Qian, B. Shi, C. Benson, A.M. Khounsary, J. Vila-Comamala, O. Bunk, J.R. Fienup, A.T. Macrander and L. Assoufid, 'Reconstruction of an astigmatic hard X-ray beam and alignment of K-B mirrors from ptychographic coherent diffraction data', Opt. Express 18, 23420–23427 (2010).
4. J. Vila-Comamala, A. Diaz, M. Guizar-Sicairos, A. Mantion, C.M. Kewish, A. Menzel, O. Bunk and C. David, 'Characterization of high-resolution diffractive X-ray optics by ptychographic coherent diffractive imaging', Opt. Express 19, 21333–21344 (2011).
5. A. Schropp, R. Hoppe, V. Meier, J. Patommel, F. Seiboth, H.J. Lee, B. Nagler, E.C. Galtier, B. Arnold, U. Zastrau, J.B. Hastings, D. Nilsson, F. Uhlén, U. Vogt, H.M. Hertz and C.G. Schroer, 'Full spatial characterization of a nanofocused x-ray free-electron laser beam by ptychographic imaging', Sci. Rep. 3, 01633 (2013).
6. B. N. Chichkov, C. Momma, S. Nolte, F. von Alvensleben and A. Tünnermann, 'Femtosecond, picosecond and nanosecond laser ablation of solids', Appl. Phys. A 63, 109–115 (1996).

Lasing on an overtone.

Self-seeding an X-ray FEL by amplifying harmonics

Harmonic lasing in free-electron lasers (FELs) can be used to reach to shorter wavelengths. To generate even brighter beams at the harmonics, X-ray FEL facilities can be operated in the harmonic lasing self-seeded free-electron laser (HLSS FEL) mode. This mode was successfully demonstrated at FLASH2 in the wavelength range between 4.5 nm and 15 nm. The spectral brightness was improved in comparison with the standard self-amplified spontaneous emmission (SASE) mode of operation by a factor of six in the exponential gain regime. The HLSS FEL also shows improved performance compared to a SASE FEL in the post-saturation regime with a tapered undulator.

In order to extend the photon energy range of high-gain X-ray FELs, one can study the emitted radiation at integer fractions of the fundamental wavelength, the so-called harmonics. In harmonic lasing, the FEL process develops at an odd harmonic of the planar undulator independent from lasing at the fundamental. Contrary to the nonlinear harmonic generation (which is driven by the fundamental in the vicinity of saturation), harmonic lasing can provide much more intense, stable, and narrow-bandwidth radiation. The most attractive feature of saturated harmonic lasing is that the spectral brightness of a harmonic is comparable to that of the fundamental [1,2].

An interesting option, proposed in [1], is the possibility to further improve the spectral brightness by setting the first part of the undulators to a multiple wavelength of the targeted fundamental. Harmonic lasing then (self-)seeds the short wavelength emission in the second part of the undulator (tuned to the desired fundamental), see Fig. 1. This scheme is then called HLSS.

Operation of a HLSS FEL at FLASH2 was successfully demonstrated during several experimental campaigns in 2016 at different electron energies and soft X-ray wavelengths in order to benchmark machine parameters [3].

The first evidence of harmonic lasing was observed on 1 May, 2016. Initially, ten undulator sections were tuned to the standard SASE mode, operating in the exponential gain regime at the desired fundamental wavelength of 7 nm. The pulse energy was 12 µJ. Then HLSS was set up: the first three sections were scanned around 21 nm (see Fig. 2). The output pulse energy at 7 nm exhibits a strong increase, when exactly 3 × 7 nm = 21 nm is lasing in the first part. Even more: the pulse energy at 7 nm with three of ten undulators tuned to the corresponding 3rd (sub)harmonic at longer wavelength and only seven undulators remaining at 7 nm (50 µJ) is significantly larger than if all undulators were tuned to 7 nm (12 µJ). This is because the gain length for harmonic lasing at 7 nm (with a fundamental at 21 nm) is shorter than the SASE gain length of 7 nm [1].

The studies of the HLSS FEL at FLASH2 continued in June 2016 at a wavelength of 11 nm. The output spectra were measured with the wide-spectral-range XUV spectrometer of FLASH2. In Fig. 3, the averaged spectra for two study cases are presented: standard SASE mode with ten undulator modules resonant at 11 nm and HLSS FEL with four modules tuned to 33 nm and six modules tuned to 11 nm. The HLSS spectral power is larger by a factor of six due to a five-fold increase of the pulse energy in the HLSS regime and a

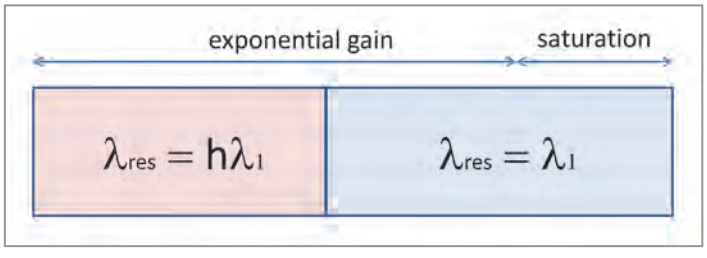

Figure 1

Conceptual scheme of HLSS FEL. Beam direction is left to right, λ_1 = 7 nm, h = 3 in the present demonstration. The harmonic emission of the first section tuned to 21 nm self-seeds the FEL operation in the second part of the undulators, tuned to 7 nm.

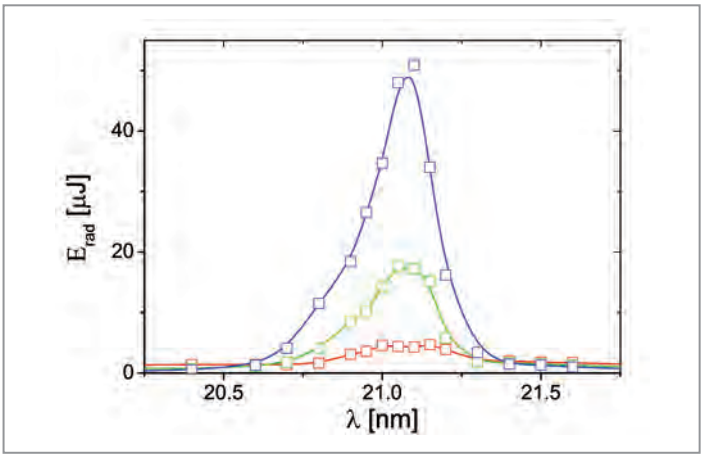

Figure 2

Scan of the resonance wavelength of the first part of the undulator with one undulator section (red), two sections (green), and three sections (blue). The second part of the undulators is tuned to 7 nm. The total pulse energy is completely dominated by the emission at 7 nm.

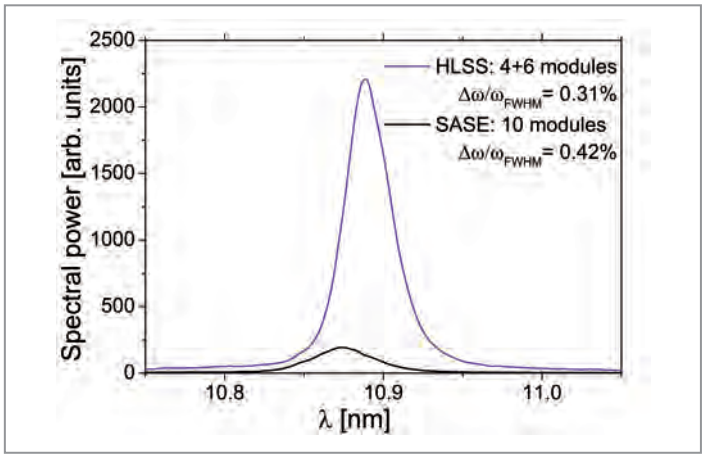

Figure 3

Spectral power of the radiation pulse energy for HLSS FEL configuration (blue) and for SASE FEL (black). $\Delta\omega/\omega$ is the resulting spectral bandwidth.

bandwidth reduction by a factor of 1.3 (the measured bandwidth is 0.31 % for HLSS versus 0.41 % for SASE). Further analysis shows that the spectral bandwidth was increased due to an energy chirp along the electron beam [3]. However, since the coherence time is independent of an energy chirp, we found an even larger (1.8 ± 0.3-fold) increase in the coherence time deduced from statistical analysis of the FEL pulses, which is in good agreement with theory [2]. Currently, the operation of HLSS FEL at FLASH2 is limited to the 3rd harmonic due to a relatively low K-value of the FLASH undulators. It is important to note that at the SASE3 undulator of the European XFEL, one can in principle use a much higher harmonic number yielding even further enhanced coherence.

In November 2016, the HLSS FEL was established with the first four undulators tuned to 45 nm and eight undulators tuned to 15 nm. FEL saturation was reached in SASE and HLSS modes, and a post-saturation taper keeping the resonance condition in the undulator was applied to even further improve the FEL efficiency. The tapering is usually designed in such a way that the undulator field decreases upstream in order to compensate the effect of the energy losses of the electron beam during light amplification. Using quadratic tapering for each FEL mode (HLSS and SASE) and optimising the taper parameters, 50 % higher HLSS pulse energies were achieved. For HLSS, the post-saturation taper regime can be improved, because of an earlier saturation and a better longitudinal coherence than for SASE. We would like to point out that HLSS was achieved at the shortest wavelength of 4.5 nm in September 2016.

In conclusion, we successfully demonstrated the harmonic lasing phenomena and the HLSS FEL principle at FLASH2 in the wavelength range between 4.5 and 15 nm. A change from the SASE to the HLSS configuration was very simple and fast, independent of the FEL wavelength and accelerator settings. One can therefore forecast that HLSS may become a standard mode of operation of the X-ray FEL facilities with gap-tunable undulators, providing an improvement of the temporal coherence, a reduction of the saturation length and the possibility to maximise the FEL output pulse energy by a more efficient post-saturation tapering.

The first evidence of harmonic lasing in a high-gain FEL and at a short wavelength (down to 4.5 nm) paves the way for a variety of different applications of this effect in X-ray FEL facilities [1].

Contact: Evgeny Schneidmiller, evgeny.schneidmiller@desy.de

Authors

Evgeny A. Schneidmiller, Bart Faatz, Marion Kuhlmann, Juliane Rönsch-Schulenburg, Siegfried Schreiber, Markus Tischer and Mikhail V. Yurkov

Deutsches Elektronen-Synchrotron DESY, Hamburg, Germany

Original publication

'First operation of a harmonic lasing self-seeded free electron laser', Phys. Rev. ST Accel. Beams 20, 020705 (2017). DOI: 10.1103/PhysRevAccelBeams.20.020705

References

1. E. A. Schneidmiller and M. V. Yurkov, 'Harmonic lasing in x-ray free electron lasers', Phys. Rev. ST Accel. Beams 15, 080702 (2012).
2. E. A. Schneidmiller and M. V. Yurkov, 'Harmonic Lasing Self-seeded FEL', Proceedings of FEL2013, New York, p. 700.
3. E. A. Schneidmiller B. Faatz, M. Kuhlmann, J. Rönsch-Schulenburg, S. Schreiber, M. Tischer and M. V. Yurkov, 'First operation of a harmonic lasing self-seeded free-electron laser', Phys. Rev. ST Accel. Beams 20, 020705 (2017).

Double flashes with attosecond precision.

Interferometric autocorrelation by making use of lamellar gratings

Phase-sensitive measurements require phase-controlled electric fields. Combining phase-control with short-wavelength laser pulses provides novel opportunities to trace electron dynamics with unprecedented spatial and temporal resolution. Thanks to a special optics design we have demonstrated the phase control of pulses from the FLASH free-electron laser with attosecond precision. This paves the way towards time-domain interferometry in the soft X-ray range, thus increasing the amount of information retrieved from nonlinear optics experiments at FELs.

Science with FELs has enabled multiple breakthroughs covering the broad range from basic research in life sciences to applications in materials science and catalysis. Particularly, the high degree of spatial coherence of the light field allows for key applications such as serial-femtosecond X-ray crystallography [1]. Recently, temporal coherence provided by seeded FELs moved into the focus of interest [2]. It has been shown that full control over the light phase in the short-wavelength limit allows for a new class of light-phase sensitive experiments, such as XUV nonlinear wave mixing and attosecond coherent control [3,4]. These novel X-ray methodologies give a new twist to modern laser science striving to unravel energy, charge and information transport phenomena on attosecond time and nanometre length scales in matter, materials and building blocks of nature.

At the heart of any atomistic understanding of complex functionality such as chemical bond formation is the ultrafast motion of electrons dictated by the laws of quantum mechanics.

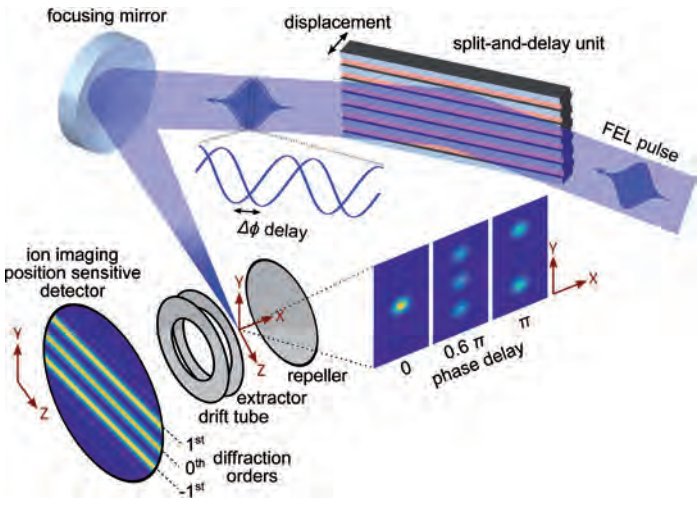

Particularly, information on the phase evolution of a wave packet, which describes electronic and/or nuclear structural changes, holds the key for its control in space and time. In optics, direct information about the light-wave phase is obtained by interferometric techniques. In the last decade, analogous methodologies have been developed to derive similar information on ultrafast electron wave packet dynamics in atoms, molecules, clusters and solid-state materials.

Time-domain interferometry is established in the optical spectral range for decades but is still in its infancy for XUV and soft X-ray photon energies. The progress in the short-wavelength limit is impeded by the usage of reflective optics and harsh requirements for accuracy and precision of experimental equipment. The workhorse of XUV pump–XUV probe studies is a double-mirror split-and-delay unit (SDU) that generates two pulse replicas with a variable delay. A conventional two-element mirror produces two spatially-separated pulses, which can be superimposed only at a skew angle thus greatly reducing the phase contrast of the pump-probe measurement [5]. To overcome this limitation we developed a smart lamellar-grating split-and-delay unit shown in Fig. 1. The device splits the wavefront of the incoming XUV pulse uniformly across the beam profile and provides two collinear pulses that have a constant phase difference in the transverse plane. This property makes the

Figure 1

FLASH pulses are split in two replicas with variable delay by the lamellar-grating split-and-delay unit and then focused on the Xe gas target. The spatial intensity distribution of the FEL light depending on the twin-pulse delay is imaged by the position-sensitive ion detector. The figure is licensed under a Creative Commons Attribution 4.0 International License.

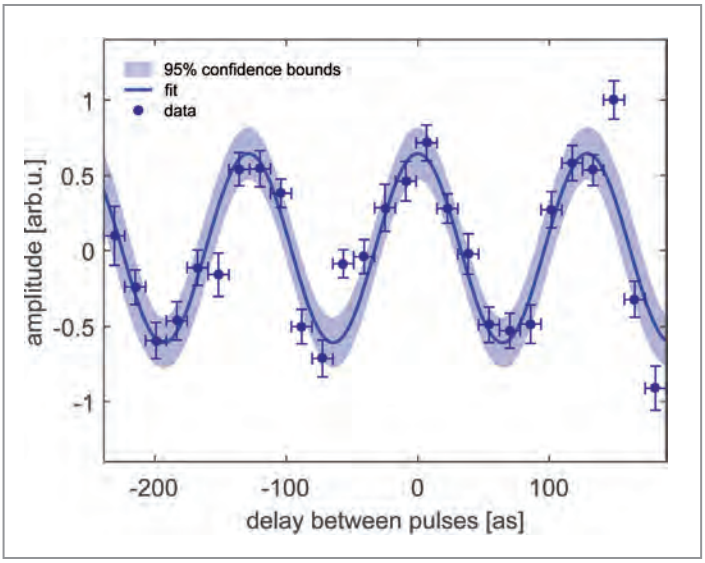

Figure 2

The oscillation of the FEL carrier light wave monitored by plotting the intensity resulting from the interference of the two pulse replicas as a function of their relative phase delay, e.g., linear autocorrelation. The measured optical cycle at the FEL wavelength of 38 nm is 129 attoseconds. The figure is licensed under a Creative Commons Attribution 4.0 International License.

SDU an all-reflective analogue of a Michelson interferometer for XUV wavelengths and allows for measurement of phase-sensitive signals with maximum contrast.

A crucial prerequisite for any interferometric measurement is the precise control over the temporal phase of the light wave on the subcycle time scale. XUV light waves oscillate a hundred times faster than visible light requiring a hundred times better precision. Thus, in our setup the SDU is combined with a diagnostics system based on an in-vacuum white light interferometer (WLI). The WLI monitors the topography of the SDU in real time and provides the precise feedback about the generated twin-pulse delay for every laser shot with attosecond accuracy. This way, the question how precisely one can control the phase is transformed into how precisely one can measure the delay for each pulse pair.

In our proof of principle experiment, performed at the PG2 monochromator beamline of FLASH1, we have demonstrated attosecond phase control of XUV light waves by generating two phase-locked replicas of FLASH pulses with the lamellar-grating SDU and observing their interference directly in the time domain. Self-amplified spontaneous emission (SASE) from the FEL was spectrally filtered by a monochromator to obtain good temporal coherence and then split in two pulse replicas by the SDU. The twin pulses focused on a Xe gas generated a spatial ion distribution that depends on the relative phase delay between the light fields. The Xe^+ ions from the ionization volume where the pulses have a fixed phase relation—a single diffraction order—were selected by an imaging time-of-flight spectrometer. The ion yield from the zeroth diffraction order plotted in Fig. 2 as a function of delay represents a linear autocorrelation of FLASH pulses and oscillates with the period of the FEL carrier wave, which is 129 attoseconds.

The successful transfer of a powerful optical method towards short wavelengths opens up the door for high-contrast time-domain interferometry in nonlinear phase-sensitive spectroscopic studies even at partially coherent SASE sources. Full control over the relative temporal phase in FEL pulse replicas provides opportunities to trace energy and charge migration in systems of increasing complexity with unprecedented spatial and temporal resolution. It makes the local electronic structure and dynamics accessible and controllable.

Contact: Sergey Usenko, sergey.usenko@desy.de
Tim Laarmann, tim.laarmann@desy.de

Authors

Sergey Usenko[1,2], Andreas Przystawik[1], Markus Alexander Jakob[2,3], Leslie Lamberto Lazzarino[3], Günter Brenner[1], Sven Toleikis[1], Christian Haunhorst[4], Detlef Kip[4] and Tim Laarmann[1,2]

1. Deutsches Elektronen-Synchrotron DESY, Hamburg, Germany
2. The Hamburg Centre for Ultrafast Imaging, Hamburg, Germany
3. Department of Physics, University of Hamburg, Hamburg, Germany
4. Faculty of Electrical Engineering, Helmut Schmidt University, Hamburg, Germany

Original publication

'Attosecond interferometry with self-amplified spontaneous emission of a free-electron laser', Nature Communications 8, 15626 (2017). DOI: 10.1038/ncomms15626

References

1. H. Chapman et al., 'Femtosecond diffractive imaging with a soft-X-ray free-electron laser', Nat. Phys. 2, 839–843 (2006).
2. E. Allaria et al., 'Highly coherent and stable pulses from the FERMI seeded free-electron laser in the extreme ultraviolet', Nat. Photon. 6, 699–704 (2012).
3. F. Bencivenga et al., 'Four-wave mixing experiments with extreme ultraviolet transient gratings', Nature 520, 205–208 (2015).
4. K. C. Prince et al., 'Coherent control with a short-wavelength free-electron laser', Nat. Photon. 10, 176–179 (2016).
5. S. Usenko et al., 'Split-and-delay unit for FEL interferometry in the XUV spectral range', Appl. Sci. 7, 544 (2017).

Straight and shaped to the red.

Mid-infrared intense single-cycle pulses

The generation of intense mid-infrared (mid-IR) pulses with customizable shape and spectra spanning a multiple octave range of vibrational frequencies is an elusive technological capability. While some recent approaches to mid-IR supercontinuum generation–such as filamentation, multicolour four-wave-mixing and optical rectification have successfully generated broad spectra, no process has been identified for achieving complex pulse shaping at the generation step. Here, we show that we can convert shaped near-IR pulses to the mid-IR spectral range lasting only 1.2 optical cycles. The method is extendable to the sub-cycle regime and enables a new class of precisely controlled nonlinear interactions, from nonlinear vibrational spectroscopy to strong light–matter interactions and single-shot remote sensing.

The mid-IR wavelength regime is of particular importance to materials science, chemistry, biology and condensed-matter physics, as it covers the fundamental vibrational absorption bands of many gaseous molecules, biomolecules and solid-state compounds. In the past decade, the advent of high-pulse-energy and ultrashort-duration mid-IR sources by nonlinear frequency conversion has ushered in a new range of nonlinear light–matter interactions. It allows for the tracking of the energy flow dynamics by multidimensional spectroscopy, the coherent control of lattice displacements through nonlinear phononics [2], or precise control of electron wave packet dynamics on the timescale of vibrational motion, making it possible to observe chemical transition states and secondary sources of coherent soft-X-ray light.

To date, octave-spanning sources of mid-IR light have not allowed pre-generation pulse shaping in order to customize the resulting amplitude and phase. Adiabatic frequency conversion [1] allows for a one-to-one transfer of the spectral phase through nonlinear frequency conversion over a larger-than-octave-spanning range and with an overall linear phase transfer function. Our approach, outlined in Fig. 1a, employs adiabatic difference frequency generation to produce energetic and octave spanning shaped pulses in the mid-IR. We used adiabatic down-conversion of shaped near-IR laser pulses in an aperiodically poled magnesium-oxide-doped congruent lithium niobate (MgO:CLN) crystal to produce a single-cycle pulse spanning range between 1.8 µm and 4.4 µm at –10 dB from the peak, with a pulse duration of 11 fs (1.2 optical cycles) and a pulse energy of 1.5 µJ. Moreover, we demonstrated an unprecedented capability to shape the mid-IR pulses over their entire bandwidth, achieved by pre-adjusting the amplitude and phase of the near-IR pulse prior to conversion with a common sub-octave-bandwidth pulse shaper. Adiabatic sum- and difference-frequency generation have been recently investigated for nonlinear wave mixing, and allow for the circumvention of the usual efficiency-bandwidth trade-off and bandwidth limitations of wave-mixing schemes. When the high- and low-frequency waves exchange photons in the presence of a strong mid-frequency pump wave, a monotonic evolution to full frequency conversion can be achieved by a nonlinear optical analogue to rapid adiabatic passage [1]. It is arranged by slowly sweeping

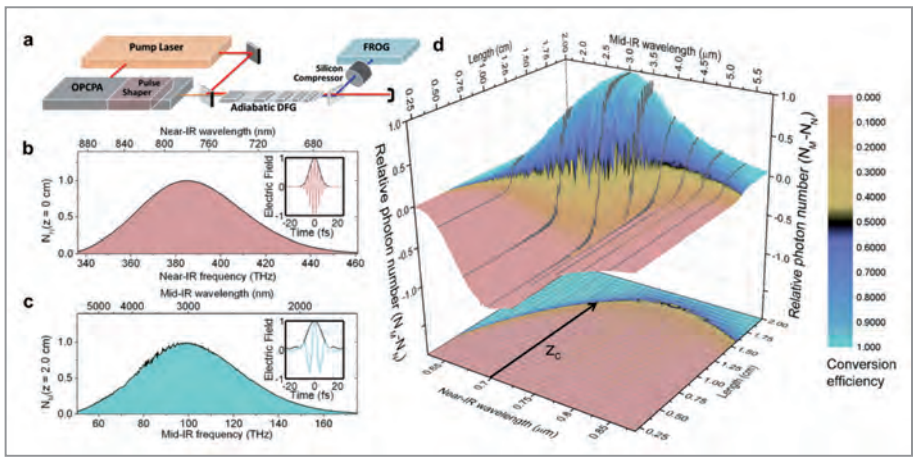

Figure 1

Octave-spanning adiabatic frequency conversion scheme (a). Shaping of the near-IR pulse is carried through to the mid-IR pulse through the broadband adiabatic frequency conversion process, which preserves the photon-number spectral density (b, c) A 4-cycle near-IR pulse can generate a 1-cycle mid-IR pulse (b, c, inset). (d) A 4D map and a 3D contour map show the evolution of relative mid-IR and near-IR photon number and conversion efficiency.

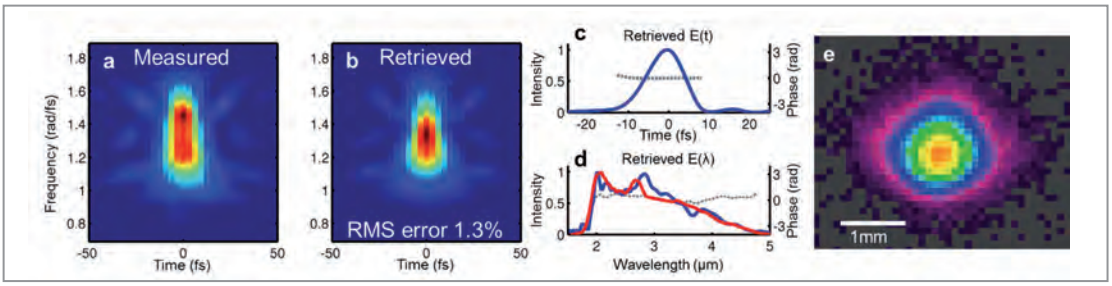

Figure 2

Characterization of single-cycle mid-IR pulses. (a) Measured SHG-FROG spectrogram. (b) Retrieved FROG spectrogram (with marginal correction applied using the measured spectrum). (c) Retrieved pulse as a function of time (blue – temporal intensity, dotted gray – temporal phase). (d) Spectral intensity (red – measured, blue – retrieved) and retrieved spectral phase (dotted gray). (e) Beam profile of collimated beam.

the wave vector mismatch during propagation with a chirped quasi-phase-matching grating. An ultra-broadband adiabatic difference frequency converter can reach full photon conversion for an octave-spanning set of frequencies [3,4], with one-to-one conversion at each frequency occurring sequentially at different longitudinal positions in the converter as each respective phase-matching condition is satisfied (Fig. 1b-d), allowing for amplitude shaping. Here, a broadband chirped mid-IR wave with centre frequency ω_M is produced through the mixing of a narrowband pump wave (ω_P) with a broadband chirped near-IR wave ($\omega_M + \omega_P$). In this case, the frequency spread is transferred from the near-IR wave to the mid-IR wave, which increases the relative bandwidth, i.e. the frequency spread divided by the mean frequency, by a factor of $\alpha = (\omega_M + \omega_P)/\omega_M$. Correspondingly, the transform-limited pulse duration of the signal is transferred to the mid-IR wave, which means that the compressed pulse duration relative to the period of the central frequency is decreased by the same factor α. The robustness of the power spectrum transfer is made possible by the one-to-one photon transfer (that is, spectrally independent, fully efficient, and back-conversion free) of the adiabatic converter. Robust transfer of spectral phase from near-IR to mid-IR, and thus octave-spanning pulse shaping, requires not only a one-to-one photon transfer, but also a linear phase transfer function. We find that the frequency-dependent group delay (that is, chirp) of the near-IR wave at the input of the device is smoothly transferred to the mid-IR wave at the output, with the addition of a smooth group delay function originating from the material dispersion of the adiabatic converter.

As an example, a two-stage 780 nm optical parametric chirped pulse amplifier (OPCPA) produces chirped near-IR pulses spanning 0.65 – 0.85 μm with 30 μJ pulse energy and 2.5 ps pulse duration, which can be shaped using the acousto-optic programmable dispersive filter between the first and second amplification stages. The amplifier output is combined with 100 μJ of pulse energy at 1.05 μm from the OPCPA pump laser and is down-converted to the mid-IR using a 20-mm adiabatically poled MgO:CLN crystal. The resulting overall dispersion from this adiabatic converter is due to the intrinsic material dispersion, as described above. The generated mid-IR wave, spanning 1.8 – 4.4 μm, is then compressed using a bulk silicon compressor and measured using frequency-resolved optical gating (FROG). The compressed pulse has 1.5 μJ energy and 11 fs duration, which is 1.2 optical cycles at the central wavelength of 2.8 μm and is within 15 % of its transform-limited duration, as shown in Fig. 2. Our study reveals that the phase transfer between near-IR and mid-IR is smooth, and the conversion device possesses a linear group delay transfer function allowing for multi-octave shaping in the mid-IR with a conventional pulse shaper in the near-IR prior to conversion.

For the first time, we achieve simultaneously multi-octave-spanning bandwidth, high-energy pulses, high conversion efficiency and complex pulse shaping capability. Recently, we also implemented another method to generate single to sub-cycle mid-IR pulses using a very short pulse high peak power pump at 2 μm and rather thin DFG/OPA crystals to generate broadband signal- and idler-pulses covering the 2 – 8 μm wavelength range [5].

Contact: Franz X. Kärtner, franz.kaertner@desy.de

Authors

Peter Krogen[1], Haim Suchowski[2], Houkun Liang[1], Noah Flemens[3], Kyung-Han Hong[1], Franz X. Kärtner[1,4] and Jeffrey Moses[1,3]

1. Department of Electrical Engineering and Computer Science and Research Laboratory of Electronics, Massachusetts Institute of Technology, Cambridge, USA.
2. Raymond and Beverly Sackler School of Physics and Astronomy, Tel Aviv University, Tel Aviv, Israel.
3. School of Applied and Engineering Physics, Cornell University, New York, USA.
4. Deutsches Elektronen-Synchrotron DESY, Hamburg, Germany

Original publication

'Generation and multi-octave shaping of mid-infrared intense single-cycle pulses', Nature Photonics 11, 222–226 (2017), DOI:10.1038/NPHOTON.2017.34

References

1. H. Suchowski, D. Oron, A. Arie and Y. Silberberg, 'Geometrical representation of sum frequency generation and adiabatic frequency conversion', Phys. Rev. A 78, 063821 (2008).
2. M. Först et al., 'Nonlinear phononics as an ultrafast route to lattice control', Nat. Phys. 7, 854–856 (2011).
3. J. Moses, H. Suchowski and F. X. Kärtner, 'Fully efficient adiabatic frequency conversion of broadband Ti:sapphire oscillator pulses', Opt. Lett. 37, 1589–1591 (2012).
4. H. Suchowski, P. R. Krogen, S.-W. Huang, F. X. Kärtner and J. Moses, 'Octave-spanning coherent mid-IR generation via adiabatic difference frequency conversion', Opt. Express 21, 28892–28901 (2013).
5. H. Liang, P. Krogen, Z. Wang, H. Park, T. Kroh, K. Zawilski, P. Schunemann, J. Moses, F. X. Kärtner and K.-H. Hong, 'High-energy mid-infrared sub-cycle pulse synthesis from a parametric amplifier', Nat. Commun. 8, 1-8 (2017).

Pink beam serial crystallography.

Protein structure determination using polychromatic X-rays

Serial X-ray crystallography allows for macromolecular structure determination at both X-ray Free-Electron Lasers (XFELs) and synchrotron sources. The polychromatic, 'pink', synchrotron beam provides more than two orders of magnitude increase in photon flux compared to the commonly-used monochromatic beam and hence allows recording diffraction patterns with much shorter exposure times. Fixed target serial crystallography experiments using polychromatic radiation were performed at the BioCARS instrument at the APS storage ring. Using a setup optimized for very low scattering background we were able to collect complete high quality data sets from different crystals with exposure times of 100 ps. The high quality of the diffraction data sets highlight the potential of this method for studying irreversible reactions at sub-microsecond timescales at high-brightness synchrotron facilities.

Serial X-ray crystallography has become the standard for structure determination of macromolecules at XFEL sources [1]. In contrast to conventional crystallography, where a diffraction dataset is collected from one or a few large crystals as they are rotated in the beam, in serial crystallography a complete data set is obtained by collecting still patterns from hundreds to hundreds of thousands of microcrystals. By taking such snapshots from each crystal with very short exposure times, serial crystallography is ideally suited to investigate structural changes in proteins as they occur for example in light-driven or chemically induced enzyme reactions.

Recently, serial crystallography was also successfully applied at synchrotron beamlines using monochromatic radiation [2]. Due to the X-ray fluence and bandwidth that is available at these beamlines, the experiments require exposure times in the millisecond range using more crystals than needed for XFEL measurements. The much larger availability of beam time, however, makes serial crystallography at synchrotrons an attractive alternative to those at XFELs. A polychromatic synchrotron beam from an undulator is referred to as 'pink' because it has a more limited spectrum than the 'white' beam originating from an X-ray tube or a bending magnet at a synchrotron. But compared to a monochromatised beam, the pink beam has more than two orders of magnitude higher X-ray flux and a much larger bandwidth of up to 4 % compared to about 0.01 %. The increase of both of these quantities are beneficial for serial crystallography experiments at synchrotrons since data can be collected with much shorter exposure times, and significantly fewer patterns (and thus crystals) are needed to collect a complete data set.

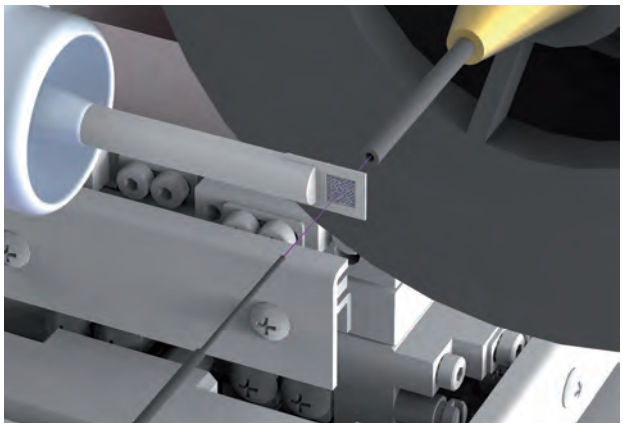

Figure 1

The newly developed setup tremendously reduces background scattering, which so far has impeded data collection from microcrystals using a polychromatic X-ray beam. To achieve this, the X-ray beam (shown in pink) is enclosed in thin metal capillaries shortly before and behind the sample and the air immediately surrounding the sample is replaced by a stream of helium gas.

A challenge for macromolecular crystallography experiments using polychromatic radiation is the typically weak signal-to-noise-ratio: due to the larger bandwidth only a small fraction of the X-rays contribute to a given Bragg reflection, whereas the background scattering level is proportional to the full flux integrated over the bandwidth. This has impeded data collection from microcrystals using polychromatic radiation so far.

To address this challenge we developed a setup which provides an extremely low background scattering level. Using a 'fixed target' approach, thousands of microcrystals are loaded onto a micro-structured silicon chip and then raster-scanned though the X-ray beam [3,4]. By using single crystalline silicon as a substrate material for the chip and efficiently removing most of the mother liquor during loading, the resulting background scattering level is extremely low. Drying out of the crystals on the chip is prevented by keeping the chips in a stream of humidified gas during the measurements [5].

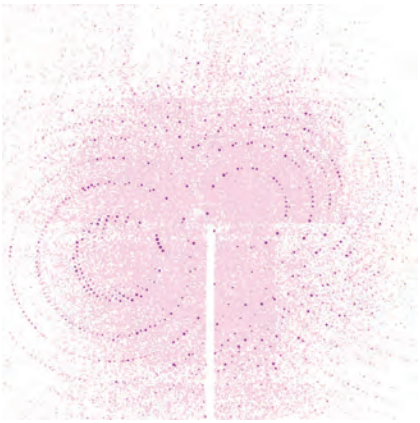

Figure 2

Diffraction pattern of a protein crystal in polychromatic, 'pink' X-rays. The new experimental setup allows for collecting diffraction patterns at very low background scattering levels. Compared to monochromatic X-ray diffraction patterns, the polychromatic pattern contains much more information, and fewer crystals are required to determine the protein's structure.

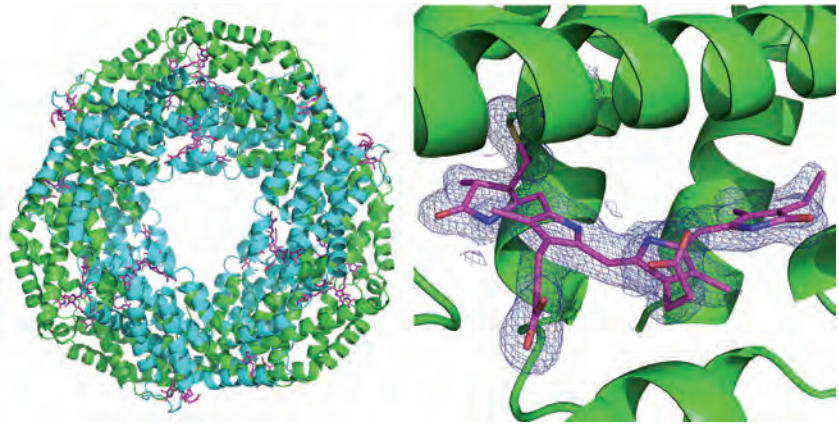

Figure 3

Left: The first measurement carried out using the new setup was performed on the protein phycocyanin that plays a role for photosynthesis in cyanobacteria. It forms a ring of six double molecules (heterodimers). At each heterodimer three phycocyanobilin molecules (pink) can bind.
Right: The blue grid represents the electron density of a bound phycocyanobilin molecule. Both structures were calculated from just 52 diffraction patterns recorded with pink beam of the Advanced Photon Source (APS) at the BioCARS beamline.

Furthermore, we combine two approaches to almost eliminate all background arising from air scattering by the direct beam. One is to enclose the direct beam in capillary shields shortly before and behind the sample (Fig. 1), leaving only a 6 mm gap where scattered rays still have a direct path to the detector. The other is to flush the remaining gap with humidified helium. The result of these approaches is a reduction of background due to air scatter by more than a factor of 100 compared to conventional X-ray crystallography setups.

Polychromatic data collection from phycocyanin and proteinase K microcrystals loaded onto our chips was performed at the BioCARS instrument at the Advanced Photon Source (APS) in Argonne National Lab (USA). A typical diffraction pattern highlighting the achievable very low background scattering level is shown in Figure 2. During the measurement the APS was operated in so called 'hybrid mode' delivering 3×10^{10} photons in a single bunch of less than 100 ps duration into an X-ray spot focused to about 20×20 µm^2. Raster scanning of one chip took less than ten minutes. Diffraction from only about 50 crystals at room temperature was sufficient to obtain a complete dataset. The electron density maps obtained (see Fig. 3) were all of high quality and compare well to data collected (also at room temperature) at the LCLS XFEL in Stanford USA.

Using our low background diffraction setup enabled us to perform pink beam serial crystallography experiments with short exposure times of only 100 ps at room temperature. This will allow the study of fast enzyme reactions which can be triggered with laser light or by micro-diffusion in a time resolved fashion at a synchrotron. A pink beam structure determination requires only 50 crystals, which is much fewer compared to current synchrotron experiments with monochromatic radiation or experiments at XFELs. This very low sample consumption and the fast and efficient data collection make the method also very well suited for ligand screening experiments of pharmaceutical relevant proteins.

Contact: Alke Meents, alke.meents@desy.de,
Max Wiedorn, max.wiedorn@desy.de

Authors

A. Meents[1,2], M.O. Wiedorn[1,3], V. Srajer[4], R. Henning[4], I. Sarrou[1], J. Bergtholdt[1], M. Barthelmess[1], P.Y.A. Reinke[5], D. Dierksmeyer[1], A. Tolstikova[1,3], S. Schaible[2], M. Messerschmidt[6] ,C.M. Ogata[7], D.J. Kissick[7], M.H. Taft[5], D.J. Manstein[5], J. Lieske[2], D. Oberthuer[1], R.F. Fischetti[7] and H.N. Chapman[1,3,8]

1. Center for Free-Electron Laser Science CFEL, Hamburg, Germany
2. Deutsches Elektronen-Synchrotron DESY, Hamburg, Germany
3. Department of Physics, University of Hamburg, Hamburg, Germany
4. Center for Advanced Radiation Sources, The University of Chicago, Argonne, IL, USA
5. Medizinische Hochschule Hannover (MHH), Institut für Biophysikalische Chemie, Hannover, Germany
6. National Science Foundation BioXFEL Science and Technology Center, Buffalo, NY, USA
7. Advanced Photon Source, Argonne National Laboratory, Lemont, IL, USA
8. Centre for Ultrafast Imaging, Hamburg, Germany

Original publication

'Pink-beam serial crystallography', Nature Communications 8, 1281 (2017).
DOI: 10.1038/s41467-017-01417-3

References

1. **L. C. Johansson, B. Stauch, A. Ishchenko and V. Cherezov, 'A bright future for serial femtosecond crystallography with XFELs', Trends Biochem. Sci. 42, 749–762 (2017).**
2. **F. Stellato et al., 'Room-temperature macromolecular serial crystallography using synchrotron radiation', IUCrJ 1, 204–212 (2014).**
3. **P. Roedig et al., 'A micro-patterned silicon chip as sample holder for macromolecular crystallography experiments with minimal background scattering', Sci. Rep. 5, 10451 (2015).**
4. **P. Roedig et al., 'High-speed fixed-target serial virus crystallography', Nat. Methods 14, 805–810 (2017).**
5. **P. Roedig et al., 'Room-temperature macromolecular crystallography using a micro-patterned silicon chip with minimal background scattering', J. Appl. Crystallogr. 49, 968–975 (2016).**

High-speed fixed-target serial virus crystallography.

First atomic structure of an intact virus deciphered with an X-ray laser

In serial crystallography (SX) still images from hundreds to hundreds of thousands crystals are recorded and subsequently combined to obtain a complete data set for structure determination. Efficient sample delivery has remained a challenge for SX as most of the currently applied methods require a large amount of sample or generate high scattering backgrounds. Using a microstructured silicon chip for sample delivery, we were able to determine the first high-resolution virus structure at an X-ray free-electron laser (XFEL) requiring a few micrograms of sample only. In combination with the high precision Roadrunner goniometer data collection could be performed at the full 120 Hz repetition rate of the XFEL Linac Coherent Light Source (LCLS) at Stanford, USA, and a complete dataset was collected in less than 10 minutes.

X-ray crystallography is a very powerful technique for structure determination of biological macromolecules. More than a hundred thousand structures of biological macromolecules have been determined with X-ray crystallography. A certain limitation of conventional crystallography is X-ray radiation damage, causing chemical changes to the macromolecules and resulting in a loss of their diffraction properties [1]. Radiation damage is in particular severe when experiments are performed at room temperature.

X-ray crystallography at XFELs allows overcoming the limitation of radiation damage that is experienced in conventional X-ray crystallography by the so-called 'diffraction before destruction' approach: The extremely short X-ray pulses are diffracted by the crystals before they destroy them [2]. This new approach has led to the development of so-called serial crystallography (SX). In contrast to conventional X-ray crystallography in SX still images from hundreds to hundreds of thousands of microcrystals are collected and afterwards combined to obtain a complete dataset [3]. A further advantage of SX in particular when carried out at XFELs is that diffraction experiments can be performed at room temperature.

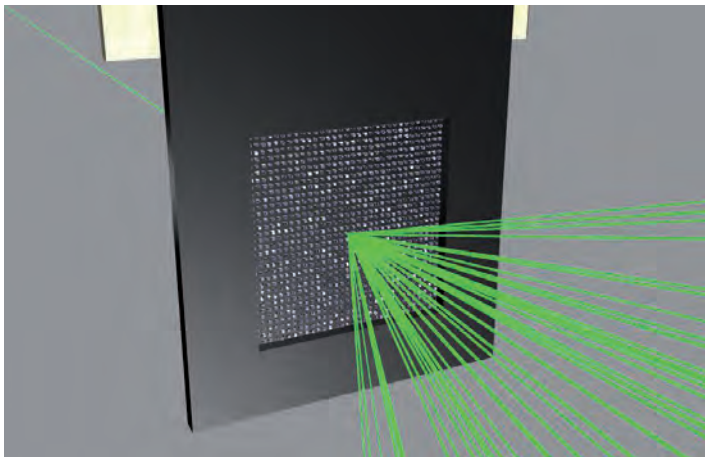

Figure 1

Schematic of a fixed target serial crystallography experiment: The chip loaded with microcrystals is scanned through the X-ray beam. Ideally, each crystal is hit by an X-ray pulse and produces a distinctive diffraction pattern (green fanned structured animation).

Sample delivery for serial crystallography has remained a challenge, as it requires exchanging the samples at the repetition rate of the FEL pulses, which is currently 120 Hz at LCLS. The most common method for sample delivery at FEL sources is the use of liquid jets, where a microcrystal suspension is pressed with high pressure through a nozzle resulting in a stable microjet with diameters of a few micrometers only. Major drawbacks of microfluidic jets are the frequent down times caused by clogging of the nozzles and the very high sample consumption required; often several tens of milligrams of microcrystals for a structure determination. One approach to reduce the very high sample consumption is to slow down the jets by using highly viscous transport media such as lipidic cubic phases (LCP). A major drawback of LCP jets is the high background signal caused by scattering of the X-rays by the jetting media with diameters of typically about 50 – 80 µm impeding high-resolution data collection in particular from large unit cell systems such as viruses or in case of very small crystals.

We have developed a new method for efficient sample delivery for SX based on so-called fixed targets. Here the microcrystals are loaded onto a microstructured sample holder, where the crystals ideally arrange themselves to the periodic pattern of the chips and are then scanned through the X-ray beam (Fig. 1) [4]. By using single crystalline silicon as material for the chips background scattering from the solid support is

kept at a minimum. Sample loading is achieved by pipetting a few microliters of sample suspension on the chip, which holds a periodic pattern of micropores slightly smaller than the crystal size. By attaching a piece of filter paper to the lower side of the chip, the liquid flows through the pores and the mother liquor is soaked-off, whilst the microcrystals are retained by the pores and arrange themselves to the periodic pore-pattern as shown in Fig. 2. The microcrystals are prevented from drying out by keeping them in a continuous stream of humidified air during sample handling [5]. Loading of sample onto the chips can be either performed directly at the experiment in case of room temperature data collection or in the lab in case of data collection at cryogenic temperatures. In the latter case the samples are preserved from drying out by flash-freezing them in liquid nitrogen directly after loading.

Virus crystals are very challenging systems for X-ray crystallography, as they are very fragile due to weak crystal contacts and thus cannot be frozen for data collection at cryogenic temperatures. They further possess large unit cells and are only available in small quantities. As a consequence room temperature SX at XFELs ideally fulfills the requirements for virus crystallography and should allow collecting higher resolution data from much smaller amounts of sample compared to synchrotron measurements.

Using our fixed target approach we were able to determine the structures of the bovine enterovirus 2 (BEV2) and the Cytoplasmic polyhedrosis virus (CPV18) polyhedra structure at the XPP instrument at LCLS. Sample scanning was performed using the specially developed Roadrunner I goniometer at the full 120 Hz repetition rate of LCLS. Data collection took less than ten minutes for a complete data set and hit rates of up to 90% were achieved. The BEV2 crystals diffracted to a resolution of up to 2.3 Å and high quality electron density maps were obtained from the data (Fig. 3). Compared to a similar structure determination carried out at a synchrotron our method required only 1/15 of the amount of much smaller crystals.

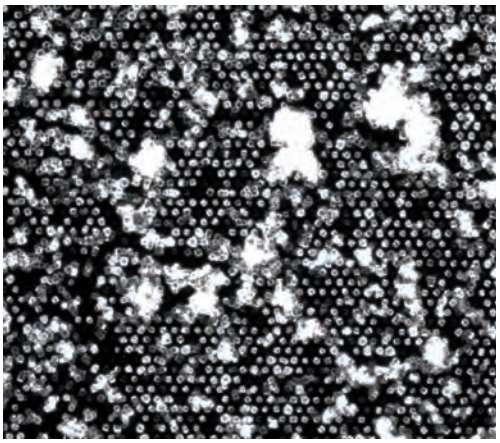

Figure 2
Micrograph of the microstructured silicon chip used for the experiment loaded with CPV microcrystals.

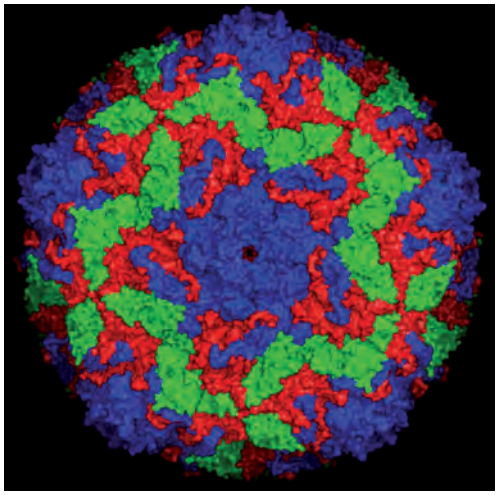

Figure 3
Surface structure of the bovine enterovirus 2, the three virus proteins are colour coded. Credit: Jingshan Ren, University of Oxford

In future we aim to collect data at higher speeds of up to several kHz, which should allow performing data collection for a structure determination in less than a minute. Such data collection times make the method also ideally suited for time resolved studies such as laser pump-probe experiments.

Contact: Alke Meents, alke.meents@desy.de

Authors

Philip Roedig[1], Helen M. Ginn[2,3], Tim Pakendorf[1], Geoff Sutton[2], Karl Harlos[2], Thomas S. Walter[2], Jan Meyer[1], Pontus Fischer[1], Ramona Duman[3], Ismo Vartiainen[4], Bernd Reime[1], Martin Warmer[1], Aaron S. Brewster[5], Iris D. Young[5], Tara Michels-Clark[5], Nicholas K. Sauter[5], Marcin Sikorsky[6], Silke Nelson[6], Daniel S. Damiani[6], Roberto Alonso-Mori[6], Jingshan Ren[2], James Kelly[7,8], Abhay Kotecha[2], David J. Rowlands[7], Elizabeth E. Fry[2], Christian David[9], David I. Stuart[2,3], Armin Wagner[3] and Alke Meents[1,10]

1. Photon Science, Deutsches Elektronen Synchrotron DESY, Hamburg, Germany.
2. Division of Structural Biology, Wellcome Trust Centre for Human Genetics, University of Oxford, Oxford, United Kingdom.
3. Diamond Light Source Limited, Harwell Science & Innovation Campus, Didcot, United Kingdom.
4. Institute of Photonics, University of Eastern Finland, Joensuu, Finland.
5. Molecular Biophysics and Integrated Bioimaging Division, Lawrence Berkeley National Laboratory, Berkeley, California, USA.
6. Linac Coherent Light Source, SLAC National Accelerator Laboratory, Menlo Park, California, USA.
7. School of Molecular and Cellular Biology, Faculty of Biological Sciences, University of Leeds, Leeds, United Kingdom.
8. The Pirbright Institute, Pirbright, United Kingdom.
9. Paul Scherrer Institut, Villigen, Switzerland.
10. Center for Free Electron Laser Science (CFEL), Hamburg, Germany.

Original publication

'High-speed fixed-target serial virus crystallography', Nature Methods 14, 805–810 (2017). DOI: 10.1038/nmeth.4335'

References

1. **A. Meents et al., 'Origin and temperature dependence of radiation damage in biological samples at cryogenic temperatures', PNAS 107, 1094–1099 (2011).**
2. **R. Neutze et al., 'Potential for biomolecular imaging with femtosecond X-ray pulses', Nature 406, 752–757 (2000).**
3. **S.Boutet et al., 'High-Resolution Protein Structure Determination by Serial Femtosecond Crystallography', Science 337, 362-364 (2012).**
4. **P. Roedig et al., 'A micro-patterned silicon chip as sample holder for macromolecular crystallography experiments with minimal background scattering', Sci. Rep. 5, 10451 (2015).**
5. **P. Roedig et al., 'Room-temperature macromolecular crystallography using a micro-patterned silicon chip with minimal background scattering', J. Appl. Crystallogr. 49, 968–975 (2016).**

THz pulse doubler at FLASH.

Double pulses for pump-probe experiments at X-ray FELs

The soft X-ray free-electron laser FLASH employs a narrowband high-field accelerator Terahertz source for ultrafast pump-probe experiments. Due to the large difference in optical paths of both beamlines – for soft X-rays (XUV) and Terahertz (THz) pulses – the full potential of FLASH is yet to be fully exploited. To solve this issue, we use the lasing of double electron bunches, timed for a temporal overlap of the THz and XUV pulses at the experimental station. Moreover, in order to optimize the experimental conditions for a typical THz-pump XUV-probe experiment, the lasing of the first bunch in the XUV is supressed to one sixth of that of the second bunch. As a result a temporal synchronization of the THz radiation pulses of around 20 fs could be achieved and further solutions for achieving higher temporal resolution by monitoring arrival times are in preparation.

A unique feature of FLASH is a THz undulator following the main XUV undulator section, which produces THz pulses enabling pump-probe experiments with ultrashort high-field THz and soft XUV pulses [1]. The central wavelength of the THz pulses can be continuously tuned from 1 – 300 µm (1 – 300 THz), depending on the electron beam energy. By producing the THz and XUV pulses with the same electron bunch, they are naturally synchronized [2]. However, the challenges of this type of experiment are caused due to significantly different optical paths of the THz and XUV pulses. The THz beam is collimated in the beamline using five toroidal mirrors, to keep the beam size within the size of the beam transport and optics (size 210 × 150 mm). Due to the extremely broad spectral range covered by the undulator, all optical elements are reflective (providing spectrally non-dispersive reflection) and have a 45° angle of incidence. Folding of the THz beam extends the optical path length, resulting in a delay of 21.5 ns with respect to XUV pulses at the experimental station. One solution to ensure temporal overlap between THz and XUV pulses at the experiment is to introduce the additional optical path for the XUV pulse in back-reflection geometry using normal-incidence multilayer mirrors specially designed for a particular wavelength. Although this method has been successfully demonstrated [3], there are two major drawbacks arising from this technique: a low reflectivity and narrow spectral range of the XUV mirrors. In addition this geometry, requires large focal length of XUV back-reflecting mirror (given by the optical path delay between THz and XUV pulses), that than produces a large focal size of the XUV beam (>100 µm FWHM). A reduced XUV fluence in the experiment due to the combined effect of low reflectivity and a large focus excludes high-intensity experiments, like for instance plasma physics or non-linear multiphoton ionizations, thus limiting FLASH's high-pulse energy advantage over other sources in the same spectral range. An alternative approach proposed by Grimm et al. [4], is to exploit the radiation of tailored electron bunches at the FLASH injector. In particular, double electron bunches at the electron gun, separated by 21.5 ns – the delay between XUV and THz pulses – are used for this purpose. In this scheme the first electron bunch is used to generate THz pulses and the second one to generate soft XUV pulses.

In general, each electron bunch generates two pulses, XUV and THz (in total four radiation pulses). For typical THz-pump – XUV-probe experiments, the first electron bunch needs to be optimized to generate maximal THz pulse energy (refer to scheme in Fig. 1), while generating little or no XUV light, to reduce its potential influence on the sample. Whereas the second bunch should be optimized to generate XUV pulses with required properties, ranging from short pulse duration to

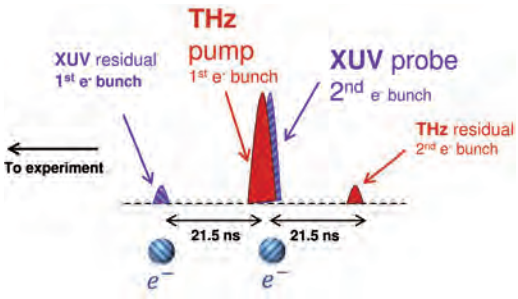

Figure 1

THz doubler timing scheme at FLASH: the first electron bunch generates a 'residual' XUV pulse (violet) and the THz pump pulse (red), while the second one generates the XUV probe temporally overlapping with the THz pump and a 'residual' THz pulse. Residual pulses are discarded and not used in the pump-probe experiment. The hatched pattern on electrons and pulses indicates their respective origin.

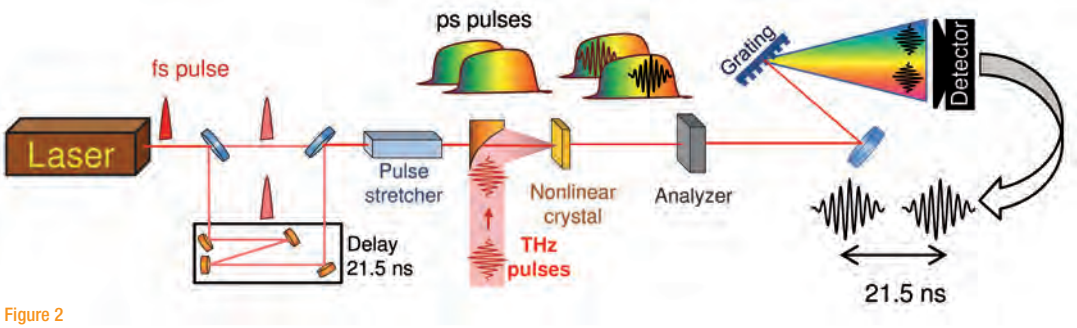

Figure 2

The principle of double THz pulses arrival-time measurement based on the spectral decoding technique at FLASH: laser pulse has been split and one part has been delayed by 21.5 ns. Pulses are recombined and temporally stretched in the high dispersion glass. Stretched pulses and THz doubler pulses are temporally and spatially overlapped in the nonlinear crystal, where THz pulses modulate polarization of the respective probing laser pulses. Modulation is detected via grating spectrometer.

high pulse energy, while suppressing the THz output. In this first study, we have demonstrated the suppression of the XUV pulse energy of the first electron bunch (11 µJ), down to a level of 16 % of the second bunch (67 µJ) of the THz doubler. These improvements will significantly widen the range of experiments that can utilize this setup. This suppression can probably be further improved by two orders of magnitude if fast kickers are used to deflect the electron bunch orbit by as little as 100 µm from the optimal orbit in the XUV undulators that would reduce the intensity of residual XUV pulse.

The arrival time stability of two THz doubler pulses is essential for accurate pump-probe experiments. We use the external optical laser pulse as a time marker, in a so-called electro-optic spectral decoding detection scheme. Inside of the nonlinear crystal (ZnTe), the field of the THz pulse modulates a temporally chirped probing laser pulse, within each single shot. This modulation can be used as an arrival-time marker of THz pulses for the external laser [5]. We adapt this technique to detect the arrival time of the THz doubler pulses simultaneously (Fig. 2) using a single probe laser pulse. We split the laser pulse into two parts and delay one part by 21.5 ns, to reproduce the time structure of the THz doubler. Since the laser pulse has been split optically, the temporal instabilities are minimal (fs or better). All laser pulses are stretched in a piece of glass (SF57) to gain linearly chirped pulses. The stretched pulses are modulated by respective THz pulses in the ZnTe crystal, mentioned above and the modulation is detected by a line camera detector mounted behind the spectrograph. The detector response is slower than the time delay between the pulses. In order to be able to detect the respective arrival time between the two THz doubler bunches, the arrival time of the probe laser pulses is adjusted so that the THz doubler pulses modulate different spectral regions of their respective probe laser pulses (Fig. 3). The modulations are well separated to avoid ambiguities in arrival-time determination. By analysing the individual arrival times we estimated the overall level of jitter over a period of 12 minutes to be ~20 fs (rms). Further solutions for achieving higher temporal resolution by monitoring arrival times are in preparation.

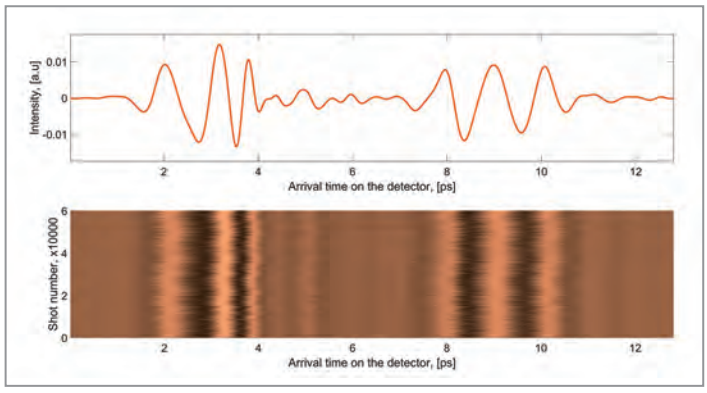

Figure 3

The arrival time detection of THz doubler pulses by spectral decoding. (above) Single shot trace, detected by grating spectrometer, modulations by the first and the second THz pulse are well separated. (below) Series of single shot measurements acquired over ~90 min (60 k shots).

Contact: Nikola Stojanovic, nikola.stojanovic@desy.de

Authors

Ekaterina Zapolnova, Torsten Golz, Rui Pan, Karsten Klose, Siegfried Schreiber and Nikola Stojanovic

Deutsches Elektronen-Synchrotron DESY, Hamburg, Germany

Original publication

'THz pulse doubler at FLASH: double pulses for pump-probe experiments at XUV FELs', J. Synchrotron Rad. 25, 39–43 (2018). DOI: 10.1107/S1600577517015442

References

1. N. Stojanovic and D. Markus, 'Accelerator-and laser-based sources of high-field terahertz pulses', Journal of Physics B: Atomic, Molecular and Optical Physics, 46, 192001 (2013).
2. F. Tavella, N. Stojanovic, G. Geloni and M. Gensch, 'Few-femtosecond timing at fourth-generation X-ray light sources', Nature Photonics 5, No. 3, 162–165, (2011).
3. T. Oelze, B. Schütte, M. Müller, J. P. Müller, M. Wieland, U. Frühling, M. Drescher, A. Al-Shemmary, T. Golz, N. Stojanovic and M. Krikunova, 'Correlated electronic decay in expanding clusters triggered by intense XUV pulses from a Free-Electron-Laser', Scientific reports, 7, 40736 (2017).
4. O. Grimm, S. Schreiber, and K. Klose, 'Double-pulse generation with the FLASH injector laser for pump/probe experiments', Proceedings of EPAC 2006, THPCH150 (2016).
5. S. Kovalev, B. Green, T. Golz, S. Maehrlein, N. Stojanovic, A. S. Fisher, T. Kampfrath, and M. Gensch, 'Probing ultra-fast processes with high dynamic range at 4th-generation light sources: Arrival time and intensity binning at unprecedented repetition rates', Structural Dynamics 4, 024301 (2017).

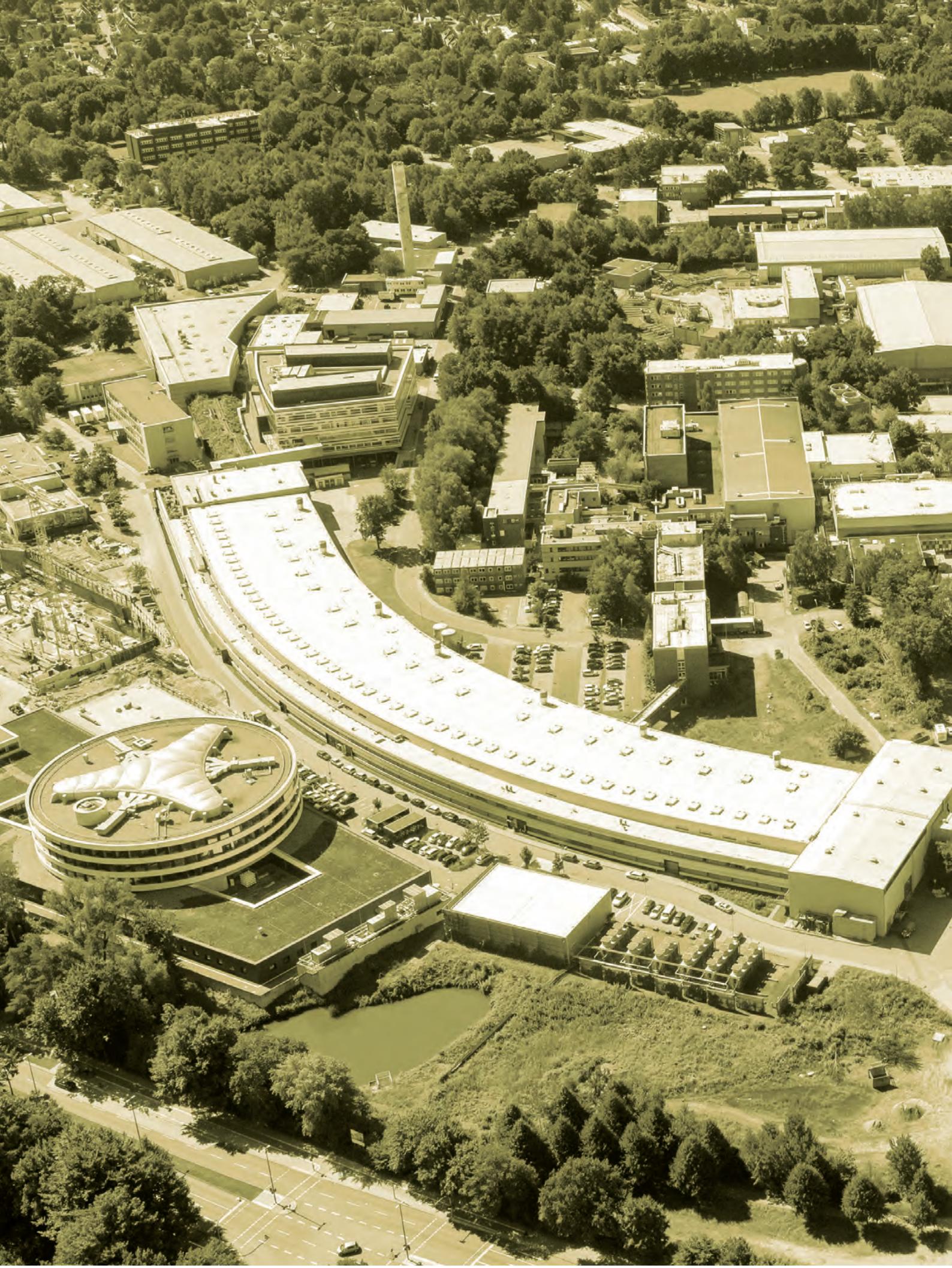

Light Sources.

FLASH.

Extending the options for exciting research

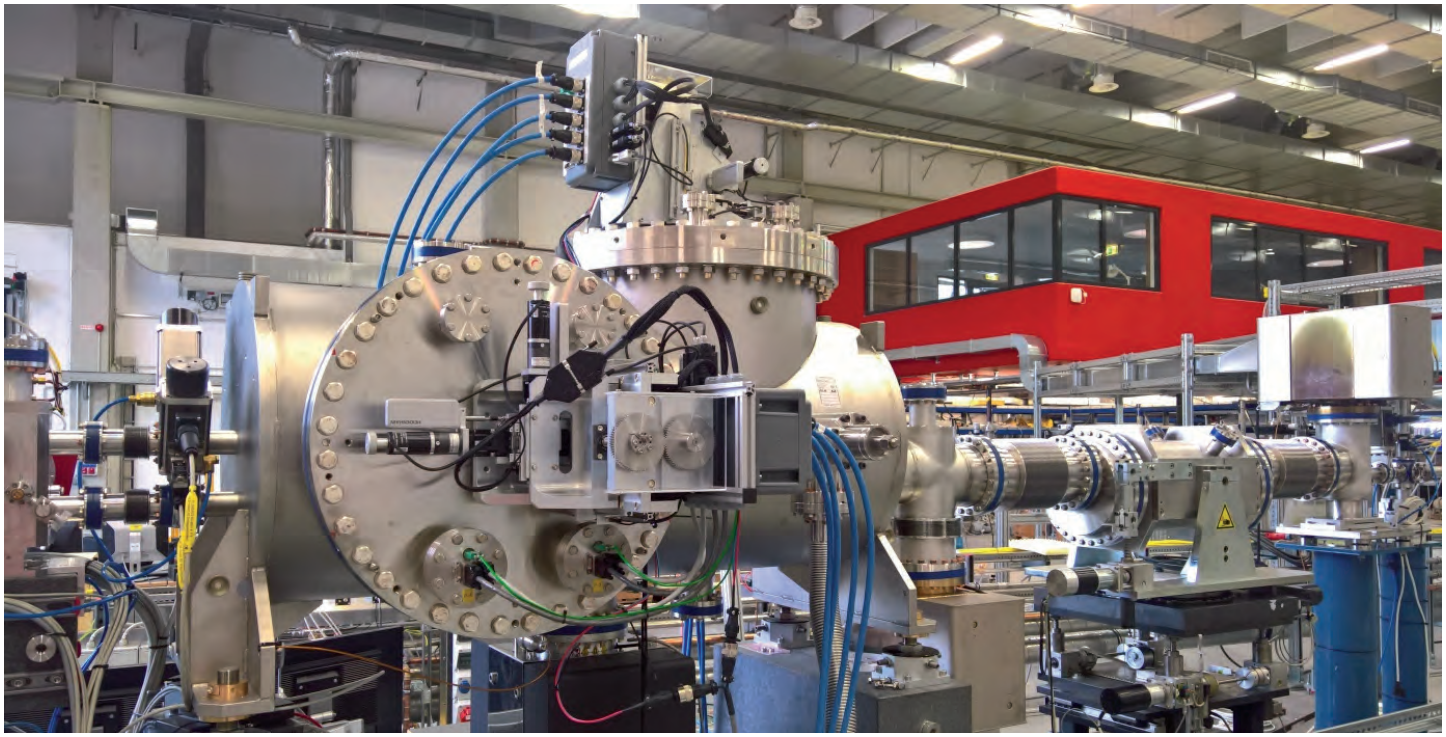

Figure 1

Side view of the beamline FL24 at FLASH2. Foreground on the left: Vacuum chamber of the Kirkpatrick-Baez focusing optics from FERMI with the outside motors for mirror manipulation. On the right: chamber of vertically deflecting pre-mirror which is required to have the FEL beam behind the focusing optics still parallel to the floor but at elevated height.

At FLASH, the beamtime for users in 2017 was allocated in two user periods and six beamtime blocks. The 9th user period took place from January to June and the 10th from July to December. The free-electron laser (FEL) was operated nearly 4500 hours for users, including time for setup, tuning and contingency, with an uptime of 97 %. During this time, FLASH provided 323 shifts of beamtime, each shift 12 h long, to 36 user experiments, including 6 in-house experiments. A large fraction of the experiments was performed using the 'CAMP' endstation at beamline BL1 and the 'WESPE' endstation (FLASH/University Hamburg) for time-resolved photoemission spectroscopy, which is 'semi-permanent' at the PG2 beamline end. The research highlights in this Annual Report give an impression of scientific opportunities available at FLASH.

In 2017, many updates and new features were added to the FLASH facility. The new installations and enhanced functionality of, e.g., data acquisition and controls, aim at expanding the range of scientific applications at DESY's free-electron laser while easing the performance of experiments. This is particularly essential for the parallel operation of two experiments in the experimental halls 'Albert Einstein' (FLASH1) and 'Kai Siegbahn' (FLASH2).

New focusing optics at beamline FL24

The FLASH2 beamline FL24 provides an open port for user supplied experiments and has recently been equipped with a Kirkpatrick-Baez (KB) focusing optics (Fig. 1) with bendable mirrors in order to adapt focus size and focal position to the users' demands. The system called 'KAOS' (Kirkpatrick-Baez Active Optics System) has been developed at FERMI in Trieste (Italy) and it was adapted to the needs at FL24 in collaboration with colleagues from FERMI. Distances from the last beamline flange to the interaction point in the experimental chamber can be varied from about 0.4 m to 2 m, while the best foci are routinely below 10 µm and for the shortest wavelengths even below 5 µm (FWHM), as verified with wavefront sensor measurements.

Reaction Microscope (REMI) features a new split-and-delay unit

At the FLASH2 beamline FL26, the permanent end station 'REMI', a reaction microscope from the MPIK Heidelberg, is installed for advanced atomic, molecular and optical (AMO)

Figure 2

Panorama-view inside the ~80 m² hutch of the FLASH2 optical pump-probe laser. The laser system, on small, modular breadboards, is still wrapped in the transport foil. The stainless steel tube at the bottom left is the front part of the transport beamline towards the experiments.

physics and molecular femto-chemistry experiments. With such a reaction microscope all fragments of a photoionisation process can be detected by means of a combination of electron and ion time-of-flight (TOF) spectrometers and a specific arrangement of electric and magnetic extraction fields. Measuring all fragments in coincidence enables kinematically complete experiments.

For time resolved experiments, REMI has been recently complemented by a grazing incidence split-and-delay unit (SDU). This unit allows to fully exploit the fast wavelength tunability of FLASH2 in contrast to the formerly used multi-layer-based SDU. The new mirror chamber simultaneously serves as an SDU and as a focusing device. The time delay can be adjusted in the range of ± 2.7 ps. A focal spot size of about 3 µm (FWHM) has been achieved during commissioning.

The new optics arrangement significantly reduces the background signal from residual gas molecules in the REMI ultra-high-vacuum and improves the data statistics. This SDU has already been used in summer/autumn 2017 for two experiments by Robert Moshammer and co-workers from MPI Heidelberg.

Pump-probe laser for FLASH2

A new type of high repetition rate laser based on the optical parametric chirped pulse amplifier (OPCPA) technology will be available for users in the second half of 2018. In summer 2017, this new laser has been put into operation according to its initial performance specifications. Afterwards, in October 2017, it moved from the laboratory where it was initially set up and tested into the laser hutch in the FLASH2 experimental hall (Fig. 2).

The laser pulses will be transported via dedicated transport beamlines (Fig. 3) to the end of the beamlines FL24 and FL26. Both will be equipped with a nearly collinear laser incoupling with approx. 1° angle with respect to the FEL beam.

The initial laser parameters expected for the operation for users in the second half of 2018 include: A fundamental centre wavelength of 800 nm at 100 nm bandwidth, 1-40 pulses at an intra-burst-repetition rate of 50 kHz, a pulse duration of 15 fs (FWHM) and variable pulse energies up to 500 µJ. 400 nm (second harmonic generation, SHG) and 266 nm (third harmonic generation, THG) wavelength will

Figure 3

FLASH2 experimental hall 'Kai Siegbahn': Stainless steel tubes of the new optical laser transport beamline during the setup phase. Mirror chambers for deflecting the laser towards beamline FL24 and FL26 are mounted on the two granite blocks in the foreground.

be generated on request with expected conversion efficiencies of >30 % and >5 %, respectively. The DESY laser group is working on more flexible parameter sets which will be available at a somewhat later time. Details and specific requirements of users will also be discussed during a satellite workshop at the users' meeting 2018.

Data acquisition changes

A variety of novel options for data analysis and storage has been implemented allowing a much more efficient and faster access to the acquired data. In order to ease the preparation before the beamtime and to keep users informed on the latest developments concerning controls, data acquisition (DAQ) and data analysis, we extended our online documentation considerably.

Important changes respectively upgrades of the DAQ include:

- access controlled storage space which is available on demand for each experiment to save acquired data from user detectors as well as data from the FLASH DAQ
- during the beamtime, pulse-synchronised data from the FLASH DAQ can be provided with few minutes delay in well-structured and easy to read HDF5 files for further analysis
- powerful DESY computing resources (Maxwell cluster) are provided for the (near) online analysis during the experiment as well as offline analysis after the beamtime
- easy remote access to the raw and processed data via web interface (gamma-portal).

New electronics for better timing and synchronisation

After the implementation of a new hardware infrastructure based on the µTCA (MTCA.4) standard several new options are now available at all FLASH beamlines, for example

- fast 2 and 4 GSample ADCs to record user data bunch-synchronised in the FLASH DAQ system. These ADCs are particularly interesting to record TOF detector traces
- 108 MHz ADCs to record 'slow' user data bunch-synchronised in the FLASH DAQ
- online viewing tools and sample scripts for efficient data analysis of the ADC user data
- additional triggers for each FEL bunch (burst trigger) as well as a set of frequencies locked to the FEL timing.

Figure 4

Participants of the workshop on the 'Future of Science at FLASH' at DESY from 25-27 September 2017.

More details on the related hardware and the data acquisition options, together with links to the corresponding documentation can be found on the FLASH webpages .

Taking spectra 'on the fly'

A particular challenge for online monitoring of FEL pulse parameters is the burst mode operation of FLASH and European XFEL, since it requires a fast detection of all parameters. Recently two new tools have been successfully implemented at FLASH to monitor the spectral distribution of individual pulses in the burst mode. These tools allow sorting of experimental data according to photon energy in the vicinity of narrow photo absorption resonances and enhancing the energy resolution of spectroscopy experiments by taking into account the exact distribution of spectral modes in a SASE pulse.

Future of Science at FLASH

More than 120 participants attended the workshop on the 'Future of Science at FLASH' at DESY from 25-27 September (Fig. 4). This 'FLASH2020+' workshop focused on the key scientific challenges that can be solved with a high-repetition-rate XUV and soft X-ray facility in the future. The programme featured six keynote and 15 contributed talks, a poster session, and breakout sessions on AMO physics, chemistry, molecular life sciences, and condensed-matter physics. Based on the discussions, the community came up with parameters for a 'dream' facility, which include 100 kHz CW operation, a fundamental wavelength up to the oxygen K-edge, flexible pump–probe schemes (THz to XUV), few-femtosecond and sub-femtosecond Fourier-limited pulses, as well as variable polarisation.

The feedback from the user community is already reflected very well in the FLASH strategy and will help to further refine it.

Contact: Rolf Treusch, rolf.treusch@desy.de

PETRA III.

New beamlines operating

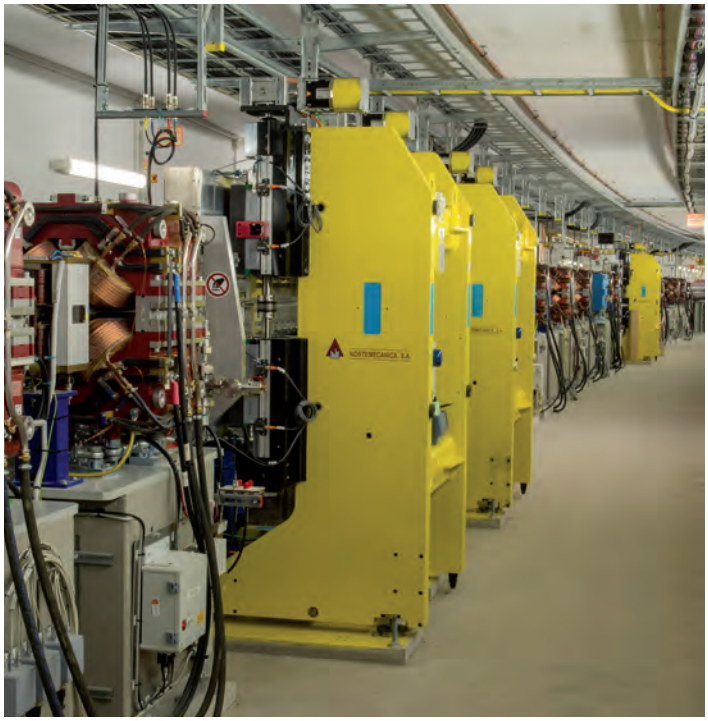

Figure 1

New 2 m undulators for beamlines P22, P23 and P24 in the PETRA III ring tunnel (left). Completed frontend of the PETRA III beamline P21 with a length of 90 m from the undulator source to the tunnel wall (right).

In 2017, separate shutdown periods in the winter and the summer were required to allow for extensive installation work in the ring tunnel and to install hardware of new beamlines at the PETRA III extension.

The PETRA III operation for users was accordingly split into two runs with the first run ranging from mid of April until beginning of July and the second from mid of August until end of December. After the winter shutdown the PETRA III operation was successfully resumed after very short commissioning on 10 April 2017. Overall 3187 hours have been planned for user beamtime in 2017. An availability of 98 % and a mean time between failures of 44 h (Update 4 December) was reached which is a significant gain as compared to the recent years. In total, 966 proposals (including 'Long term projects' (LTPs) and 'Block Allocation Group' proposals (BAGs)) have been submitted for beamlines P01 – P11, P24, P64 and P65 upon the two proposal calls in 2017. In addition, 190 proposals (incl. BAGs) have been collected for the EMBL beamlines P12 – P14 at PETRA III.

The 2017 beamtime for users ended on 22 December 2017. In the subsequent shutdown period installation work for the new beamlines will continue in the ring tunnel. In particular, the 4 m long in-vacuum high-energy undulator of P21 will be integrated into the PETRA III storage ring.

Storage ring operation and new beamline frontends

In 2017 the PETRA III operation was, as in the previous years, equally split into the two operation modes 'timing' with 40 bunch mode filling and 'continuous' with 480 or 960 bunches. This distribution is proven to be optimised for a maximum number of timing mode shifts and minimum activation of ring components as well as radiation induced degradation of the undulators due to particle losses.

The top-up procedure has been further improved at PETRA III. The injection to refill the ring current from 100 mA to 101 mA is done off-axis and is causing horizontal orbit oscillations which increase the horizontal emittance. In continuous filling mode operation, the top-up filling takes a few seconds every 5 1/2 minutes, whereas in timing mode operation it is needed every 50 seconds due to the shorter beam lifetime. Therefore, the top-up procedure itself is a significant part of the user run. In order to reduce its detrimental effect on the horizontal emittance, the kicker pulse has been optimised during several machine commissioning runs. The original increase of the emittance by 17 % for as long as 200 µs after each injection has been reduced to 5 %.

During the winter shutdown in the beginning of 2017, all four canting dipole magnets in the storage ring sections accommodating the new beamlines were replaced by modified

magnets to eliminate the influence of magnetic dipole stray fields on the undulator magnet structures and enables now optimal beamline operation at the XAFS beamlines P64 and P65 in the experimental hall 'Paul P. Ewald'. Media installation at the frontends of the PETRA III beamlines P22, P23 and P24 was finalised and all three undulators are placed at their final position. In parallel, the first frontend section of beamline P21 was installed, while the remaining major part had to be completed in the summer shutdown. Beamline P21, the Swedish materials science beamline, is by far the longest beamline at PETRA III, with a frontend length of 90 m up to the tunnel wall (Fig. 1) and a maximum beamline length of 165 m.

New beamlines coming up

At the PETRA III extension, commissioning of the second X-ray absorption beamline for advanced XAFS applications P64 was completed in spring 2017 and full user operation started in April 2017.

In the experimental hall 'Ada Yonath', the second phase of beamline installation had been in full swing with the new chemical crystallography beamline P24 getting first monochromatic light in April 2017. As part of the beamline commissioning, the instrumentation in both experimental hutches was completed and put into operation: a heavy load Kappa diffractometer for single crystal diffraction in complex sample environments in the first hutch (Fig. 2) and a 4-circle diffractometer for small molecule crystallography in the second hutch (Fig. 3). A 'Chemical Crystallography Beamline P24' user workshop was organised on 4 – 5 May to present the new beamline and to discuss possibilities for first experiments. Proposals for beamline P24 were already accepted in the call in September 2017, regular user operation will start in April 2018.

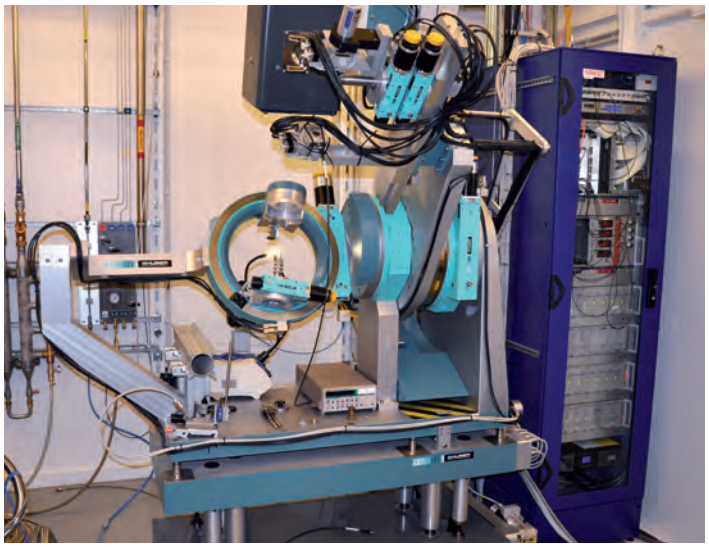

Figure 3

4-circle diffractometer in experiment hutch 2 of the PETRA III beamline P24.

Significant progress was also made at beamlines P22 for Hard X-ray photoelectron spectroscopy (HAXPES) and P23, the Russian-German *in situ* and nano-diffraction beamline. Both beamlines got first monochromatic beam in November 2017 and entered the commissioning phase. In the summer of 2018, the very successful HAXPES instrument currently in

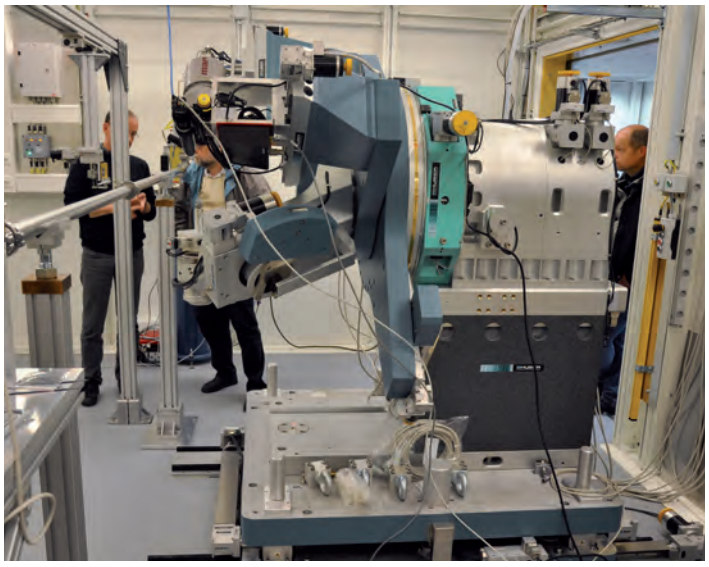

Figure 2

Heavy load Kappa diffractometer in experiment hutch 1 of PETRA III beamline P24.

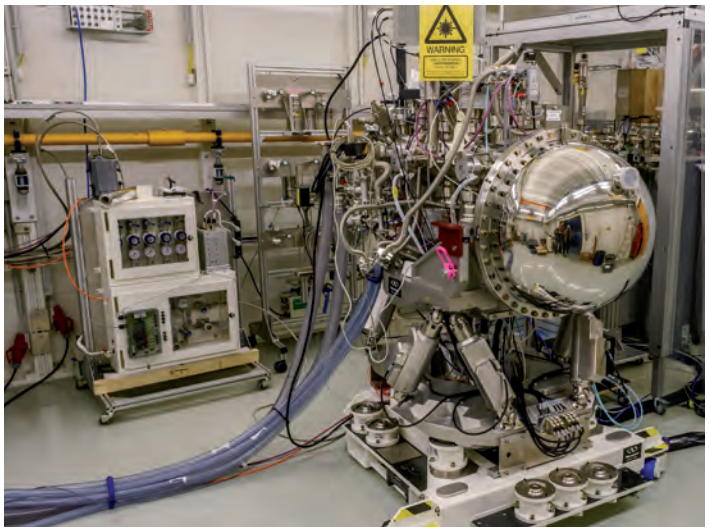

Figure 4

HAXPES instrument for ambient and high pressure from Stockholm University (A. Nilsson et al.) at the PETRA III beamline P22.

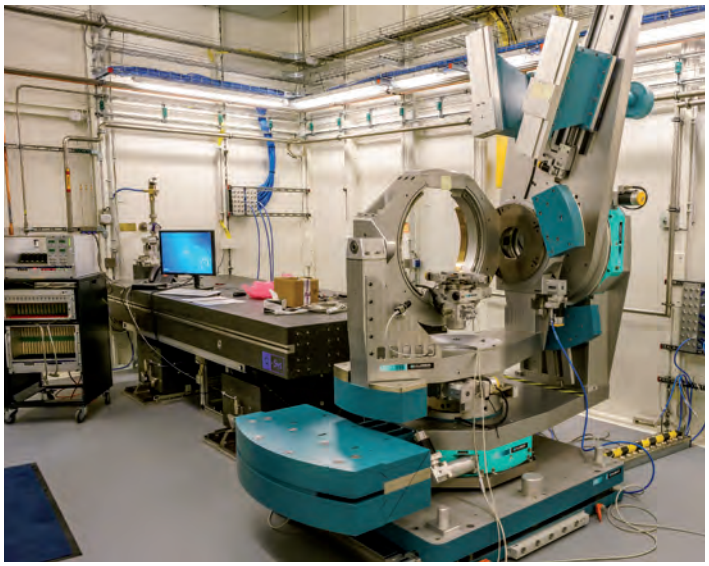

Figure 5

Heavy load diffractometer at the Russian-German beamline P23 at PETRA III.

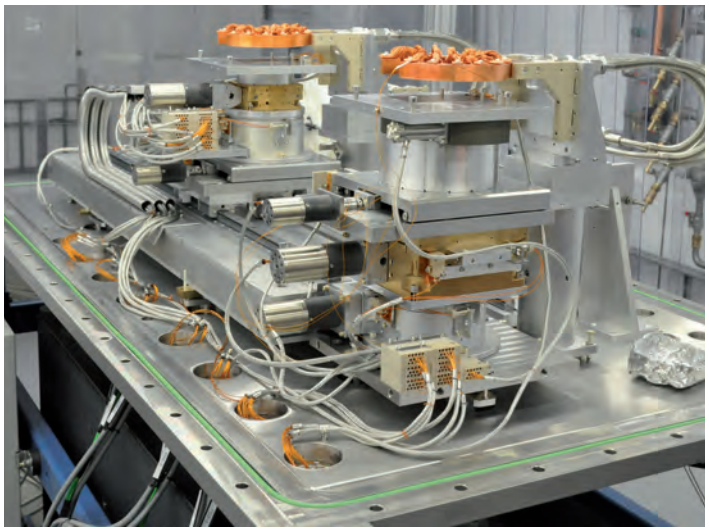

Figure 6

Cryogenically cooled double Laue monochromator (vacuum vessel removed) of the straight branch of the PETRA III beamline P21.

operation at beamline P09 will be relocated to P22. Until then it is planned to commission further instruments at P22 such as a novel high-pressure HAXPES machine designed and built by a user group of Stockholm University (Fig. 4). This setup will potentially allow photoelectron spectroscopy at pressures up to 10 bars for catalysis research, making use of the brilliant beam available at P22. The capabilities of the beamline and future applications of the various instruments were discussed at a 'Hard X-Ray Photoelectron Spectroscopy at PETRA III' user workshop on 23 – 24 November.

At PETRA III beamline P23, the optical instrumentation will be completed parallel to the initial beamline commissioning. A user workshop will be organised at the annual DESY Photon Science users' meeting 2018. For both beamlines P22 and P23 first user proposals will be accepted in the upcoming call for proposals in March 2018 and they will gradually progress into full user operation following the summer shutdown in 2018.

The Swedish materials science (SMS) beamline (P21) also made considerable progress in 2017. As mentioned above, the beamline frontend is almost completed and further downstream the beamline infrastructure and instrumentation is being set up. The undulators will be installed in the upcoming winter shutdown. Crucial components are, e.g. the Laue monochromators which have been installed in the fall of 2017 (Fig. 6). The installation of beamline components in the optics hutch will continue in the spring of 2018 and first beam is expected end of May. The beamline capabilities and its potential for materials science applications were discussed with the Swedish user community during a workshop on 9 – 10 November 2017.

In 2018, the remaining beamlines, the High-energy wiggler beamline P61, Small angle X-ray scattering P62, and 'Superlumi' beamline for time-resolved VUV-spectroscopy P66 will be in the focus of the upcoming construction work.

Operating beamlines and experiments

Since 2013 all PETRA III beamlines in the experimental hall 'Max von Laue', P01 – P14, are fully operational. Some beamlines had already been upgraded with additional optics, experiments or detectors in the recent years. The first new beamlines P65 and P64 of the PETRA III extension for XAFS experiments started full user operation in June 2016 and April 2017, respectively.

Staff from PETRA III and the Max-Planck-Society (MPG) has finished the reconstruction of beamline P01 to accommodate resonant inelastic scattering experiments at around 2.8 keV, which enables investigation of new types of topological matter based on ruthenium. The work included the installation of new undulators, an in-vacuum diffractometer and differentially pumped vacuum lines to connect to the machine vacuum. Since 2017, the beamtime at P01 is split with 40 % available for the MPG and 60 % for the general user community.

Beamline P04 finished the installation of a second branch which is basically a copy of the first branch. Both branches can be operated alternately: A switching mirror directs the X-ray beam to the corresponding experiment. This operation mode makes more efficient use of the beamtime because it could now be scheduled in alternating 12 hour shifts. For instance a new experiment can be setup or samples can be

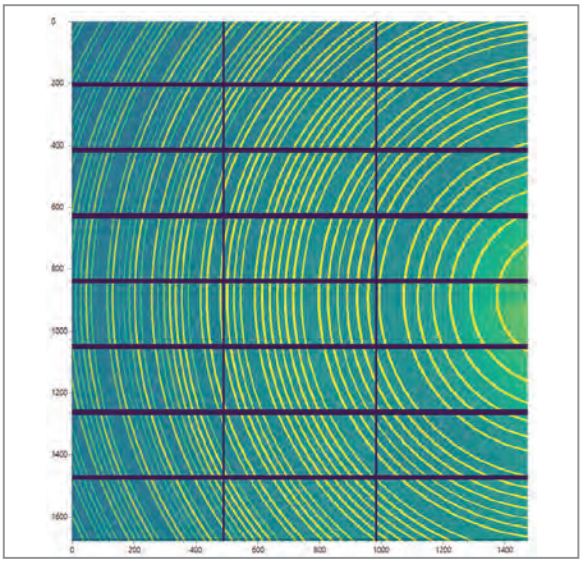

Figure 7

New 2M CdTe detector at the powder diffraction beamline P02.1 at PETRA III. The first image of LaB_6 was taken at 60 keV.

prepared at one branch while user experiments can be performed at the other branch.

For the high energy beamlines at PETRA III a photon counting pixel detector (PILATUS 2M CdTe) has been delivered in 2017 (Fig. 7). This detector has the advantage to be fast (250 Hz), to lack electronic noise and to have an electronic gate. The case of this particular detector has specially designed holes to allow the small angle scattering signal passing the PILATUS for detection at a further detector.

At the new advanced XAFS beamline P64, first time-resolved user experiments using the quick scanning extended X-ray absorption fine structure (QEXAFS) monochromator, implemented in collaboration with University of Wuppertal (R. Frahm et al.) have been successfully performed. Also, the van-Hamos fluorescence spectrometer (Fig. 8), built in collaboration with the University of Paderborn (M. Bauer et al.), has been applied for XAFS experiments with high-energy resolution fluorescence detection (HERFD).

Further instrumental achievements at PETRA III beamlines in 2017 are: At the experiment for nuclear resonant scattering at beamline P01 a high resolution monochromator for the Mößbauer-active iridium isotop ^{193}Ir has been installed. First measurements of the magnetic properties of $SrIrO_3$ have been performed. Moreover at the Extreme conditions beamline P02.2 a dynamic compression setup in combination with two GaAs LAMBDA pixel detectors yielded a time resolution of 250 µs at a compression rate of 124 TPa/s.

In February 2017 the first internal workshop of all staff members of PETRA III and colleagues from groups on-site was held to strengthen the cooperation and to discuss technical, computing and scientific achievements and challenges at PETRA III beamlines. All these activities will help to further advance developments at PETRA III.

Contact: Wolfgang Drube, wolfgang.drube@desy.de,
Oliver H. Seeck, oliver.seeck@desy.de,
Rainer Wanzenberg, rainer.wanzenberg@desy.de

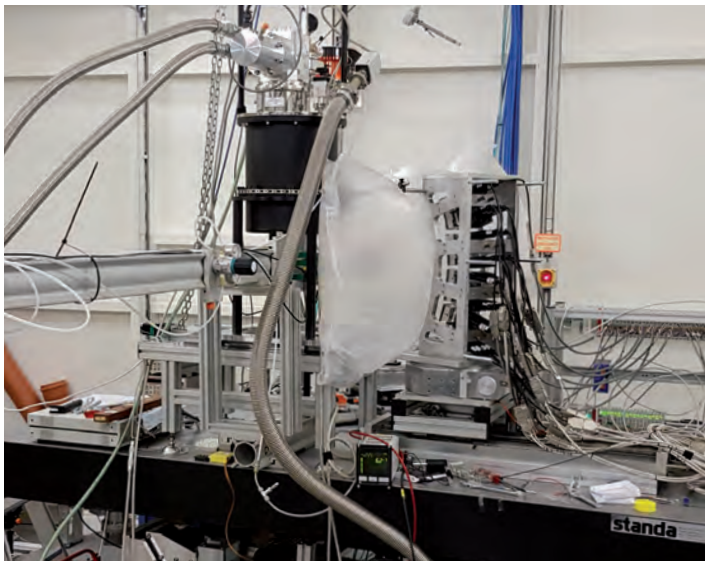

Figure 8

Van-Hamos fluorescence spectrometer at the PETRA III XAFS beamline P64.

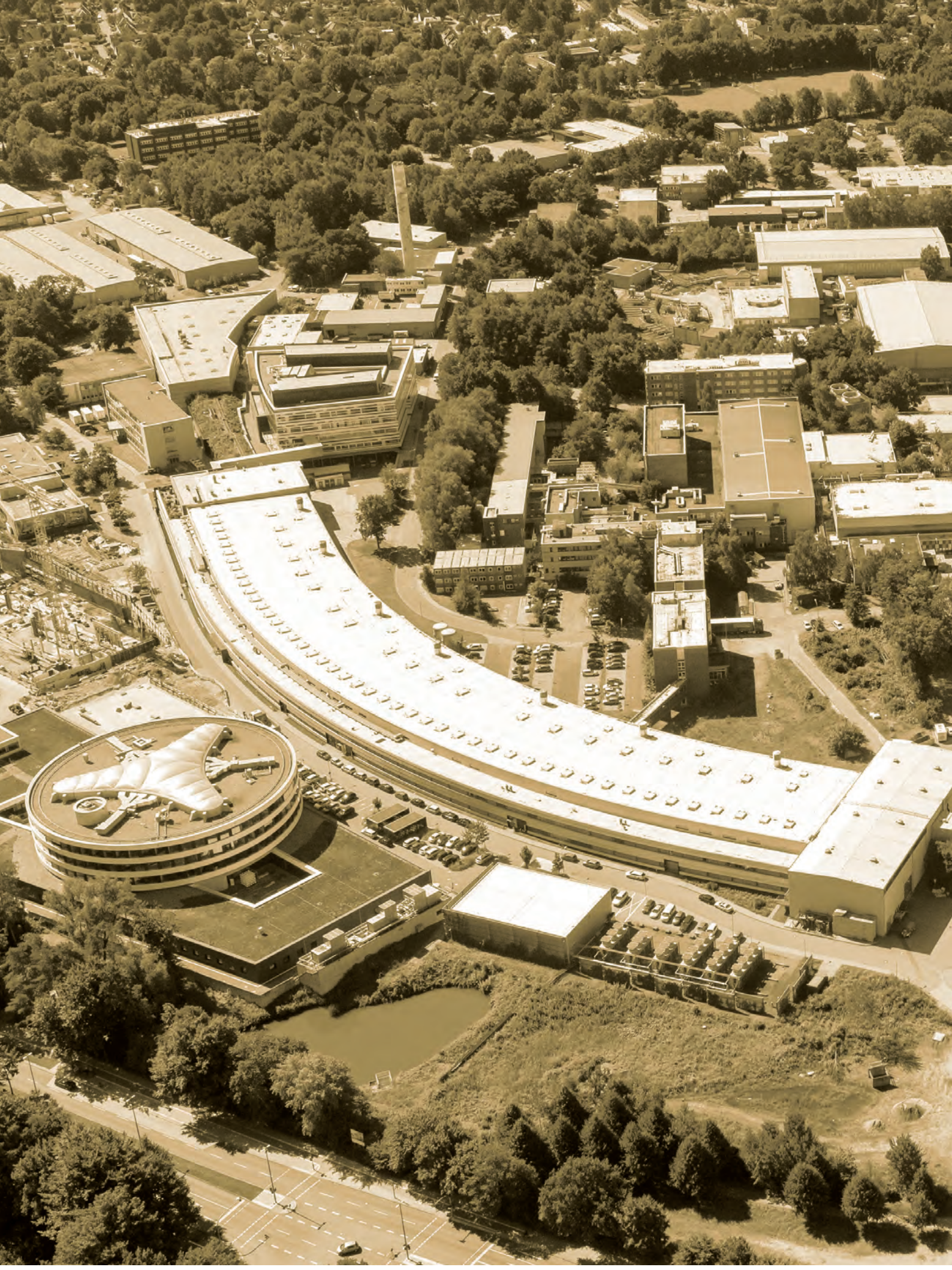

Campus and Collaborations.

Overview – campus and collaborations.

DESY Photon Science is part of many national and international collaborations. Cooperation creates new scientific and technological opportunities at DESY's facilities, increases the pool of talents and is also indispensable to further coordinate research roadmaps and agendas. The full collaboration landscape at DESY Photon Science is diversified and involves local as well as national and international partners.

Universities

A strong connection to the Universität Hamburg (UHH) is established through the 'Partnership for Innovation, Education and Research' (PIER). This structural cooperation has provided the ground for a joint graduate school (PIER Helmholtz Graduate School, PHGS), joint professorships and a seed fund facility for research projects. Together with colleagues from the Max Planck Institute for the Structure and Dynamics of Matter (MPSD) and European XFEL, DESY and UHH run common research projects in the DFG funded Cluster of Excellence CUI ('The Hamburg Centre for Ultrafast Imaging') and the collaborative research centre SFB 925 'Light induced dynamics and control of correlated quantum systems'. DESY is expanding collaborations with further German universities through joint professorships, common research projects and BMBF Collaborative Research at PETRA III and FLASH. With some of the universities joint laboratories and outstations on the DESY campus are being formed. Examples of current partnerships are the TU Hamburg, and the Universities of Göttingen, Kiel and Erlangen-Nürnberg.

Centre for Structural Systems Biology (CSSB)

Within the CSSB – a cooperation of nine partner institutions – scientists use a novel approach which combines integrative structural biology with systems biology to advance our understanding of the molecular mechanisms of some of the world's most widespread infections.

European Molecular Biology Laboratory (EMBL) Hamburg

At EMBL Hamburg, scientists investigate the structure of challenging molecules that impact human health. The Hamburg site's service teams develop methods and software to support scientists from around the world in every step of biological structure determination. EMBL runs three beamlines at PETRA III: one for Small Angle X-ray Scattering experiments and two for Macromolecular Crystallography.

Center for Free-Electron Laser Science (CFEL)

The Center for Free-Electron Laser Science as a joint enterprise of DESY, the Max Planck Society (MPG), and the Universität Hamburg is designed to advance science with next generation light sources and lasers.The three partners join forces to explore structural changes of atoms, molecules, condensed, biological, or warm dense matter on femto-second time scales. CFEL envisions uncovering the 'dynamics of matter' by uniting expertise from various disciplines and research institutions into a new interdisciplinary and synergistic effort.

DESY within User Consortia at the European XFEL

Besides being responsible for the construction and the operation of the European XFEL linear accelerator, DESY plays an important role as user of the European XFEL. DESY is partner in several user consortia, which have been formed to prepare for the facility's user operation in an optimal way. These user consortia are:

- the Serial Femtosecond Crystallography (SFX) user consortium,
- the Helmholtz International Beamline for Extreme Fields (HIBEF),
- the Heisenberg Resonant Inelastic X-ray Scattering (h-RIXS) user consortium,
- the DataXpress consortium for data analysis,
- the consortium State-, size-, and isomer-selected samples of polar molecules and clusters at the European XFEL (COMO).

Moreover, DESY scientists develop lasers and detectors for usage at the European XFEL.

DESY Innovation and Technology Transfer

With support of the DESY department for Innovation and Technology Transfer (ITT) scientists from DESY Photon Science contribute to the DESY innovation strategy including the transfer of knowledge and technology from the laboratory to industry.

DESY NanoLab

The DESY NanoLab provides nano-characterisation, spectroscopy and nano-structuring methods, which are complementary to the photon based techniques available for users at the DESY X-ray facilities PETRA III and FLASH. The access to the DESY NanoLab is granted for external users via regular PETRA III or FLASH proposals (through DOOR) or via proposals from the European transnational user platform Nanoscience Foundries Fine Analysis (NFFA Europe).

Helmholtz-Zentrum Geesthacht (HZG)

The German Engineering Materials Science Centre (GEMS) is a user platform of HZG for the complementary research with photons and neutrons with an outstation at DESY. GEMS research groups work in X-ray diffraction and imaging on the DESY campus. HZG operates several beamlines and end stations at PETRA III focusing on research in the field of engineering materials science.

International cooperation

DESY is engaged in international cooperation, for example to leverage new resources and contributions to DESY facilities and installations. Significant examples for DESY Photon Science in that respect are the international contributions to PETRA III by Sweden through the Röntgen-Angström-Cluster (RAC), by Russia through the Ioffe-Röntgen-Institute (IRI) and by India via the India@DESY collaboration.

Cooperation for research and education.

News from the universities

Figure 1

The new building of the Center for Hybrid Nanostructures (CHyN) on the campus.

Universität Hamburg (UHH)

On the occasion of the New Year's Reception of the Hamburg Centre for Ultrafast Imaging (CUI) on 17 January 2017 the Mildred Dresselhaus Award 2016 was given to Prof. Dr. Christiane Morais Smith (Utrecht University) and Dr. Friederike Ernst (Stanford University). The award for the two excellent female scientists includes prize money and a guest professorship at the Universität Hamburg.

On 19 July 2017 the new Center for Hybrid Nanostructures (CHyN) was inaugurated. The new centre which was built by the Sprinkenhof GmbH on behalf of the Hamburg Ministry for Science, Research and Gender Equality will host 8 working groups from the Institute of Nanostructure and Solid State Research (INF) of the Physics Department of the Universität Hamburg. CHyN is another building block of the on-going relocation of the Physics Department to the Science Campus Bahrenfeld (Fig. 1). In the framework of CHyN the scientists will focus on an interdisciplinary approach towards nano-structure research including physics, chemistry, biology and medicine. The direct neighborhood to DESY will further foster the already existing strong collaborations with DESY scientists and the DESY NanoLab.

In the framework of the Federal Excellence Initiative the Universität Hamburg was successful with a total of four pre-proposals as announced by the Deutsche Forschungsgemeinschaft in the end of September. One of the successful initiatives is 'Advanced Imaging of Matter: Structure, Dynamics and Control on the Atomic Scale' (AIM), which is centred on photon science and nanoscience and involves scientists from the Universität Hamburg, DESY and the European XFEL as principal investigators. The initiative is now preparing for a full proposal for the final round in 2018.

On 9 November 2017 the prestigious Hamburg Prize for Theoretical Physics was presented to the American physicist Andrew Millis from Columbia University. Millis received the prize in recognition of his work in the field of solid-state physics. In particular, his research on high-temperature superconductivity is considered to be pioneering. The prize which was established in 2010 was awarded by the Hamburg Centre for Ultrafast Imaging (CUI) and the Joachim Herz Stiftung. Millis accepted the prize at a ceremony held on the Campus Bahrenfeld in the presence of Hamburg's Deputy Mayor and Minister of Science Katharina Fegebank. The prize winner is expected to come to Hamburg for extended teaching and research visits in the following years.

Christian-Albrechts-Universität zu Kiel (CAU)

The Christian-Albrechts-Universität zu Kiel and DESY continue their successful cooperation. Two joint professor appointments, Melanie Schnell and Kai Rossnagel, strengthen the already close collaboration between CAU and DESY and enhance the 'Kiel Nano, Surface and Interface Science' (KiNSIS) co-operation. One highlight this year was the sod turning ceremony for the new Photon Science building, where the Kiel 'Ruprecht Haensel Laboratory' will be housed (Fig. 2). A further collaboration through a workshop 'High resolution diffraction at solid and liquid interfaces' organised jointly by Bridget Murphy (CAU) and Florian Bertram (DESY) highlighted recent developments in this field.

Figure 2

Joint ground breaking: HZG director Wolfgang Kaysser, Hamburg state secretary for science Eva Gümbel, Schleswig-Holstein research minister Kristin Alheit, Matthias Kalläne (CAU), Martin Müller (HZG/CAU), Kai Rossnagel (CAU), Olaf Magnussen (CAU), DESY director Helmut Dosch, Cristel Haensel, CAU president Lutz Kipp, Bridget Murphy (CAU). Image: Claudia Eulitz, copyright CAU

BMBF funding continues to provide excellent support for new CAU science and instrumentation at PETRA III, including biodegradable magnesium at P05 and ultra-fast investigation of liquids at the X-ray diffractometer dedicated to liquid interfaces (LISA) at P08. CAU continues to support science at both the joint CAU/Helmholtz-Zentrum Geesthacht (HZG) nanofocus end station at the MiNaXS Beamline P03 and the spin and momentum resolved photoemission experimental station at the soft X-ray beamline P04, ASPHERE III.

Figure 3

Attendees of the research and students' workshop 'Energy Research at DESY Photon Sources' between DESY and the Collaborative Research Center 'Atomic Scale Control of Energy Conversion', Göttingen Campus.

Georg-August-Universität Göttingen (GAU)

During the year 2017 the interaction between DESY and Göttingen's Collaborative Research Center 'Atomic Scale Control of Energy Conversion' of the physics and chemistry faculties have been strengthened. In November 2017, at DESY a research and students' workshop has been hosted (Fig. 3). Goal of the workshop was an exchange about energy research capabilities at the DESY campus and materials-research-driven ideas of studying novel types of energy conversion mechanisms. The workshop has been sponsored by the German Science Foundation (DFG).

Goal of a novel project funded by the BMBF Verbundforschung (Köster, Salditt) is to study biomolecular structures in cells by combining coherent X-ray scanning diffraction and holography techniques at the P10 beamline of PETRA III with optical super-resolution microscopy. Furthermore, Göttingen University was successful within the proposal preselection round of the Federal Excellence Initiative, and DESY is an important contributing partner within the 'Campus Laboratory for Advanced Imaging, Microscopy and Spectroscopy' (CL-AIMS).

Friedrich-Alexander-Universität Erlangen-Nürnberg (FAU)

Within the framework of the DESY-FAU-HZG competence anchor (collaboration in the framework of the excellence initiative) joint laboratory collaboration between FAU and DESY, pilot projects are focused on catalysis, electronics, and lightweight materials. The goal of the first project is to investigate the catalytic adsorption behavior of liquid organic hydrogen carrier molecules for the storage of energy obtained from unsteady renewable sources. The key parameter is to find a proper metal catalyst for the de-/hydrogenation process. Pt- and Pd-based catalysts are the most efficient catalysts for this reaction. In 2017 the adsorption and hydrogenation of molecules on the nanoparticles surfaces and the solid/liquid interface was studied in Erlangen, DESY NanoLab and at the High Energy Materials Science Beamline P07 at PETRA III. The second project is related to the development of efficient electronic devices from organic thin film materials for solar cells, displays and light sources. Scientists at FAU designed a dedicated setup for *in situ* Doctor-Blading, which is a technique for creating thin organic films on industrial levels, and the high resolution diffractometer at beamline P08 at PETRA III has been adopted by DESY to accommodate this setup. During beamtimes at this instrument the in-plane and out-of plane properties of phospholipid films have been successfully measured. Scientist of FAU and DESY have been alternately visiting the partner institutes during the Condensed Matter in Physics and Chemistry Workshop at DESY and the Symposium of the competence anchor and the X-ray scattering summer school in Erlangen.

Technische Universität Hamburg (TUHH)

Several research groups at DESY Photon Science work in cooperation with TUHH. Examples of joint projects, which also include other partners, are the collaborative research centre Sonderforschungsbereich (SFB) 986 'Tailor-Made Multiscale Material Systems' coordinated by TUHH, two projects in the framework of the DESY strategy fund and a project funded by the 'Landesforschungsförderung' on new reactor technologies for chemical and biochemical synthesis techniques.

Contact: Wilfried Wurth, UHH and DESY, wilfried.wurth@desy.de
Bridget Murphy,CAU, murphy@physik.uni-kiel.de
Simone Techert, GAU and DESY, simone.techert@desy.de
Andreas Stierle, UHH and DESY, andreas.stierle@desy.de
Oliver Seeck, DESY, oliver.seeck@desy.de

Center for Free-Electron Laser Science CFEL.

Three institutions working successfully together

The fruitful collaboration between participating CFEL institutions (DESY, the Max Planck Institute for the Structure and Dynamics of Matter MPSD, and the University of Hamburg UHH) has continued in 2017 with great success.

The collaboration between the MPSD Theory Group of Angel Rubio and the DESY Ultrafast X-ray Optics Group of Franz Kärtner has demonstrated that ellipticity provides an additional knob to experimentally control high-order harmonic generation (HHG) in solids [1]. Solids are one promising route towards compact, brighter HHG sources. However, their use is currently hampered by the lack of a microscopic understanding of the mechanism leading to HHG from solids. The researchers have now shown that it is possible to unravel the complex interplay between the two mechanisms responsible for HHG in solids using elliptically polarized light, see Fig. 1. By means of extensive first-principles simulations they have shown how these two mechanisms are differently affected by the ellipticity of the driving laser field. The complex interplay between these effects can be used to tune and improve harmonic emission in solids, in particular, increasing the maximal obtained photon energy by as much as 30 %.

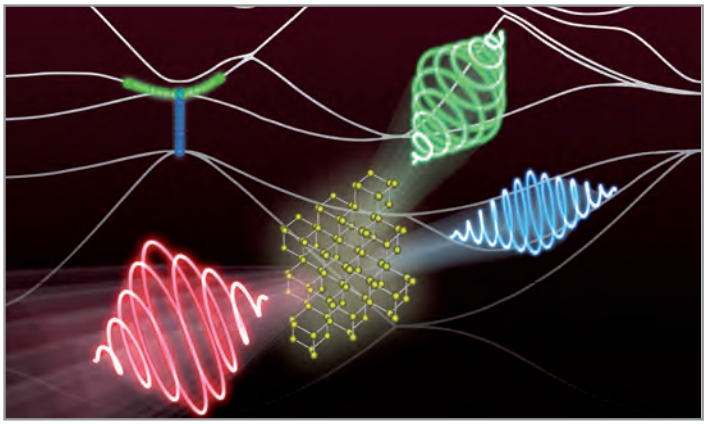

Figure 1

When exciting crystals such as silicon by an intense elliptically or circularly polarized light pulse (red), circularly polarized higher harmonics (green & blue) can be generated. Image: Nicolas Tancogne-Dejean + Joerg M. Harms, MPSD

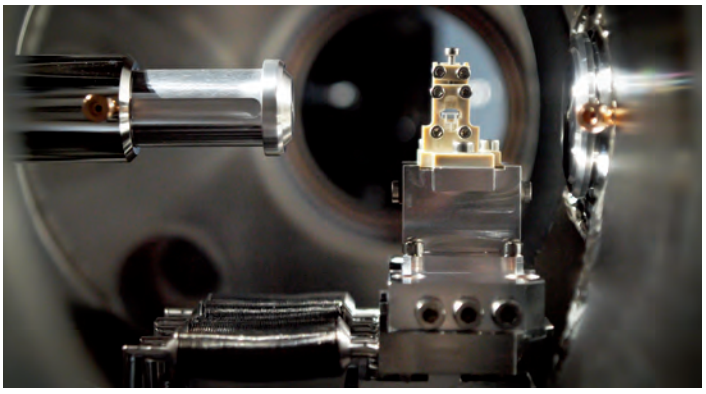

Figure 2

LUX plasma accelerator: The plasma cell (center) accelerates the electrons. Image: Niels Delbos, University of Hamburg.

Besides internal collaborations another CFEL highlight in 2017 was the start of the first scientific experiments at Europe's new X-ray laser European XFEL which were led by the CFEL Division for Coherent Imaging. The aim of the team headed by Anton Barty (DESY) and Henry Chapman (DESY) is to decode the atomic structure of different biomolecules at the SPB/SFX instrument of the European XFEL. For these experiments they recorded diffraction patterns from protein crystals every 220 nanoseconds. To accomplish this, they used the fastest X-ray camera in the world, the tailor-made Adaptive Gain Integrated Pixel Detector (AGIPD). It was designed and produced by an international consortium led by CFEL's Detector Research and Developments Group of Heinz Graafsma (DESY).

In summer 2017, the LUX (Latin for 'light') project led by the CFEL researcher Andreas Maier of the University of Hamburg in collaboration with DESY's Accelerator Division has produced first ultra-short pulses of X-rays (Fig. 2). LUX is part of the LAOLA collaboration between DESY and the UHH. LUX uses a laser with a power of 200 trillion watts (TW) to create electron beams from the interaction with hydrogen plasma. In the plasma, electrons accumulate behind each laser pulse, and are then accelerated by the positively charged plasma wave in front of them, thereby gaining up to 800 million electron volts (MeV) within a distance of just a few millimetres. For comparison, this is more energy than is supplied by the 70 metre long linear pre-accelerator LINAC II at DESY. For the first time on DESY campus, the plasma-based LUX electron beams were sent down a 50 centimetres long undulator, a periodic arrangement of small dipole magnets, to produce soft X-ray pulses with a wavelength of 9 nm. This is based on the same principle used by the large X-ray sources at DESY, such as the storage ring PETRA III, or the free-electron lasers FLASH and European XFEL.

Contact: Ralf Koehn, ralf.koehn@cfel.de

References

1. N. Tancogne-Dejean et al., Nature Communications 8, 745 (2017).

DESY NanoLab.

Preselecting and relocating single nano-objects

2017 stands out for a significant demand for sophisticated nano-structuring methods offered by DESY NanoLab in preparation for PETRA III experiments. With the dual beam Focussed Ion Beam (FIB) instrument at DESY NanoLab, micro- and nano-scale objects were selected, cut by the gallium (Ga) ion beam and fixed on dedicated sample holders. Figure 1 shows one step of this sample preparation: a copper sulphate nano-wire bundle is transferred with a micromanipulator and fixed on a fine tip. Gluing involves electron (E-BID) or ion beam (I-BID) induced deposition of a platinum (Pt) containing precursor material.

One crucial aspect is the need to position such nano-objects in the X-ray beam of PETRA III. E-BID and I-BID can be used to write markers in the vicinity of the nano-objects and relocate them by, e.g. their Pt fluorescence or their Pt Bragg peak.

Based on such hierarchically arranged guiding markers, DESY NanoLab develops tests and implements jointly with five European institutions a software tool that permits to transfer position coordinates inside the FIB to motor positions of the sample translation stage at an X-ray beamline. This 'Advanced Nano-Object Transfer and Positioning' protocol is supported by the European user platform Nanoscience Foundries and Fine Analysis (NFFA Europe, www.nffa.eu). The first NFFA user experiment making use of the Pt markers and the positioning protocol is scheduled for spring 2018.

A Physical Property Measurement System (PPMS) has become operational in 2017. It permits to condition properties of magnetic samples and to characterise them by a variety of magnetic field-dependent measurements up to 14 T and down to 1.6 K, both compatible with the conditions available at the resonant scattering PETRA III beamline P09.

Since December 2017 a multi-purpose Atomic Force Microscope (AFM) is available at DESY NanoLab that broadens the available analytic tools by providing high resolution surface topographic imaging in air, liquid or in an electrochemical environment.

The DESY NanoLab instrumentation is currently located in building 3 on the DESY Campus until the new building for the Center for X-ray and Nano Science (CXNS) is completed, which is foreseen for 2019.

In its basement, the new building will provide room for laboratories; more lab space is planned in the old DORIS hall and in building 25b. On additional four office floors, the CXNS building will host DESY Photon Science groups and outstations of the Helmholtz-Zentrum Geesthacht (HZG) and the University of Kiel, thus fostering a collaborative atmosphere.

Contact: Andreas Stierle, andreas.stierle@desy.de

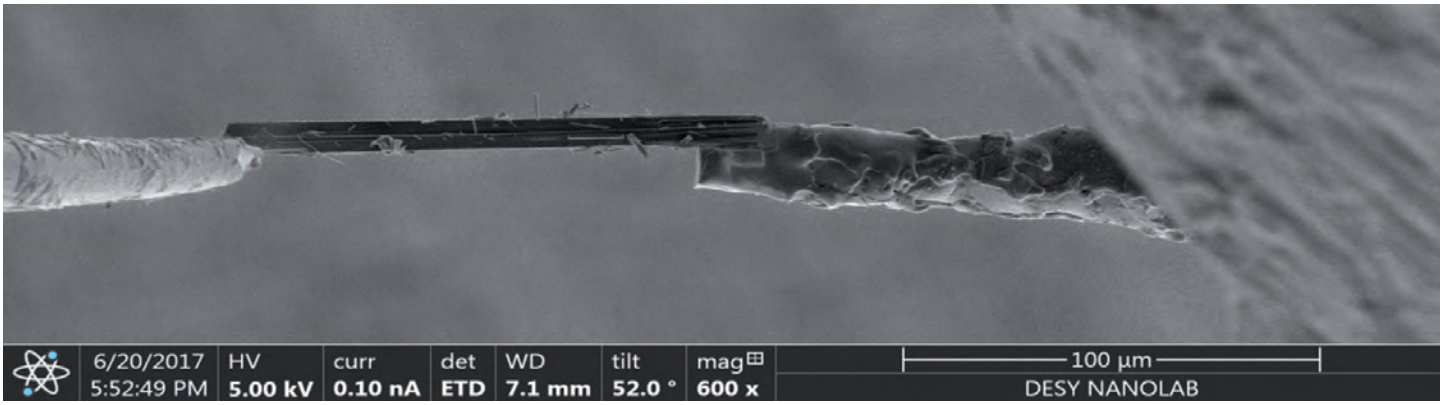

Figure 1

Hand-over of a preselected copper sulphate nano-wire bundle (centre) from the micromanipulator (left) of the Focussed Ion Beam instrument at DESY NanoLab to a fine tip, permitting to analyse the nano-wire bundle in a focussed PETRA III X-ray beam. As glue serves a Pt containing precursor dosed through a nozzle outlet (upper right corner).

DESY within user consortia at the European XFEL.

Contribution to first user experiments

SFX

With the first experiments performed at the European XFEL at the 'Single Particles, Clusters, and Biomolecules and Serial Femtosecond Crystallography' (SPB/SFX) instrument (Fig. 1), the SFX consortium reached an important milestone together with the beamline and facility. The experiments carried out the first serial femtosecond crystallography data collection of protein microcrystals at megahertz rates, which should eventually allow macromolecular structure determination to be performed in seconds. The capability also opens up the possibility for large surveys of macromolecular structural changes that occur after activation by light or other physical or chemical triggers, to gain insights into the functions of proteins and their complexes. The consortium will contribute a second end station as part of the integrated beamline, incorporating a large (4 million pixel) AGIPD detector, automated sample delivery apparatus, and diagnostics. The second end station will be able to operate simultaneously with the first, by re-focusing the 'spent' beam that passes through the sample in the first chamber and the hole in the detector used there. This second end station is under construction, led by the SPB/SFX project leader, Adrian Mancuso, with contributions from over 15 consortium-funded scientists and engineers and many in-kind contributions from the consortium partners, comprising members of the scientific communities in Germany, United Kingdom, Sweden, Slovakia, Switzerland, United States, and Australia.

HIBEF

DESY is part of the 'Helmholtz International Beamline for Extreme Fields' (HIBEF) consortium, headed by the Helmholtz-Zentrum Dresden-Rossendorf (HZDR), which contributes experimental setups, optical laser systems and pulsed magnets to the 'High Energy Density' (HED) instrument at the European XFEL. In 2017 DESY has finished the design and started the procurement of the second interaction chamber dedicated to 'Diamond Anvil Cell' (DAC), shock, and ramp compression experiments (Fig. 2). The design of the sample environment for the DACs and shock targets is nearing completion and a detector bench for the integration of the AGIPD detector and smaller detection systems, e.g. for phase contrast imaging, has been finalised. At the same time the construction of the HIBEF 1M GaAs AGIPD detector continues (see text on AGIPD in 'Campus and Collaborations'). With its GaAs chip, this detector will allow to efficiently exploit the unique bunch train pattern of the European XFEL for diffraction experiments at high energies. Two laser systems are currently manufactured: 'Amplitude' for ultrahigh intensity short pulses (HZDR) and 'DiPOLE' for high energy long pulses (UK Consortium). One subsystem of the latter has already undergone factory acceptance tests. At the HED hutch the installation of the laser beam transport developed at HZDR has started, and the laser clean room for the large lasers will be handed over in spring 2018. In 2017, the scientific case for pulsed magnetic field studies has

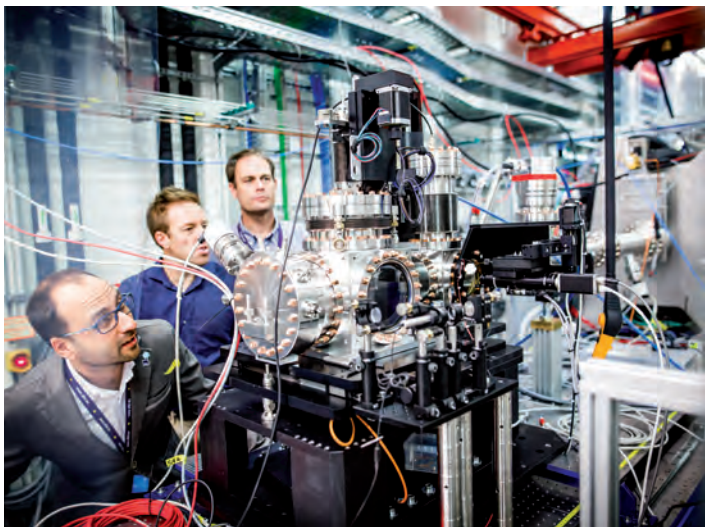

Figure 1

The image shows scientists working at the SPB/SFX instrument at European XFEL.

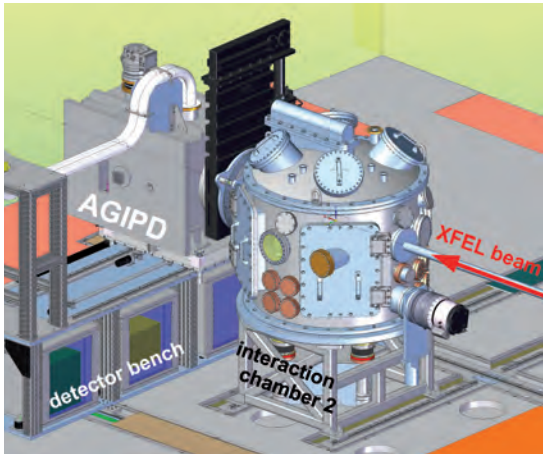

Figure 2

3D view of the second interaction area at the HED instrument of European XFEL: Interaction chamber 2 for DAC and shock experiments. The HIBEF AGIPD 1M detector and the detector bench are shown.

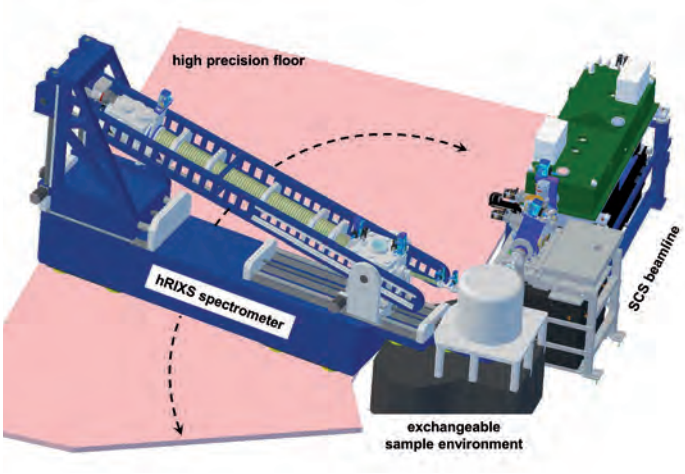

Figure 3

Preliminary layout by the hRIXS consortium of the hRIXS spectrometer to be installed at the SCS instrument at European XFEL beginning of 2019.

been reiterated leading up to a satellite meeting during the joint DESY Photon Science and European XFEL users' meeting in 2018. Furthermore, the Dresden High Magnetic Field Laboratory made progress on the integration of pulsed magnets in the sensitive environment by devising an efficient way to significantly reduce the stray fields generated by magnets reaching up to 60 T. In addition, safety concepts that allow deploying the required electrical energy of up to 1 MJ without risk were developed.

hRIXS

The Heisenberg RIXS consortium will bring resonant inelastic soft X-ray scattering (RIXS) to the transform limit in energy and time at the European XFEL. Unique insights to chemical dynamics, driven phases as well as fundamental X-ray matter interaction open up new directions in science. The optical design of the spectrometer is based on spherical variable line-spacing gratings with the ability to achieve resolving powers ≥ 20.000 over an energy range of 250 – 1600 eV. hRIXS will be the world leading instrument to detect static properties and transient excitations in structure, charge, spin and orbital polarisation for chemical processes as well as a wide range of energy- and bio-relevant materials. To enable this vast range of experiments, the hRIXS spectrometer will be operated with two complementary, exchangeable end stations optimised for measurements on solid-state and liquid/gas phase targets.

The contract for the mechanical design and construction of the spectrometer including the two end stations has recently been awarded (Fig. 3). After the current mechanical construction phase at the company's site, the installation in the 'Spectroscopy & Coherent Scattering' (SCS) hutch at the European XFEL is scheduled for early 2019. The hRIXS spectrometer will be equipped with a multi-hit compatible delay-line detector, which will allow taking full advantage of the large photon densities delivered by the XFEL beam.

Funding is provided by the Helmholtz Association via strategic investment in the Helmholtz-International Users consortium hRIXS. The project is partially supported by the ERC Advanced Grant 'EDAX' of A. Föhlisch at Potsdam University. The hRIXS consortium includes partners from Germany, Switzerland, Finland, France, Sweden, Italy, and the UK. The project is coordinated by Potsdam University in close collaboration with DESY and European XFEL.

DataXpress

The DataXpress consortium has developed software for data analysis and real time experiment feedback for serial crystallography and single particle coherent diffraction at the high data acquisition rates of European XFEL. DataXpress software was installed and tested in five of the first user experiments conducted at the SPB/SFX instrument of the European XFEL in 2017, enabling high-quality results to be obtained within a short space of time (Fig. 4). Installed centrally on the Maxwell cluster (High-Performance-Cluster and resource for data analysis at CFEL, CSSB, DESY and European XFEL), this software is available for use by all users, enabling serial crystallography experiments to focus immediately on scientific output without having to handle the data processing and reduction challenges in each group individually. Rapid feedback makes experiments more effective. The consortium builds on research performed within groups at CFEL/DESY developing the OnDA, Cheetah and CrystFEL analysis packages, and includes partners from Germany, Sweden, and the USA.

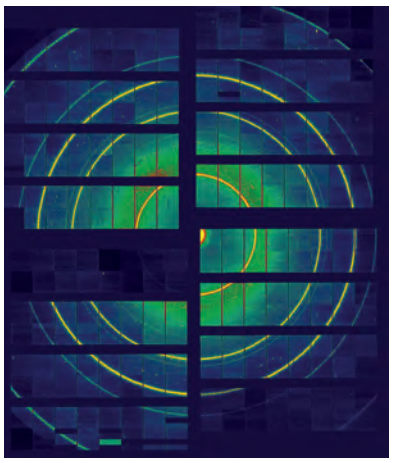

Figure 4

Diffraction data measured during the very first user experiment at European XFEL. The image shows measured test data ($Li_4Ti_5O_{12}$ powder) obtained at the SFX/SPB instrument using the AGIPD detector.

Scientific coordinators of User Consortia at European XFEL with DESY contributions:
SFX: Henry Chapman, CFEL/DESY, henry.chapman@desy.de
HIBEF: Thomas Cowan, HZDR, t.cowan@hzdr.de
hRIXS: Alexander Föhlisch, Potsdam University and HZB, alexander.foehlisch@helmholtz-berlin.de
DataXpress: Anton Barty, CFEL/DESY, anton.barty@desy.de
COMO: Jochen Küpper, CFEL/DESY and Univ. Hamburg, jochen.kuepper@desy.de

The Adaptive Gain Integrating Pixel Detector (AGIPD) for the European X-ray Free-Electron Laser.

The fastest X-ray eye in the world

The first 1 million pixel AGIPD camera (Fig. 1) was successfully used during start up and first user experiments at the Single Particles, Clusters, and Biomolecules & Serial Femtosecond Crystallography (SPB/SFX) instrument at the European X-ray Free-Electron Laser (XFEL) in September this year. In a concerted effort by DESY and European XFEL the system was commissioned and integrated into the XFEL environment in record time. The vast amount of data collected during the first beamtimes is currently being analysed by the different user consortia, and first scientific publications are already in preparation.

The X-ray detector is one of the most critical instruments at many experimental stations of the European XFEL. Due to its extreme brilliance and unique bunch structure, custom-made imaging detectors needed to be developed. The AGIPD system was constructed over the last 10 years by a consortium led by DESY together with the Swiss Paul Scherrer Institute (PSI) and the Universities of Hamburg and Bonn, and utilises a new concept where every pixel adapts its gain automatically to the incoming flux. This is done in each pixel during the few tens of nanoseconds it takes for the pixel to collect the signal pulse generated by the X-rays. It allows both single photon sensitivity and the ability to handle intensities of up to 10^4 photons per pixel in a single pulse. To cope with the characteristic bunch train structure of the European XFEL, AGIPD can take images at 4.5 million frames per second. The images are stored in a 352-images-deep analogue memory inside each pixel and are read out and digitised in the 99 milliseconds between two bunch trains. To allow for a more efficient use of the 352 storage cells, the system includes a high speed vetoing capability so known non-optimal images, e.g. images where the FEL pulse did not hit the sample, can be overwritten already during the bunch train.

The excellence of the scientific data that can be obtained critically depends on the quality of the calibration of the system. With 1 million pixels, each having 3 gain stages and 352 storage cells, this is a non-trivial task. To achieve sufficient precision, various electronic calibration circuits are implemented in each pixel, allowing for a well-defined and reproducible signal to be injected. Nevertheless, final calibration has to be performed at the experimental station, under real experimental conditions.

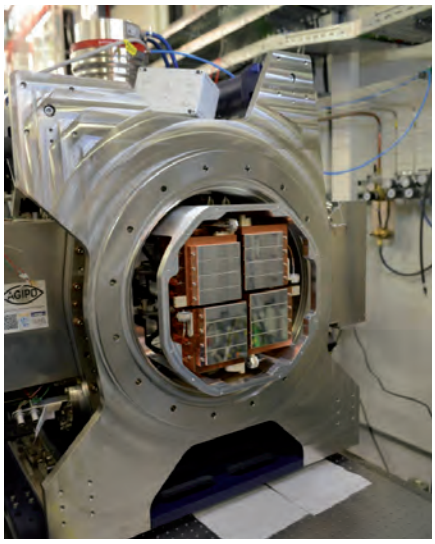

Figure 1

1 million pixel AGIPD camera installed at the SPB/SFX instrument at European XFEL. Clearly visible are the four independently moveable quadrants, each consisting of four detector tiles.

In addition to implementing the unique electronic capabilities described above, another challenge was to provide as much flexibility as possible for the mechanical layout of the system. The 1 million pixel camera consists of four fully independently moveable quadrants (Fig. 1). This allows not only for the direct beam to pass through unobstructed, but also to position the quadrants in such a manner as to achieve an optimal coverage of the scattering plane.

After this first successful deployment of a 1 million pixel AGIPD system, a second system, for the Materials Imaging and Dynamics (MID) instrument, is currently under commissioning, and will be operational at the experimental station before the first user experiments. In addition, a 4 million pixel variant for the SFX user consortium and a high-energy version for the Helmholtz International Beamline for Extreme Fields (HIBEF) user consortium are being constructed.

Contact: Heinz Graafsma, heinz.graafsma@desy.de

New photocathode laser for the European XFEL.

DESY develops a second photocathode laser for the European XFEL

The brilliant X-rays of the new 3 km-long European X-ray free-electron laser (European XFEL) are generated by accelerated high energetic electrons in long undulator sections. These electrons are initially created by photons from an ultrafast ultraviolet (UV) laser at the very beginning of the European XFEL linear accelerator. Those photons are hitting a Cs_2Te photocathode inside European XFEL's electron gun, utilising the photoelectric effect for electron emission. Needless to say that high reliability and availability of this laser are of key importance to the entire facility, since its failure will immediately bring the FEL's X-ray production to a standstill. But also its parameters and performance influences many important electron beam properties, such as bunch charge and emittance. Unfortunately, the combined requirements for this laser, especially the burst-mode timing structure of the European XFEL, cannot be met by any standard commercially available laser product.

The first electron beams of the European XFEL were generated using UV laser technology developed by the Max Born Institute Berlin, similar to DESY's FLASH XUV-FEL [1]. Even though this laser (laser 1) performs nearly flawless during its 24 hours per day, 7 days per week operation, it became clear early on, that a laser failure might require significant repair time and be a severe disruption to European XFEL's tight schedule.

To mitigate risks, DESY's Laser Science and Technology Group (FS-LA) started 2016 an in-house development of a 'backup' photocathode laser system (laser 2). This system was designed to ensure a fully performing and stable European XFEL. Only the requirement for short pulse options (available with laser 1) which is currently not used but might be of importance in future, was dropped. This allowed a significantly simpler design using Nd-doped power amplifiers. Additionally it turned out that suitable Nd:YVO_4 gain blocks were commercially available from neoLASE, a spin-off company of the Laser Zentrum Hannover e.V., which developed this technology for the Laser Interferometer Gravitational-Wave Observatory LIGO [2,3]. The project was completed in record time, so that already in October 2017 the first XFEL electrons were produced by the new laser. Compared to laser 1, there was little change in electron properties observed, which allows fast switching times without long re-tuning of the accelerator's injector section.

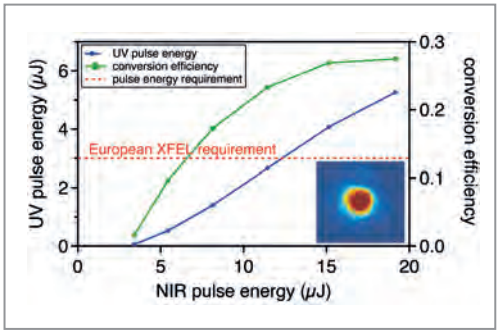

Figure 2
Frequency converter performance and beam quality (inset).

The laser (Fig. 1) consists of three building blocks, an accelerator-synchronised Yb-fibre laser front-end, the Nd:YVO_4 power amplifier stages and a frequency conversion unit, converting the near-infrared (NIR) output to UV photons. The laser comprises a second amplifier chain which can drive the laser-heater of the European XFEL. Overall the laser produces simultaneously 10 ps long UV and NIR pulses of > 5 µJ and 50 µJ energy, respectively, in bursts of up to 600 µs length and 2700 pulses with 10 Hz burst-repetition frequency. It delivers more than twice the required energy for daily operation (Fig. 2).

Redundancy in the UV-conversion unit is of particular importance, since the nonlinear materials need to be driven close to their damage threshold. The newly designed unit shows a record conversion efficiency of > 20% with excellent beam quality (Fig. 2) and operated already several weeks without degradation.

In conclusion, DESY developed a second photocathode laser for the European XFEL which helps to boost the facility's availability.

Figure 1
Second photocathode laser system installed in the European XFEL's photocathode laser lab.

Contact: Lutz Winkelmann, lutz.winkelmann@desy.de
Ingmar Hartl, ingmar.hartl@desy.de

References

1. I. Will et al., Opt. Express 19, 23770-23781 (2011).
2. M. Frede et al., Opt. Express 15, 459 (2007).
3. L. Winkelmann et al., Appl. Phys. B 102, 529 (2011).

European Molecular Biology Laboratory Hamburg Unit.

Structural biology research and service provision

The European Molecular Biology Laboratory (EMBL) operates from six sites across Europe. The focus of the Hamburg Unit is to provide state-of-the art research services for applications in structural biology to the external research community. This is complemented by in-house research activities, which are focussed on the development of new approaches in structural biology and infection biology.

Provision of research services in structural biology

Beamlines for structural biology

The EMBL Hamburg Unit operates three beamlines for structural biology applications at the PETRA III storage ring; one for Small Angle X-ray Scattering (SAXS) experiments (P12) and two for Macromolecular Crystallography (P13, P14).

Key developments in 2017 were:

- At P12 high-flux optics were installed utilising a multilayer monochromator (MLM) constructed in-house by the EMBL Hamburg instrumentation group. The MLM yields the beam up to $5*10^{14}$ photons/sec, about 70 times higher than the standard crystal monochromator. The MLM, together with the fast EIGER 1M detector with a 750 Hz frame rate, enables the routine collection of full SAXS curves from protein solutions in msec exposure time. Surprisingly, the extremely high flux offers a possibility to 'outrun' the radiation damage, allowing to record the scattering data before the solution starts aggregating. The high flux option also opens up advanced possibilities for time-resolved SAXS experiments at P12. To fully utilise this possibility a neodymium-doped yttrium aluminium garnet (Nd:YAG) laser with tuneable wavelength, short pulse and high energy was installed in a special hutch adjacent to the beamline providing various options of fast triggering of biological reactions.
- A new EIGER 16M detector was installed at P14. The new detector offers smaller pixel size, higher frame-rates, and shorter readout time, therefore delivering higher data quality in shorter data collection times. Enabled by the EIGER detector at P14, several pump-probe experiments were successfully carried out by research groups associated with the Center for Free-Electron Laser Science (CFEL). The experiments were, in part, preparation for the set-up of a second experimental station at P14 (see Fig. 1) for time-resolved experiments, funded by an external project to implement Hadamard crystallography as a method for the time-resolved investigation of the structural dynamics of biomolecules. The experimental station is being built in collaboration with Arwen Pearson and her group at the Centre for Ultra-Fast Imaging (CUI). It will be constructed in a modular fashion so that external users, together with in-house support staff, can spend time

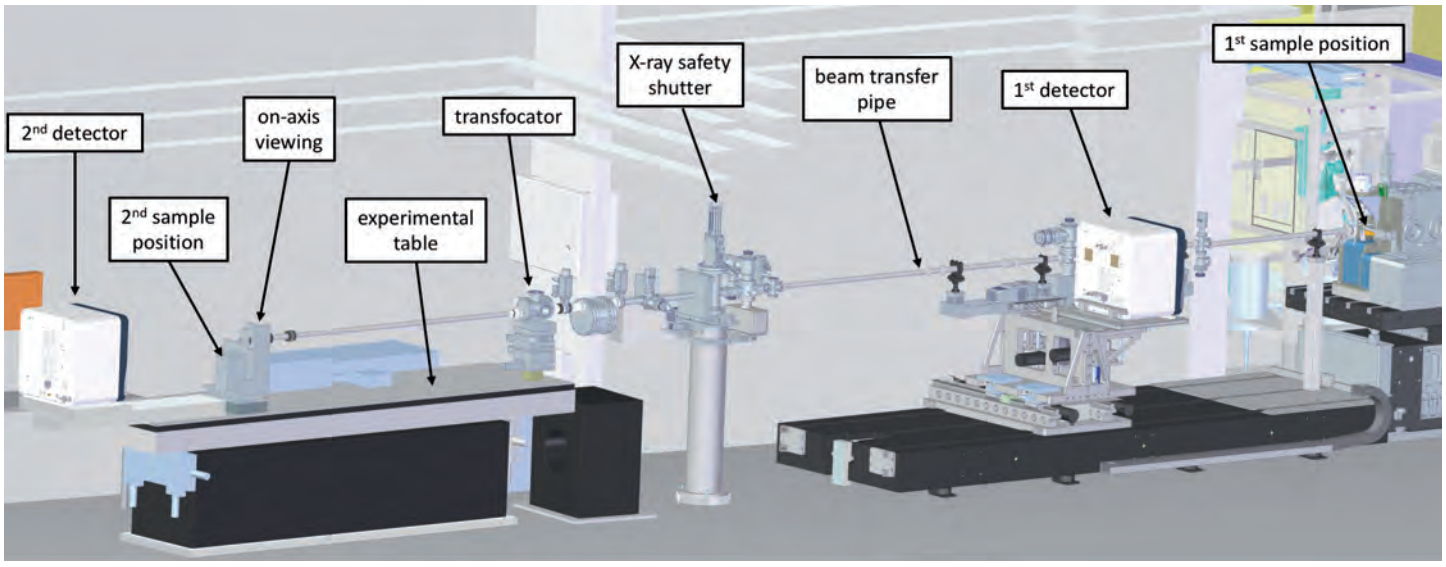

Figure 1

Second experimental station at the EMBL beamline P14 at PETRA III.

designing and setting up the complex experiments to suit their particular needs ahead of the beamtime. The experimental station is scheduled to be ready for first experiments in 2018.

- A CrystalDirect™ harvester was also installed and commissioned at the beamlines that will change the handling and transfer of crystals that are often highly sensitive to changes of environmental conditions such as temperature, humidity and mechanical stress. Designed and developed by the EMBL Unit in Grenoble, the CrystalDirect™ approach allows X-ray data collection from crystals without the need of adding cryo-protectants, avoiding a step that often leads to a serious decrease in crystal quality.

Sample preparation and characterisation facilities

EMBL also offers users a pipeline of sample preparation and characterisation facilities prior to their measurements at the EMBL beamlines. Within the framework of the establishment of the core facilities at the newly inaugurated Centre for Structural Systems Biology (CSSB), EMBL received additional external resources to expand its facilities, so they can also serve CSSB research groups with their specific needs. The funding has been used to purchase several state-of-the-art instruments and to pay for additional staff. Part of the EMBL facilities will be housed within the new CSSB building a short walk across the 'science bridge' connecting the two buildings.

EMBL is also a major contributor to the biological sample preparation infrastructure at the newly inaugurated European XFEL facility just outside Hamburg. The 'XFEL Biology Infrastructure (XBI)' is a user consortium focussed on providing state-of-the-art preparation facilities for researchers visiting the European XFEL for experiments with biological samples. EMBL participates in the XBI team with two staff members. Not only in terms of sample preparation, but also with respect to developments at the European XFEL instruments, EMBL fosters close ties to European XFEL with involvement in projects and networks uniting the two institutes.

Software development and provision

EMBL also develops software for data processing and evaluation for the international user community. The ATSAS data analysis suite developed by Dmitri Svergun and his group is a key software product for the SAXS community. In summer 2017, the latest release (ATSAS 2.8) reached over 14,000 users [1].

Research at the EMBL Hamburg Unit

In June this year the CSSB building was inaugurated on the DESY campus. EMBL is one of nine founding partners and Matthias Wilmanns, Head of the EMBL Hamburg unit, has also been Scientific Director at the CSSB until the end of 2017. As such, the EMBL Hamburg Unit has a close connection to the growing CSSB network. This year EMBL recruited Jan Kosinski, who, as of September, joined the CSSB as an additional EMBL group leader. Both Kosinski and fellow EMBL group leader Christian Löw have started to create many synergies between CSSB and EMBL.

Research highlights this year include work by the Svergun group in collaboration with the Lemke group from EMBL in Heidelberg, about finally understanding the long-standing discrepancy between SAXS and Förster Resonance Energy Transfer (FRET) results on intrinsically unfolded proteins. Their work shows that decoupling size and shape fluctuations in heteropolymeric sequences reconciles the discrepancies between the two measurements [2].

Patrick Cramer's group from the Max Planck Institute for Biophysical Chemistry in collaboration with Thomas Schneider from the EMBL Hamburg Unit was able to resolve the structure of the Core Mediator, a key regulator of RNA polymerase, at 3.4 Å resolution using collimated X-ray radiation at various energies on P14. This research is described in the highlight section of this report [3].

Using a combination of small-angle X-ray scattering, electron microscopy and biophysical studies, the Wilmanns group together with collaborators in Vienna and Amsterdam were able to gain significant insights into the unusual shape of a membrane protein complex the tuberculosis pathogen *Mycobacterium* uses to infect its hosts. Details of the work on the ESX-5 secretion system are presented in the highlights section of this report [4].

References

1. D. Franke et al., J. Appl. Crystallogr. 50, 1212-1225 (2017).
2. G. Fuertes et al., Proc. Natl. Acad. Sci. USA 114, E6342-E6351 (2017).
3. K. Nozawa et al., Nature 545, 248-251 (2017).
4. K. S. H. Beckham et al., Nature Microbiology 2, 17047 (2017).

Contact: Matthias Wilmanns, matthias.wilmanns@embl-hamburg.de

Centre for Structural Systems Biology CSSB.

New frontiers in infection biology research

Figure 1

Schleswig-Holstein´s Scientific Senator Oliver Grundei, DESY Director Helmut Dosch, Bärbel Brumme-Bothe from the Federal Ministry for Education and Research, CSSB´s Scientific Director Matthias Wilmanns, Lower Saxony´s Minister for Science Gabriele Heinen-Kljajić and Hamburg´s First Mayor Olaf Scholz and CSSB partner institution representatives at the CSSB Grand Opening.

On 29 June, CSSB celebrated its grand opening in the presence of 700 guests including several leading representatives from funding bodies and partner institutions. Helmut Dosch, Chairman of the DESY Board of Directors, presented Matthias Wilmanns, CSSB Scientific Director, and Dirk Heinz, Chair of CSSB Council with a ceremonial key thus marking the official begin of CSSB's scientific activity in the new building (Fig. 1). CSSB scientists began setting up their laboratories in April and are now actively working together to elucidate the structures, dynamics and mechanisms of infection processes (Fig. 2). The opening of the CSSB building marks the beginning of a new era during which all nine research partners will be able to interact and work together under one roof. All partners are enthusiastic about this opportunity.

In September of this year, CSSB's overall performance as well as that of individual group leaders was reviewed for the first time by a panel of international experts. The results of this review, together with regular recommendations from CSSB's Scientific Advisory Board, will provide the necessary guidance to help CSSB become an internationally recognised centre of excellence.

Collaborative research highlights

Published in early 2017, the CSSB Research Programme outlines the Centre's strategic scientific focus and direction thus laying a solid foundation for collaborative and interdisciplinary research projects.

Figure 2

Biosafety S2 level laboratory in CSSB building.

Figure 3

CSSB Opening Symposium group photo.

An international collaboration including scientists from two CSSB groups – Matthias Wilmanns from the EMBL Hamburg Unit and Thomas Marlovits from University Medical Center Hamburg-Eppendorf (UKE) – revealed the first molecular structure of the type VII secretion system of Mycobacterium tuberculosis. This project is detailed in the highlights section of this report [1].

Thomas Marlovits, in collaboration with colleagues from Massachusetts Institute of Technology (MIT), developed a simplified version of the type III secretion system's molecular needle thus unveiling key insights regarding the regulatory elements of the system [2].

CSSB group leader Jörg Labahn was part of an international team of researchers involved in the elucidation of the atomic-level three-dimensional structure of an amyloid fibril. The fibrils of the body's own amyloid beta (Aβ) protein are the main constituent of Alzheimer's disease related and characteristic pathological protein deposits in the brain [3].

New recruitments

The new EMBL group leader Jan Kosinski moved into the CSSB building in September. He is a leading expert in structural modelling of diverse experimental data sets, as proven by his previous postdoctoral work at EMBL in Heidelberg. He plans to expand his portfolio to include functional modelling of viral infection pathways and has already established multiple collaborations with CSSB colleagues.

Infrastructure investments

The German Research Council (DFG) granted the Universität Hamburg co-financing for the establishment of a 15.6 million Euro cryo-electron microscopy facility in the new CSSB building. Five cryo-electron microscopes are currently being installed in the basement of the CSSB building and the facility is expected to be open for experiments in early 2018.

CSSB Opening Symposium

Understanding host-pathogen interaction was the focus of the CSSB Opening Symposium entitled 'Frontiers in Structural Systems Biology of Host-Pathogen Interactions'. From 13-15 November 2017 international experts discussed how new methods and technologies in structural systems biology can be used to develop a more in-depth understanding of the infection process (Fig. 3).

CSSB governance

Matthias Wilmanns from the European Molecular Biology Laboratory (EMBL) will complete his term as CSSB's first Scientific Director at the end of 2017. Chris Meier from the Universität Hamburg will become the next CSSB Scientific Director in January of 2018.

Contact: Ina Plettner, ina.plettner@desy.de
Matthias Wilmanns, matthias.wilmanns@embl-hamburg.de

References

1. K. S. H. Beckham et al., Nature Microbiology 2, 17047 (2017).
2. M. Song et al., Nature Communications 8, 14737 (2017).
3. L. Gremer et al., Science 358, 116–119 (2017).

CSSB Partner Institutions

- Bernhard Nocht Institute for Tropical Medicine (BNITM)
- Deutsches Elektronen-Synchrotron (DESY)
- European Molecular Biology Laboratory (EMBL)
- Forschungszentrum Jülich (FZJ)
- Hannover Medical School (MHH)
- Heinrich Pette Institute (HPI)
- Helmholtz Centre for Infection Research (HZI)
- Universität Hamburg (UHH)
- University Medical Center Hamburg-Eppendorf (UKE)
- Research Center Borstel (FZB) (associated partner)

CSSB Investors

- Federal Republic of Germany
- Free and Hanseatic City of Hamburg
- Federal State of Lower Saxony
- Federal State of Schleswig-Holstein

The Helmholtz-Zentrum Geesthacht Outstation at DESY.

GEMS – Instruments with world-leading engineering materials science sample environments

At the German Engineering Materials Science Centre (GEMS) special sample environments are developed and used for *in situ* studies of processes in the field of engineering materials science, e.g. an *in situ* laser beam welding device (FlexiLas) or a quenching and deformation dilatometer (FlexiTherm). These sample environments were rated as world-leading by the reviewers at the Helmholtz-Zentrum Geesthacht (HZG) evaluation in November 2017 in the frame of the Program-oriented Funding of the Helmholtz Association.

One example of a new sample environment is a zone melting furnace (FlexiDS) which will be installed and used at P07/HEMS within the framework of a BMBF collaborative research project with partners from Karlsruhe Institute of Technology (KIT) and University of Magdeburg. This full-scale zone melting device will be used, e.g. for the study of directed solidification of TiAl-based alloys. A device for *in situ* selective laser melting experiments is planned (FlexiSLM). Cooperation with partners from University of Erlangen-Nürnberg (FAU) and TU Berlin as well as an in-house partner has started.

Diffraction

The preparations for the construction of the new hutches of beamline P61.1 in the PETRA III experimental hall 'Paul P. Ewald' move on quickly. P61.1 will be the only white-beam beamline at PETRA III allowing, e.g. depth-resolved residual stress measurements. The option for monochromatic experiments will be maintained and it can be accomplished based on future needs.

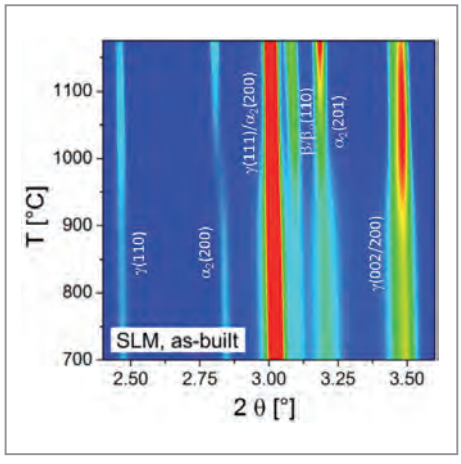

Figure 1
Evolution of reflections during heating of a TiAl sample produced by selective laser melting (P07/HEMS beamline).

In order to be able to make use of the flux increase from the new undulator at P07/HEMS, a new PILATUS3 X CdTe area detector, enabling full frame rates of up to 250 Hz, was purchased together with DESY. The DECTRIS detector for high photon energies will be used at DESY and HZG beamlines for experiments that require high time resolution. The DECTRIS detector is currently being tested.

At P07/HEMS the microstructure stability of γ-TiAl produced by selective laser melting was studied. Current products of γ-TiAl alloys are restricted to conventional processing routes, i.e. casting and forging or powder processing. The development of suitable processing conditions for additive manufacturing of γ-TiAl alloys would allow more complex geometries, e.g. components with cooling channels and hollow structures, as well as the reduction of development time and material savings. However, additive manufacturing of TiAl is still demanding and the stability of the product has to be assessed. Significant microstructural transformations are induced by heating the metastable as-built alloy Ti-44.8Al-6Nb-1.0Mo-0.1B up to 1200 °C, which was carried out in the dilatometer. The resulting microstructure differs strongly from the corresponding annealing experiment of a material that was more stabilised and closer to thermodynamic equilibrium due to hot isostatic pressing (HIP) at 1200 °C followed by relatively slow cooling (Fig. 1) [1].

Imaging

At the Imaging Beamline P05 the new multilayer monochromator was successfully put into operation and has increased the photon flux by up to two orders of magnitude, laying the ground for high-speed microtomography. At the P05 nanotomography end station a new high-speed detector system was successfully implemented in the beginning of 2017. It allows for a fivefold total scan time reduction as well as for a

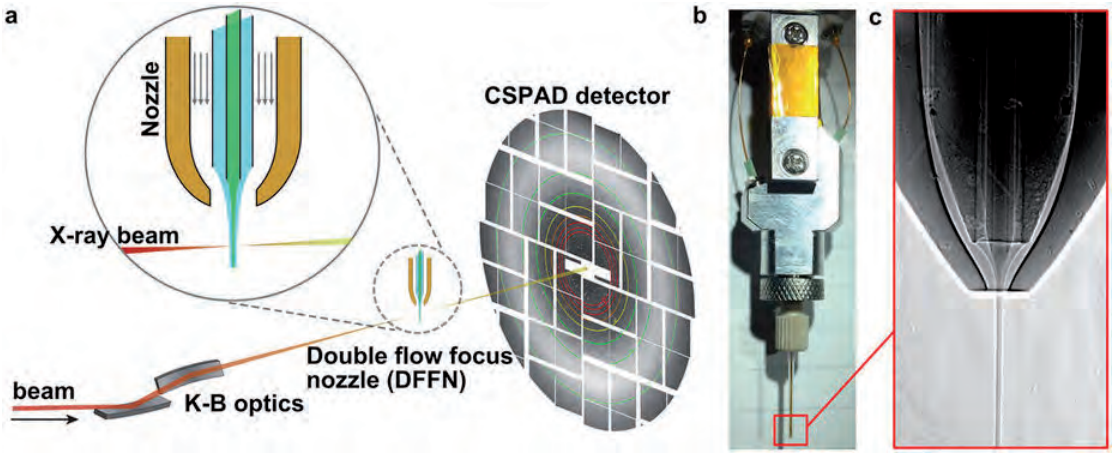

Figure 2
Projection of a double-flow focused liquid injector. The injector is used for sample injection into an XFEL beam for efficient serial femtosecond crystallography.

worldwide uniquely long, lense-less sample-detector distance of up to 20 m with excellent conditions for 'cone-beam' X-ray microscopy.

In collaboration with the CFEL group of Henry Chapman a double-flow focused liquid injector (Fig. 2) was investigated *in situ* using the well-established microtomography setup at the Imaging Beamline P05. Development of the liquid injectors is important for efficient crystal injection into an XFEL X-ray focus for serial femtosecond crystallography. With the help of the *in situ* measurements it was possible to characterise properties of the liquid jet and verify the flow focusing of the injector nozzle [2].

At the Nanofocus end station of P03 beamline, spatially resolved scanning wide-angle X-ray scattering (WAXS) experiments were performed to study the oriented crystallisation of barium sulfate confined in hierarchical cellular structures. This diffraction-enhanced imaging study was performed on biomineralised wood samples, involving the controlled formation of inorganic matter within hierarchical biological scaffolds. Mimicking the crystallisation of biominerals in such confinement is an important goal in the field of crystal engineering. Natural porous materials offer an interesting platform for studying mineral morphogenesis and texturing through template-directed mineralisation. Here, users from the ETH Zürich studied barium sulfate precipitates from aqueous salt solutions in the constrained micro- and nanoenvironment of pristine wood cells and cell walls. The spatially resolved scanning WAXS experiments delivered important insights into the deposition pattern, morphology, and crystallographic orientation of barite crystals in the plant cell anatomy. The experimental findings suggest directed crystallisation of $BaSO_4$ at different hierarchical levels and a crystallographic co-orientation of barite and cellulose, suggesting epitaxial crystal growth (Fig. 3) [3].

Contact: Christina Krywka, christina.krywka@hzg.de
Peter Staron, peter.staron@hzg.de
Martin Müller, martin.mueller@hzg.de

References

1. J. Gussone et al., Scripta Mater. 130, 110–113 (2017).
2. D. Oberthuer et al., Scientific Reports 7, 44628 (2017).
3. V. Merk et al., Cryst. Growth Des. 17, 77–684 (2017).

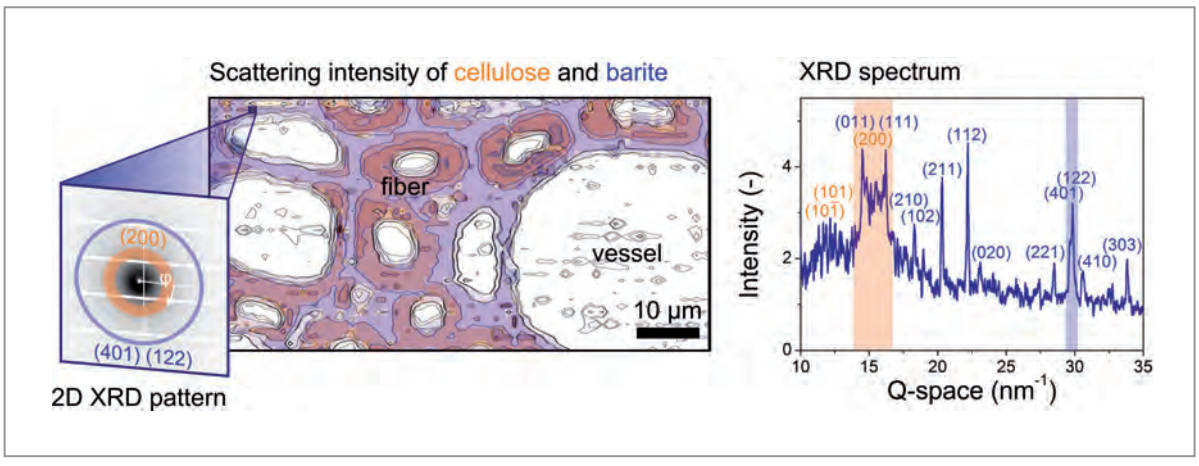

Figure 3
Diffraction enhanced imaging of the distribution of barite ($BaSO_4$) inside the cell walls of wood. Each pixel corresponds to the information extracted from individual diffractograms recorded at the same position.

DESY Innovation and Technology Transfer.

Towards a new innovation strategy

Figure 1
Architect concept of the Innovation Centre to be constructed at the Luruper Hauptstraße on the campus and adjacent to the CFEL building and PETRA III experimental hall 'Max von Laue' (DFZ Architekten GmbH).

The field of Innovation and Technology Transfer at DESY has evolved substantially in 2017. The former department of 'Technology Transfer' was integrated into the new administrative department of 'Innovation & Technology Transfer' (ITT). ITT is implementing the newly developed DESY Innovation Strategy in close cooperation with all divisions at DESY. As a result, the joint activities with the DESY Photon Science division are also increasing.

Regarding DESY Photon Science, successful activities can be noted for 2017 in all 3 fields of actions outlined in the DESY Innovation Strategy: innovation services, exploitation and start-ups. The field of innovation services is determined by industrial clients booking beamtime at PETRA III or FLASH. The involvement of so-called 'provider companies', who carry out experiments on behalf of industrial clients, has increased in 2017. These small companies play an important role for DESY, as the collaboration offers a high reliability in terms of beamtime bookings, and time-consuming client acquisition is taken over by the provider. Complex scientific infrastructures, such as the DESY NanoLab with its equipment and methods specifically adapted to nanoscience, complete the services provided at the research facilities run by DESY.

In the field of exploiting DESY technologies, a validation project, successfully obtained from the Helmholtz Association, was started for a technology developed at DESY Photon Science. The coating technology for magneto sensors has the potential for application in the automobile and other industrial sectors. This potential shall be investigated in the next 2 years to identify market requirements and to transfer the technology to an industrial level.

So far, all of DESY's start-ups have evolved from the Photon Science division and are currently successful in positioning themselves on the market. Together with DESY scientist Tim Laarmann, the start-up 'Class 5 Photonics' has successfully gained sponsorship by the 'Investitions- und Förderbank Hamburg' PROFI Program and has grown solidly, like the other start-ups as well. For 2018, DESY has decided to accommodate all start-ups for now in the 'DESY Innovation Village' on the DESY campus. This will provide additional office space and increase the visibility of founding activities. It is an interim solution until the Innovation Centre (Fig. 1), with construction planned to start in 2018, will be completed.

Contact: Arik Willner, arik.willner@desy.de

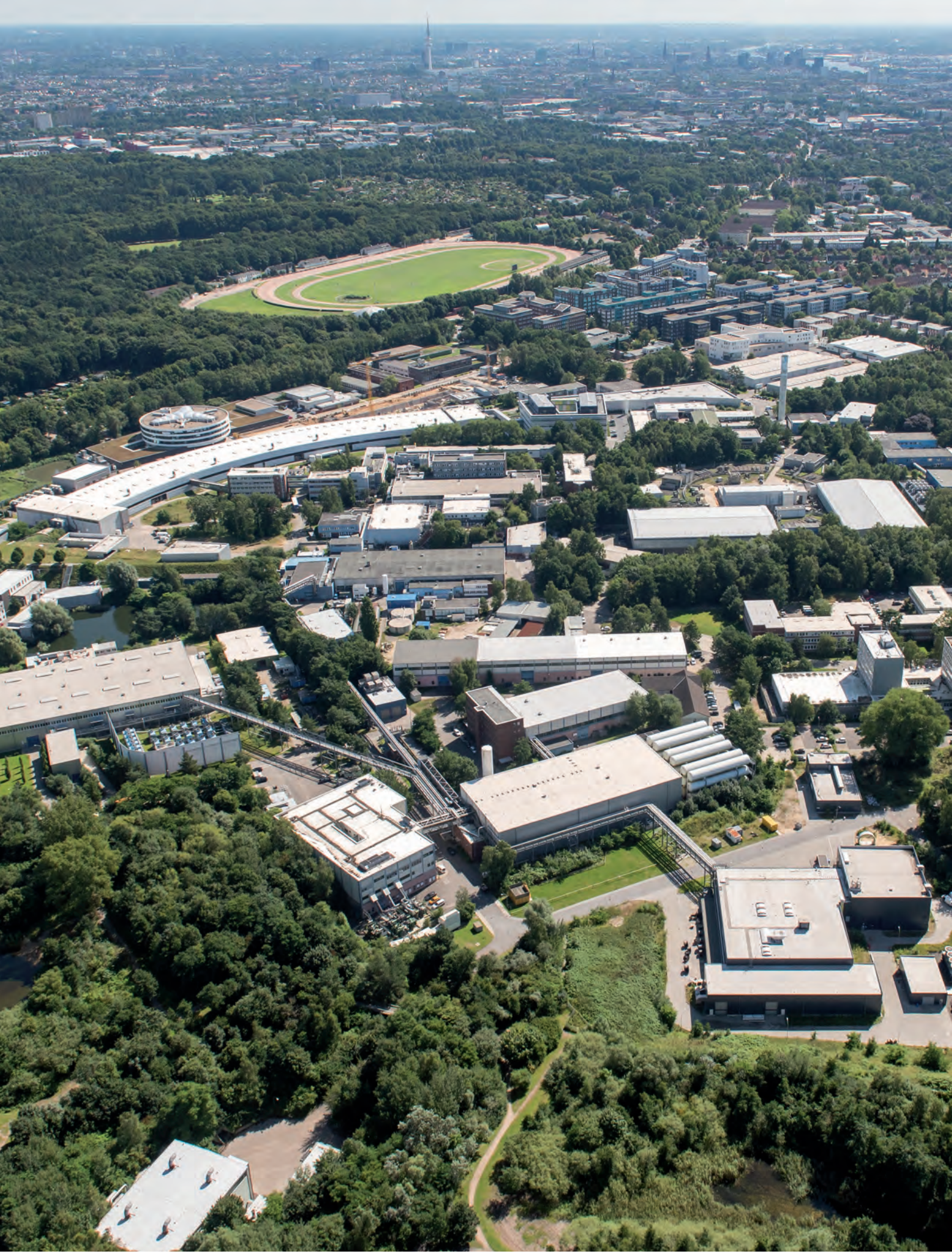

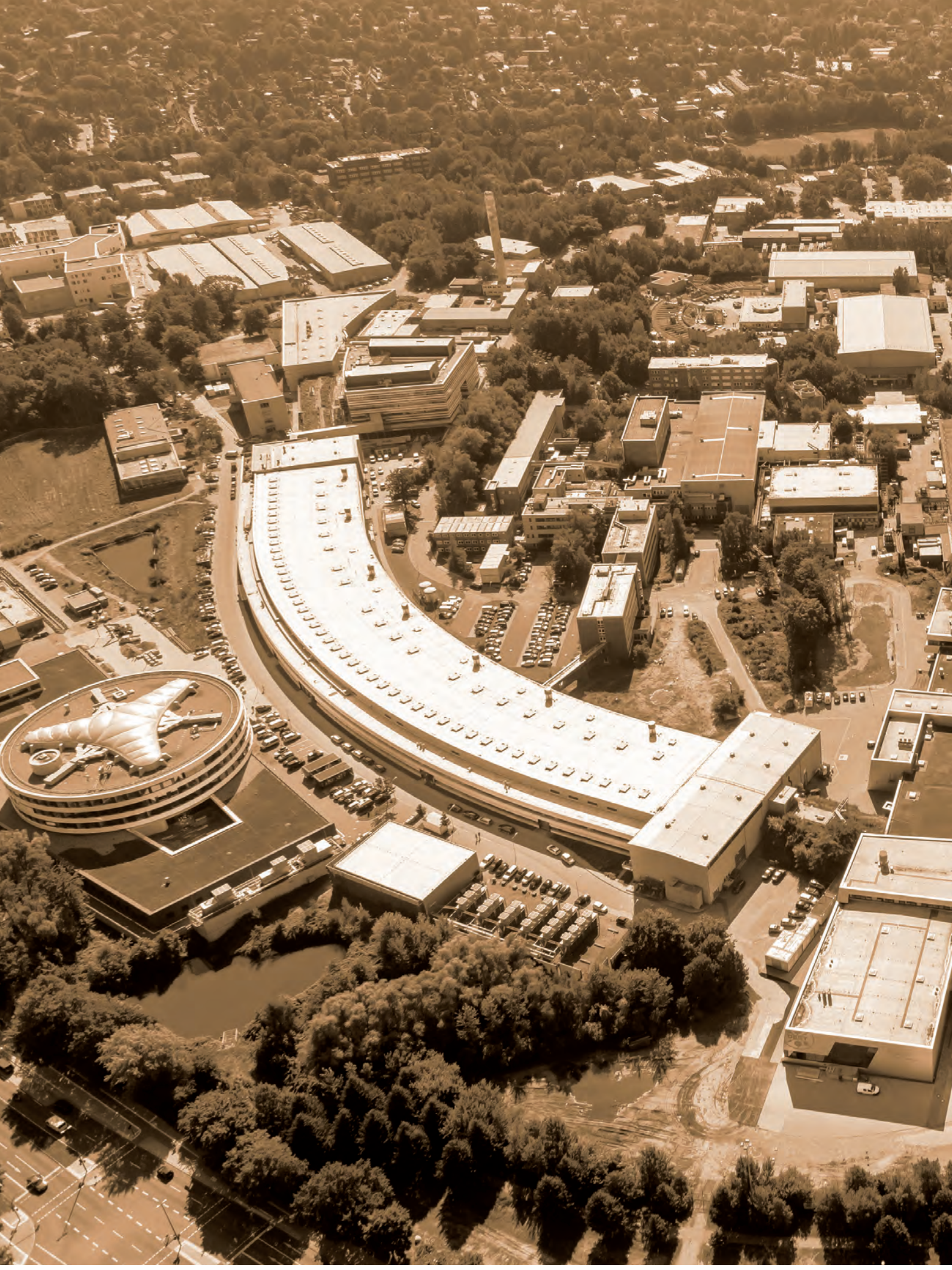

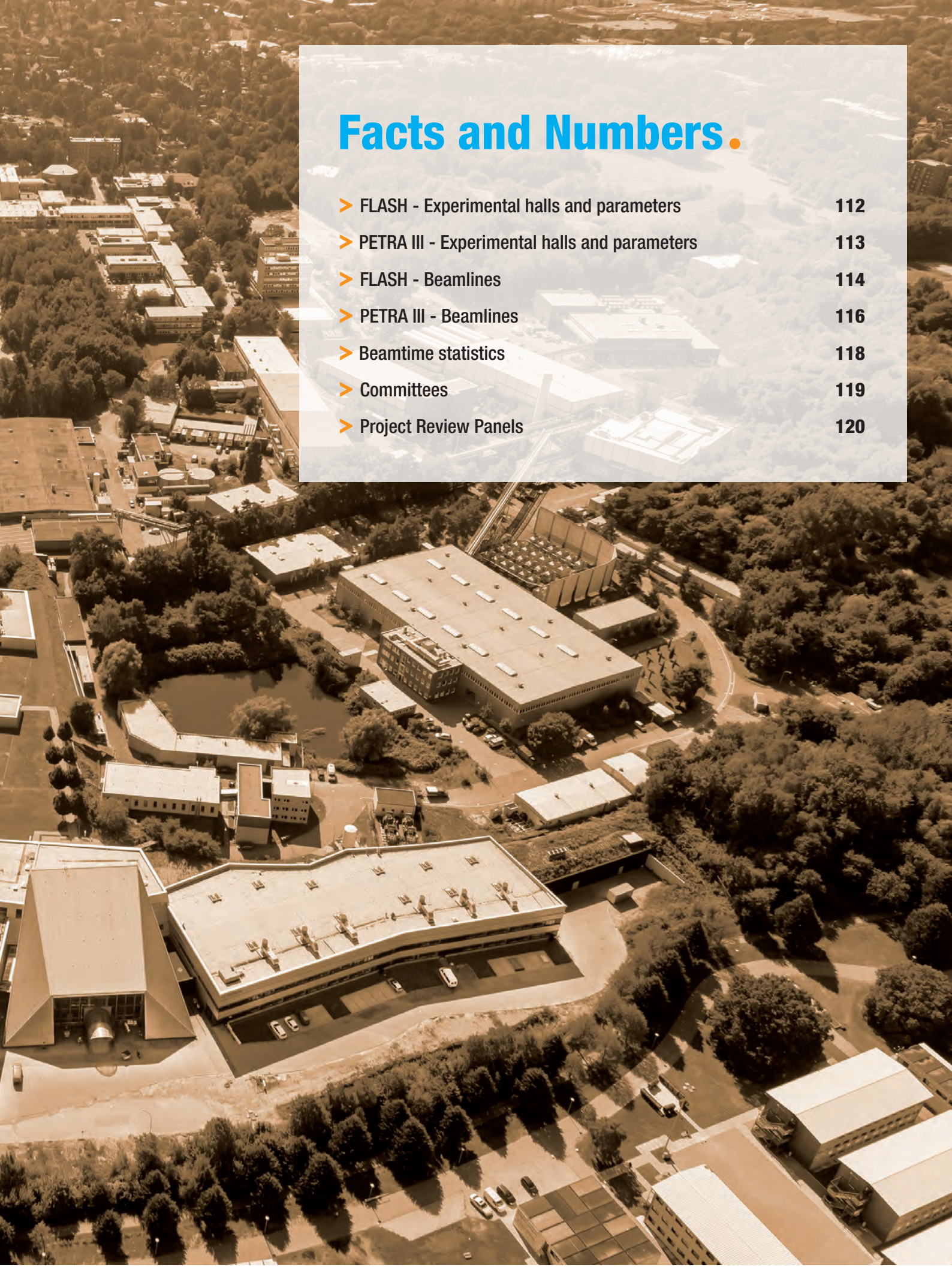

Facts and Numbers.

FLASH.

Experimental halls and parameters

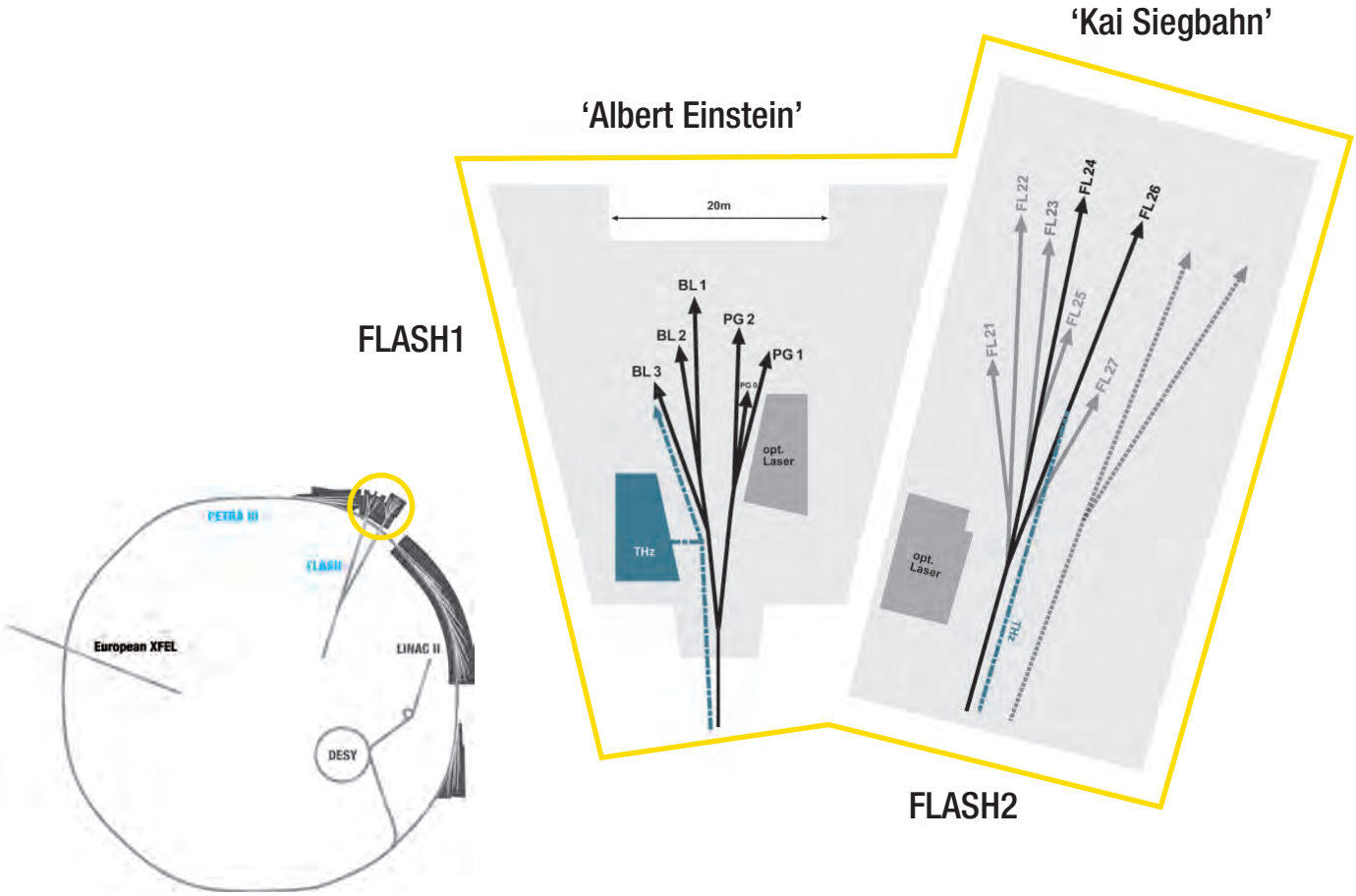

FLASH - machine parameters

	FLASH1	FLASH2
Electron energy range	0.35 – 1.25 GeV	0.4 – 1.25 GeV
Normalised emittance at 1 nC (rms)	1.4 mm mrad	1.4 mm mrad
Energy spread	200 keV	500 keV
Electron bunch charge	0.1 – 1.2 nC	0.02 – 1 nC
Peak current	1 – 2.5 kA	1 – 2.5 kA
Electron bunches per second (typical/maximum)	300 / 5000	300 / 5000

FLASH - lasing parameters

	FLASH1	FLASH2
Photon energy fundamental	24 – 295 eV	14 – 310 eV
Wavelength fundamental	51 – 4.2 nm	90 – 4 nm
Photon pulse duration (FWHM)	30 – 200 fs	10 – 200 fs (estimated)
Peak power	1 – 5 GW	1 – 5 GW
Single photon pulse energy (average)	1 – 500 µJ	1 – 1000 µJ
Spectral width (FWHM)	0.7 – 2 %	0.5 – 2 %
Photons per bunch	10^{11} – 10^{14}	10^{11} – 10^{14}
Peak brilliance photons/sec/mm²/mrad²/0.1 %	10^{28} – 10^{31}	10^{28} – 10^{31}

PETRA III.

Experimental halls and parameters

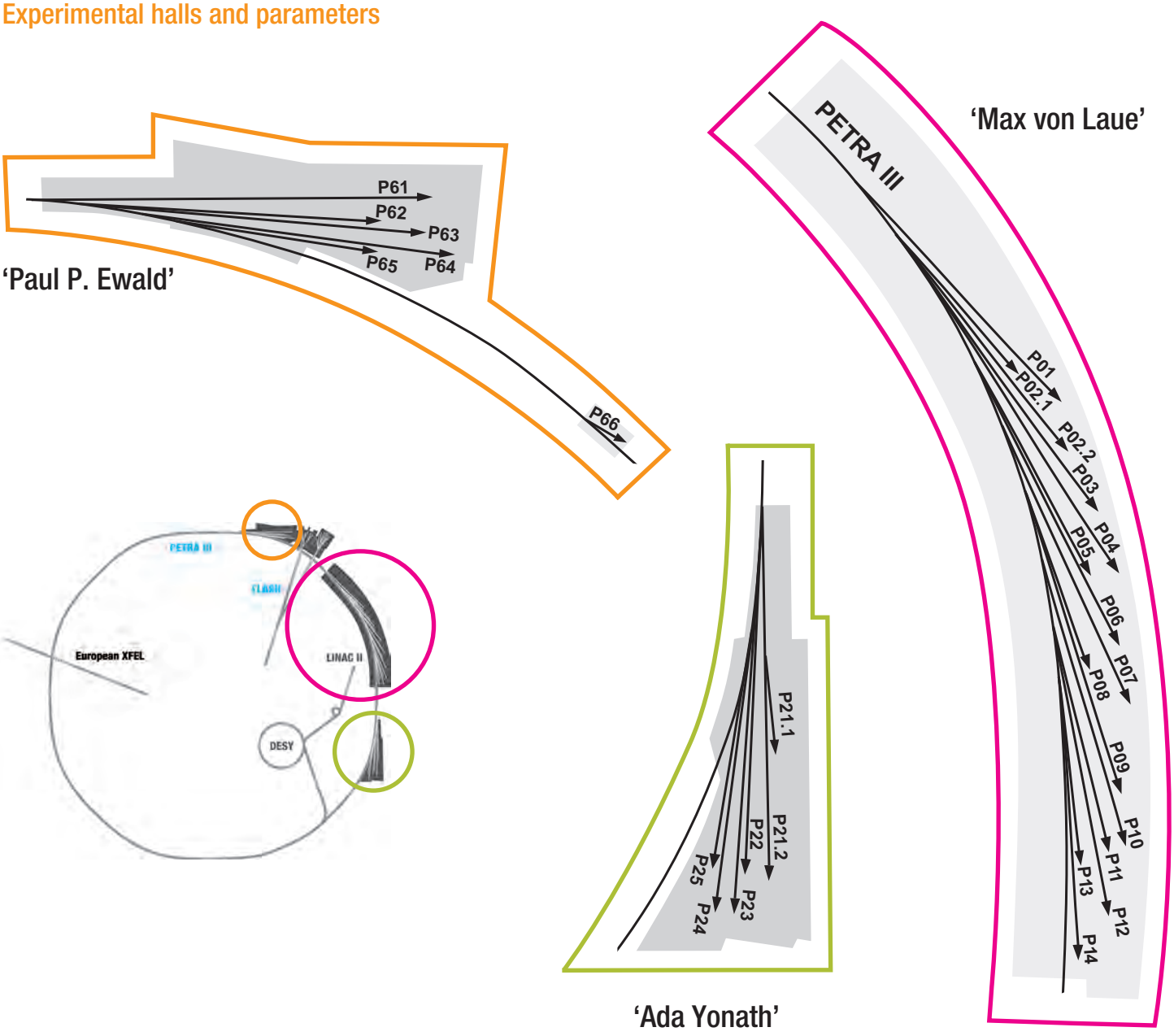

PETRA III - machine parameters

Electron energy	6.08 GeV
Circumference of the storage ring	2304 m
Number of bunches	960, 480, 60, and 40
Bunch separation	8 ns, 16 ns, 128 ns, and 192 ns
Electron beam current	100 mA (top-up)
Horizontal electron beam emittance	1.2 nmrad
Vertical electron beam emittance	0.01 nmrad
Electron beam energy spread (rms)	0.1%
Horizontal x vertical beam size (rms) at 5 m undulator (high β section) and 10 keV photon energy	141 µm x 5.2 µm
Horizontal x vertical beam size (rms) at 5 m undulator (low β section) and 10 keV photon energy	36 µm x 5.7 µm

FLASH1

BL1	non-monochromatic FEL photons Kirkpatrick-Baez (KB) focusing optics, FEL focal spot of ~7 µm × 8 µm (FWHM)	
	split-and-delay unit for XUV pump – XUV probe experiments (under commissioning, -30 ps to 650 ps delay)	*TU Berlin**
	optional pump – probe experiments using FLASH1 optical laser system	
	4-mirror polarizer for variable FEL polarization from 30 – 70 eV	*TU Berlin**
	permanent end station: multipurpose CAMP chamber with pnCCD detectors, electron and ion spectrometers and collinear incoupling optics for optical laser	
BL2	non-monochromatic FEL photons focused to ~20 µm(>4.5 nm) / unfocussed beam size ~5 – 10 mm (FWHM, depending on wavelength)	
	XUV beam splitter with variable time delay (-3 ps to 15 ps) for photon diagnostics and XUV pump – XUV probe experiments	
	optional pump-probe experiments using FLASH1 optical laser system	
	4-mirror polarizer for variable FEL polarization from 30 – 70 eV	*TU Berlin**
	about 3 × 4 m footprint for user-provided end station	
BL3	non-monochromatic FEL photons, spectral range: >4.5 nm (carbon coated optics) focused to ~20 µm / unfocussed beam size ~5 – 10 mm (FWHM, depending on wavelength)	
	optional pump – probe experiments using FLASH1 optical laser system	
	4-mirror polarizer for variable FEL polarization from 30 – 70 eV	*TU Berlin**
	optional pump – probe experiments using **THz radiation**: - tunable: 10 – 230 µm; up to 150 µJ/pulse; ~10 % bandwidth - broadband at 200 µm; up to 10 µJ/pulse; ~100 % bandwidth - synchronized and phase stable to X-ray pulses (down to 5 fs) - delivered to the experiment via vacuum beamline as: (i) ultra-high vacuum (~10^{-8} mbar), shorter delay between THz and X-ray (~4 m path difference), can accommodate up to 0.3 m wide setup (ii) high vacuum (~10^{-6} mbar), longer delay between THz and X-ray (~7 m path difference); can accommodate up to 2 m wide setup - available UHV chamber with mounts for refocusing XUV optics to compensate for XUV/THz path delay	
	about 3 × 4 m footprint for user-provided end station	
PG1	high resolution plane grating XUV monochromator (SX 700 type, <10^{-4} bandwidth, carbon coated optics): - variable combination of photon flux and resolution (from high flux to high resolution) - controlled temporal-spectral properties at moderate resolution for pump – probe experiments - high photon flux with harmonic filtering Kirkpatrick-Baez (KB) refocusing optics, FEL focal spot of 5 µm (vertically)	
	permanent end station: in commissioning two-stage VUV-Raman spectrometer for high-resolution measurements close to Rayleigh line	
PG2	uses the same monochromator as PG1 50 µm focus	
	XUV beam splitter with variable time delay (±6 ps) for time resolved studies	
	optional pump – probe experiments using FLASH1 optical laser system	
	about 3 × 4 m platform for user-provided end station	

FLASH1 optical / NIR laser system for pump – probe experiments

10 Hz single pulse	a)	compressed pulse transported over beamline 810 nm, 1.5 mJ, 60 fs FWHM pulse duration, 25 nm FWHM spectral bandwidth synchronization to FEL better than 60 fs rms
	b)	stretched pulse (chirped) transported over beamline pulse compressor must be included in experimental set-up 810 nm, 15 mJ, 200 ps FWHM uncompressed, 25 nm FWHM bandwidth 810 nm, 10 mJ, 60 fs FWHM with external pulse compressor, 25 nm FWHM bandwidth SHG 407 nm, 600 µJ, 5 nm FWHM spectral bandwidth THG 270 nm, 200 µJ, 2.5 nm FWHM spectral bandwidth synchronization to FEL better than 60 fs rms, corrected for drifts
burst-mode		up to 400 pulses / burst 805 nm, 20 µJ per single pulse, 120 fs FWHM pulse duration synchronization to FEL better than 60 fs rms
all laser options are available at Beamlines PG2, BL1-3, from summer 2018 on the laser beam transport of the burst mode laser to PG1 will be available		

FLASH2

FL24	non-monochromatic FEL photons wavelength range: 4 – 16 nm for the fundamental with 6σ acceptance, for harmonics down to 0.8 nm Kirkpatrick-Baez (KB) focusing optics, FEL focal spot of ~7 µm × 9 µm (FWHM)	
	grazing incidence (1.8 °) split-and-delay unit with ±12 ps time delay (to be installed 2018) optional pump – probe experiments using FLASH2 optical laser system (to be installed middle 2018)	*Univ. Münster**
	about 3 × 4 m footprint for user-provided end station	
FL26	non-monochromatic FEL photons wavelength range: 6 – 40 nm with 6σ, up to 80 nm with 3σ acceptance	
	permanent end station: - reaction microscope (REMI) for time-resolved AMO spectroscopy - grazing incidence delay-line and refocusing optics: FEL focal spot <10µm × 10µm (FWHM), ±2.7 ps time delay range, 1 fs precision	*MPI-K Heidelberg**

All FLASH beamlines provide online photon diagnostics for intensity, wavelength, and beam position; fast shutter, aperture and filter sets.

FLASH2 optical / NIR laser system for pump – probe experiments

By mid-2018 a pump-probe laser will be available for the FLASH2 beamlines FL24 and FL26 with the parameter set below

wavelength:	800 nm (fundamental centre wavelength)
bandwidth:	100 nm
intra-burst-repetition rate:	50 kHz
number of pulses per burst:	1 – 40
pulse duration:	15 fs FWHM (compressed), 1 ps FWHM (uncompressed)
timing jitter to FEL:	<50 fs rms
pulse energy:	0 – 500 µJ
polarization:	flexible
focus size ($1/e^2$ diameter):	FL24: <100 µm, FL26: <50 µm
peak intensity	$>10^{14}$ W/cm^2
time delay to FEL:	-4 ns to +4 ns, 10 fs resolution, larger delays optional
energy instability:	<10 % pulse-to-pulse peak (3 % rms)

400 nm and 266 nm will be available on a best effort basis with expected conversion efficiencies of >30 % SHG, >5 % THG

We would like to acknowledge all contributions to instrument development and operation provided within the framework of BMBF Verbundforschung.

PETRA III.

Beamlines

PETRA III experimental hall 'Max von Laue'

Beamline and instruments		Operated by
P01	High resolution dynamics 10 (20) m U32 | 4.5 – 40 keV	DESY
	Nuclear resonant scattering	DESY
	Resonant inelastic scattering	DESY / MPG
	X-ray Raman scattering	DESY / MPG
P02.1	Powder diffraction 2 m U23 | 60 keV	DESY
	Standard & time resolved powder diffraction	DESY
	High resolution powder diffraction	DESY
P02.2	Extreme conditions 2 m U23 | 10 – 60 keV	DESY
	Laser heated diamond anvil cells	DESY
	General purpose high pressure	DESY
P03	Micro- and Nano-SAXS / WAXS 2 m U29 | 8 – 23 keV	DESY
	Micro-small and wide angle scattering	DESY
	Nano-beam scattering and diffraction	DESY
P04	Variable polarization soft X-rays 5 m UE65 | 200 – 3000 eV	DESY
	UHV diffractometer	DESY
	Photon-ion spectrometer (PIPE)	DESY
	Ultra-high resolution photoelectron spectroscopy (ASPHERE)	DESY
	Soft X-ray absorption spectrometer	DESY
	Nano focus apparatus for spatial and time resolving spectroscopy	DESY
P05	Micro- and nanoimaging 2 m U29 | 8 – 50 keV	HZG
	Micro-tomography	HZG
	Nano-tomography	HZG (in commissioning)
P06	Hard X-ray micro-/nanoprobe 2 m U32 | 5 – 100 keV	DESY
	Microprobe	DESY
	Nanoprobe	DESY
P07	High energy X-ray materials science 2 m U29 (planned: 4 m U19) | 50 – 200 keV	HZG
	Multi-purpose triple-axis diffractometer	DESY
	Heavy load diffractometer	HZG
	Grain mapper	HZG
	High energy tomography	HZG
P08	High resolution diffraction 2 m U29 | 5.4 – 29.4 keV	DESY
	High resolution diffractometer	DESY
	Liquid surface diffractometer	DESY
	Langmuir trough in-plane diffractometer	DESY
P09	Resonant scattering and diffraction/HAXPES 2 m U32 | 2.7 – 50 keV	DESY
	High precision psi-diffractometer	DESY
	Heavy load diffractometer	DESY
	Hard X-ray photoelectron spectroscopy	DESY
P10	Coherence 5 m U29 | 4 – 20 keV	DESY
	X-ray photon correlation spectroscopy (4 – 20 keV)	DESY
	Vertical rheometer (8.388 keV)	DESY
	Coherent imaging (8 – 15 keV)	DESY
	Multi-purpose diffractometer (8 – 20 keV)	DESY
P11	Bio-imaging and diffraction 2 m U32 | 2.4 – 30 keV	DESY
	Imaging of biological samples (2.4 – 10 keV)	DESY (in commissioning)
	Macromolecular crystallography (5.5 – 30 keV)	DESY / MPG / HZI

Beamline and instruments		Operated by
P12	Bio SAXS 2 m U29 | 4 – 20 keV	EMBL
	Solution small-angle scattering	EMBL
P13	Macromolecular crystallography I 2 m U29 | 4.5 – 17.5 keV	EMBL
	Macromolecular crystallography	EMBL
P14	Macromolecular crystallography II 2 m U29 | 6 – 20 keV	EMBL
	Macromolecular crystallography	EMBL

PETRA III experimental hall 'Ada Yonath'

Beamline and instruments		Operated by
P21	Swedish materials science (SMS) beamline 4 m IVU21 | 40 – 150 keV side branch: 2 m U29 | 50, 80, 100 keV	Swedish institution / DESY
	Diffraction and imaging Broad band diffraction	Swedish institution / DESY (commissioning 2018)
P22	Hard X-ray photoelectron spectroscopy 2 m U33 | 2.4 – 15 keV	DESY
	HAXPES, ambient and high pressure, HAXPEEM (relocated from P09),	DESY (operation from fall 2018)
P23	Russian-German *in-situ* and nanodiffraction beamline 2 m U32 | 5 – 35 keV	DESY
	Nano-XRD, *in situ* and complex environments	DESY (operation from fall 2018)
	2nd hutch instrument t.b.d.	not yet funded
P24	Chemical crystallography 2 m U29 | 8, 15 – 45 keV	DESY
	Single crystal diffraction in complex sample environments	DESY
	Small molecule crystallography	DESY
P25	t.b.d.	not yet funded

PETRA III experimental hall 'Paul P. Ewald'

Beamline and instruments		Operated by
P61	High-energy wiggler beamline 40 m damping wiggler | 50 – 200 keV / pink beam	DESY
	High-energy engineering materials science	HZG
	Large volume press - Extreme conditions (LVP-EC)	DESY (commissioning 2018/19)
P62	Small-angle X-ray scattering 2 m U32 | 4 – 44 keV	DESY
		(operation planned 2020)
P63	t.b.d.	not yet funded
P64	Advanced X-ray absorption spectroscopy 2 m U32 | 4 – 44 keV	DESY
	Time-resolved *in situ* XAFS, QEXAFS, bioXAFS	DESY
P65	Applied X-ray absorption spectroscopy 36 cm U32 | 4 – 44 keV	DESY
	Ex-situ and *in-situ* XAFS of bulk samples	DESY
P66	Superlumi Bending magnet | 4 – 40 eV	DESY
	Time-resolved luminescence spectroscopy *(separate building)*	DESY (commissioning 2019)

We would like to acknowledge all contributions to beamline & instrument development and operation provided within the framework of BMBF-Verbundforschung, the Röntgen-Ångström-Cluster (RAC), the Ioffe-Röntgen-Institute (IRI), the Department of Science & Technology (Government of India) within the India@DESY collaboration, the Ruprecht-Haensel-Laboratory (University of Kiel), Forschungszentrum Jülich, University of Stockholm.

Beamtime statistics 2017.

FLASH
Operation period 2017

	User beamtime	Machine studies and user experiment preparation	Maintenance	Shutdown and commissioning
FLASH1				
1 Jan – 6 Nov	3806 h	2094 h	59 h	
planned for 7 Nov – 31 Dec	690 h	378 h	12 h	
				1721 h
FLASH2				
1 Jan – 6 Nov	1369 h			
planned for 7 Nov – 31 Dec	480 h			

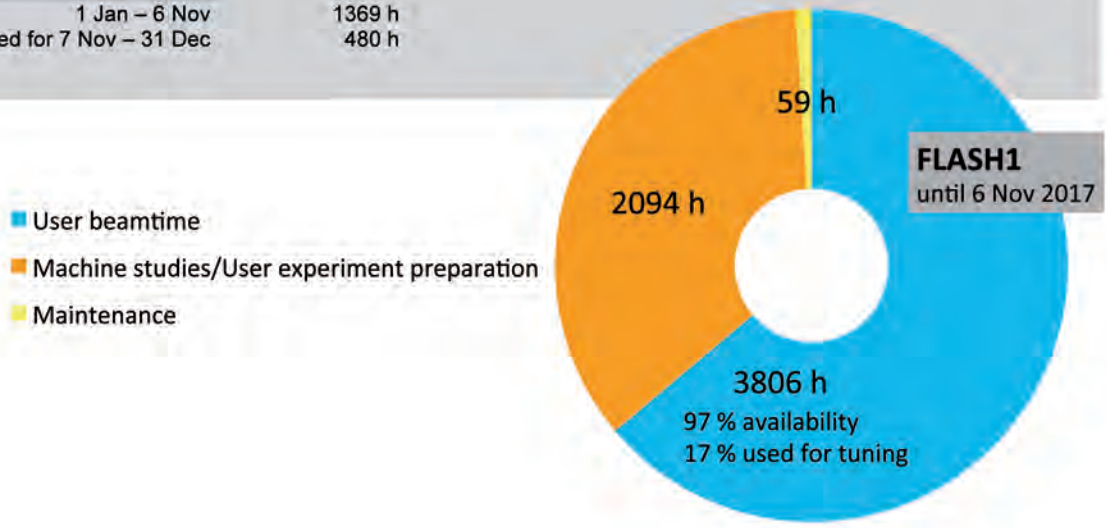

PETRA III
Operation period 2017

	User beamtime	Machine studies and test runs	Maintenance	Shutdown
1 Jan – 11 Dec	3773 h	1391 h	378 h	
planned for 12 Dec – 31 Dec	228 h	24 h	0 h	
				2966 h

run periods:
10 Apr – 6 Jul
17 Aug – 22 Dec

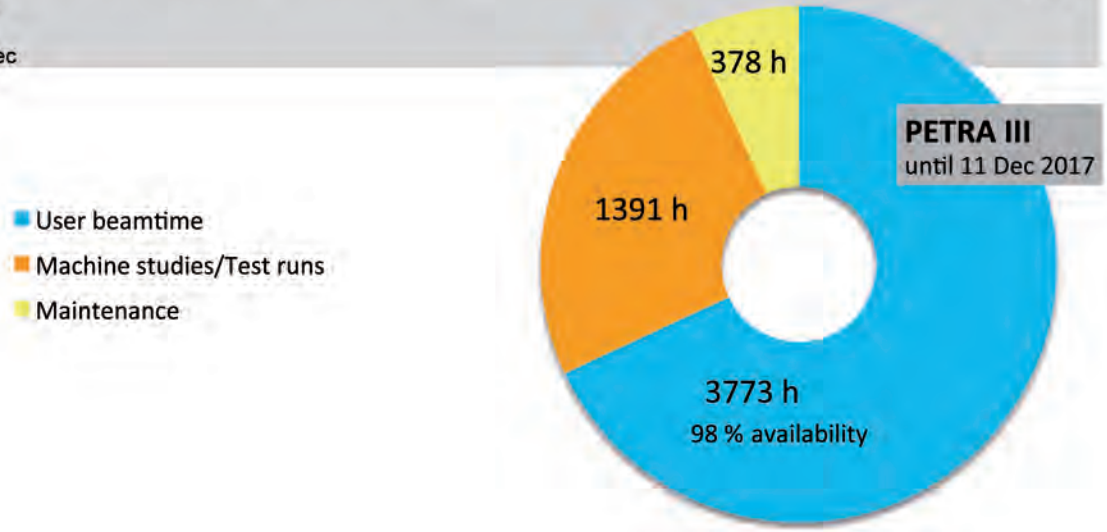

Committees 2017.

Photon Science Committee PSC — advises the DESY Photon Science management

Christian David (chair)	PSI, Villigen, CH
Melissa A. Denecke (vice chair)	University of Manchester, UK
Stefan Eisebitt	MBI and Technische Universität Berlin, DE
Gwyndaf Evans	Diamond Light Source Ltd., Didcot, UK
Jan-Dierk Grunwaldt	KIT, Karlsruhe, DE
Simo Huotari	University of Helsinki, FI
Maya Kiskinova	Elettra-Sincrotrone, Trieste, IT
Arwen Pearson	CUI, Universität Hamburg, DE
Thomas Pfeifer	MPI for Nuclear Physics, Heidelberg, DE
Henning Friis Poulsen	DTU Fysik, Lyngby, DK
Harald Reichert	ESRF, Grenoble, FR
Bernd Schmitt	PSI, Villigen, CH
Andrea Somogyi	Synchrotron SOLEIL, Saint-Aubin, FR
Julian Stangl	Johannes Kepler Universität, Linz, AT
Stefan Vogt	Argonne National Laboratory, Lemont, US
Nele Müller (PSC secretary)	DESY, Hamburg, DE

Laser Advisory Committee LAC — shared between DESY and the European XFEL

Uwe Morgner (chair)	Laser Zentrum Hannover, DE
Giulio Cerullo	Politecnico di Milano, IT
Miltcho Danailov	Elettra-Sincrotrone, Trieste, IT
Patrick Georges	CNRS, FR
Alfred Leitenstorfer	Universität Konstanz, DE
Robert W. Schoenlein	LBNL, Berkeley, US
William E. White	SLAC, Menlo Park, US
Jonathan Zuegel	LLE, Rochester, US
Andreas Galler (LAC secretary)	European XFEL GmbH, Schenefeld, DE
Oliver D. Mücke (LAC secretary)	CFEL-DESY, Hamburg, DE

DESY Photon Science User Committee DPS-UC — represents the user community

Peter Müller-Buschbaum (chair)	Technische Universität München, DE
Markus Mezger	MPI für Polymerforschung, Mainz, DE
Daniela Rupp	Technische Universität Berlin, DE
Chrystèle Sanloup	Institut des Sciences de la Terre de Paris, FR
Gregor Witte	Ludwig-Maximilians-Universität München, DE

Komitee Forschung mit Synchrotronstrahlung KFS
representative body of the German SR and FEL user community

Bridget Murphy (chair)	Christian-Albrechts-Universität Kiel, DE
Jan-Dierk Grunwaldt (vice chair)	KIT, Karlsruhe, DE
Peter Albers	AQura GmbH, DE
Stefan Eisebitt	MBI and Technische Universität Berlin, DE
Ronald Frahm	Universität Wuppertal, DE
Christian Gutt	Universität Siegen, DE
Birgit Kanngießer	Technische Universität Berlin, DE
Sarah Köster	Georg-August-Universität Göttingen, DE
Kai Rossnagel	Christian-Albrechts-Universität Kiel, DE
Hermann Schindelin	Universität Würzburg, DE

Project Review Panels 2017.

PRP X-ray Spectroscopy	
Iztok Arčon	University of Nova Gorica, SL
Matthias Bauer	Universität Paderborn, DE
Ralph Claessen	Julius-Maximilians-Universität Würzburg, DE
Jörg Evers	MPI für Kernphysik, Heidelberg, DE
Raphael Hermann	Oak Ridge National Laboratory, US
Greg Hughes	Dublin City University, IE
Marco Moretti	ESRF, Grenoble, FR
Maarten Nachtegaal	PSI, Villigen, CH
Håkan Rensmo	Uppsala University, SE
Svetoslav Stankov	Karlsruher Institut für Technologie KIT, DE
Max Wilke	Universität Potsdam, DE
Wolfgang Drube (PRP secretary)	DESY, Hamburg, DE

PRP High Pressure and Extreme Conditions	
Leonid Dubrovinsky	Bayerisches Geoinstitut, Bayreuth, DE
Diego Gatta	University of Milan, IT
Malcolm McMahon	University of Edinburgh, UK
Sébastien Merkel	Lille University, FR
Clemens Prescher	Universität Köln, DE
Sergio Speziale	GFZ, Potsdam, DE
Hanns-Peter Liermann (PRP secretary)	DESY, Hamburg, DE

PRP Engineering Materials Science	
Jens Gibmeier	Karlsruher Institut für Technologie KIT, DE
Patrick Huber	Technische Universität Hamburg-Harburg, DE
Rolf Kaufmann	Empa, CH
Jozef Keckes	Montanuniversität Leoben, AT
Svea Mayer	Montanuniversität Leoben, AT
Thomas Niendorf	Universität Kassel, DE
Wolfgang Pantleon	Technical University of Denmark, DK
Walter Reimers	Technische Universität Berlin, DE
Guillermo Requena	DLR and RTWH Aachen, DE
Carsten Siemers	Technische Universität Braunschweig, DE
Axel Steuwer	University of Malta, MT
Dieter Lott (PRP secretary)	HZG, Geesthacht, DE
Ulrich Lienert (DESY representative)	DESY, Hamburg, DE

PRP Soft Condensed Matter – Bulk	
Stephan Förster	Universität Bayreuth, DE
Christian Gutt	Universität Siegen, DE
Thomas Hellweg	Universität Bielefeld, DE
Daniel Söderberg	KTH, Stockholm, SE
Joachim Wagner	Universität Rostock, DE
Rainer Gehrke (PRP secretary)	DESY, Hamburg, DE

PRP Soft Condensed Matter – Surfaces and Interfaces	
Tiberio A. Ezquerra	CSIC, Madrid, ES
Alexander Gerlach	Universität Tübingen, DE
Markus Mezger	Universität Mainz, DE
Frank Schreiber	Universität Tübingen, DE
Tobias Unruh	Technische Universität München, Garching, DE
Andreas Zumbühl	University of Fribourg, CH
Oliver Seeck (PRP secretary)	DESY, Hamburg, DE

PRP Imaging (full-field, scanning, coherent)	
Martin Bech	Lund University, SE
Oliver Bunk	PSI, Villigen, CH
Manfred Burghammer	ESRF, Grenoble, FR
Frank Friedrich	Universität Hamburg, DE
Julia Herzen	Technische Universität München, DE
Koen Janssens	University of Antwerp, BE
Hendrik Küpper	University of South Bohemia, České Budějovice, CZ
Stephan Peth	Universität Kassel, DE
Sebastian Schoeder	Synchrotron SOLEIL, Saint-Aubin, FR
Jürgen Thieme	Brookhaven National Laboratory, Upton NY, US
Stefan Vogt	Argonne National Laboratory, Lemont, US
Gerald Falkenberg (PRP secretary)	DESY, Hamburg, DE
Felix Beckmann (HZG representative)	HZG, Geesthacht, DE

PRP Methods and Instrumentation	
Yngve Cerenius	MAX IV Laboratory, Lund University, SE
Cameron Kewish	Australian Synchrotron, Melbourne, AU
Raymond Barrett	ESRF, Grenoble, FR
Anatoly Snigirev	I. Kant Baltic Federal University, Kaliningrad, RU
Horst Schulte-Schrepping (PRP secretary)	DESY, Hamburg, DE

PRP Hard Condensed Matter – Surface and Coherent Scattering	
Johan Gustafson	Lund University, SE
Václav Holý	Charles University, Prague, CZ
Alexander Komarek	MPI CPfS, Dresden, DE
Guido Meier	MPI MPSD, Hamburg, DE
Bogdan Sepiol	Universität Wien, AT
Julian Stangl	Johannes Kepler Universität Linz, AT
Jesper Wallentin	University Lund, SE
Peter Wochner	MPI für Festkörperforschung, Stuttgart, DE
Michael Sprung (PRP secretary)	DESY, Hamburg, DE

PRP Hard Condensed Matter – Bulk (diffraction and scattering)	
Emil Bozin	Brookhaven National Laboratory, Upton NY, US
Johan Chang	University of Zurich, CH
Robert Dinnebier	MPI für Festkörperforschung, Stuttgart, DE
Jochen Geck	IFW Dresden, DE
Hermann Gies	Ruhr-Universität Bochum, DE
Markus Huecker	Weizmann Institute of Science, Rehovot, IL
Mads Ry Vogel Jørgensen	Aarhus University, DK
Helen Walker	ISIS, Didcot, GB
Xiaodong Zou	Stockholm University, SE
Ann-Christin Dippel (PRP secretary)	DESY, Hamburg, DE

PRP VUV- and Soft X-ray	
Lucia Aballe	CELLS-ALBA Barcelona, ES
Stephan Fritzsche	Helmholtz Institut Jena, DE
Michael Meyer	European XFEL GmbH, Schenefeld, DE
Luc Patthey	PSI, Villigen, CH
Emma Sokell	University College Dublin, IE
Jens Viefhaus, Jens Buck (PRP secretaries)	DESY, Hamburg, DE

PRP Soft X-Ray – FEL Experiments (FLASH)	
Katharina Al-Shamery	Universität Oldenburg, DE
Michael Bonitz	Universität Kiel, DE
Christoph Bostedt	Argonne North Western University, US
Hermann Dürr	SLAC Nat. Accelerator Laboratory, Menlo Park, US
Chris Jacobsen	APS, Argonne National Laboratory, US
Steven Johnson	ETH Zürich, CH
Claudio Masciovecchio	Elettra Sincrotrone Trieste, IT
Ronald Redmer	Universität Rostock, DE
Robert W. Schoenlein	SLAC Nat. Accelerator Laboratory, Menlo Park, US
Kiyoshi Ueda	Tohoku University, Sendai, JP
Marc Vrakking	MBI, Berlin, DE
Martin Weinelt	FU Berlin, DE
Elke Plönjes-Palm, Rolf Treusch (PRP secretaries)	DESY, Hamburg, DE

PEC: EMBL Life Science beamlines P12-P14 / PRP Bio-crystallography at P11	
Savvas Savvides (chair)	Ghent University, BE
Pau Bernadó	CBS/CNRS, Montpellier, FR
Kristina Djinovic-Carugo	Universität Wien, AT
Gwyndaf Evans	Diamond Light Source, Didcot, GB
Robert Fischetti	Argonne National Laboratory, US
Mariusz Jaskolski	Adam Mickiewicz University of Poznan, PL
Javier Pérez	Synchrotron SOLEIL, Saint-Aubin, FR
Zehra Sayers	Sabanci University, Istanbul, TR
Joel Sussman	Weizmann Institute of Sciences, Rehovot, IL
Maria Vanoni	University of Milan, IT
Bente Vestergaard	University of Copenhagen, DK
Gregor Witte	Ludwig-Maximilians-Universität München, DE
Christian Schroer (DESY observer)	DESY, Hamburg, DE

Photographs and Graphics:

Lars Berg, Münster
Julian Bergtholdt, DESY
DESY
DFZ Architekten GmbH
EMBL
European XFEL
Axel Heimken, Hamburg
HZG
LEAPS
Tina Mavric, Hamburg
Marta Mayer, DESY
MPG
Eberhard Reimann, DESY
Reimo Schaaf, Hamburg
Dae Seon Seo, DESY
Bente Stachowske, Hamburg
Rie Tanaka, RIKEN
Universität Hamburg
Marco Urban, Berlin
Edgar Weckert, DESY

Figures of the Research Highlights were reproduced by permission from authors or journals.

Acknowledgement

We would like to thank all the authors and all those who have contributed to the realisation of this Annual Report.

Imprint

Publishing and Contact:
Deutsches Elektronen-Synchrotron DESY
A Research Centre of the Helmholtz Association

Hamburg location:
Notkestr. 85, 22607 Hamburg, Germany
Tel.: +49 40 8998-0, Fax: +49 40 8998-3282
desyinfo@desy.de

Zeuthen location:
Platanenallee 6, 15738 Zeuthen, Germany
Tel.: +49 33762 7-70, Fax: +49 33762 7-7413
desyinfo.zeuthen@desy.de

Photon Science at DESY
Tel.: +49 40 8998-2304, Fax: +49 40 8998-4475
photon-science@desy.de
photon-science.desy.de

www.desy.de

ISBN 978-3-945931-15-8

Online version:
photon-science.desy.de/annual_report

Realisation:
Wiebke Laasch, Daniela Unger

Editing:
Sadia Bari, Martin Beye, Lars Bocklage, Rainer Gehrke, Daniel Horke, Thomas Keller, Tim Laarmann, Wiebke Laasch, Wolfgang Morgenroth, Nele Müller, Ralf Röhlsberger, Sang-Kil Son, Daniela Unger, Hans-Christian Wille

Layout: Sabine Kuhls-Dawideit, Büro für Grafik und Design, Halstenbek

Printing: EHS Druck GmbH, Schenefeld

Copy deadline: December 2017

HELMHOLTZ
RESEARCH FOR GRAND CHALLENGES

Deutsches Elektronen-Synchrotron
A Research Centre of the Helmholtz Association

The Helmholtz Association is a community of 18 scientific-technical and biological-medical research centres. These centres have been commissioned with pursuing long-term research goals on behalf of the state and society. The Association strives to gain insights and knowledge so that it can help to preserve and improve the foundations of human life. It does this by identifying and working on the grand challenges faced by society, science and industry. Helmholtz Centres perform top-class research in strategic programmes in six core fields: Energy, Earth & Environment, Health, Aeronautics, Space and Transport, Matter, and Key Technologies.

www.helmholtz.de